2014-11-01

Gasification of Biomass, Coal, and Petroleum Coke at High Heating Rates and Elevated Pressure

Aaron D. Lewis
Brigham Young University - Provo

Gasification of Biomass, Coal, and Petroleum Coke at High Heating Rates and Elevated Pressure

Aaron Dudley Lewis

A dissertation submitted to the faculty of
Brigham Young University
in partial fulfillment of the requirements for the degree of

Doctor of Philosophy

Thomas H. Fletcher, Chair
David O. Lignell
Randy S. Lewis
Larry L. Baxter
Thomas A. Knotts

Department of Chemical Engineering

Brigham Young University

November 2014

ABSTRACT

Gasification of Biomass, Coal, and Petroleum
Coke at High Heating Rates and
Elevated Pressure

Aaron Dudley Lewis
Department of Chemical Engineering, BYU
Doctor of Philosophy

Gasification is a process used to convert any carbonaceous species through heterogeneous reaction to obtain the desired gaseous products of H_2 and CO which are used to make chemicals, liquid transportation fuels, and power. Both pyrolysis and heterogeneous gasification occur in commercial entrained-flow gasifiers at pressures from 4 to 65 atm with local gas temperatures as high as 2000 °C. Many gasification studies have been performed at moderate temperatures, heating rates, and pressures. In this work, both pyrolysis and char gasification experiments were performed on coal, petroleum coke, and biomass at conditions pertinent to commercial entrained-flow gasifiers.

Rapid biomass pyrolysis experiments were performed at atmospheric pressure in an entrained-flow reactor for sawdust, switchgrass, corn stover, and straw mostly using a peak gas temperature of 1163 K at particle residence times ranging from 34 to 113 ms. Biomass pyrolysis was modeled using the Chemical Percolation Devolatilization model assuming that biomass pyrolysis occurs as a weighted average of its individual components (cellulose, hemicellulose, and lignin). Thermal cracking of biomass tar into light gas was included using a first-order model with kinetic parameters regressed in the current study.

Char gasification rates were measured for biomass, petroleum coke, and coal in a pressurized entrained-flow reactor at high heating-rate conditions at total pressures between 10 and 15 atm. Peak centerline gas temperatures were between 1611 and 1879 K. The range of particle residence times used in the gasification experiments was 42 to 275 ms. The CO_2 gasification rates of biomass and petroleum coke chars were measured at conditions where the reaction environment consisted of approximately 40 and 90 mol% CO_2. Steam gasification rates of coal char were measured at conditions where the maximum H_2O concentration was 8.6 mol%. Measured data was used to regress apparent kinetic parameters for a first-order model that describes char conversion. The measured char gasification rates were far from the film-diffusion limit, and are pertinent for pulverized particles where no internal particle temperature gradients are important. The modeling and measured data of char gasification rates in this research will aid in the design and efficient operation of commercial entrained-flow gasifiers, as well as provide validation for both existing and future models at a wide range of temperatures and pressures at high heating-rate conditions.

Keywords: biomass, sawdust, corn stover, switchgrass, petroleum coke, coal, pyrolysis, gasification, thermal conversion, pressure, heating rate, tar, CPD model, tar cracking, Aaron Lewis

ACKNOWLEDGEMENTS

I would like to thank my lovely wife Brittany for her constant support and for allowing me to work most Saturdays to make progress on this research. I would also like to thank my kids, Connor and Annemarie, for being a source of motivation. I express my appreciation to my parents who taught me the importance of an education and how to work hard. I also wish to recognize the support that my in-laws have been to me while I have pursued my graduate studies.

I would like to thank my graduate advisor, Dr. Thomas H. Fletcher, for his support during this research project and for allowing me to continue working on petcoke research following my Master's degree. He gave me the freedom to conduct my own research, but provided valuable correction and guidance when necessary.

I appreciate the financial support for this research, which was funded in part by Grant 2009-10006-06020 from the US Department of Agriculture/NIFA, and also by Award Number DE-NT0005015 from the Department of Energy. However, any opinions, findings, conclusions, or other recommendations expressed herein do not necessarily reflect the views of NIFA, the United States Government, or any agency thereof.

I wish to thank Randy Shurtz for making the learning curve of research less steep by sharing his experience with me when I first started graduate school. Like Randy often said, experience is really nice to have but is often only painfully obtained. Gratitude is expressed to the undergraduate researchers Emmett Fletcher, Mitch Withers, Nate Marchant, Daniel Henley, and Eric Fuller for their assistance in this research. I also wish to thank Mike Standing for his assistance on the SEM microscope, and Duane Tucker for delivering the countless bottles of gas cylinders to our lab over the years that experiments were conducted. Lastly, I wish to acknowledge God for anything helpful, original, or creative in this work.

TABLE OF CONTENTS

LIST OF TABLES

LIST OF FIGURES

NOMENCLATURE

A	pre-exponential factor
A_p	particle external surface area of an assumed spherical particle ($4 \cdot \pi \cdot r^2$)
BSG	entrained-flow Bench Scale Gasifier reactor of GE Global Research
C_p	particle heat capacity
$C_{reactant,\infty}$	concentration of CO_2 or H_2O in the bulk gas
C_{tar}	daf tar fraction from biomass pyrolysis
CCK	Char Conversion Kinetics model developed by Shurtz (2011)
CPD	Chemical Percolation Devolatilization model
CS	corn stover
D_{AB}	diffusion coefficient
d_m	particle diameter mass mean
d_p	particle diameter
d_0	diameter of feedstock material
d_1	diameter of collected char after an experiment
daf	dry and ash-free
E	activation energy
FFB	entrained-flow flat-flame burner reactor; operates at atmospheric pressure
h_c	heat transfer coefficient ($Nu \cdot k_{gas}/d_p$)
h_m	mass transfer coefficient ($Sh \cdot D_{AB}/d_p$)
ILL #6	Illinois #6 coal
HPFFB	entrained-flow High-Pressure Flat-Flame Burner reactor
k_1	rate constant of biomass tar cracking
k_{gas}	gas thermal conductivity
k_{rxn}	gasification rate constant
m_0	mass of material fed during an experiment on a dry basis
m_1	mass of char collected after an experiment on a dry basis
$m^0_{ash,fed}$	dry mass of ash in the fed feedstock
$m_{char\ collected}$	dry mass of char collected after an experiment
m^0_{fed}	dry mass of feedstock fed
m_p	particle mass
MR	particle mass release
n	number of experimental data points
Nu	Nusselt number
$P_{CO2,surf}$	CO_2 partial pressure at particle surface
$P_{CO2,\infty}$	CO_2 partial pressure in bulk gas
$P_{H2O,surf}$	partial pressure of H_2O at the particle surface
$P_{reactant,surf}$	partial pressure of CO_2 or H_2O at the particle surface
$P_{reactant,\infty}$	partial pressure of CO_2 or H_2O in the bulk gas
Pitt #8	Pittsburgh #8 coal
PS	poplar sawdust
R	ideal gas constant
r''_p	char reaction rate per external surface area (i.e., $dm_p/dt/A_p$)

SG	switchgrass
Sh	Sherwood number
t	time
T_{gas}	gas temperature
$T_{gas,max}$	maximum measured centerline gas temperature
T_p	particle temperature
T_{surr}	surroundings temperature (500 K in this study)
Utah	Utah Skyline coal
v_p	particle velocity
w	mass fraction
x_{ash}	mass fraction of ash
$x^0_{ash,fed}$	mass fraction of ash in dry feedstock fed in an experiment
$x_{ash,char\ collected}$	mass fraction of ash in the dried collected char after an experiment
X_i^M	modeled particle mass release point
X_i^E	experimental particle mass release point
ΔH_{rxn}	heat of reaction
Δz	distance a particle travels in a single time step
ε_b	inter-particle void fraction or packing factor
ε_p	emissivity of char
μ_{gas}	dynamic gas viscosity
ρ_0	apparent density of dried feedstock material
ρ_1	apparent density of dried char collected from an experiment
$\rho_{apparent}$	apparent density
ρ_{bulk}	bulk density
ν	mass of carbon (i.e., char) that react per mole of CO_2 or H_2O reactant
σ	Stefan-Boltzmann constant
χ	ratio of observed rate to maximum film diffusion limited rate
ψ	structural parameter for the random pore model

1. Introduction

One way that carbonaceous solids can be transformed into useful products such as chemicals and energy is through gasification, which converts carbonaceous fuels through partial oxidation into a gaseous fuel termed *synthesis gas* (or *syngas*) for the desired products of H_2 and CO. Both homogeneous and heterogeneous reactions occur during gasification of a solid fuel. Homogeneous gas-phase reactions in most commercial entrained-flow gasifiers achieve thermodynamic chemical equilibrium (Smoot and Smith, 1985; Higman and Burgt, 2003). However, the heterogeneous reactions between solid char and gasification agents (such as steam and CO_2) do not achieve equilibrium, and heterogeneous gasification rates must include particle size effects, pore diffusion, temperature and pressure variations, evolution of char structure, ash composition, diffusion of reactants through the particle boundary layer, and reactions with multiple reactant gases (Smoot and Smith, 1985). Predicting char gasification kinetics therefore relies heavily on measured rate data. Being able to predict char gasification rates is of research interest because the heterogeneous reaction between char and gas often governs the overall reaction rate in gasification processes (Liu et al., 2010b). Other processes such as pyrolysis or volatiles combustion occur more quickly during the gasification of a solid fuel.

Entrained-flow gasifiers are very common in industry (Minchener, 2005; Liu et al., 2010b), although several gasifier types exist. Some of the advantages of the entrained-flow gasifier are that it allows the highest throughput per reactor volume and can be operated with a

variety of fuels (Smoot, 1991; Minchener, 2005). Entrained-flow gasifiers convert pulverized particles, and use high temperature (1200-2000 °C) and pressure (4-65 atm) to ensure high carbon conversion in the time frame of a few seconds (Minchener, 2005; Liu et al., 2010b; Ren et al., 2013). Particles can be fed dry or carried by a water slurry into pressurized entrained-flow gasifiers. The small entrained particles experience initial particle heating rates near 10^5-10^6 K/s (Essenhigh, 1981; Fletcher et al., 1997), and react in cocurrent flow in the presence of a high-temperature flame.

Char gasification rates are seldom measured at the experimentally challenging, yet industrially significant conditions of high temperature, pressure, and initial particle heating rate. The vast majority of gasification reactivity data in the literature have been measured using thermal gravimetric analyzers (TGA) at relatively low temperatures using chars generated at atmospheric pressure and low heating rates. While TGA reactors are certainly valuable in providing insights to reaction processes, it is known that char-generation conditions affect gasification reactivity (Mermoud et al., 2006). Hence, measuring gasification rates of chars prepared at low heating rates and low temperature will yield different results than measuring gasification rates of chars prepared at conditions characteristic of commercial entrained-flow gasifiers (i.e., high temperature, pressure, and heating rates). When performing experiments to learn more about a complicated process, it is valuable to match as many experimental variables as possible. In this research, char gasification rates were measured for various fuels (biomass, petroleum coke, & coal) at conditions representative of commercial entrained-flow gasifiers using a pressurized entrained-flow reactor operated at high temperature using short particle residence times. This makes the measured and modeled gasification rates in this work very realistic and meaningful. The modeling and measured data of char gasification rates in this

research will aid in the design and efficient operation of commercial entrained-flow gasifiers, as well as provide a test case to evaluate both existing and future models at a wide range of temperatures and pressures at high heating-rate conditions.

Part of this research also involved the pyrolysis of biomass. Pyrolysis or devolatilization is the thermal decomposition of a solid fuel into permanent gases, tar (condensable vapors), and char (solid residue) (Ranzi et al., 2008). Studying pyrolysis is important since pyrolytic char yields act as a source of reactants for the heterogeneous reactions of combustion or gasification. Additionally, pyrolysis sometimes serves as a stand-alone process for certain fuels (Scott and Piskorz, 1984). In this work, the pyrolysis yields of biomass were measured at conditions of rapid initial particle heating rates using short residence times in an entrained-flow reactor at atmospheric pressure. The measured biomass pyrolysis yields were modeled assuming that biomass pyrolysis occurs as a weighted average of its individual components (cellulose, hemicellulose, and lignin). Thermal cracking of biomass tar into light gas was also implemented in the biomass modeling.

2. Literature Review

This section gives background in several areas to better understand this research, and includes a review of pertinent literature. Some of the topics include fuel description, pyrolysis, gasification, and a review of recent char gasification kinetic studies in the literature.

2.1 Fuel Descriptions

2.1.1 Biomass

Biomass can be a sustainable fuel source that allows energy generation from biological material such as sawdust, switchgrass, corn stalks, yard clippings, etc. Interest in converting biomass to fuels and chemicals was sparked in the 1970s due to the oil crisis (Bungay, 1981). Biomass is similar to fossil fuels in that they both contain high percentages of carbon and hydrogen, but biomass has a much higher oxygen content. The majority of biomass research for energy use has focused on wood.

The three major components of any type of biomass are cellulose, hemicellulose, and lignin. Although present in lesser amounts, biomass contains an inorganic fraction as well as organic extractives, some of which extractives include fats, proteins, waxes, resins, terpenes, pectins, and

essential oils (Mohan et al., 2006). Biomass also contains a significant amount of moisture that can be as high as 50 to 60 wt% on a wet basis (Demirbas, 2004).

Cellulose provides support to the primary cell wall with its strong fiber-structure, making up about a third of all plant matter. Cellulose is made up of 5000 to 10,000 repeating glucose units (Crawford, 1981). Hydrogen bonding between strands and between molecules allows the cellulose network to lie flat (Mohan et al., 2006).

Hemicellulose is a group of carbohydrates that surround the cellulose fibers in plant cells, and makes up about 25 wt% of dry wood (Rowell, 1984). Hemicellulose is composed of polymerized monosaccharides such as glucose, mannose, galactose, xylose, and arbinose (Mohan et al., 2006). Hemicellulose has a less rigid structure than cellulose, partially caused by hemicellulose containing 30 to 65 times fewer repeating saccharide monomers than cellulose (Soltes and Elder, 1981).

Lignin is found mostly between plant cell walls and makes up about 20 wt% of wood (Bridgwater, 2004). Lignin includes a variety of phenylpropanoids linked in a branched, three-dimensional network containing many ether bonds (Mohan et al., 2006). Lignin has a very stable structure that includes the only aromatic compounds typically found in raw biomass.

2.1.2 Coal

Coal is a sedimentary rock that is composed primarily of carbon but also contains hydrogen, oxygen, nitrogen, sulfur, and ash. Coal seams formed from deposited plant matter that was protected from both microbial destruction and excessive oxidation, and exposed to elevated temperature and pressure for millions of years (Smith et al., 1994). The process of dead

vegetation slowly transforming into coal requires both peatification and coalification stages, which are biochemical and geochemical transformations, respectively.

Ranks are used to classify different coals, and stem from coal being at different degrees in the coalification process. The ranks of coal include lignite, sub-bituminous, bituminous, and anthracite. Anthracite represents the highest rank of coal, or the most mature coal type in the coalification process. As coal rank increases, the following general trends are observed: less oxygen content and volatiles, but increased aromaticity and heating value. When compared to biomass, coal has a higher heating value and a more aromatic structure.

2.1.3 Petroleum Coke

Petroleum coke, or petcoke, is a by-product from oil refining, resembles coal in appearance, and consists primarily of carbon. Petcoke comes from the Coker process, where heavy residual fuel oil is heated until it cracks into more valuable light compounds that are eventually incorporated into jet fuel, diesel, and other components (Ellis and Paul, 2000a). Petcoke has a lower amount of ash, moisture, and volatiles than most coals. Some of the advantages of petcoke are its cheap cost and high calorific value, although it has the drawbacks of high sulfur and vanadium contents (Yoon et al., 2007). Even though petcoke can be used in feeding systems designed for pulverized coal, the behavior of petcoke during gasification is more similar to heavy oil fractions (Higman and Burgt, 2003). Current estimates of worldwide petroleum coke generation as of 2012 were 100 million metric tons per year (Fisher, 2014), and petcoke production is expected to increase as coker units are added to oil refineries to process cheaper and heavier crudes.

2.2 Thermal Conversion Background

Combustion and gasification are commonly used to thermally convert biomass, petroleum coke, and coal into useful products. Although this research focuses on gasification, some discussion of combustion is given here due to the similarities of these processes, and to emphasize that pyrolysis research is important for both gasification and combustion. The first step that a particle passes through in either combustion or gasification is evaporation of any moisture from the particle. At higher temperatures, pyrolysis occurs, where the particle thermally decomposes into light gases, condensable vapors (tar), and solid residue (char) (Ranzi et al., 2008). Lastly, the primary pyrolysis products are either oxidized or gasified, depending on whether the process is combustion or gasification, respectively. Evaporation and pyrolysis are common to both combustion and gasification. Figure 2.1 provides a visual summary of important steps in thermochemical conversion of a solid fuel (gasification in this case).

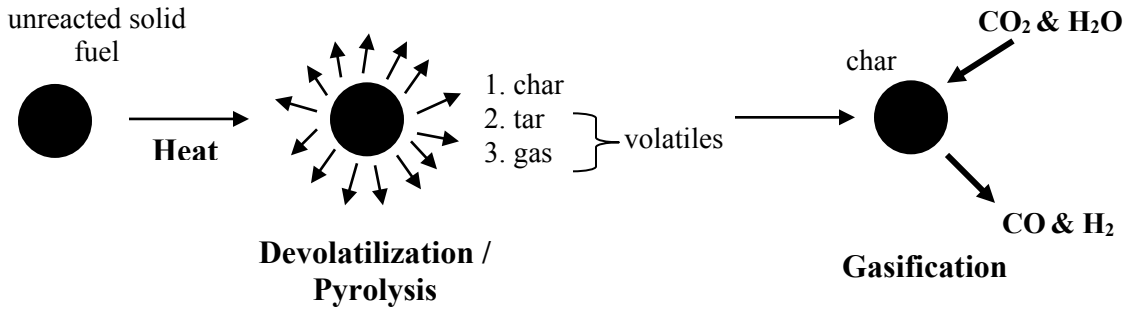

Figure 2.1. Simplified summary of important steps to gasify a solid particle.

2.2.1 Primary Pyrolysis

Primary pyrolysis is defined as the initial thermal decomposition of a particle into gas, tar, and char upon heating, without secondary reactions. During pyrolysis, volatile gases and tars escape from the heated particle as bonds thermally rupture (Smoot, 1991). Variables that affect devolatilization rates include temperature, pressure, particle size, residence time, and fuel type. The terms 'pyrolysis' and 'devolatilization' are often used synonymously.

Typical pyrolysis volatile yields of biomass and petcoke are near 90 and 10 wt% (dry ash-free basis), respectively (Jenkins et al., 1998; Milenkova et al., 2003). However, volatile yields of coal vary greatly depending on coal rank (Smith et al., 1994). Studying pyrolysis is important since it precedes combustion or gasification, and acts as a source of reactants for the aforementioned thermochemical processes. It is of modeling interest to be able to predict the extent of devolatilization and also the relative amounts of the devolatilization products (i.e., light gas, tar, and char).

2.2.2 Secondary Pyrolysis

Secondary pyrolysis refers to processes such as cracking, polymerization, condensation, or carbon deposition that result from the reaction of the primary pyrolysis products at high temperatures and sufficiently long residence times (Smoot and Smith, 1985). These reactions occur homogeneously in the gas phase and heterogeneously at the surface of the solid fuel or char particles (Wurzenberger et al., 2002). Generally speaking, secondary pyrolysis receives much less research attention than primary pyrolysis. However, the secondary reaction of tar cracking has a very important influence on biomass product distribution and usability.

Although tar yields can be as high as 75 wt% following the primary pyrolysis of wood (Scott and Piskorz, 1984; Bridgwater, 2004), tar cracking can cause light gas to be the major product of pyrolysis provided a sufficiently hot reactor temperature. Tar yields from wood pyrolysis pass through a maximum near 500 °C (Scott et al., 1988; Fagbemi et al., 2001), and then decrease at higher temperatures as the light gas yield increases proportionately. Exposing wood tar to high temperatures at long residence times causes most of the tar to crack into light gas.

2.2.3 Biomass Pyrolysis

Prakash and Karunanithi (2008) wrote a review concerning the many biomass pyrolysis models available in the literature. Di Blasi (2008) authored an excellent review regarding the modeling of wood pyrolysis. White et al. (2011) recently published a review article summarizing biomass kinetic models with a focus on agricultural residue studies. Pyrolysis rate constants are available in literature, but they are often specific to a certain type of biomass in a particular reactor.

A more universal method of modeling biomass pyrolysis is representing biomass pyrolysis as a sum of its main components, namely cellulose, hemicellulose, and lignin (Koufopanos et al., 1989; Raveendran et al., 1996; Miller and Bellan, 1997; Pond et al., 2003). This approach of using an additivity law to model biomass pyrolysis has also been used in conjunction with the Chemical Percolation Devolatilization (CPD) model (Fletcher et al., 1992), which was originally developed to model coal devolatilization yields as a function of time, temperature, pressure, and heating rate using a description of the coal's chemical structure. Fletcher et al. (2012) determined the structural and kinetic parameters for cellulose,

hemicellulose, and lignin for use in the CPD model. Their parameters allowed a satisfactory prediction of volatile yields from the pyrolysis of black liquor, cellulose, hemicellulose, and lignin. Fletcher's parameters enabled a prediction of volatile yields from *primary* pyrolysis since modeling secondary tar-cracking reactions was not attempted. The CPD model has also been used in conjunction with a first-order tar cracking model to predict accurate sawdust pyrolysis yields (Lewis, 2011).

2.2.4 Effect of Heating Rate on Pyrolysis

The conditions at which pyrolysis data are collected can greatly influence the measured results. This section describes the effect of heating rate on pyrolysis in the thermal conversion process.

Maximum initial heating rate of a particle is defined as the maximum derivative of particle temperature with respect to time (i.e., $dT_p/dt)_{max}$ during initial heating. The calculation of particle heating rate often assumes no internal temperature gradients, which is justified when the Biot number is less than 0.1 (Incropera and Dewitt, 2002). The most extreme heating rates occur when cold particles are injected into hot gases. While a typical heating rate in a thermogravimetric analyzer is on the order of 20 K/min, pulverized particles in industrial gasifiers and combustors experience initial heating rates on the order of 10^5-10^6 K/s (Essenhigh, 1981; Fletcher et al., 1997).

The rate at which particles heat strongly influences thermal conversion processes. Heating rate can affect both pyrolysis volatile yields and the temperature at which devolatilization occurs. A standard method of quantifying the volatile yield of a sample is often determined by proximate analysis, as defined by the American Society for Testing Materials

(ASTM). The ASTM volatile yield can be thought of as one produced at low heating rate since it requires a bed of dry particles (1 g) to be placed in a crucible in a muffle furnace for 7 minutes set at 950 °C. Borrego et al. (2009) measured up to 13% greater volatile yields (or 11 wt% daf) than the daf ASTM volatile yield when pyrolyzing wood chips, forest residues, and rice husks at high heating rate in a drop tube furnace. Sufficiently high particle heating rates result in a higher volatiles yield since crosslinking reactions kinetically compete with the release of material from a devolatilizing particle (Borrego et al., 2009). Enhanced volatile yields at high heating rate are not unique to biomass since the same effect has been noticed in coal pyrolysis studies (Jamaluddin et al., 1986; Solomon et al., 1993; Borrego and Alvarez, 2007). To the knowledge of the author, the effect of heating rate on petcoke volatile yields has not been reported in the literature.

A higher heating rate causes devolatilization to occur at a higher temperature. For example, Figure 2.2 shows the effect of heating rate on the extent of devolatilization for Montana lignite, a low-rank coal. The particle temperature reaches 400 °C at a heating rate of 1 °C/s before devolatilization is 10% completed and 840 °C at 10^5 °C/s. For 90% completion, the particle temperature reaches 860 °C at 1 °C/s and 1700 °C at 10^5 °C/s. Figure 2.2 shows how heating rate affects devolatilization temperature for a low-rank coal, but the same general trend that a more extreme heating rate causes a higher devolatilization temperature holds true for other fuels such as biomass and petroleum coke.

Both the pyrolysis and char gasification data measured in this research project will be at high initial particle heating rates, comparable to those characteristic of commercial entrained-flow gasifiers.

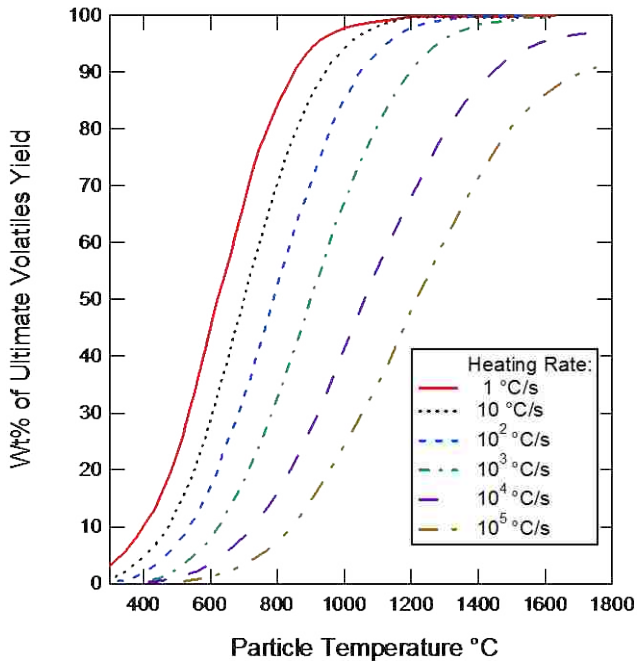

Figure 2.2. Effect of heating rate on weight loss at different temperatures for a Montana lignite (low-rank coal) (Howard, 1981).

2.2.5 Gasification

Gasification is the process by which any carbonaceous species can be converted through heterogeneous reaction into a gaseous fuel termed *synthesis gas* (or *syn gas*) that is mainly composed of H_2 and CO. This process is preceded by devolatilization and usually takes place at high temperatures and pressures to speed along the relatively slow gasification kinetics.

Both gas-phase and heterogeneous reactions occur during gasification of a solid fuel. While thermodynamic equilibrium calculations adequately predict the homogeneous gas phase reactions in most commercial gasifiers (Smoot and Smith, 1985; Higman and Burgt, 2003), the heterogeneous reaction between solid char and gasification agents (such as steam and CO_2) can become very complicated when considering all the influencing factors. Some of these include diffusion of reactants through the external boundary layer, reactions with both H_2O and CO_2,

particle size effects, pore diffusion, char ash content, temperature and pressure variations, and changes in surface area (Smoot and Smith, 1985). Predicting char gasification kinetics therefore relies heavily on measured rate data. Being able to predict char gasification rates is of research interest because the heterogeneous reaction between char and gas often governs the overall reaction rate in gasification processes (Liu et al., 2010b). Other processes such as pyrolysis or volatiles combustion occur more quickly during the gasification of a solid fuel.

The most common gasifying agents are steam and CO_2. These gases react with the char through dissociative chemisorption onto the carbon surface (Essenhigh, 1981). As long as the gasification reactions are not controlled by film diffusion, the internal surface area of the char plays an important role since it provides many more reacting sites than are available on the external char surface area. Even though all chars are primarily composed of carbon, the gasification reactivity of chars from different feedstocks can vary by several orders of magnitude (Mermoud et al., 2006). Biomass chars are typically more reactive than fossil carbons due to a more disordered carbon structure (Antal and Gronli, 2003; Williams et al., 2012).

The simplified global reactions that are important in char gasification are listed in Table 2.1.

Table 2.1. Major global reactions of carbon combustion and gasification

	ΔH_{rxn}° (kJ/mol) (Higman and Burgt, 2003)	Approximate Relative Global Rates at 1073 K and 0.1 atm (Walker et al., 1959)	
$C + O_2 \rightarrow CO_2$	- 394	1×10^5	R2.1
$C + H_2O \rightarrow CO + H_2$	+ 131	3	R2.2
$C + CO_2 \rightarrow 2CO$	+ 172	1	R2.3
$C + 2H_2 \rightarrow CH_4$	- 75	0.003	R2.4

This table also contains the relative rates of the global reactions of various sources of carbon with O_2, H_2O, CO_2, and H_2 from a review by Walker et al. (1959). The char combustion reaction

(R2.1of Table 2.1) is about 10^5 times faster than the gasification reactions (R2.2 and R2.3) at 1073 K and 0.1 atm (Walker et al., 1959). The gasification reaction with steam (R2.2) is about three times faster than the gasification reaction with CO_2 (R2.3) at the aforementioned conditions. The hydrogenation reaction (R2.4) is several orders of magnitude slower than the gasification reactions and is usually ignored in gasification studies (Smith et al., 1994). Note also that the combustion and hydrogenation reactions (R2.1 and R2.4) are exothermic, while the main gasification reactions (R2.2 and R2.3) are endothermic. In a typical gasifier, roughly 20% of the oxygen needed for stoichiometric combustion is provided (Simbeck et al., 1983). The oxygen reacts primarily with the volatiles from pyrolysis, and is entirely consumed in about 10 ms at the high temperatures in a gasifier (Batchelder et al., 1953). Although oxygen is present for only a short time in a gasifier, oxygen is important since the exothermic combustion reaction provides the heat that drives the endothermic gasification reactions.

The product of gasification is a gaseous fuel that is rich in both CO and H_2. According to the National Energy Technology Laboratory's (NETL) Gasification Worldwide Database (NETL, 2010), the synthesis gas from commercial gasifiers is used mainly for chemical production (45%), although other uses include liquid transportation fuels (38%), power (11%), and gaseous fuels (6%). The current syngas capacity combined with projected growth in the years 2011 to 2016 for coal, petcoke, and biomass are 75,500, 12,900, and 400 MW_{th}, respectively (NETL, 2010). Although coal is the leading gasifier feedstock in commercial gasification, this research advances the understanding of coal, petcoke, *and* biomass gasification processes.

2.2.6 Types of Gasifiers

The three basic types of commercial gasifiers are moving- or fixed-bed, fluidized-bed, and entrained-flow reactors. Among these, entrained-flow gasifiers are the most widely used in industry for gasifying coal (Minchener, 2005; Liu et al., 2010b) and petroleum coke. Some of the advantages of this type of gasifier are that it allows the highest throughput per reactor volume and can be run with a variety of solid and liquid fuels (Smoot, 1991; Minchener, 2005). Entrained-flow reactors convert pulverized particles, and use high temperatures (1200-2000 °C) and pressures (20-80 atm) to ensure high carbon conversion in the time frame of a few seconds (Minchener, 2005). Particles can be fed dry or carried by a water slurry into pressurized entrained-flow gasifiers. The entrained particles then react in cocurrent flow in the presence of a high-temperature flame. Pulverized particles in commercial entrained-flow reactors experience high initial heating rates, which are reported as 10^5-10^6 K/s (Essenhigh, 1981; Fletcher et al., 1997). The optimal dimensions of an entrained-flow gasifier are affected by particle size, fuel reactivity, reaction temperature, and gas phase velocities (Hebden and Stroud, 1981).

Most commercial processes that gasify biomass use fluidized-bed reactors (Gomez-Barea et al., 2006), even though biomass gasifiers are currently somewhat rare in industry. Fluidized bed reactors differ from entrained-flow reactors in that fluid beds typically use bigger particles, longer residence times, and lower temperatures (Smoot, 1991). The biomass gasification rates measured in the current project will be useful if the high throughput of entrained-flow gasifiers is desired in the future or if co-firing with coal or petroleum coke is desired.

2.2.7 Three Zone Theory

Both chemical and mass transfer effects can influence the rate of char gasification. It is important to understand how the observed rate can be influenced by these two factors to interpret measured kinetic data correctly. Temperature primarily determines the degree to which chemical or mass transfer effects influence the rate of char conversion.

Walker et al. (1959) and Gray et al. (1974) use the existence of three temperature regimes that help explain the rate-limiting step in solid-gas reactions (see Figure 2.3). The chemical reaction limits the conversion of solid particles in *Zone 1*, which occurs at low temperature. Laboratory data measured in *Zone 1* conditions provides intrinsic kinetics. In this zone, gaseous diffusion occurs quickly compared to the slow chemical reaction, allowing the concentration of the reactant gas to be the same throughout the particle as in the bulk gas.

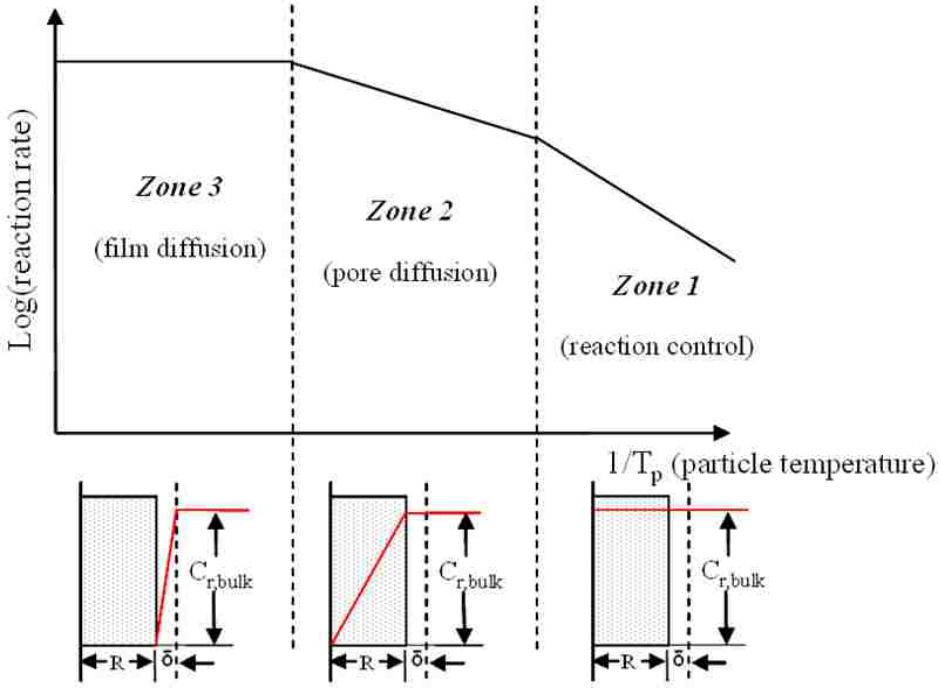

Figure 2.3. Three-zone theory and concentration profiles of a gaseous reactant applicable to heterogeneous reactions of porous particles (Walker et al., 1959; Hodge, 2009) where R equals particle radius, δ is the boundary layer thickness, and $C_{r,bulk}$ is the reactant concentration in the bulk gas stream.

Zone 2 occurs at higher temperatures where the observed rate of solid conversion is limited by a combination of chemical reaction and pore diffusion. The increased temperature results in a chemical reaction rate that becomes comparable to the rate of pore diffusion since the reaction rate increases exponentially with temperature (Hodge, 2009). An oxidizer concentration gradient is present within a particle that is reacting under *Zone 2* conditions because the oxidizer gas reacts before it can diffuse into the deepest pores of the particle. Small particles that are typically converted in industrial entrained-flow combustors and gasifiers react under *Zone 2* conditions, where particle size and pore structure affect the rate at which gaseous reactants can diffuse to internal surfaces of the char (Shurtz, 2011). Therefore, kinetic data measured at low temperature under *Zone 1* conditions cannot simply be extrapolated to higher temperatures to model the gasification rates in industrial reactors.

The diffusion of reactant gas through the boundary layer of the particle limits the conversion of solid particles in *Zone 3*, which occurs at even higher temperatures than *Zone 2*. In *Zone 3*, the chemical reaction is sufficiently rapid that the gaseous reactants are consumed entirely at the exterior surface of the particle before they can diffuse into the porous network of the particle interior.

2.2.8 Effect of Pyrolysis Conditions on Char Gasification Reactivity

Pyrolysis conditions such as final temperature, heating rate, soaking time (i.e., time at elevated temperature), and pressure are also known to affect char gasification reactivity. In this section, the effect of the aforementioned variables on *biomass* gasification reactivity will be summarized.

2.2.8.1 Effect of Pyrolysis Temperature on Biomass Gasification Reactivity

Gasification reactivity of biomass char is believed to decrease with increasing pyrolysis temperature. Min et al. (2011) reported that biomass char gasification reactivities, $1/(1-X)\cdot dX/dt$, at 850 °C in CO_2 decreased with increasing pyrolysis temperature for corn and wheat straws pyrolyzed in a quartz fixed-bed reactor at slow heating rate in the temperature range of 500-800 °C. Kumar and Gupta (1994) found that the reactivity ($mg\ min^{-1}\ mg^{-1}$) of wood char to CO_2 decreased with increasing final pyrolysis temperature (800-1200 °C) for two varieties of wood. The aforementioned researchers explained that a higher pyrolysis temperature results in an increased structural ordering of the carbon matrix that lowers the concentration of active sites available for reaction.

2.2.8.2 Effect of Heating Rate on Biomass Gasification Reactivity

It is generally well accepted in the literature that the gasification reactivity of biomass char increases with increased pyrolytic heating rates, although the explanations for this phenomenon vary. Okumura et al. (2009) compared the CO_2 reactivity using the random pore model (Bhatia and Perlmutter, 1980) for Douglas-fir char that had been prepared at pyrolysis heating rates over the range of 15-600 K/min, and found that chars generated at higher heating rates gasified more quickly. The increased reactivity of the high heating-rate char was attributed to the coarseness and rough texture of the wood char. Kumar and Gupta (1994) showed that two varieties of cubic shaped wood chars that had been pyrolyzed at 30 K/min had a higher reactivity ($mg\ min^{-1}\ mg^{-1}$) to CO_2 than chars prepared at 4 K/min. They explained that the higher heating-rate char was more reactive due to a lower amount of deposition of reactivity-hindering pyrolytic

carbon and a higher concentration of active sites from defective microcrystallites on the carbon matrix. Cetin et al. (2005a) compared the CO_2 gasification reactivity, $-dm/dt \cdot (1/(m-m_{ash}))$, of pine chars pyrolyzed at 1 bar in two separate reactors with very different heating rates. The pine char prepared in a wire-mesh reactor at 500 K/s with a 20-sec hold time at 950 °C had an apparent CO_2 gasification reactivity about twice that of pine char pyrolyzed at 20 K/s in a tubular reactor to 950 °C with a 5-min hold time. The higher reactivity of the rapid pyrolyzed char was attributed to higher total surface areas measured by both CO_2 and N_2 adsorption. The low heating-rate char generated at 20 K/s was found to have a surface area that mainly comprised of micropores, while the surface area of the char generated at 500 K/s mainly consisted of macropores as a result of melting.

Other researchers have also noticed an increase in biomass gasification reactivity for chars pyrolyzed at high heating rates, although they did not offer explanations for this occurrence. Zanzi et al. (1996) reported that both biomass and coal chars that were generated at high heating-rate pyrolysis conditions in a free-fall reactor were more porous and more reactive ($-dm/dt$) to steam than chars produced at low heating rate. Chen et al. (1997) found that the gasification reactivity, $-dm/dt$, of birch char produced at high heating-rate pyrolysis conditions in a free-fall tubular reactor was about 3 times more reactive to both steam and CO_2 than slow-pyrolyzed char that was generated in a thermogravimetric analyzer (TGA). Fushimi et al. (2003) reported that a higher pyrolytic heating rate in the range 1-100 K/s resulted in a more porous lignin char that was more reactive (s^{-1}) to steam even though the elemental composition of the char was unaffected by heating rate. The work of Mermoud et al.(2006) also showed that a higher pyrolytic heating rate resulted in a more reactive biomass char. They reported that 10-mm spheres of beech wood char took 2.6 times longer to completely react with steam when

comparing chars that had been prepared using heating rates of 2.6 and 900 K/min during pyrolysis.

2.2.8.3 Effect of Pyrolysis Soaking Time on Biomass Gasification Reactivity

Pyrolysis soaking time is defined as the length of time that char remains at the final temperature during pyrolysis. The effect of pyrolysis soaking time on biomass gasification reactivity is generally thought to produce a less reactive char through thermal annealing (Nandi and Onischak, 1985; Mermoud et al., 2006). Chen et al. (1992) compared the reactivity of a mixture of aspen and birch wood under different pyrolyzing conditions in a pressurized fluidized bed reactor from 3.4 to 10 bar using wood feed rates near 2.5 kg/hr. They reported that increased soaking time of the char at high temperature during pyrolysis negatively affected the steam gasification rate constant, k, of the wood char when using the first-order expression ($- dW/dt = k \cdot W$) to analyze their data. This conclusion was reached by comparing reactivities of wood that were pyrolyzed in N_2 for 1 hr and then steam gasified for 1 hr to experiments where wood was pyrolyzed and gasified simultaneously in the presence of steam for 1 hr. The lesser reactivity of the wood chars pyrolyzed in N_2 was attributed to increased pyrolysis soaking time since it was assumed that the pyrolyzing gas atmosphere had no effect on gasification reactivity. Kumar and Gupta (1994) reported that two varieties of cubic shaped wood chars that had been pryolyzed in argon at 800 and 1000 °C were less reactive ($mg\ min^{-1}\ mg^{-1}$) to CO_2 upon increased pyrolysis soaking times over the range 1-3 hours. Mermoud et al. (2006) agree that increased pyrolysis soaking time negatively influences the reactivity of biomass chars, although they report that increasing the soaking time at the final temperature of 1200 K from 8 min to 1 hr for 1-cm beech wood spheres that were heated at 900 K/min did not affect the time for the chars to reach full

conversion in 20% steam at atmospheric pressure. It was therefore concluded that 1 hr at 1200 K was insufficient time for beech wood char to undergo thermal annealing.

2.2.8.4 Effect of Pyrolysis Pressure on Biomass Gasification Reactivity

Increasing pyrolysis pressure is generally thought to produce a less reactive biomass char. Cetin et al. (2005b) compared the char CO_2 gasification reactivity of pine chars pyrolyzed at 500 °C/s in a wire mesh reactor from 1 to 20 bar, and found that higher pyrolysis pressure resulted in a less reactive wood char from CO_2 gasification experiments conducted on all of the chars at 1 bar and 850 °C. The apparent gasification reactivity, $-dm/dt \cdot (1/(m-m_{ash}))$, of char pyrolyzed at 1 bar was approximately three times that of pine char prepared at 20 bar. Both N_2 and CO_2 surface area measurements decreased by about 25% over the pyrolysis pressure range 1-20 bar, but the difference in apparent gasification reactivity of chars prepared over 1-20 bar was too large to be explained solely by differences in surface areas. X-ray diffraction (XRD) was used to characterize the pine chars that were produced at different pyrolysis pressures from 1-20 bar. The XRD results led to the explanation that increased graphitization in the structure of chars generated at higher pyrolysis pressure was responsible for their reduced CO_2 gasification reactivity.

Okumura et al. (2009) compared the CO_2 reactivity using the random pore model (Bhatia and Perlmutter, 1980) for Douglas-fir chars which had been pyrolyzed at total pressures of 1, 10, and 30 bar at 800 °C using a heating rate of 15 °C/min. The gasification experiments were all carried out at 900 °C and 1 bar, utilizing a 10-15 mg bed of char particles with diameters 2-3 mm. The reported data of Okumura et al. showed that the char which had been pyrolzyed at 1 bar fully reacted to completion in about half the time as the 30-bar char. When the physical

properties of the wood chars were examined, Raman spectroscopy measurements revealed that the char pyrolyzed at 30 atm had a lower amount of amorphous carbon when compared to the char pyrolyzed at 1 atm. It was concluded that increased pyrolysis pressure results in a more uniform carbonaceous structure with suppressed cavity growth during gasification.

Illerup and Rathmann (1996) tested the effect of pyrolysis pressure on CO_2 gasification reactivity, $-dm/dt \cdot (1/(m-m_{ash}))$, using wheat chars prepared in a pressurized entrained-flow reactor (EFR) from 2-15 bar. From CO_2 reactivity experiments at 20 bar in a TGA on the wheat straws, they came to the conclusion that pyrolysis pressure in the range 2-15 bar does not significantly impact the char reactivity. However, Illerup and Rathmann note that there may have been some issues in generating reproducible char in the EFR at the same pyrolysis pressure with repeatable CO_2 reactivities. Two replicate pyrolysis runs at 4 bar in the EFR yielded wheat chars whose gasification reactivity varied by nearly a factor of two in a TGA.

Pyrolysis pressure has been shown to affect the size and shape of radiata pine char pryolyzed at 300 °C/s in a single particle reactor using initial particle sizes near 300 μm (Cetin et al., 2005a). Comparing the digital cinematography of chars generated at different pressures revealed that larger char particles were formed at a pyrolysis pressure of 20 bar when compared to 1 bar. The same study revealed that increased pyrolysis pressure led to char particles with larger cavities, a higher proportion of voids, and thinner walls. This finding resulted by comparing SEM cross-sectional images of pine chars prepared at 5, 10, and 20 bar in a wire mesh reactor near 500 °C/s.

2.2.8.5 Effect of Total Pressure on Biomass Gasification Reactivity

The previous section described the effect of *pyrolysis* pressure, whereas this section reports on the effect of *total* pressure on biomass gasification reactivity. Literature concerning the effect of total pressure on biomass reactivity remains somewhat scarce, but the limited studies found indicate that total pressure at which a biomass char is gasified does not have a significant impact.

Cetin et al. (2005b) compared the total pressure effect on the gasification of pine by reacting chars at 4-bar constant CO_2 partial pressure at a total pressure of 5-20 bar. The pyrolysis pressure and the total gasification pressure were the same (i.e., a 5-bar total pressure gasification experiment used pine char that had been pyrolyzed at 5 bar). Even though the 5-bar char had a higher reactivity, $-dm/dt \cdot (1/(m-m_{ash}))$, than the 10- and 20-bar chars, the difference in reactivities was shown to correspond to the difference in pyrolysis pressures and not total gasification pressure. This conclusion was drawn by using XRD analysis on the chars, which allowed the char atomic structure to be characterized by looking at specific carbon-peak intensities.

Illerup and Rathmann (1996) studied the effect of total pressure on the CO_2 gasification reactivity, $-dm/dt \cdot (1/(m-m_{ash}))$, of wheat straw by varying gasification total pressure 2-20 bar at 800 °C with constant partial pressure of CO_2 of 1 bar. The gasified chars were all generated at the same pyrolysis pressure of 15 bar. Even though it was claimed that total pressure did not significantly impact the char gasificiation reactivities over the range of 5-20 bar, the reactivity of the char gasified at 2 bar was nearly twice the reactivity of the chars at the other pressures.

Sections 2.2.8.1 to 2.2.8.5 summarized the effect of pyrolysis conditions on measured biomass gasification rates. Matching pyrolysis conditions for a process of interest is very important if meaningful char gasification rates are to be measured. The gasification rates measured in this project for biomass, petcoke, and coal will use chars that try to match the pyrolysis conditions characteristic of entrained-flow gasifiers (i.e., high temperature, elevated pressure, rapid initial particle heating rates, and short soaking times).

2.2.9 Recent Biomass Gasification Studies

A summary of recent kinetic studies involving the CO_2 gasification of biomass char is shown in Table 2.2. Di Blasi's recent review (2009) is also a good source for kinetic information regarding the gasification of biomass. Studies involving solely steam gasification were precluded from Table 2.2 since the focus of this work is CO_2 gasification of biomass.

As can be seen in Table 2.2, the majority of the kinetic studies involving the CO_2 gasification of biomass involve thermogravimetric measurements at atmospheric pressure in *Zone 1* conditions (see Section 2.2.7) using chars that were generated at relatively low temperatures, pressures, and heating rates. However, kinetic data measured at low temperature under *Zone 1* conditions cannot simply be extrapolated to higher temperatures to model gasification rates in *Zone 2* conditions that are typical of industrial reactors, due to the complex interactions between the many phenomena involved (Shurtz, 2011). Thus, there is a need for more data at conditions pertinent to commercial entrained-flow gasifiers.

Table 2.2. Recent biomass CO_2 gasification kinetic studies

Reference	Biomass Type	Pyrolysis Apparatus, Particle Size, Heating Rate	Pyrolysis Temperature & Pressure	Gasification Reactor, Reactant(s), & Sample Size	Gasification Temperature & Total Pressure
Barrio and Hustad (2001)	birch wood	TGA 32-45 μm 24 °C/min	600 °C for 30 min 0.101 MPa	TGA CO_2 w/ CO 5 mg	750-950 °C 0.101 MPa
Bhat et al. (2001)	rice husk	batch pyrolyzer 10 μm & unground heat rate not given	600-700 °C 0.101 MPa	TGA,SiO_2 tube CO_2, H_2O 500 mg in tube	750-900 °C 0.101 MPa
Marquez-Montesinos et al. (2002)	grapefruit skin	furnace size not given heat rate not given	700 °C for 2 hrs 0.101 MPa	TGA CO_2, H_2O 10 mg	725-800 °C 0.101 MPa
Ollero et al. (2003)	olive residue	TGA <150 μm 30 °C/min	900 °C for 7 min 0.101 MPa	TGA CO_2 w/ CO 10 mg	800-950 °C 0.101 MPa
Cetin et al. (2005b)	radiata pine, spotted gum, & sugar cane bagasse	WMR[a], TR[b] 120-180 μm 20 & 500 °C/s	950 °C for 20 s, 5 min 0.1-2 MPa	HPTGA[c], TR[b] CO_2, CO_2 w/ CO 0.3 & 5 g	800-1050 °C 0.1-2 MPa
Klose and Wolki (2005)	beech wood & oil palm shell	vertical tube furnace <125 μm 3 °C/min	900 °C for 30 min 0.101 MPa	TGA CO_2, H_2O 10 mg	740-800 °C 0.101 MPa
Senneca (2007)	pine seed shells, olive husk, & wood chips	fluidized bed[d] < 300 μm heat rate not given	850 °C for 5 min 0.101 MPa	TGA CO_2, H_2O 0.5-1 mg	750-910 °C 0.101 MPa
Fermoso et al. (2009)	slash pine	drop tube reactor 75-106 μm ~ 10^4 °C/s	1000,1400 °C for 7 s 0.101 MPa	HPTGA[c] CO_2 10 mg	750-900 °C 0.1, 1 MPa
Matsumoto et al. (2009)	Japan cedar, cedar bark, hardwood mixture, & lawngrass	2 ton/day plant[e] 240 kg/day plant[e] 50-100 μm heat rate not given	900-1000 °C 0.101 MPa	drop tube CO_2, H_2O fed at 1-10 g/hr 0.5-3 s res time	900-1200 °C 0.405 MPa
Khalil et al. (2009)	pine & birch	furnace 45-63 μm heat rate not given	500 °C for 150 min 0.101 MPa	TGA CO_2 1-2 mg	600-1000 °C 0.101 MPa
Link et al. (2010)	reed, douglas fir, & pine pellets	fixed bed reactor size not given 20 °C/min	800 °C for 15 min 0.101 MPa	TGA CO_2 size not given	750-900 °C 0.101 MPa
Ahmed and Gupta (2011)	yellow pine woodchips	custom reactor size not given heat rate not given	900 °C for 1 hr 0.1-0.2 MPa	custom reactor CO_2, H_2O 20-35 g	900 °C 0.2 MPa
Mani et al. (2011)	wheat straw	TR[b] in furnace <60-925[f] μm 12 °C/min	500 °C for 45 min 0.101 MPa	TGA CO_2 10 mg	750-900 °C 0.101 MPa
Yuan et al. (2011)	rice straw, chinar leaves, & pine	HF[g] furnace 56-180 μm heat rate not given	800-1200 °C 0.101 MPa	TGA CO_2 size not given	850-1050 °C 0.101 MPa

[a]wire mesh reactor, [b]tubular reactor, [c]high-pressure TGA, [d]bubbling, [e]these chars were pyrolyzed in O_2 and H_2O, [f]<60, 250, 638, 925 μm, [g]high-frequency

2.2.10 Summary of Petcoke Gasification Studies

A summary of kinetic studies involving the CO_2 gasification of petroleum coke is shown in Table 2.3. The recent review by Murthy et al. (2014) is also a good source for petcoke gasification rates. The studies summarized in the table mainly reported petcoke gasification rates measured in TGA reactors using chars prepared at atmospheric pressure and low initial particle heating rates. However, there is much to be learned about petcoke gasification rates at conditions characteristic of commercial entrained-flow gasifiers.

Table 2.3. Petcoke gasification kinetic studies

Reference	Pyrolysis Apparatus, Particle Size, & Heating Rate	Pyrolysis Temperature & Pressure	Gasification Reactor, Reactant(s), Sample Size; Particle Size	Gasification Temperature & Total Pressure
Tyler and Smith (1975)	fixed bed reactor 220, 900, 2900 µm heat rate not given	745-905 °C *in-situ pyrolysis* 0.101 MPa	fixed bed reactor CO_2 ~1.6 g; 220, 900, 2900 µm	745-905 °C 0.101 MPa
Harris and Smith (1990)	fixed bed reactor 700 µm heat rate not given	650-900 °C *in-situ pyrolysis* 0.101 MPa	fixed bed reactor CO_2, H_2O 700 µm	650-900 °C 0.101 MPa
Zamalloa et al. (1995)	TGA 105-150 µm 20 °C/min	900-1300 °C for 20 min *in-situ pyrolysis* 0.101 MPa	TGA CO_2 30 mg; 105-150 µm	900-1300 °C 0.101 MPa
Trommer and Steinfeld (2006)	TGA 250-355 µm 10-20 °C/min	227-1250 °C *in-situ pyrolysis* 0.101 MPa	TGA CO_2, H_2O, CO_2+H_2O 40 mg; 250-355 µm	227-1250 °C 0.101 MPa
Zou et al. (2007)	TGA 85-125 µm 25 °C/min	975-1050 °C *in-situ pyrolysis* 0.101 MPa	TGA CO_2 10 mg; 85-125 µm	975-1050 °C 0.101 MPa
Gu et al. (2009)	TGA < 73 µm 30 °C/min	950-1400 °C for 3 min *in-situ pyrolysis* 0.101 MPa	TGA CO_2 8 mg; < 73 µm	950-1400 °C 0.101 MPa
Wu et al. (2009)a	muffle furnace 0.4-0.63 mm 6 °C/min	950-1400 °C for 20 min 0.101 MPa	TGA CO_2 < 73 µm	950 & 1000 °C 0.101 MPa
Wu et al. (2009)b	pressurized furnace 0.4-0.63 mm > 650 °C/s	950 °C for 2 min 0.1, 1, 2, 3 MPa	TGA CO_2 < 73 µm	950 °C 0.101 MPa
Malekshahian and Hill (2011b)	fixed bed reactor < 90 µm 20 °C/min	975 °C for 1 hr 0.101 MPa	HPTGA[h] CO_2 15 mg; < 90 µm	900-975 °C 0.1-2.4 MPa

[h]high-pressure TGA

Only few research groups study char gasification rates at the experimentally challenging, yet industrially significant conditions of high temperature, pressure, and initial particle heating rate. While it can be implied that petcoke gasification occurs quickly in entrained-flow gasifiers where the maximum residence time is on the order of seconds, the reported petcoke gasification rates in the current literature (see Table 2.3) are on the order of minutes and even hours (at lower temperatures, pressures, and heating rates). Thus, the need for additional data and modeling of petcoke gasification rates at conditions more pertinent to commercial entrained-flow gasifiers is clear.

2.2.11 Recent Coal Gasification Studies

A summary of recent kinetic studies involving the gasification of coal char is shown in Table 2.4. Recent literature involving solely CO_2 gasification of coal were precluded from the table since the coal work in this research primarily involves the measurement of steam gasification rates of coal char. The summary of coal studies over the years 1995-2010 prepared by Shurtz and Fletcher (2013) is also a good source for gasification rates of coal char.

Coal gasification rates have been studied much more extensively than either biomass or petcoke gasification rates since coal is the leading gasification feedstock used commercially (NETL, 2010). However, many of the research groups that measured coal gasification rates utilized coal chars prepared at heating rates and pressures not representative of commercial entrained-flow gasifiers, even though heating rate and pressure can affect pore structure and morphology of the char (Wall et al., 2002). While Shurtz (2011) provided valuable CO_2 gasification rates of coal char at conditions pertinent to commercial entrained-flow gasifiers, the

current study measures and models H_2O gasification rates of coal char at commercially relevant conditions and explores gasification rates when both H_2O and CO_2 are present in the same reacting atmosphere.

Table 2.4. Recent coal gasification kinetic studies (2010-2014)*

Reference	Pyrolysis Apparatus, Particle Size, & Heating Rate	Pyrolysis Temperature & Pressure	Gasification Reactor, Reactant(s), Sample Size; Particle Size	Gasification Temperature & Total Pressure
Fermoso et al. (2010)	fixed-bed reactor 1-2 mm 15 °C/min	1100 °C for 30 min 0.101 MPa	TGA H_2O 5 mg; < 150 μm	727-1127 °C 0.101 MPa
Huang et al. (2010)	fluidized bed reactor pulverized particles 1000 °C/s	840 °C for 20 min 0.101 MPa	TGA CO_2, H_2O 10 mg; < 200 μm	850-950 °C 0.101 MPa
Liu et al. (2010a)	fluidized bed (*in-situ*) 177-210 μm rapid heating rate	1000-1500 °C for up to 10 min 0.101 MPa	fluidized bed H_2O 177-210 μm	1000 -1500 °C 0.101 MPa
Fermoso et al. (2011)	fixed-bed reactor 75-150 μm 5000 °C/s	800-1000 °C 0.101-2.03 MPa	TGA H_2O 5 mg; 75-150 μm	850-1050 °C 0.101 MPa
Xu et al. (2011)	electric oven 6x10 mm pellets heat rate not given	900 °C for 7 min 0.101 MPa	tube reactor in oven H_2O 1g; 6x10 mm pellets & pulverized sizes	850-950 °C 0.101 MPa
Li et al. (2012)	TGA particle size not given 10 °C/min	900-1100 °C *in-situ pyrolysis* 0.101 MPa	TGA CO_2, H_2O 15-20 mg	900-1100 °C 0.101 MPa
Fan et al. (2013)	tube furnace 0.5-1 mm heat rate not given	900 °C for 5 min 0.101 MPa	TGA CO_2, H_2O 15 mg; 0.5-0.8 mm	850-1050 °C 0.101 MPa
Ren et al. (2013)	DIFBR[i] 2-4 mm single particle ~490-790 °C/s	1000-1600 °C *in-situ pyrolysis* 0.101 MPa	DIFBR[i] CO_2, H_2O 50 ± 1 mg particle	1000-1600 °C 0.101 MPa
Tremel and Spliethoff (2013)	entrained-flow reactor particle size not given 10^4-10^5 °C/s	1200-1600 °C for 1.3 to 1.7 s 0.5, 2.5 MPa	HPTGA[j] CO_2, H_2O 40-60 mg; > 42 μm	600-1000 °C 0.5, 1.0, 2.5 MPa
Huo et al. (2014)	fixed bed reactor < 40, 100, 250, 500 μm 25 °C/min	850 °C for 30 min 0.101 MPa	TGA CO_2, H_2O 5 mg	850-1300 °C 0.101 MPa
Yan et al. (2014)	fixed bed reactor particle size not given 150 °C/s	900 °C for 30 min likely 0.101 MPa	PFBDR[k] H_2O 20 mg	950 °C 0.1, 1.0, 2.0 MPa
Bai et al. (2014)	apparatus not specified <125 μm 10 °C/min	800-1100 °C for 30 min 0.101 MPa	TGA CO_2, H_2O, CO_2+H_2O ~15 mg; <125 μm	750-1100 °C 0.101 MPa

* See Shurtz and Fletcher (2013) for a summary of coal gasification studies over the years 1995-2010
[i]drop-in fixed bed reactor, [j]high-pressure TGA, [k]pressurized fixed-bed differential reactor

2.3 Summary

High throughput entrained-flow gasifiers allow biomass, petroleum coke, and coal to be thermally converted into a fuel-rich gas, which can then be used to make useful commodities such as energy and chemicals. Measuring and modeling char gasification rates are of research interest because the heterogeneous reaction between char and gasification agents (typically H_2O and CO_2) is slow and therefore rate-limiting in the overall gasification process.

The reaction conditions of entrained-flow gasifiers (i.e., high temperature, elevated pressure, and rapid initial particle heating rates) present many experimental challenges when trying to mimic them in a lab setting, yet it is important to match the reaction conditions if the most meaningful gasification rates are to be obtained. Although most char-gasification rates have been measured in TGAs, the reaction conditions of these reactors do not well represent the conditions in commercial entrained-flow gasifiers. Many researchers ignore pyrolysis conditions when measuring char-gasification rates, even though the conditions at which char is generated can affect measured rates. The primary focus of this work will be to measure and model the char-gasification rates of biomass, petroleum coke, and coal in similar reaction conditions as used in commercial entrained-flow gasifiers, which will provide insight to reactor volume requirements and optimal operating conditions.

3. Objectives and Approach

The objective of this research was to characterize char gasification at conditions pertinent to commercial entrained-flow gasifiers for biomass, petroleum coke, and coal. The work mainly focuses on the measurement and modeling of char gasification rates at conditions of high initial particle heating rates at elevated temperature and pressure. In addition, biomass pyrolysis yields at conditions of high heating rate and atmospheric pressure were also measured and modeled. This research will aid in the design and efficient operation of commercial entrained-flow gasifiers, as well as provide a test case to evaluate both existing and future models at a wide range of temperatures and pressures at high heating-rate conditions. This project is divided into the following tasks:

1) *Modify the high-pressure flat-flame burner (HPFFB) reactor to enable steam gasification reactivity tests of coal chars*. The HPFFB reactor that was originally developed by Shurtz (2011) was modified in this study to enable steam gasification experiments. Water condensation in the HPFFB collection system was avoided by utilizing heating tape, while steam traps were used to condense water from the post-flame gases downstream of the collection system. Improvements were also made to the particle feeder, the char collection system, and the glow-plug ignition system. Furthermore, additional safety features were implemented.

2) *Measure and model biomass pyrolysis yields at high initial heating rates at atmospheric pressure*. Pyrolysis experiments of 45-75 μm sawdust, switchgrass, corn stover, and straw were performed in a flat-flame burner reactor at atmospheric pressure using peak gas temperatures of 1163 to 1433 K. Yields of tar and char were measured, and yields of light gas were calculated by difference. Biomass pyrolysis was modeled using the Chemical Percolation Devolatilization (CPD) model combined with a tar-cracking model.
3) *Measure and model CO_2 gasification rates of biomass at high temperature and elevated pressure*. Biomass chars of sawdust, switchgrass, and corn stover were generated at high initial particle heating rates (~ 10^4 K/s) in a drop tube reactor at atmospheric pressure using short residence times. The biomass chars were then fed separately in the HPFFB reactor to measure CO_2 gasification rates of the biomass chars at conditions of 10 and 15 atm where the peak gas temperature exceeded 1800 K. A global first-order model was used to fit the gasification data.
4) *Measure and model CO_2 gasification rates of petroleum coke at high temperature and elevated pressure*. CO_2 gasification rates were measured for 2 commercially obtained petroleum coke samples following rapid *in-situ* pyrolysis in the HPFFB reactor at 10 and 15 atm at conditions where the peak gas temperature exceeded 1800 K. A global first-order model was used to fit the gasification data. The morphology of the 2 petroleum coke chars was studied from SEM images of the chars. A CO_2 gasification rate comparison between petroleum coke and coal char was also performed.
5) *Measure and model H_2O gasification rates of coal char at high temperature and elevated pressure*. Steam gasification rates were measured for 3 re-injected coal chars in the HPFFB reactor at 10, 12.5, and 15 atm using maximum gas temperatures exceeding

1600 K. The measured steam gasification data for the coal chars were fit to a global first-order model. In addition, the particle mass release of a single coal char was both measured and modeled at conditions where significant particle mass release was caused by both H_2O and CO_2.

The char gasification modeling from measured data in this research will allow a prediction of char conversion for pulverized particles in entrained-flow conditions when given 1-D input profiles of residence time, reactant gas concentration, and temperature. Therefore, the gasification modeling can find use in CFD codes, by accounting for the exchange of gas species and enthalpy between the char particles and the gas phase (Shurtz and Fletcher, 2013). The insight gained about fuel reactivities will also be of value to determine optimal dimensions of future entrained-flow gasifiers, where high char conversions are desired in short times, and where any over-design of the gasifier results in hefty capital equipment costs. The gasification modeling of this research can also aid in the optimal operation of existing entrained-flow gasifiers, since there is an optimal balance between stoichiometry, temperature, char conversion, and desired product gases (Liu et al., 2010b).

The work is presented in the following order: Chapter 4 describes the experimental equipment and procedures used in this research, and includes documentation concerning the modifications made to the HPFFB reactor (see Task 1). The results of the experimental and modeling work of biomass pyrolysis are presented in Chapter 5 (see Task 2). The experimental and modeling work of char gasification rates of biomass, petroleum coke, and coal are found in Chapters 6, 7, and 8, respectively (see Tasks 3, 4, & 5). Lastly, Chapter 9 contains the summary and conclusions of this research as well as recommendations for future work.

4. Experimental Equipment and Procedures

4.1 Atmospheric Flat-Flame Burner Reactor

An entrained-flow flat-flame burner (FFB) reactor operating at atmospheric pressure was primarily used in this study to measure pyrolysis yields of biomass (sawdust, switchgrass, corn stover, and straw) at conditions of high initial particle heating rates. A Hencken flat-flame burner created well characterized conditions at high temperature. The FFB reactor is useful for combustion or pyrolysis experiments, but is not ideal for collecting char gasification data due to the limited residence times available (< ~225 ms) in the reactor and the relatively slow kinetics of the char-gasification reaction at atmospheric pressure. Flat-flame burners are useful since they provide particle heating rates around 10^5 K/s, which approaches particle heating rates characteristic of commercial entrained-flow reactors (Fletcher et al., 1997). Since the FFB reactor (see Figure 4.1) has been described previously in great detail (Ma, 1996), only a quick overview is given here.

The flat-flame burner used many small-diameter tubes to create hundreds of diffusion flamelets by feeding gaseous fuel through the tubes while introducing oxidizer in-between the tubes. The numerous small flamelets created a flat flame about 1-mm thick above the burner. Particles were entrained in N_2 and carried to the middle of the burner surface through a small metal tube (0.052" ID; 304H16.5 from MicroGroup) that is referred to as the feeding tube. The

particles then pyrolyzed while traveling upward in laminar flow in a quartz tower for a known residence time before the reacting particles were quickly quenched with N_2 in a water-cooled collection probe. Nitrogen transpired through the walls of the porous inner tube of the collection probe to prevent deposition of tar or aerosols in the probe. A virtual impactor and cyclone in the collection system separated the char aerodynamically while the tar/soot collected on glass fiber filters (part# F-2771-9 from ISC BioExpress). Permanent gases were pulled through the filters by a vacuum and released in a vent hood.

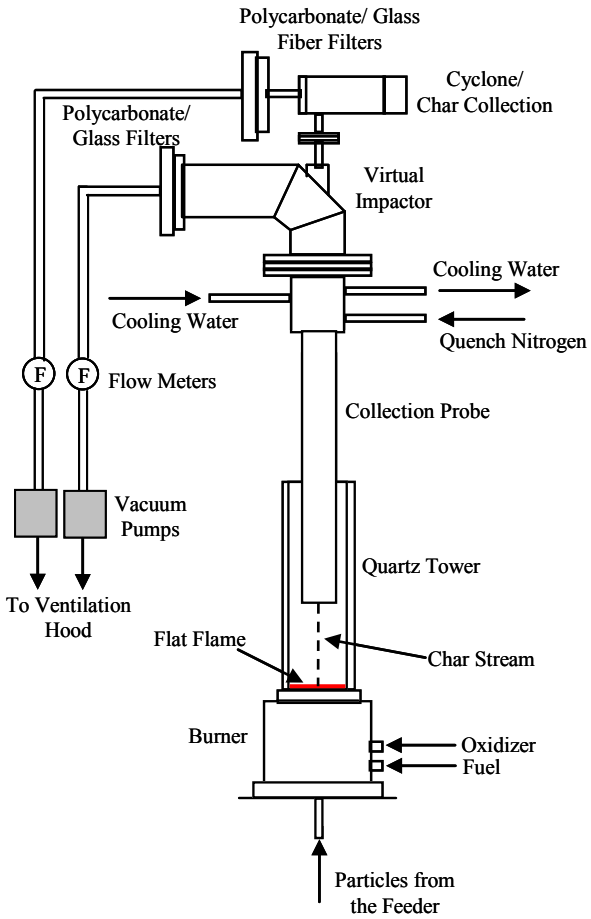

Figure 4.1. FFB reactor with separation system (Ma, 1996).

Particle residence time was controlled in the FFB experiments by adjusting the distance between the moveable burner and stationary collection probe. Measured particle velocities from

a high-speed camera (Kodak EktaPro) operated at 125 frames per second (fps) were used in particle residence time calculations. Slow biomass feeding rates near 0.5 g/hr were used to ensure single-particle behavior and to prevent clogging in the same plunger-type particle feeder that has been documented elsewhere (Ma, 1996). The gaseous fuel supplied to the FFB was mainly CO with a trace amount of H_2 to stabilize the flame. A CO flame offered a wide temperature range (~1100 – 2000 K) and did not form soot, in contrast to a fuel-rich methane flame which had a more limited temperature range and formed soot at pressurized conditions.

The CO passed through a 'carbonyl trap' on its way to the burner, where iron and nickel carbonyls were captured using activated charcoal (20-40 mesh) and a small amount of iodine. The aforementioned contaminants are common in pressurized CO cylinders, and can cause a red deposit in the post-flame regions of the reactor and collection system if unaddressed (Williams and Shaddix, 2007). Note that it is very important to use the correct size of activated charcoal in the 'carbonyl trap' since smaller charcoal sizes can potentially pass through the glass wool filters and clog the many small fuel tubes of the burner.

4.2 High-Pressure Flat-Flame Burner Reactor

The char gasification data measured in this research project (see Figure 4.2) was collected using BYU's high pressure flat-flame burner (HPFFB) reactor, which had many similarities to the FFB reactor. The HPFFB reactor has been used previously to research both coal swelling and char CO_2 gasification rates at a total pressure up to 15 atm (Lewis, 2011; Shurtz, 2011; Shurtz et al., 2012; Shurtz and Fletcher, 2013). Only a few reactors in the world exist that are similar to BYU's HPFFB reactor (Ma, 2006). The high-pressure reactor is useful since it can be used to approximate the reaction conditions characteristic of industrial entrained-flow reactors by

reacting small particles in cocurrent flow at high temperatures and pressures with rapid initial particle heating rates (~10^5 K/s) and short reaction times (< 1 s).

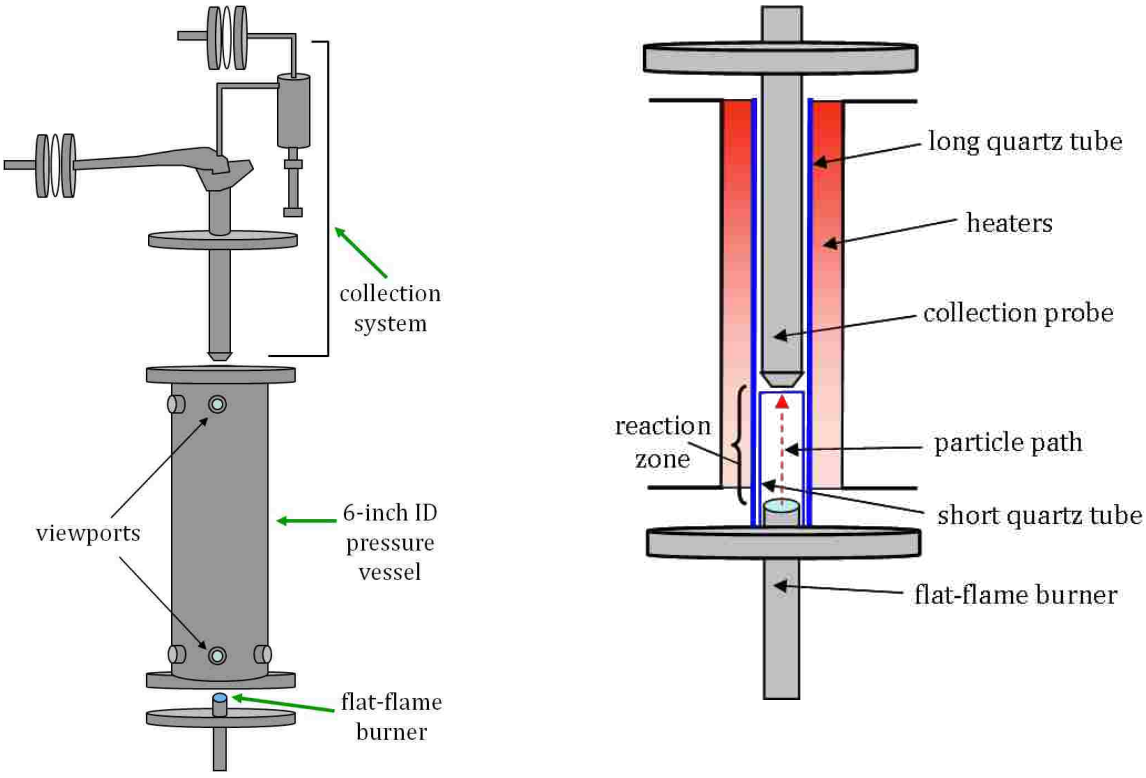

Figure 4.2. External and cutaway views of BYU's HPFFB reactor.

A quick comparison between TGAs and pressurized flat-flame burner reactors is given here to emphasize the difference in experimental challenges between the two reactor types. Kinetic data measured in TGAs are very common in the literature because data collection is relatively cheap, fast, and easy in this type of purchasable reactor. On the other hand, data from pressurized flat-flame burner reactors are much more rare because these reactors need to be custom designed, which typically includes many failed first attempts and high machining costs. Data collection from pressurized flat-flame burner reactors is usually expensive, slow, and difficult with the potential of a myriad of problems. A few examples of difficulties from

pressurized flat-flame burner reactors include initial flame ignition, maintaining pressure seals, particle feeding issues, obtaining a stable flame, and measuring centerline gas temperatures in a pressurized vessel.

A ~1" diameter flat-flame burner served as the heat source of the HPFFB reactor. The gaseous fuel which fed the fuel-rich flame of the HPFFB was CO and H_2. The use of CO avoided gaseous-fuel soot formation at the elevated pressures (10, 12.5, & 15 atm) and fuel-rich conditions used in this study. Similar to the FFB reactor, the HPFFB reactor also utilized a 'carbonyl trap' to capture iron and nickel carbonyls before the CO was burned.

Particles were entrained in nitrogen and carried to the middle of the burner surface through a small metal tube (0.0535" ID; 304H16TW from MicroGroup) at a low feed rate (< ~1 g/hr). The particles then reacted while traveling upward in laminar flow before the particles were collected in a very similar collection system as the FFB reactor. The particles were assumed to stop reacting upon their entrance into the collection probe due to the high flow rate of inert gas and the sudden decrease in temperature.

The particle reaction zone between the burner and collection probe consisted of a circular quartz tube (26 mm ID) of different lengths to adjust the residence time. The reaction environment in the HPFFB reactor was determined by the post-flame gas composition. Gas temperature was controlled by adjusting gas flow rates to the burner and thus the stoichiometry. Increased char gasification was achieved in the HPFFB reactor at hotter gas temperatures, higher partial pressures of gasification agent, and increased particle residence times. Additional information about the HPFFB reactor is located in Appendix G.

4.2.1 Modifications to the HPFFB Reactor

The HPFFB collection system is shown in Figure 4.3. The figure illustrates the separation of solid char during operation mode through use of red arrows, and also provides a visual summary of the changes made to the reactor since its last documentation (Lewis, 2011; Shurtz, 2011). The char trap and glow-plug ignition system were both modified, and water traps were added.

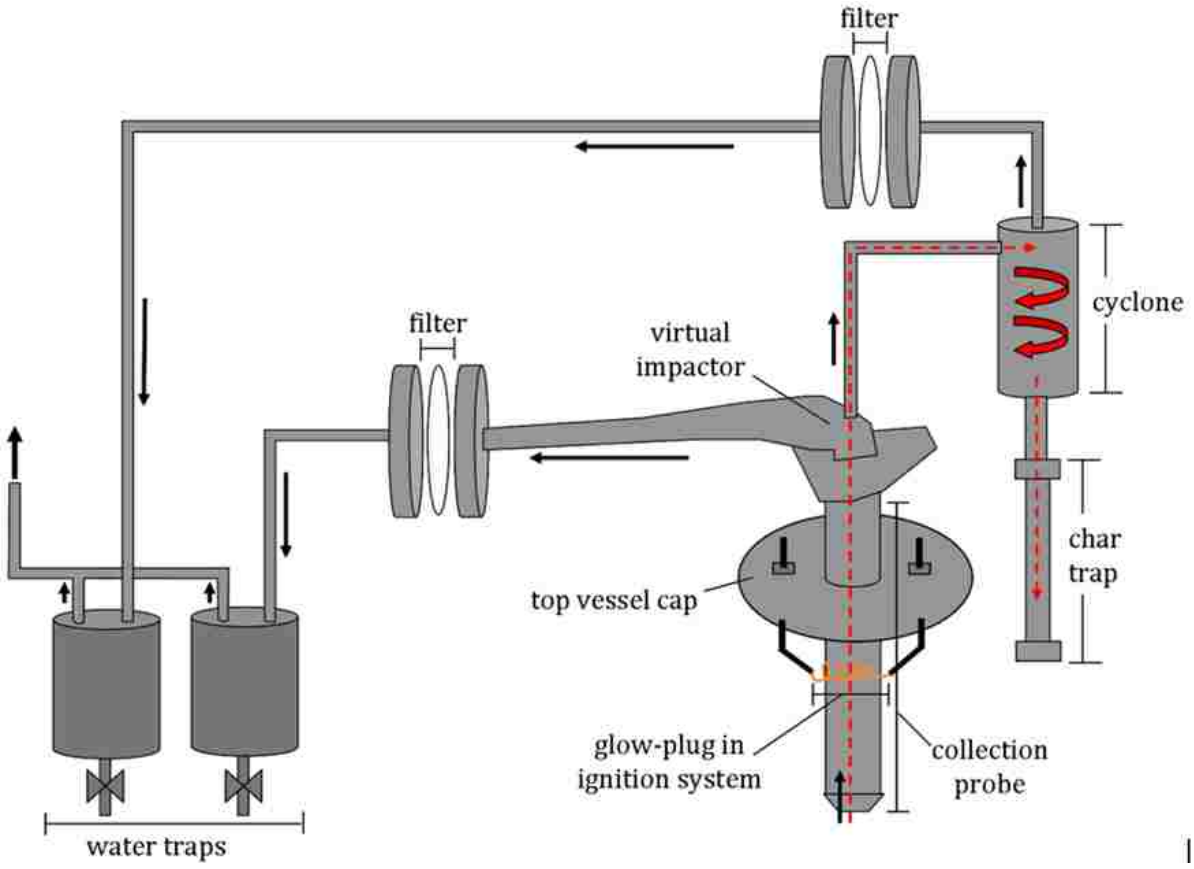

Figure 4.3. Collection system of the HPFFB reactor.

The previous char trap was secured to the collection system by screwing on by hand a threaded and hollowed-out stainless steel cylinder (3" long with diameter 2.25") that was closed

on one end. This design was discontinued after the char trap consistently began to unscrew by itself at pressurized conditions. As a replacement char trap, a ½" stainless steel tube (0.5" OD) with compression fittings was used. The use of a low-capacity (tube 6" long) or a high-capacity (tube 20" long) char trap depended on whether a gasification experiment or a coal char-generation experiment was being performed, respectively.

The custom glow-plug ignition system (see Figure 4.3) of the HPFFB reactor worked by using an AC power supply to heat a wire, which then ignited the flowing flammable gas mixture. The top viewport of the reactor allowed viewing of the glow plug wire as well as the ignition event. The bottom viewport of the reactor allowed verification that the flame had dropped to the burner surface. At the start of this project, the glow plug wire was a ~6" coiled segment of B-type thermocouple wire of 0.010" diameter. The thermocouple wire with higher rhodium content (i.e., 30% vs 6%) was used as the glow plug due to the higher melting point of rhodium when compared to platinum. Copper made up the rest of the ignition-system circuit, and Conax® fittings enabled the copper to pass through insulated and pressure-tight fittings on the top cap of the vessel. The costly B-type thermocouple wire in the ignition system was replaced by an inexpensive 22 gauge nichrome 60 wire that was found to also function as the coiled glow-plug wire. The thicker and more durable nichrome wire seemed to last longer as a glow plug when compared to the B-type wire. About 3 volts was found sufficient to allow the glowing nichrome wire to cause ignition without burning out. When using the B-type thermocouple wire as the glow plug, ignition events would often occur where the flame would remain at the top of the vessel without ever dropping to the burner surface. However, use of the nichrome wire eliminated this problem. Either the burner would light when using the nichrome wire, or the entire gas mixture contained by the quartz tube in the reactor would combust nearly

instantaneously but not light the burner. The ignition pressure was lowered to 5 atm (even when operating pressure was 10 atm or higher after ignition) as a precaution when using the nichrome wire due to the sometimes rapid ignition events that occurred with no warning. Proper ignition was very closely tied to the proper amount of H_2. When too much H_2 was present, the burner would not light since the flame would drop too quickly due to its high flame speed.

Water traps were added to the HPFFB reactor during this project (see Figure 4.3) since steam gasification experiments were conducted, and it was desired to condense out the water in the post-flame gases before they passed through flow meters. The water traps were essentially small stainless-steel pressure vessels that enabled liquid water to collect while allowing permanent gases to continue traveling through the exhaust plumbing. Valves on the bottom of the steam traps allowed water to be drained after the reactor had depressurized and been purged with N_2 after an experiment.

4.2.2 Running HPFFB Reactor in Steam Gasification Mode

Steam gasification experiments were conducted in the HPFFB reactor for this project using coal as feedstock material. Steam in the post-flame region of the reactor was generated by supplying extra H_2 to the burner, although steam generation was also considered using a combination of a HPLC pump, furnace, and heat-traced lines to the burner. The steam concentrations used in this study were limited to less than 9 mol% in the post-flame HPFFB environment due to concerns about damaging the burner head. Supplying extra H_2 to the burner resulted in higher concentrations of steam in the post-flame environment, but also caused the flame to 'sit' closer to the burner surface due to the high flame speed of H_2. Supplying the burner with excessive amounts of H_2 can greatly reduce the life of the burner, thus explaining why only

conservative amounts of H_2 were used in this study. Shurtz (2011) reported that a former HPFFB burner head suffered from high-temperature corrosion after months of using 84 mol% H_2 in the *fuel* stream to the burner. In this project, using H_2 to compose up to 36 mol% of the total fuel stream did not cause visible damage to the burner head during the 1.5 years that steam gasification experiments were conducted.

Using the HPFFB reactor for steam gasification experiments required several operational modifications. For example, the collection system was wrapped in heating tape and insulation in order to prevent water condensation upstream of the filters. In addition, cooling water to the filter flanges was not used during steam experiments. After ignition, non-steam gas conditions were used to feed the burner for about 30 minutes until the temperature behind both filter flanges (see Figure 4.3) registered ~ 110 °C, as measured using sheathed K-type thermocouples. After this approximate temperature was attained in the collection system, steam condensation upstream of the filters was no longer a concern and the flow rates of gases to the burner were then adjusted to the desired steam gas conditions while the burner remained lit. Char collected from steam gasification experiments was dried at 107 °C, and typically contained ~ 10 wt% moisture or less on a wet basis. After drying, the apparent density of the char was measured and the moisture content of the collected char was used to accurately assign mass release to the experiment. As an aside, steam condensation negatively affected particle feeding when the water-cooled collection probe was positioned 5" above the burner (without the use of heaters) when the peak gas temperature inside the HPFFB reactor was near 1600 K.

4.2.3 HPFFB Particle Feeder

A schematic of the pressurized plunger-type particle feeder used to feed coal and biomass separately to the HPFFB reactor is shown in Figure 4.4. A stepper motor was used to slowly progress forward an aluminum plunger, which pushed particles from the open end of the feeding tube down into a funnel which channeled the particles into the double-tubed feeder line. Particles then traveled to the middle of the burner surface due to their entrainment by N_2.

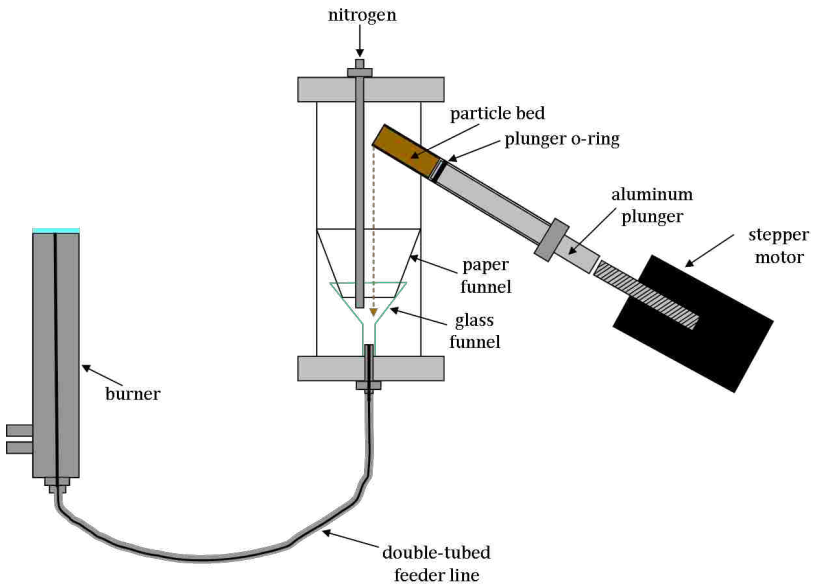

Figure 4.4. HPFFB particle feeder.

A few improvements were made to the particle feeder since its documented initial design (Lewis, 2011). These improvements involved the use of an o-ring on the end of the aluminum plunger, a paper funnel, and an additional feeder tube assembly of decreased diameter. An o-ring was strategically placed around the aluminum plunger on one end (see Figure 4.4) in order to feed the maximum percentage of loaded particles by preventing particles from falling behind the plunger. A laminated paper funnel (see Figure 4.4) whose top diameter was the same diameter as

the inside feeder wall and whose bottom end was inside the glass funnel ensured that falling particles made their way into the glass funnel and feeder line. The use of the paper funnel improved mass balances of the experimental runs since the weight difference of the particle bed before and after an experiment more accurately represented the mass of particles fed. Using a feeder tube assembly with a reduced internal diameter (see Figure 4.5) improved particle feeding by providing tighter control of the feed rate. The original feeder tube assembly measured 0.5" OD and 0.413" ID with an aluminum plunger of 3/8" diameter. However, particle clogging issues were experienced when feeding biomass since intermittent clumps of particles fell into the funnel rather than a steady stream of particles. The biomass feeding issue was resolved by utilizing a feeder tube assembly with 0.5" OD and 0.335" ID and an aluminum plunger of 5/16" diameter.

(a) (b)

Figure 4.5. Two views of the feeder tube assemblies of different internal diameter.

Adequate vibration was pivotal for good particle feeding. Vibration was provided on the feeder tube assembly, the double-tubed feeder line, and on the fittings where the feeder line entered the bottom of the burner body. A small coat of vacuum grease was applied on the front o-ring of the aluminum plunger before every run so that the o-ring would glide smoothly past the inside walls of the feeder tube assembly. It was important to have correct alignment between stepper motor screw and the aluminum plunger for proper feeding. Weighing the particle bed

before and after an experimental run rather than the feeder tube assembly resulted in improved mass balances.

A schematic of the stepper motor and its wiring is included as Figure 4.6. For convenience, the colored wires were drawn in the figure to match the actual wiring. An external power supply was used to provide power to the stepper motor, and a parallel port from a desktop computer in combination with transistor arrays (ULN2003) provided ground to individual coils of the stepper motor in a sequence that caused the stepper motor screw to move axially. Ten transistor arrays were wired in parallel on a breadboard in order to handle the necessary current to the stepper motor, even though only a single transistor array is shown in Figure 4.6. A Zener diode positioned between the power supply and pin 9 of the transistor array (top left pin in the figure) prevented electricity from traveling back to the computer. Additional details of the HPFFB particle feeder and stepper motor can be found elsewhere (Lewis, 2011; Shurtz, 2011).

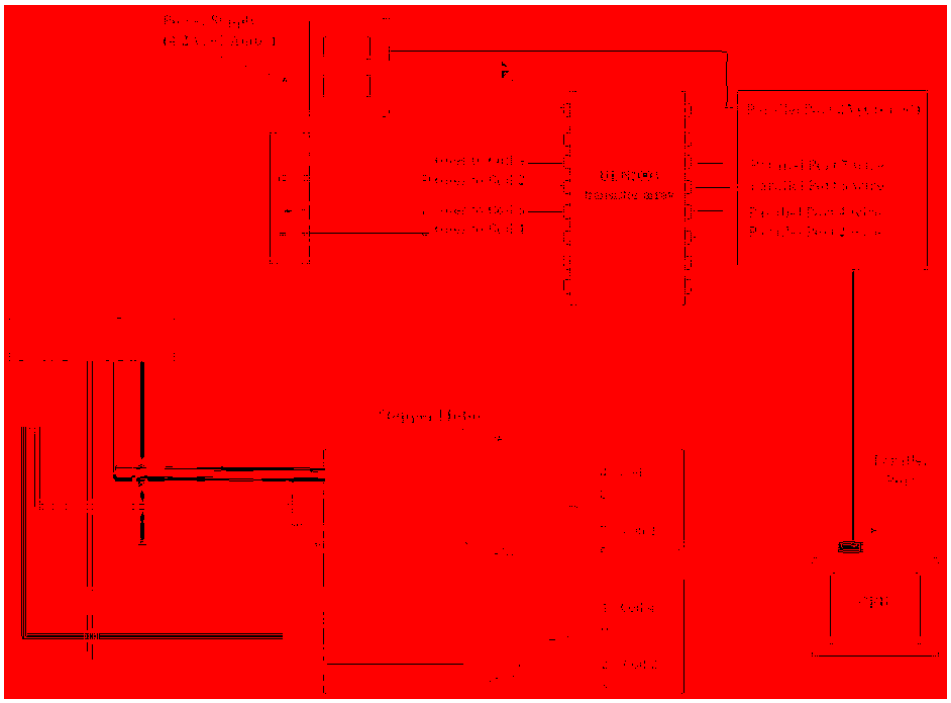

Figure 4.6. Wiring schematic of the HPFFB stepper motor.

4.2.4 Attempt at Utilizing Heaters in HPFFB Reactor

The purpose of using heaters (see Figure 4.2) in the HPFFB is to overcome heat losses and maintain a sufficiently hot environment beyond the near-burner region of the reactor to permit measurable amounts of char gasification for longer times. Since the char gasification reaction is slow, it is possible for char particles to essentially stop gasifying before they enter the collection probe if the temperature has dropped too low to permit continued char gasification in the limited residence times available in the HPFFB reactor.

Use of nichrome cylindrical heaters (18" long 2" ID) that were rated to 1200 °C and manufactured by Watlow did not maintain high enough temperatures in the HPFFB reactor to allow points of extended char gasification to be measured. Centerline gas temperature profiles corrected for radiation losses (see Appendix A) are shown in Figure 4.7 at two probing gas conditions of the HPFFB reactor where nichrome heaters were used. Both Figure 4.7a and b show that the nichrome heaters affected gas temperatures after ~4" above the burner at conditions where the peak gas temperature was at least 1900 K. However, the effect of the nichrome heaters on the centerline gas temperature was not sufficient to extend the useable distance above the burner where char mass release was measurable (at least at conditions of peak gas temperature near 1900 K at pressures up to 15 atm using post-flame environments containing ~20 mol% CO_2). Hence, the use of the nichrome heaters was discontinued.

Use of a different set of heaters was attempted in the HPFFB which were rated for higher temperature. These cylindrical molybdenum disilicide heaters (8" long) were manufactured by Micropyretics Heaters International. The heating element in these heaters broke early in this project even while cooling N_2 blew past their power leads. Fortunately, an appreciable amount of char mass release was measurable until roughly 6" above the burner without the use of heaters in

the HPFFB reactor at total pressures of 10-15 atm where the peak gas temperature was near 1900 K. Therefore, heaters were *not* utilized in any HPFFB experiments for this research.

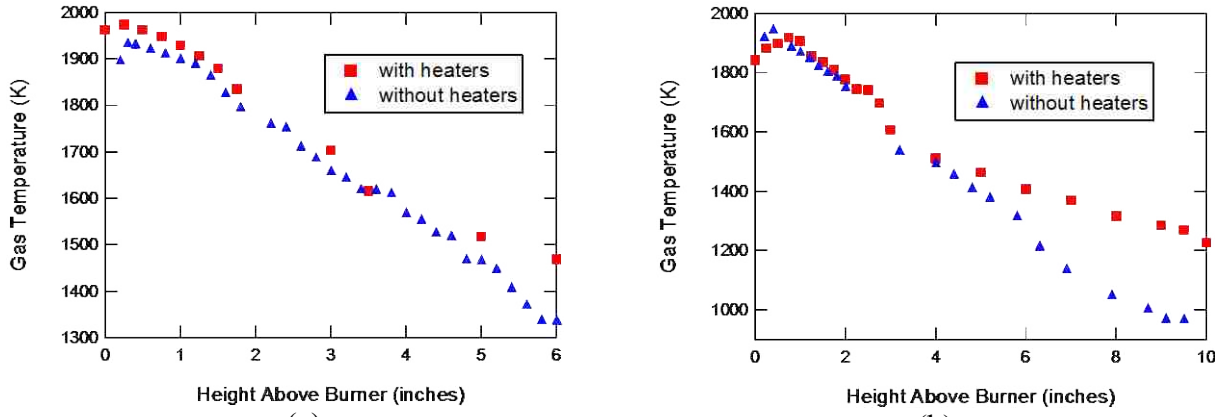

Figure 4.7. Centerline gas temperature profiles in the HPFFB reactor in a post-flame environment containing ~20 mol% CO_2 at total pressures of (a) 10 and (b) 15 atm where nichrome heaters were tested.

4.3 Safety Upgrades to FFB and HPFFB Reactors

Two safety upgrades were made to both the FFB and the HPFFB facilities. The first upgrade would not permit the burner from being lit in the case that cooling water to the collection probe was lost or if cooling water was not turned on (see Figure 4.8). The stainless steel collection probe typically resided about one to a few inches away from a live flame during an experiment, and had high potential to suffer from heat damage due to its proximity to a live flame. A rate meter (with relay card) received input from the measured flow rate of cooling water to the collection probe, and closed a valve on the fuel line to the burner (hence extinguishing the flame) in the case that the cooling water was below a set value. The water meter, solenoid valve, and rate meter had Omega part numbers FTB4605, SV121, and DPF701-R, respectively.

The second safety upgrade involved the installation of pressure relief valves in the gas cabinets that housed cylinders of toxic CO. In the event that the gas regulators on the CO tanks failed to drop gas pressure to a safe and low pressure during an experiment, the CO would leak through the pressure relief valves in the gas cabinets rather than be released elsewhere. After CO was detected in the ventilated gas cabinets by a gas detection system, another safety valve (upstream of the pressure relief valve) would close and stop the flow of high-pressure CO.

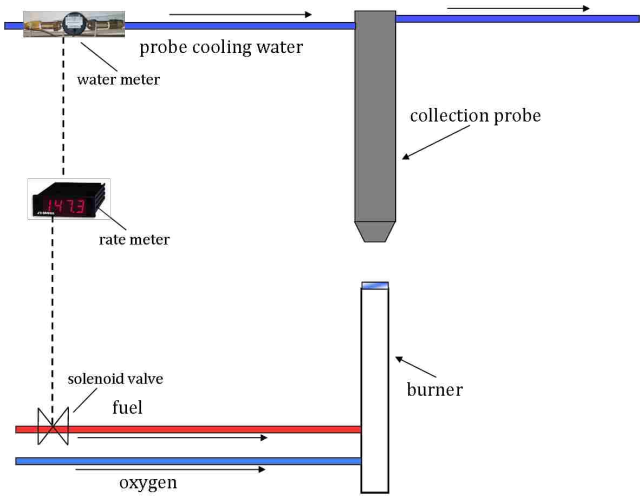

Figure 4.8. Safety system that extinguishes the burner flame if the cooling water flow rate to the collection probe falls below a specified value.

4.4 Methods of Producing Sphere-Like Biomass Char

A method was developed in this research to generate sphere-like biomass char since using spherical char as feedstock material for gasification experiments simplified the calculation of residence times, particle temperatures, and gasification rate constants. Several attempts were made to obtain the desired sphere-like biomass char. The first method involved the construction

of an aerodynamic particle separator that was similar to the separator of Lu (2006) (see Figure 4.9a and b).

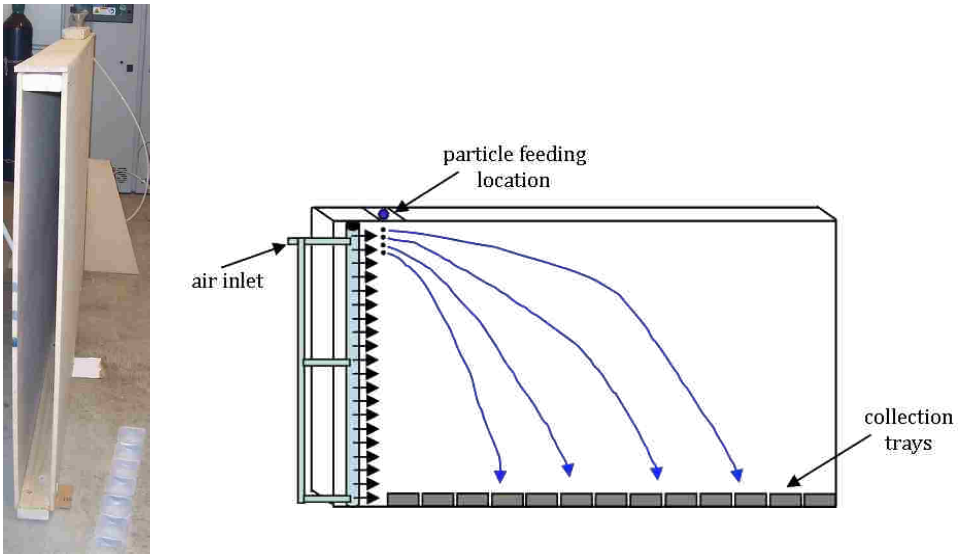

(**a**) (**b**)

Figure 4.9. Aerodynamic particle separator (a) built during this project and (b) its ideal operation.

To operate this separator, particles were released from the top of the particle separator and fell near a compressed-air distributor that blew air horizontally. Ideally, differences in drag force would allow separation by particle shape since each shape would be carried different horizontal distances in the separator. Raw and finely ground biomass samples (< 100 μm) were fed in the particle separator during testing in order to preserve the limited supply of biomass chars and to not risk contamination of the char. The aerodynamic particle separator approach to collect spherical biomass char particles was eventually abandoned after making several unsuccessful improvements to the separator. Uniform air flow was difficult to achieve in the separator, but even if the particle separator had functioned ideally, the aerodynamic separator was thought to be ill-suited for instances where recoverable yields are of concern, as was the case in this project where only limited supply of biomass char was available.

In a second attempt to separate spherical biomass char particles, char was loaded across the top of 600-grit sand paper. The sand paper was then held at an angle and tapped lightly on the side, which caused the more sphere-like particles to fall more quickly than other-shaped particles (see Figure 4.10).

Figure 4.10. Separating char by shape using an inclined piece of 600-grit sandpaper.

The spherical particles were collected on a piece of paper that lay underneath the sandpaper. This method of particle separation was used to successfully separate the sphere-like particles of corn stover char (see Figure 4.11).

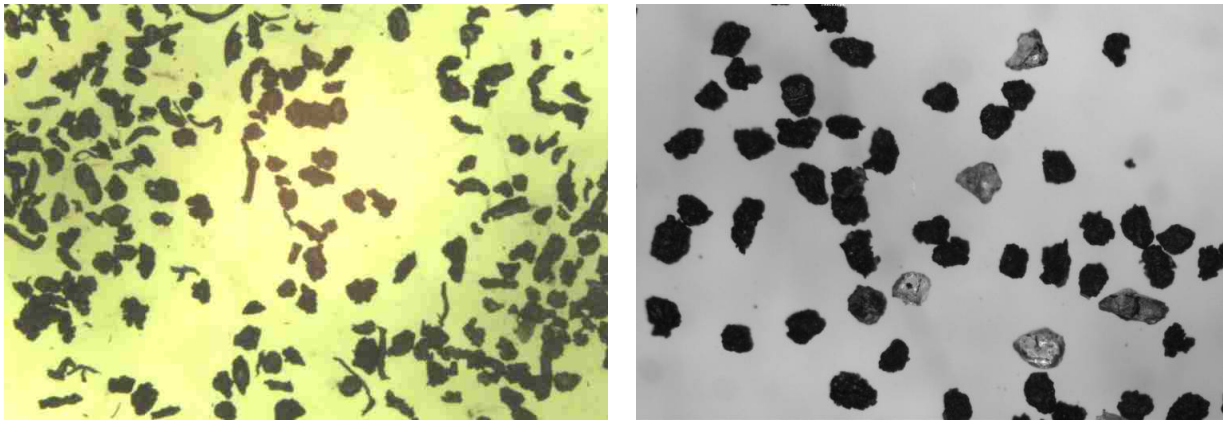

(a) (b)

Figure 4.11. Corn stover char (a) before and (b) after separation by the sandpaper technique.

However, collection of spherical char was extremely slow using this method. In addition, the collected spherical corn stover char particles had appreciably higher ash content than the starting

sample (84 wt% vs 52 wt% on a dry basis, respectively). The high ash content of the spherical corn stover char was concerning since it was not clear how high ash content would affect gasification reactivity measurements. Ash can act as a catalyst to the gasification reaction (Di Blasi, 2009; Yuan et al., 2011), but high ash content can also have an inhibiting effect to reactivity (Hurt et al., 1998). The sand paper approach to separate spherical biomass char particles was therefore abandoned due to these concerns.

The most favorable method of producing sphere-like biomass char particles from non-spherical biomass char involved feeding biomass char though a wheat grinder (Blendtec Kitchen Mill). Improved grindability of biomass after torrefaction is well known (Bergman et al., 2005). A variable transformer (Powerstat® 3PN116B) was used to control voltage delivered to the wheat grinder since manipulating the voltage directly affected the rate at which the grinder rotated. Experiments were performed to determine the optimal voltage to grind the biomass chars. It was found that operating the wheat grinder at 25 to 35 volts produced the highest yields of near-spherical biomass char. This method of grinding biomass char with a wheat grinder using low grinder speeds is ideally suited when limited quantities of biomass char are available (as was the case in the present study) due to its ability to produce relatively high yields of uncontaminated near-spherical biomass char. For example, coverable yields up to 70% (weight basis) were obtained using batch sizes of ~14 g. The ability to control particle shape by grinding is only achieved when grinding biomass char, not raw biomass. Grinding raw biomass usually results in fibrous particles, whereas grinding biomass char typically results in short and round particles since biomass char is much more brittle than raw biomass (Abdullah and Wu, 2009; Jarvis et al., 2011). This new method of generating near-spherical biomass char from non-spherical biomass chars may be useful in future studies.

4.5 Centerline Gas Temperature Measurements

Centerline gas temperature profiles were measured in both the FFB and HPFFB reactors by positioning a B-type thermocouple at different heights above the burner. A correction was applied to the raw temperature measurements in order to account for radiation losses of the thermocouple bead (see Appendix A). These measured gas temperature profiles were utilized to calculate particle temperatures, of which the particle kinetics were dependent. To measure gas temperatures in the atmospheric-pressure FFB reactor, a B-type thermocouple was held stationary on the centerline while a crank system was used to move the burner vertically. One set of temperature measurements were recorded as the burner was moved closer to the thermocouple bead, and replicate measurements were obtained as the burner was brought back to its starting position. The crank-system method of measuring temperature in the HPFFB reactor also had the advantage of being able to measure gas temperature inside the collection probe to evaluate quench characteristics of the probe.

Centerline gas temperature measurements were more difficult in the pressurized HPFFB reactor since they required a pressure seal to be maintained on the system during the measurements. The thermocouple was moved vertically above the stationary burner surface using a crank system (Shurtz, 2011) for the HPFFB measurements. The crank system shown in Figure 4.12 allowed the thermocouple to travel vertically while the collection probe remained stationary. The near-burner centerline gas temperatures (i.e. from ~0.2” to 3” above the burner) were most accurately measured when the collection probe was positioned 3” above the burner surface while also utilizing the appropriate length of short quartz tube (see Figure 4.2) since it was difficult to maintain a centered thermocouple bead at extended distances beyond the

entrance of the collection probe. Replicate HPFFB gas temperature measurements were taken in a similar manner as was done in the FFB reactor.

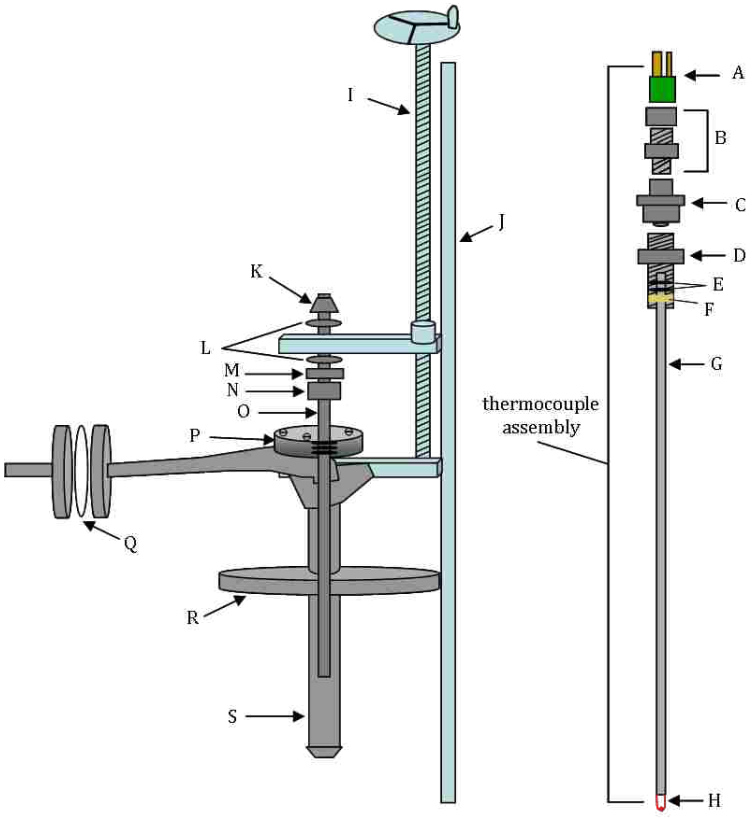

Figure 4.12. HPFFB reactor setup during centerline gas temperature measurements. A= electrical connector which hooked to a thermocouple reader; B = Conax® fitting that provided a pressure-tight seal for the thermocouple wires that passed through it; C = compression/NPT adapter fitting; D = through-wall compression fitting; E = o-rings to help secure part G to part D; F = epoxy to help secure part G to D as well; G = ceramic thermocouple shaft; H = B-type thermocouple bead; I = crank system that allowed raising or lowering of the thermocouple assembly; J = reactor stand; K = ferrules; L = metal washers; M = nut; N = 3/8" compression nut that screws onto part D; O = 3/8" OD stainless steel tube through which part G passes; P = water-cooled piece used during gas temperature measurements that maintains pressure seal with part O by use of 3 o-rings; Q = filter; R = top cap of vessel; S = collection probe.

4.6 Determination of Particle Residence Times

Accurate reaction times of particles are very important when determining particle kinetics. The particle reaction time in this research was taken as the time for a particle to travel from the burner surface to the entrance of the collection probe in an entrained-flow reactor. Particle residence time was controlled by adjusting the height between burner and collection probe, and was calculated using particle velocity measurements from a high-speed camera (Kodak EktaPro) at 125 fps. A lens effect had to be taken into account when measuring particle velocities through the bottom viewport of the HPFFB reactor. The calculations and method used to determine particle residence times in the BYU flat-flame burner reactors have been thoroughly documented (Lewis, 2011), but a brief summary is included here.

A force balance that included the effects of gravity, buoyancy, and drag on spherical particles was used to predict particle velocity profiles from the burner surface to the first measured particle velocity, typically 1" above the burner surface. A quadratic scaling factor was used in conjunction with the force balance to transition from a purely theoretical particle velocity at the burner surface to the measured particle velocity at 1" above the burner. Boundary conditions were chosen for the quadratic scaling factor such that the scaling factor had a closed-form solution. In the FFB reactor, the measured particle velocities were then used to complete the remaining velocity profile at increased heights above the burner. However, particle velocities at the $T_{gas,max}$ = 1163 K condition in the FFB reactor could not be measured since the particles were not sufficiently bright to be detected by the high-speed camera. For this particular condition, the velocity profile was calculated using ratios (Lewis, 2011) from FFB conditions of higher temperature where the particle velocities were measurable. Since the sole optical access to the HPFFB was a viewport at the bottom of the reactor (see Figure 4.2), the particle velocity

profiles beyond 1" above the burner surface were obtained by scaling the measured particle velocity by centerline gas temperatures (Lewis, 2011). After complete particle velocity profiles were obtained, the total particle residence time (t_{total}) was then calculated using Equation (4.1). This equation was a summation of small time steps of the particle as it traveled through the reactor to the collection probe. The variable Δz is the distance a particle traveled in a single time step.

$$t_{total} = \sum_{i=1}^{n} \frac{\Delta z}{v_{p_i}} \tag{4.1}$$

Dynamic gas viscosity (μ_{gas}) was used in the model that predicted particle velocities from the burner surface to the first measured particle velocity. Since empirical μ_{gas} correlations different than have previously been documented (Lewis, 2011) were used in this work, they are documented here. The gas viscosity data to which Equations (4.2) and (4.3) were fit were obtained using DIPPR correlations (Rowley et al., 2010) to calculate the molar weighted average viscosity of each gas condition at both the lowest and highest gas temperatures for each gas condition. Equation (4.2) was used to model the FFB gas conditions as well as the HPFFB conditions where the post-flame CO_2 concentrations in the HPFFB reactor were near 40 and 90 mol%. Equation (4.3) was used to model the gas viscosity for the coal steam HPFFB conditions. Both correlations are dependent on gas temperature in units Kelvin and had r^2 values of at least 0.98.

$$\mu_{gas} = \left(2.241 \times 10^{-8}(T) + 1.883 \times 10^{-5}\right) Pa \cdot \sec \tag{4.2}$$

$$\mu_{gas} = \left(2.286 \times 10^{-8}(T) + 1.93 \times 10^{-5}\right) Pa \cdot \sec \tag{4.3}$$

4.7 Particle Mass Release

Accurate particle mass release measurements are of pivotal importance when fitting measured mass release data to char gasification models. The typical equations used to calculate particle mass release on a dry and ash-free (daf) basis from a mass balance and ash-tracer respectively follow:

$$\%\ MR(daf) = \left(\frac{m^0{}_{fed} - m_{char\ collected}}{m^0{}_{fed} - m^0{}_{ash,fed}} \right) \cdot 100 \tag{4.4}$$

$$\%\ MR\ (daf) = \left(\frac{1 - \frac{x^0{}_{ash,fed}}{x_{ash,char\ collected}}}{1 - x^0{}_{ash,fed}} \right) \cdot 100 \tag{4.5}$$

where m^0_{fed} is the dry mass of feedstock fed, $m_{char\ collected}$ is the dry mass of collected char after the experiment, and $m^0_{ash,fed}$ is the dry mass of ash in the fed feedstock. The mass fraction of ash in the dry feedstock fed during experimentation is $x^0_{ash,fed}$, and $x_{ash,char\ collected}$ is defined as the mass fraction of ash in the dried collected char. Although not performed in this study, it is also possible to calculate particle mass release using specific elements in the ash as tracers (Lewis, 2011). Details about measuring accurate particle mass release are discussed in Appendix B.

Equation (4.5) is convenient because it does not depend on collection efficiency, and allows accurate mass release to be calculated (assuming that original ash remains with the particle) even if a mass balance is ruined by spills, clogs, forgetting to record necessary weights, etc. However, mass release calculated by Equation (4.5) should only be considered when the corresponding mass release values using Equation (4.4) are higher, assuming again that the original ash remained with the collected char.

Both Equations (4.4) and (4.5) assume that ash is not released from the particle during the experiments. If ash leaves the particle, Equations (4.4) and (4.5) will overestimate and underestimate the particle daf mass release, respectively. The numerator in Equation (4.4) reflects the organic mass that leaves the particle *if* ash is not liberated. However, when ash leaves the particle, the numerator in Equation (4.4) reflects the mass of ash that was released in combination with the organic mass lost from the particle. Equation (4.6) was derived in this work to calculate particle mass release on a daf basis when ash was determined to have been released from an ash mass balance (see Section 5.3). The numerator in the equation reflects the amount of organic mass of the particle that was released:

$$\%MR\ (daf) = \left(\frac{m^0{}_{fed} \cdot (1 - x^0{}_{ash,fed}) - m_{char\ collected} \cdot (1 - x_{ash,char\ collected})}{m^0{}_{fed} - m^0{}_{ash,fed}} \right) \cdot 100 \qquad (4.6)$$

It is important to note that Equation (4.6) depends on an accurate mass balance, which is regularly achieved in both the FFB and HPFFB reactors. The average collection efficiency of the FFB reactor was measured to be 99.6% when feeding 45-75 μm petroleum coke using collection heights of 2 to 8 inches above the burner. The collection efficiency of the HPFFB reactor was measured to be 98.0% from 5 tests when feeding the same petroleum coke feedstock at a gas condition in the HPFFB where the CO_2 partial pressure and temperature were not sufficiently high to gasify the petcoke in the allotted residence time. This condition was at a total pressure of 5 atm with a post-flame gas composition near 20 mol% CO_2 and a peak centerline *gas* temperature of 1804 K. Collection heights in the range 3 to 9.5 inches (with corresponding particle residence times 161-626 ms) were used.

The most accurate mass balance was ensured by blowing out the collection system after each experiment to most correctly assign weights of material fed and collected. To blow out the HPFFB collection system after a run (see Figure 4.3), a valve upstream of the bottom filter

flange was closed and compressed air was blown from the top filter flange towards the cyclone (while the entrance to the collection probe was blocked off) causing any residual char in the collection system to collect in the char trap.

4.8 Means of Measurements for Particle Properties

This section summarizes the means by which several different char properties were measured in this study including ash fractions, elemental composition, surface areas, ash composition, apparent density, etc.

Ash tests were performed in this study to determine ash fraction of a feedstock or collected char. These ash tests took place overnight in a muffle furnace by slowly heating the furnace to 750 °C and holding that temperature for 10 hours. Ceramic crucibles of 5 mL volume were often used in the ash tests. From sensitivity studies performed on the Mettler Toledo AB104 digital scale, a sample needed to contain at least ~8 mg of ash for an accurate ash fraction to be determined. Proximate analyses were performed in-house at BYU following the methods documented by Zeng (2005). The ultimate analyses of the feedstocks were performed by Huffman Labs in Golden, Colorado. Moisture tests were performed in a muffle furnace by holding a sample at 107 °C until constant weight was obtained.

Both N_2 and CO_2 surface area particle measurements in this study were performed at BYU using adsorption isotherms from a TriStar Micromeritics 3000 instrument. Nitrogen surface areas were measured at 77 K (using liquid N_2) and calculated using the Brunauer-Emmett-Teller (BET) equation. These measurements provide information regarding the mesopore structure. Carbon dioxide surface areas were measured at 298 K (using an ice water bath), and provides insight regarding the micropores of the particles. Filler rods and isothermal jackets were not

utilized in CO_2 measurements. CO_2 surface areas were calculated using density functional theory (DFT), and represent the total area in the pores greater than ~4.5 angstroms. The Tristar 3000 instrument was used to measure the CO_2 isotherms, but a free executable file was required from a Micromeritics representative to post-process the measured CO_2 data to obtain a CO_2 surface area.

Optical pictures in this work were taken with a Leco Olympus SZX12 microscope with PAX-it imaging software. Scanning electron microscope (SEM) images were taken using a FEI XL30 ESEM instrument with a FEG emitter. The ash compositions reported in this document were from energy-dispersive x-ray spectroscopy measurements collected on an EDAX Genesis system mounted on the aforementioned ESEM instrument.

Apparent density, $\rho_{apparent}$, is the mass of the particle divided by the volume of the particle, and includes voids inherent in the material. Apparent densities were obtained in this work by taking the average of 2-3 bulk density measurements and assuming a packing factor using the following equation:

$$\rho_{apparent} = \frac{\rho_{bulk}}{1 - \varepsilon_b} \tag{4.7}$$

where ρ_{bulk} and ε_b are defined as the bulk density and inter-particle void fraction or packing factor. The bulk density was measured using a technique similar to that used by Tsai and Scaroni (Tsai and Scaroni, 1987), where particles were added to a graduated cylinder of known volume. The bulk density was then calculated by dividing the mass of particles added by the volume of the bed. The graduated cylinder was also tapped repeatedly to ensure the minimum volume of the bed. The value for ε_b was taken as 0.45 (Tsai and Scaroni, 1987; Gale et al., 1995).

Using Equation (4.7) and the method described above to determine the apparent density of finely ground (45-75 μm) raw poplar sawdust yielded encouraging results even though

biomass does not consist of uniformly shaped particles. For example, the measured apparent densities of two separate blocks of poplar wood (weighing 13 and 583 g) were on average within 3% of the apparent density measured when using Equation (4.7). It was therefore assumed that Equation (4.7) could be used to calculate accurate apparent densities of other biomass feedstocks when using a compact bed of 45-75 μm particles and the method described above.

5. Biomass Pyrolysis Experiments and Modeling

High-temperature biomass pyrolysis experiments were conducted at atmospheric pressure in the flat-flame burner reactor (FFB) for four different samples: poplar sawdust, switchgrass, corn stover, and straw. This chapter focuses on the experimental results and addresses mass release, tar and gas yields, increased volatile yields at conditions of high heating rate, and ash release. Biomass devolatilization modeling efforts are also discussed using the Bio-CPD model with a tar-cracking model.[1]

5.1 Samples for Biomass Pyrolysis Experiments in FFB Reactor

The biomass samples used in pyrolysis experiments in the FFB reactor (see Section 4.1) at atmospheric pressure were barkless poplar sawdust (PS), switchgrass (SG), corn stover (CS), and straw (ST). The chosen feedstocks included energy crops as well as both woody and agricultural residues. The source for the corn stover was pelletized material that was ground to the desired size. The four biomass samples were ground using an electric wheat grinder (Blendtec Kitchen Mill) and sieved to collect the 45-75 μm size range. These small biomass particles were used in pyrolysis experiments in order to ensure a high initial heating rate of the particles and to assume that the temperature gradients within the particle are insignificant (for

[1] A portion of the biomass pyrolysis modeling work in this chapter has been published: Lewis, A. D. and T. H. Fletcher, "Prediction of Sawdust Pyrolysis Yields from a Flat-Flame Burner Using the CPD Model," *Energy & Fuels,* **27**, 942-953 (2013). Parts of this chapter were also included in a technical report (McDermott et al., 2014).

simplified modeling), which is only true when the Biot number is less than 0.1 (Incropera and Dewitt, 2002). Properties and ash composition of the raw 45-75 μm biomass feedstocks are given in Table 5.1 and Table 5.2, respectively. Details about measurement techniques were included in Section 4.8. The balance of the ash composition values in Table 5.2 is composed of elemental oxygen since the elements existed as oxides (i.e., Na_2O, MgO, Al_2O_3, SiO_2, etc.) after they were collected from an ash test in air at 750 °C. The reported biomass ash composition values in Table 5.2 agree well with values in the literature (Jenkins et al., 1998; Vassilev et al., 2010; Vassilev et al., 2012).

Table 5.1. Properties of the raw biomass feedstocks (45-75 μm)

Feedstock	PS	SG	CS	ST
sieved particle size (μm)	45-75	45-75	45-75	45-75
C (wt% daf)	48.84	46.38	46.47	48.69
H (wt% daf)	5.91	5.93	5.85	6.32
N (wt% daf)	0.11	0.53	1.35	0.50
S (wt% daf)	0.0	0.14	0.09	0.15
O (wt% daf, by diff.)	45.14	47.02	46.24	44.33
volatiles (wt% daf)[a]	88.79	85.66	81.28	85.91
ash (wt% dry) [a]	0.82	8.23	23.46	4.93
moisture (as rec'd) [a]	2.38	5.62	3.15	4.39
apparent density (g/cm^3)	0.653	0.457	0.865	0.348
N_2 surface area (m^2/g)	0.67	0.88	0.80	0.73
CO_2 surface area (m^2/g)	59.33	53.17	43.58	46.12

[a] ASTM

Table 5.2. Biomass ash composition

	Composition of Ash[b] (wt %)			
	PS	**SG**	**CS**	**ST**
Na	0.77	0.25	0.99	0.64
Mg	11.70	2.09	2.84	5.92
Al	0.70	0.86	4.36	0.36
Si	2.69	34.34	22.31	17.02
P	0.53	2.22	2.19	2.70
S	1.43	1.15	1.03	4.93
K	5.30	6.93	11.98	19.18
Ca	40.69	9.11	9.14	12.64
Ti	0.24	0.14	0.46	—
Fe	1.18	1.14	7.00	1.07
Cr	—	—	0.77	—
Mn	0.93	—	—	—

[b] prepared at 750 °C. These elements appear as oxides in the ash, but the wt% oxygen is not reported here since the performed analysis reported the non-oxidized metal form.

5.2 Results and Discussion

5.2.1 Pyrolysis Mass Release of Biomass in FFB Reactor

Ground and sized (45-75 μm) raw samples of poplar sawdust, switchgrass, corn stover, and straw were fed separately through the FFB reactor at atmospheric pressure to measure pyrolysis yields of char, tar, and light gas at different residence times using fuel-rich conditions with peak gas temperatures of 1163-1433 K. Temperature profiles from the $T_{gas,max}$ = 1163 K FFB condition are shown in Figure 5.1 since the vast majority of the biomass pyrolysis experiments were conducted at this condition. These gas temperature measurements as well as any other cited gas temperatures in this chapter have been corrected for radiation losses from a 555 μm-diameter B-type spherical thermocouple bead (see Appendix A). The average correction of gas temperature at the FFB pyrolysis conditions was approximately 70 K. Figure 5.1 shows the measured centerline gas temperature profile, in addition to the calculated particle temperature profile of poplar sawdust from a particle energy balance.

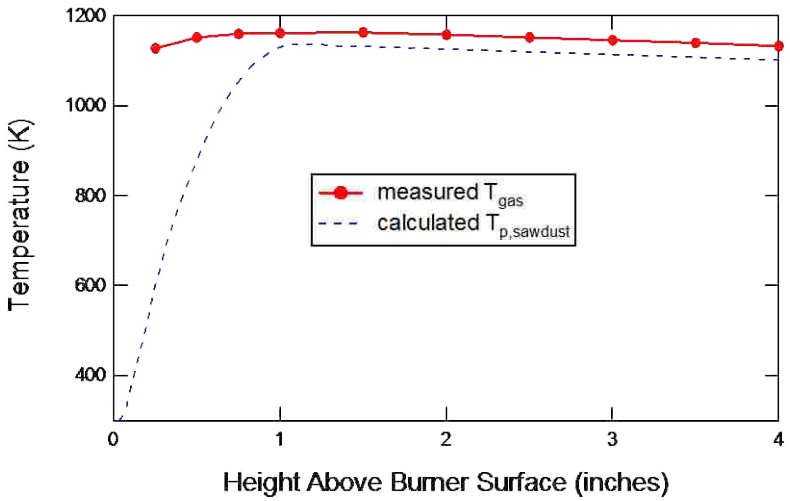

Figure 5.1. Measured centerline gas temperature and calculated particle temperature profile of sawdust at the $T_{gas,max}$ = 1163 K pyrolysis FFB condition.

Figure 5.2 shows biomass particles being pyrolyzed in the FFB reactor at the $T_{gas,max}$ = 1433 K pyrolysis condition. Although the $T_{gas,max}$ = 1433 K condition was only used in a limited number of experiments, it was chosen for Figure 5.2 because the particle stream was brightest at this condition of relatively high temperature. Slow biomass feeding rates near 0.5 g/hr were used to prevent the biomass particles from clogging the feeding tube during the pyrolysis experiments. The calculated maximum initial particle heating rates of poplar sawdust, switchgrass, and straw at the $T_{gas,max}$ = 1163 K gas condition were 6.0×10^4, 7.9×10^4, and 8.2×10^4 K/s, respectively. Additional details about all the FFB pyrolysis gas conditions as well as a complete set of measured data from the biomass pyrolysis experiments are included in Appendix C.

Figure 5.2. Biomass particles being pyrolyzed in the FFB reactor at the $T_{gas,max}$ = 1433 K condition.

Figure 5.3 shows a summary of the measured mass release from the FFB biomass pyrolysis experiments as calculated using a mass balance (using weights of raw biomass fed and collected char). The poplar sawdust had the highest mass release (99.3 wt% daf) from pyrolysis while straw had the lowest (92.4 wt% daf). Note the small char yields, which are the difference between 100 and the reported values in Figure 5.3. Each data point of mass release in Figure 5.3 is the average of at least 2 experiments. The average 95% confidence interval of mass release

data points in Figure 5.3 for poplar sawdust, switchgrass, and straw were 0.5, 0.9, and 1.7 wt% daf, respectively (± $T_{stat} \cdot \sigma$ / *sqrt(#points)* at points where ≥3 replicate experiments had been performed).

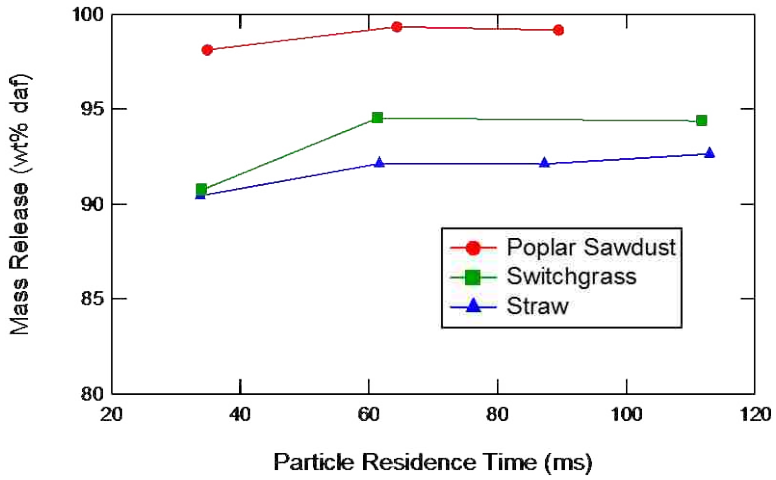

Figure 5.3. Mass release (daf) from biomass pyrolysis experiments at atmospheric pressure at the $T_{gas,max}$ = 1163K condition in the FFB reactor.

The data points at the earliest residence time (~ 35 ms) in Figure 5.3 were the only experiments where partial pyrolysis of the biomass fuels was measured. Poplar sawdust, switchgrass, and straw all reached full pyrolysis by at least ~60 ms, which is indicated in Figure 5.3 by the asymptotic mass release values. A few additional biomass pyrolysis experiments run at peak gas temperatures up to 1433 K in the FFB reactor confirmed that asymptotic mass release values from pyrolysis were indeed measured (see Appendix C).

Obtaining additional data of partial pyrolysis (besides at a residence time of ~35 ms) was beyond the ability of the FFB reactor since this would require lower temperatures and/or shorter particle residence times. Trying to decrease gas temperatures below 1163 K resulted in an unstable flame, and obtaining shorter residence times than ~35 ms would require a distance less than 1" between burner and collection probe (making the temperature history difficult to quantify). Although it was difficult to measure partial pyrolysis for the biomass feedstocks in the

FFB reactor, pyrolysis yields were measured and reported from feeding the same biomass feedstocks (poplar sawdust, switchgrass, & corn stover) in a drop tube reactor at lower temperatures (Maghzi and Rizeq, 2011). These drop tube measurements were part of the collaboration that took place between BYU and GE Global Research to study the thermal conversion of biomass. However, there are concerns about the accuracy of the reported residence times and temperatures from the biomass drop tube measurements (see Appendix C).

Mass release values of corn stover were not summarized in Figure 5.3 because only limited experiments could be run with this biomass feedstock. Corn stover posed serious feeding problems since it routinely clogged at the end of the feeding tube (0.052" ID) near the lit burner. Other researchers have also reported feeding problems when using corn stover and attributed it to the fact that corn stover 'pyrolyzed very readily' causing 'feed inlet blockages' (Scott et al., 1985). Using about 1.5 times the usual carrier N_2 in the feeding tube allowed corn stover to be fed without clogging in the FFB reactor, which allowed meaningful data of corn stover to be measured at some conditions. The pyrolysis mass release of corn stover at high heating-rate conditions was 93.3 wt% (daf basis).

Figure 5.4 shows the difference in biomass mass release at low and high heating rate conditions at atmospheric pressure for poplar sawdust, straw, switchgrass, and corn stover. The low heating-rate mass release values in Figure 5.4 came from an ASTM volatiles test (see Table 5.1). The high heating-rate mass release values came from FFB experiments where complete pyrolysis was obtained. The difference between low and high heating rate mass release values was greatest for corn stover (12.0 wt% daf difference), followed by poplar sawdust (10.5 wt% daf difference), switchgrass (9.1 wt% daf difference), and straw (6.4 wt% daf difference). Other researchers (Zanzi et al., 1996; Borrego et al., 2009; Lewis and Fletcher, 2013) have also noticed

a difference in volatile content of biomass when comparing data from low and high heating-rate conditions. For example, Borrego et al. (2009) measured up to 12% greater volatile yields than the ASTM volatiles test when pyrolyzing wood chips, forest residues, and rice husks at high heating rate in a drop tube furnace. The initial particle heating rate influences the effect of cross-linking reactions in a devolatilizing particle (Borrego et al., 2009). Sufficiently high particle heating rates result in a higher volatiles yield since cross-linking reactions kinetically compete with the release of material from a biomass particle during pyrolysis.

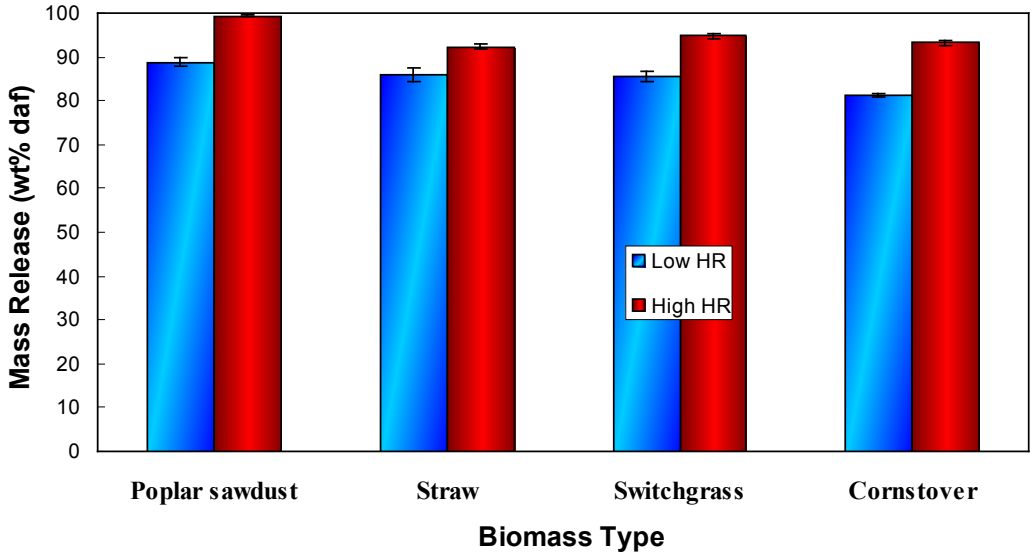

Figure 5.4. Comparison of mass release (daf basis) at low and high heating-rate (HR) conditions for poplar sawdust, straw, switchgrass, and corn stover at atmospheric pressure (95% confidence intervals of the mean are shown).

5.2.2 Tar and Gas Yields of Biomass Pyrolysis in FFB Reactor

Biomass tar and gas yields from the FFB pyrolysis experiments at atmospheric pressure are shown in Figure 5.5, and correspond to the mass release data in Figure 5.3. The tar yields were calculated based on the mass that collected on the water-cooled glass fiber filters (see Figure 4.1) in the FFB collection system (i.e., tar yield = weight of collected tar/weight of daf biomass fed). Note that the gas yields in Figure 5.5b were determined by difference, i.e., (100%

– % char yield (daf) – % tar yield (daf)). Each data point of tar yield in Figure 5.5a is the average of at least 2 experiments. The average 95% confidence interval of biomass tar yields in Figure 5.5a was ~0.5 wt% daf (at points where ≥3 replicate experiments had been performed). Corn stover tar and gas yields were not included in Figure 5.5 since only limited experiments were conducted using this feedstock due to feeding problems, as documented above. However, the asymptotic tar and gas yields from the corn stover FFB pyrolysis experiments were 2.1 wt% and 91.2 daf wt%, respectively.

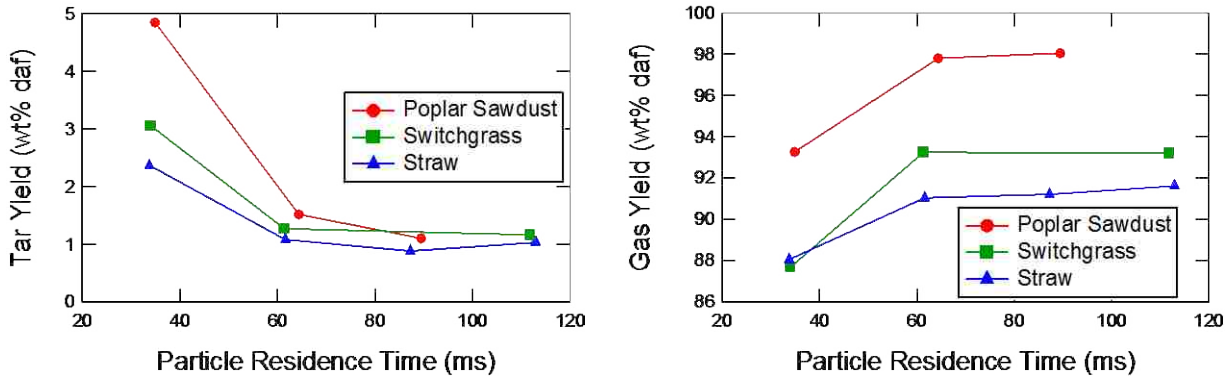

(a) (b)

Figure 5.5. Measured yields (wt% daf) of (a) tar and (b) gas from biomass pyrolysis experiments at different residence times in the FFB reactor at atmospheric pressure at the $T_{gas,max}$ = 1163 K condition.

The decreasing yields of biomass tar in Figure 5.5a were the result of tar-cracking reactions, which results in a gas yield that increases proportionately to the destruction of tar. The high temperatures used in the FFB biomass pyrolysis experiments resulted in the very low tar yields (see Figure 5.5a), especially considering that biomass tar yields can be as high as ~75 daf wt% (Scott and Piskorz, 1984; Bridgwater, 2003). It is important to note that the following discussion regards cracking of tar from *wood*, although the findings likely apply to other biomass feedstocks as well. There is much literature that indicates wood tar begins to thermally crack into light gas near 500 °C (Fagbemi et al., 2001). Scott et al.(1988) report that it is unlikely that a

wood particle can still be in the primary pyrolysis phase at any temperature above 500 °C and that secondary reactions must occur above this temperature. Other researchers have studied the conditions at which maximum biomass tar yields occur, and have concluded that these conditions involve short residence times with high heating rates at a maximum temperature near 500 °C (Higman and Burgt, 2003; Li et al., 2004; Mohan et al., 2006). Data in the literature such as shown in Figure 5.6 indicate that tar yields from wood pyrolysis pass through a maximum near 500 °C, and then decline at higher temperatures due to secondary tar-cracking reactions. Both high temperature and residence time contribute to the cracking of the wood tar into light gas.

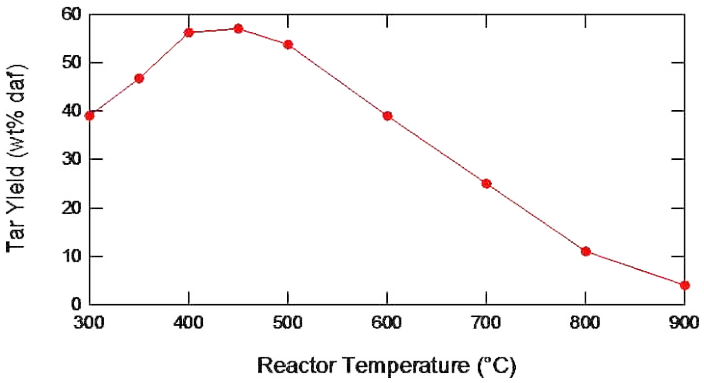

Figure 5.6. Silver birch tar yields from a fluidized bed reactor at a volatile residence time of 1.21 s (*Adapted from the work of Stiles and Kandiyoti* (1989), with permission from Elsevier).

It is interesting to note that the tar yields in Figure 5.5a from the biomass pyrolysis experiments conducted in a *reducing* environment leveled off near 1 to 1.3 daf wt%. This is important because even low tar yields in industrial processes can cause problems by corroding equipment, causing damage to motors and turbines, lowering catalyst efficiency, and condensing in transfer lines (Vassilatos et al., 1992; Brage et al., 1996; Baumlin et al., 2005). It is suggested in the literature that there exists a small fraction of biomass tar that is or becomes refractory which does not thermally crack to light gas at reasonable temperatures (Antal, 1983; Rath and Staudinger, 2001; Bridgwater, 2003; Di Blasi, 2008). Other researchers have shown that hotter

reactor temperatures result in an increased fraction of aromatic compounds and condensed ring structures in the biomass tar (Stiles and Kandiyoti, 1989; Zhang et al., 2007; Jarvis et al., 2011). In order to test for refractory tar, poplar sawdust was fed in the FFB reactor at a condition where the peak gas temperature was 1751 K using a particle residence time near 75 ms (6" collection height). The collected tar yield from the $T_{gas,max}$ = 1751 K condition was not any lower than the $T_{gas,max}$ = 1163 K condition, suggesting that the asymptotic biomass tar yields in Figure 5.5a were the result of collecting refractory tar. However, Zhang et al. (2006) reported to have measured complete tar destruction when pyrolyzing Hinoki cypress sawdust in a drop-tube furnace above 1473 K. The measured sawdust tar yield in the FFB reactor at a hotter condition differs from the findings of Zhang et al., but could possibly be explained by a difference in residence time, sawdust type, or how experimental tar was defined.

5.3 Ash Release When Feeding Raw Biomass in FFB Reactor

The inorganic matter transformation of biomass during thermal conversion is important due to its effect on many different facets including slagging, fouling, corrosion, and emission of fine particles (Wu et al., 2011). This section provides some insight into biomass ash release in *reducing* conditions during the pyrolysis of 45-75 μm biomass particles in entrained-flow in the FFB reactor at high initial particle heating rates. These results are likely be pertinent to *oxidizing* conditions as well since the net mass of material away from the biomass particle is so high during pyrolysis at high initial particle heating rates that external conditions (i.e., reducing vs oxidizing) likely would not have a noticeable effect, at least on the initial ash release. Several other researchers have also studied ash release during the thermal conversion of biomass

(Jimenez and Ballester, 2006; van Lith et al., 2006; Frandsen et al., 2007; van Lith et al., 2008; Johansen et al., 2011; Wu et al., 2011).

Ash release in the biomass pyrolysis FFB experiments was calculated using Equation (5.1), which uses a mass balance of the ash:

$$\%\ ash\ release = \left(\frac{m^0{}_{fed} \cdot x^0{}_{ash} - m_{char,collected} \cdot x_{ash,char}}{m^0{}_{fed} \cdot x^0{}_{ash}} \right) \cdot 100 \qquad (5.1)$$

where m^0_{fed} is the mass of dry biomass fed, $m_{char,collected}$ is the mass of dry char collected, x^0_{ash} is the ash mass fraction in the dry raw biomass fed, and and $x_{ash,char}$ is the ash mass fraction in the dry collected char. Equation (5.1) requires a good mass balance to provide accurate ash release results; however, the collection efficiency of the FFB has been previously measured as 99.6% (see Section 4.7).

Figure 5.7 summarizes the ash release results from the biomass FFB pyrolysis experiments. Ash release is not reported for poplar sawdust in Figure 5.7 because the low ash content of this feedstock (i.e., 0.82 wt% dry basis) made accurate quantification of ash release difficult. Switchgrass, corn stover, and straw had on average 17, 13, and 19 wt% of their initial ash content released to the gas phase, respectively. Although straw had the highest percentage of its ash released to the gas phase when compared to the other 2 biomass feedstocks, straw had the lowest *total* ash being released due to its relatively low initial ash fraction (4.93 wt% dry basis). Corn stover had the highest *total* ash released, and on average had 3.0 wt% (i.e., 23.46 wt% x 0.13) of its fed dry mass transform to inorganics in the gas phase. It is also interesting to note from Figure 5.7 that temperature and residence time did not significantly affect ash release in these limited experiments. Also note that the results in Figure 5.7b for corn stover were from

experiments where about twice the carrier N_2 was utilized in the feeding tube since this feedstock otherwise tended to pyrolyze early and clog the feeding tube to the burner (see Section 5.2.1).

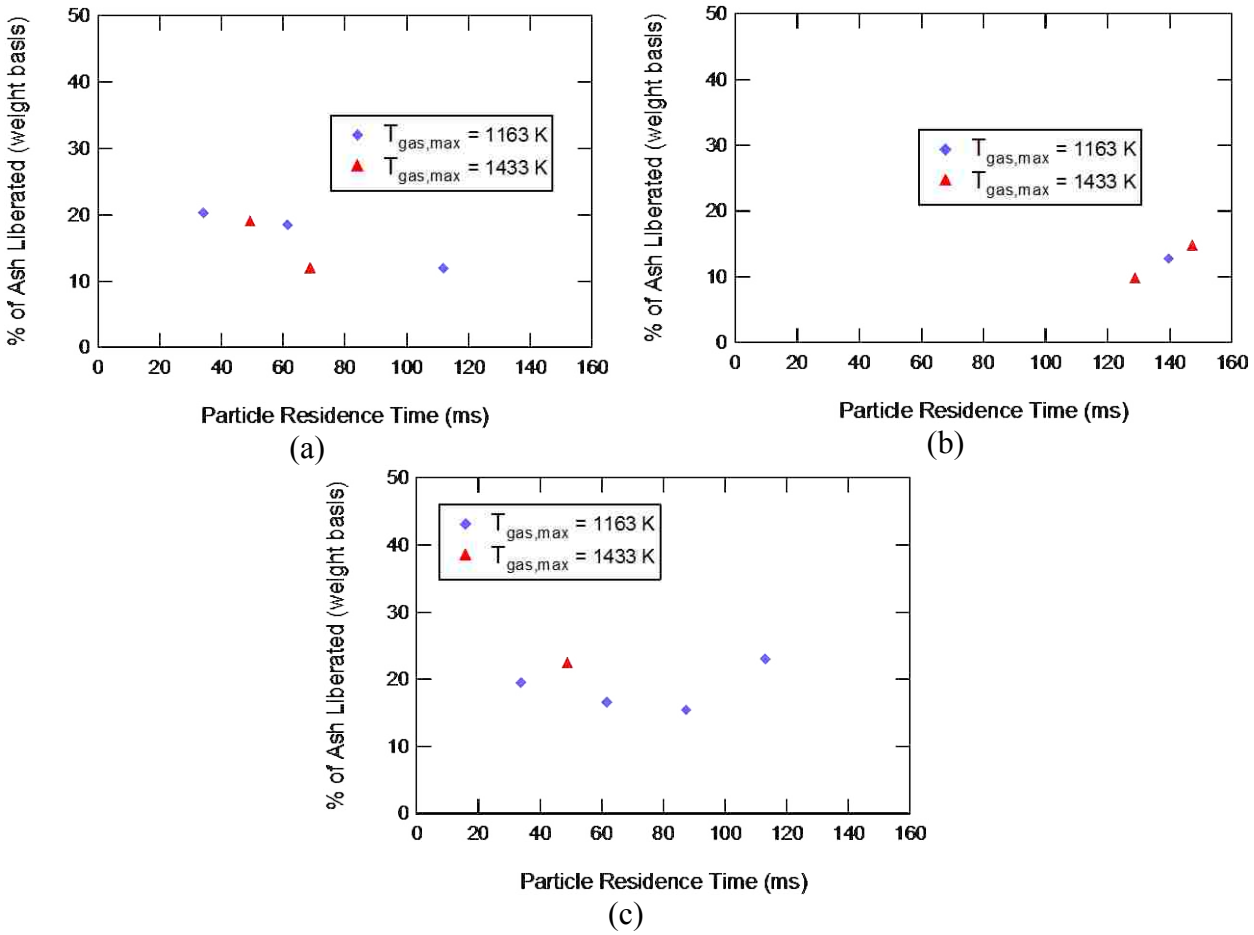

Figure 5.7. Release of ash to the gas phase during biomass pyrolysis in reducing conditions in the FFB at high initial heating rates for (a) switchgrass, (b) corn stover, and (c) straw at conditions where the maximum gas temperatures were 1163 and 1433 K.

5.4 Biomass Pyrolysis Modeling Using the CPD Model

5.4.1 Bio-CPD Model

The model used to predict biomass pyrolysis in this research project was the Chemical Percolation Devolatilization (CPD) model (Fletcher et al., 1992). The CPD model was originally

developed to predict coal devolatilization yields as a function of time, temperature, pressure, and heating rate using a description of the coal's chemical structure. Coal is modeled as aromatic clusters connected by labile bridges. Upon heating during pyrolysis, the bridges become activated and can proceed through two competing pathways. The intermediate bridges can either break to form side chains and subsequent light gas or else release light gas and simultaneously form a char bridge that will remain stable at typical pyrolysis temperatures. The competing reaction rates are a function of kinetic parameters, including activation energy, pre-exponential factor, and a standard deviation for the activation energy. The rate at which bridges rupture is modeled, and percolation statistics for Bethe lattices predict the relationship between the number of cleaved bridges and detached clusters. The tar yields are calculated using Raoult's law, a vapor pressure correlation, and a flash calculation at every time step. Secondary reactions of tar (i.e., tar cracking into light gas; see Section 5.2.2) are not part of the CPD model. It is important to recognize that the pyrolysis predictions of the CPD model assume that temperature gradients within the particle are insignificant, which is only true for sufficiently small particles when the Biot number is less than 0.1 (Incropera and Dewitt, 2002). Hence, care should be taken when comparing predictions of the CPD model to measured values.

The CPD model uses structural and kinetic parameters to describe a particular fuel. The structural parameters in the CPD model are molecular weight of the cluster (MW_{c1}), molecular weight of side chains (M_δ), initial fraction of intact bridges (p_0), coordination number ($\sigma + 1$), and initial fraction of char bridges (c_0). The structural parameters typically come from ^{13}C NMR measurements, except c_0, which must be determined empirically. The structural and kinetic parameters used to model the pyrolysis of cellulose, hemicellulose, and lignin using the CPD model have been documented previously (Fletcher et al., 2012).

The CPD model requires a base structural unit, which, for coal, is an aromatic cluster. Fletcher et al. (2012) defined the base unit for biomass components of cellulose, hemicellulose, and lignin. The base unit for lignin was coniferyl, coumaryl, and sinapyl alcohols. The fixed anomeric carbon and attached hydrogen were considered the base cluster for cellulose and hemicellulose. This definition of the base cluster for cellulose and hemicelluose translated into three intact bridges, an ether bridge, and two bridges that make up the sugar ring with their attached side chains. The chemical similarity between lignin and a low rank coal makes lignin a good candidate for Bethe lattice statistics, which the CPD model uses to predict the number of detached clusters as a function of cleaved bridges. Perhaps different statistical models besides that for Bethe lattices would better model the linear polymers of cellulose and hemicellulose, but the initial results (Fletcher et al., 2012) of the CPD model are promising for predicting measured pyrolysis yields of all 3 biomass components.

The char-to-gas kinetic ratio, ρ, was changed for hemicellulose from 1.08 to 1.35 in this work to more accurately predict fully pyrolyzed tar, char, and light gas yields of xylan-based hemicellulose from the literature (Shen et al., 2010). Fletcher et al. (2012) previously used ρ = 1.08 to model xylan pyrolysis at a heating rate of 20 K/min and demonstrated good agreement between predicted and measured xylan char yields from a thermogravimetric analyzer (TGA) (Alen et al., 1995). The accurate prediction of xylan char yields from the CPD model would also indicate that the xylan volatiles (i.e., tar + gas) yield would be accurate from the TGA experiments. However, because tar and gas yields from xylan pyrolysis were not reported in the TGA experiments (Alen et al., 1995), the ability of the CPD model to predict accurate tar and gas yields individually from xylan pyrolysis was not previously evaluated (Fletcher et al., 2012). When using ρ = 1.35 in the CPD model to predict the final pyrolysis yields of xylan at a heating

rate of 20 K/min, the code predicted tar, char, and light gas fractions of 0.45, 0.23, and 0.32, respectively. Using the previous value of ρ = 1.08, the CPD model predicted tar, char, and light gas fractions of 0.35, 0.27, and 0.38, respectively. Changing the kinetic parameter ρ for xylan only changed the fully pyrolyzed char yield by 4 wt%, but mostly changed the tar and light gas fractions to more accurately match the measured xylan pyrolysis yields (Shen et al., 2010) at temperatures of 475−500 °C, where the effects of tar cracking were minimal. For documentation purposes, measured pyrolysis yields of xylan by Shen et al. (2010) near 500 °C were about 43, 24, and 33 wt% tar, char, and light gas, respectively.

To predict the *primary* pyrolysis yields for biomass, the CPD model was run separately for cellulose, hemicellulose, and lignin using the kinetic and structural parameters which have been published (Lewis and Fletcher, 2013). Running the CPD model separately for each of the three biomass components resulted in the predicted devolatilization yields from *primary* pyrolysis of pure cellulose, hemicellulose, and lignin. The char, tar, and light gas yields of a particular biomass were then calculated as the weighted average of the pyrolysis yields of cellulose, hemicellulose, and lignin (using normalized fractions of biomass components). Any effect of extractives on the mechanism of biomass pyrolysis is not addressed in the Bio-CPD model. The biomass content of the studied biomass fuels in this project were measured for modeling purposes, and the results from the UC Davis Analytical Lab are summarized in Table 5.3.

Table 5.3. Measured and normalized biomass fractions of biomass feedstocks

Biomass Component	Poplar Sawdust	Straw	Corn Stover	Switchgrass
Cellulose	0.629	0.512	0.510	0.462
Hemicellulose	0.242	0.399	0.384	0.415
Lignin	0.129	0.089	0.106	0.123

5.4.1.1 Biomass Tar Predictions when Tar Cracking was Included

Recall that the sole use of the Bio-CPD model allows a prediction of the *primary* pyrolysis yields of biomass as the weighted sum of the *primary* pyrolysis yields of cellulose, hemicellulose, and lignin. To accurately predict biomass pyrolysis yields above 500 °C (see Section 5.2.2), a first-order tar-cracking rate was utilized in conjunction with the predicted tar generation rate by the CPD model. The differential material balance of tar when considering tar cracking is:

$$\frac{dC_{tar}}{dt} = r_{tar\ generation} - r_{tar\ cracking} \tag{5.2}$$

$$\text{where } r_{tar\ generation} = from\ CPD\ \text{model}$$

$$r_{tar\ cracking} = k_1 \cdot C_{tar} = \left[A \cdot \exp\left(\frac{-E}{R \cdot T_{gas}} \right) \right] \cdot C_{tar}$$

where C_{tar} is the daf tar fraction, $r_{tar\ generation}$ is the rate at which tar is generated, $r_{tar\ cracking}$ is the rate at which biomass tar thermally cracks into light gas, k_1 is the rate constant of tar cracking, A is the pre-exponential factor, E is the activation energy, R is the ideal gas constant, and T_{gas} is the gas temperature. It is important to note that the tar-cracking reaction occurs as a function of *gas* temperature, whereas the CPD model predicts primary pyrolysis yields as a function of *particle* temperature. Tar-cracking kinetic parameters (i.e., A and E in Equation (5.2)) were regressed in this study by fitting measured tar data from the FFB reactor (see Section 5.2.2) and also silver birch tar data from Stiles and Kandiyoti (1989) at lower temperatures of 500-900 °C for residence times 0.25-3.08 s in a fluidized bed reactor. The regressed values of A and E for the first-order tar cracking rate were 4.65×10^8 s^{-1} and 145.32 kJ/mol, respectively. Figure 5.8 shows the predicted and measured tar yields from the pyrolysis of straw in the FFB reactor at the

$T_{gas,max}$ = 1163 K condition. The predicted tar yields in the figure include cases where tar cracking was (a) included and (b) ignored.

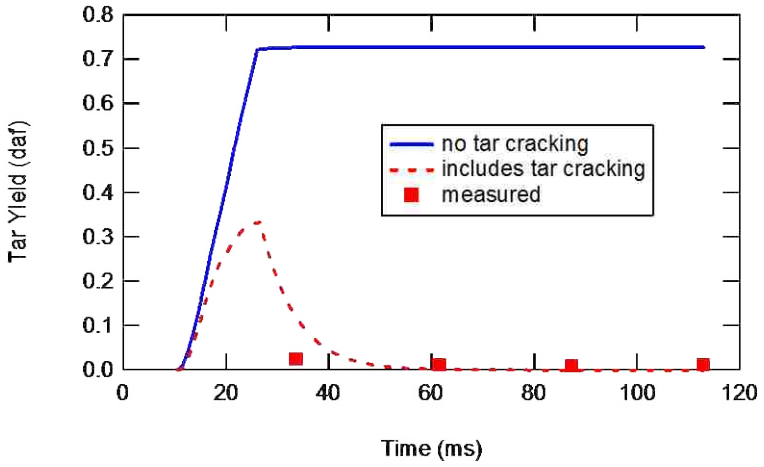

Figure 5.8. Prediction of tar yields from the pyrolysis of straw at the $T_{gas,max}$ = 1163 K condition in the FFB reactor.

The fraction of tar that was calculated to thermally crack to light gas was added to the gas yields. The char yield predicted by the CPD model remained unchanged when considering secondary tar-cracking reactions. Figure 5.9 provides a visual summary of the predictions of the first-order tar-cracking model as a function of time and temperature for the simplified case when a tar fraction of 0.7 exists at time zero.

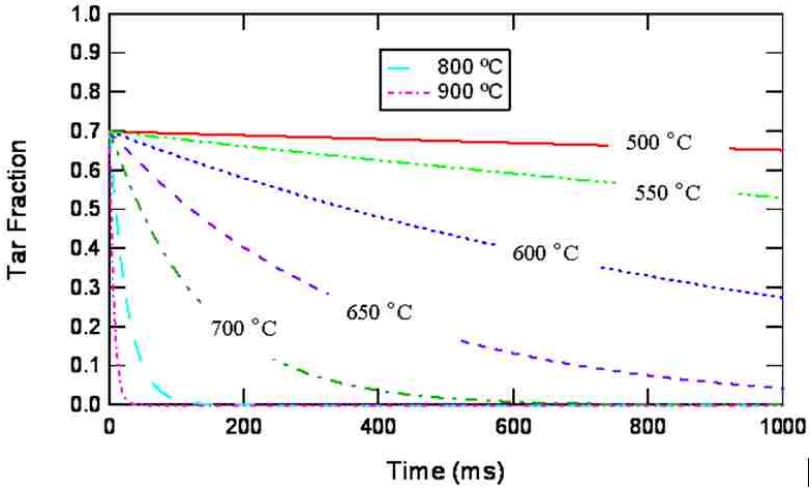

Figure 5.9. Predicted biomass tar yields as a function of time and temperature using a first-order tar-cracking model using A and E values of 4.65×10^8 s^{-1} and 145.32 kJ/mol respectively.

Given sufficient time, the biomass tar-cracking model predicts complete tar cracking into light gas and does not consider the small amount of refractory biomass tar measured in the FFB experiments at reducing conditions (see Section 5.2.2).

5.4.2 Predictions of the Bio-CPD Model with FFB Experiments

The Bio-CPD model was used previously to accurately predict the pyrolysis yields (i.e., char, tar, & gas) of a *softwood* sawdust (Lewis, 2011; Lewis and Fletcher, 2013). In this project, the performance of the Bio-CPD model was evaluated for a *hardwood* sawdust (poplar), as well as straw and switchgrass using data summarized in Section 5.2. Predictions of corn stover pyrolysis are not included here due to the inability to measure a complete set of pyrolysis data for this feedstock in the FFB reactor due to feeding problems (see Section 5.2.1).

The comparison between measured and modeled biomass pyrolysis yields of poplar sawdust and straw are summarized in Figure 5.10a and b, respectively. The Bio-CPD model when used in combination with the first-order tar-cracking model essentially predicted full pyrolysis after the first measured collection point, just as was measured.

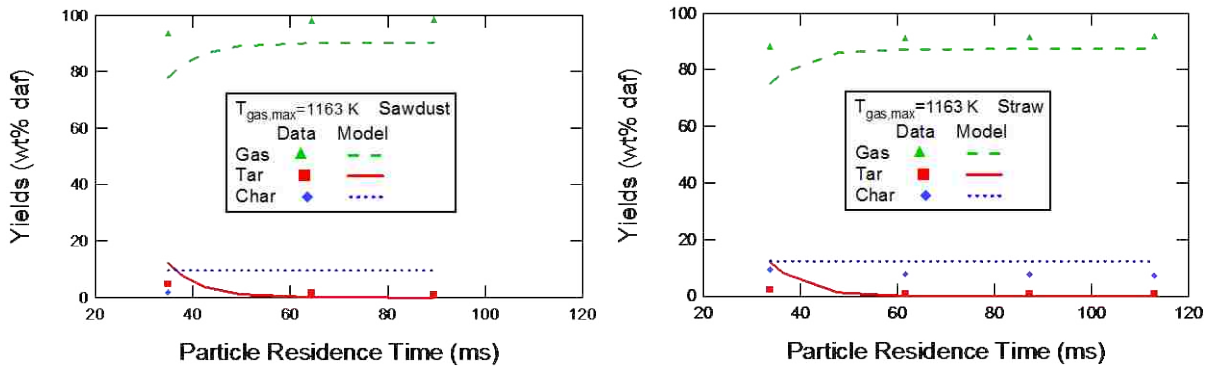

Figure 5.10. Comparison of measured and modeled (a) poplar sawdust and (b) straw pyrolysis yields at atmospheric pressure in the FFB reactor at the $T_{gas,max}$ = 1163 K condition.

Although the model correctly predicted that the measured biomass yields would be comprised almost entirely of gas, the model over-predicted the char yield at complete pyrolysis (≥ ~60ms) by 8.9 and 4.9 wt% daf for poplar sawdust and straw, respectively.

The comparison between measured and modeled biomass pyrolysis yields of switchgrass is summarized in Figure 5.11a when using the Bio-CPD model in combination with the tar-cracking model in Equation (5.2). Similarly as with poplar sawdust and straw, the model over-predicted the fully pyrolyzed char yields (8.0 wt% daf), but predicted essentially complete pyrolysis at residence times ≥ ~60 ms, as was measured in the FFB reactor. Figure 5.11b is a comparison of measured and modeled pyrolysis yields of switchgrass solely from the Bio-CPD model (*without* use of the tar-cracking model). Note that the predicted tar yield is close to the measured gas yield in Figure 5.11b, rather than the measured tar yield. This comparison demonstrates the importance of combining the results of the Bio-CPD model with a tar-cracking model, since tar-cracking reactions greatly affect tar and gas yields above 500 °C (see Section 5.2.2). The ability of the Bio-CPD model (when used in combination with a tar-cracking model) to correctly predict the pyrolysis yields from a wide range of biomass feedstocks is encouraging.

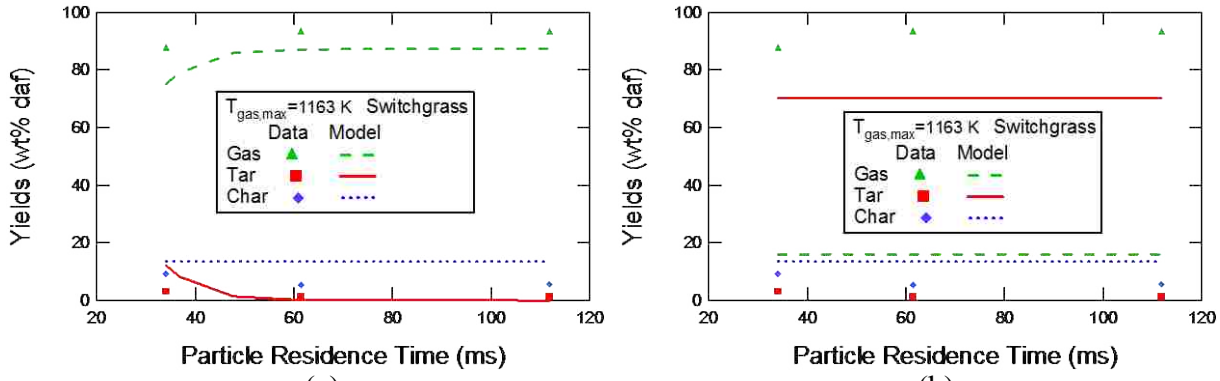

Figure 5.11. Comparison of measured and modeled switchgrass pyrolysis yields in the FFB at atmospheric pressure and peak gas temperature of 1163 K (a) with and (b) without use of the tar-cracking model in Equation (5.2).

5.4.3 Modeling of Primary Pyrolysis of Pine Sawdust

The Bio-CPD model using the kinetic and structural parameters that have been previously published (Lewis and Fletcher, 2013) was also evaluated with a data set from literature that was obtained at conditions where minimal tar cracking occurred. This allowed an assessment of the predicted biomass yields of the CPD model considering primary pyrolysis only, without use of a tar-cracking model. Figure 5.12a shows the CPD model predictions of fully pyrolyzed yields of 100-212 μm Pine sawdust in a drop-tube reactor (Wagenaar et al., 1993). The biomass component fractions used to model the Pine sawdust were taken as the average of several values from the literature (Ward and Braslaw, 1985; Orfao et al., 1999; Franco et al., 2003; Kang et al., 2006; Yuan et al., 2010; Vassilev et al., 2012) since the component fractions were not reported for this experiment. The resulting cellulose, hemicellulose, and lignin fractions used in modeling were 0.427, 0.29, and 0.283, respectively. Even though some of the measured data in Figure 5.12a were at temperatures above 500 °C, tar cracking was not taken into account since secondary reactions were suppressed by quickly removing the pyrolysis vapors during experimentation at short residence times (Wagenaar et al., 1993).

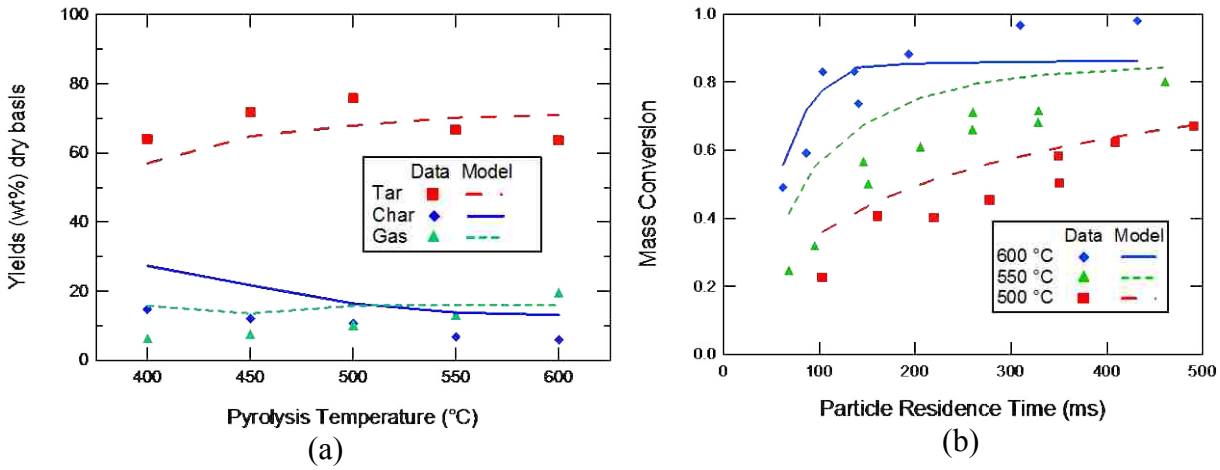

Figure 5.12. Comparison of measured and modeled Pine sawdust primary pyrolysis yields from a drop-tube reactor (Wagenaar et al., 1993).

Despite using short residence times and low temperatures to suppress tar-cracking reactions in their experimental setup, a small fraction of tar cracking would explain the slight decreasing tar yields and increasing gas yields from 500 to 600 °C in the data.

To model the measured data in Figure 5.12a and b, an isothermal gas temperature profile was assumed in the reactor since measured temperature profiles were not reported (Wagenaar et al., 1993). To collect the measured sawdust pyrolysis yields shown in Figure 5.12a, the researchers modified their drop tube reactor by inserting a steel-wire plug that completely covered the cross sectional area of the tube. The steel plug captured all the pyrolyzing particles and was inserted 0.05 m downstream of where the sawdust particles were introduced into the reactor (Wagenaar et al., 1993). Since the sawdust particles on the steel-wire plug were continually subjected to high temperature, the measured sawdust pyrolysis yields in Figure 5.12a are those from complete pyrolysis. Thus, the modeled pyrolysis yields in Figure 5.12a were those from complete pyrolysis as predicted by the CPD model. The discrepancy between measured and modeled sawdust pyrolysis yields in Figure 5.12a can mostly be explained by material losses in the collection system, which was reported to be between 3.7 and 15.6 wt% (10 wt% on average) (Wagenaar et al., 1993).

Figure 5.12b shows the modeled and measured mass conversion of Pine sawdust in drop-tube experiments as a function of particle residence time at temperatures between 500 and 600 °C. The predicted mass conversions from the CPD model were within 10.0 wt% on average of measured data for the three temperatures tested. One explanation of the under-prediction of mass conversion at residence times above 200 ms at 600 °C is incomplete collection efficiencies in the reactor, as was previously mentioned. Another possible explanation is that there is an effect of

high heating-rate on biomass volatile yields (Borrego et al., 2009; Lewis and Fletcher, 2013) that is not fully captured by the CPD model.

5.4.4 Modeling of Beech Sawdust Pyrolysis at Low Heating Rates

The Bio-CPD model was also evaluated by comparing the measured and modeled solid mass fraction of Beech sawdust that was heated at a relatively low heating rate in a TGA. Figure 5.13 shows the CPD model's predictions of weight loss curves from the pyrolysis of <80 μm sawdust at a heating rate of 1000 K/min to final temperatures ranging from 573-708 K with an isothermal stage upon heating to the final temperature (Branca and Di Blasi, 2003). The reported biomass component fractions (Branca and Di Blasi, 2003) of the beech sawdust were normalized for CPD modeling. The resulting cellulose, hemicellulose, and lignin fractions were 0.459, 0.337, and 0.204, respectively. No tar cracking model was utilized in the prediction of the CPD model summarized in Figure 5.13 since tar cracking does not have any appreciable effect on char yields.

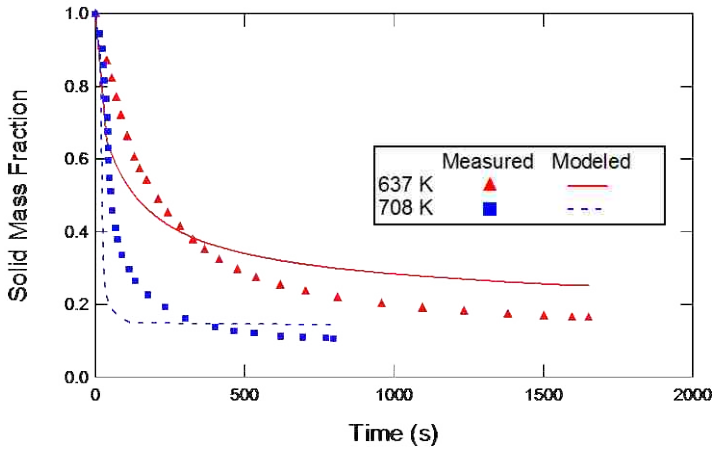

Figure 5.13. Comparison of measured and modeled char yields from beech sawdust pyrolysis in a TGA (Branca and Di Blasi, 2003).

The modeled solid mass fraction in Figure 5.13 was typically within 9 wt% of the measured beech data at 637 K, and the final solid mass fraction at 1650 s was only over-predicted by 8.9 wt%. Although the CPD model predicted a quicker initial mass release of the solid beech sawdust than was measured at 708 K, the model captured the general character of the measured mass-loss curve at 708 K (see Figure 5.13). The predicted final solid mass fraction at 708 K was within 3.9 wt% of the measured value.

Although not shown in Figure 5.13, the prediction of the CPD model was also compared with the aforementioned TGA data (Branca and Di Blasi, 2003) at the lower temperatures of 573 and 593 K. The CPD model over-predicted the final char yield at 2000 s by an average of 24 wt% at both temperatures. Although there was a wide discrepancy between the measured and modeled data at these lower temperatures, biomass pyrolysis of industrial significance typically occurs at higher temperatures, except for torrefaction which is a mild form of pyrolysis at approximate temperatures of 200-300 °C (Bergman et al., 2005). The predictions of the Bio-CPD model at 573, 593, 637, and 708 K were all obtained without adjusting any model parameters. If being able to predict biomass pyrolysis at very low temperatures is of interest, the Bio-CPD model has the potential for improvement by modifying kinetic parameters. Nevertheless, the ability of the Bio-CPD model to predict measured biomass pyrolysis data over a wide variety of feedstock varieties, heating rates, and final temperatures is notable.

5.5 Summary

Pyrolysis experiments were performed at conditions of high initial particle heating rates by feeding finely ground poplar sawdust, switchgrass, corn stover, and straw in an entrained-flow flat-flame burner reactor at atmospheric pressure. Most of the biomass pyrolysis

experiments were conducted at a peak gas temperature of 1163 K using particle residence times ranging from 34 to 113 ms. Only limited experiments could be performed with corn stover since this feedstock posed serious feeding problems. The measured maximum volatile yields from pyrolysis were 99.3, 94.8, 93.3, and 92.4 wt% daf for poplar sawdust, switchgrass, corn stover, and straw, respectively. Volatile yields of the 45−75 μm biomass in the FFB reactor exceeded the ASTM volatiles value by ~10 wt% daf. A refractory biomass tar yield near 1-2 wt% daf was measured in the reducing environment of the FFB reactor for all 4 biomass feedstocks. Biomass ash vaporization was measured to occur during the FFB experiments where 13-19% of the initial ash content was released to the gas phase (on a weight basis).

Biomass pyrolysis was modeled using the Chemical Percolation Devolatilization (CPD) model assuming that biomass pyrolysis occurs as a weighted average of its individual components (cellulose, hemicellulose, and lignin). Thermal cracking of tar into light gas was included using a first-order tar-cracking model. Biomass tar cracking can greatly affect the distribution of the pyrolysis products between tar and light gas, and becomes important above ~500 °C. Biomass devolatilization yields from three different reactors (flat-flame burner, drop-tube, and TGA) were predicted.

6. CO_2 Gasification of Biomass Char

Biomass chars of sawdust, switchgrass, and corn stover were generated at high initial particle heating rates (~10^4 K/s) in a drop tube reactor at atmospheric pressure using short residence times. The chars (~100 μm) were then re-injected separately in a high-pressure flat-flame burner reactor at elevated temperatures ($T_{gas,max}$ > 1800 K) and pressures (10-15 atm) to measure CO_2 gasification rates of the biomass chars. The measured char gasification data were fit to a global first-order model and the optimal kinetic parameters are reported.[2]

6.1 Biomass Gasification Experiments

The high-pressure flat-flame burner reactor (HPFFB; see Section 4.2) allowed biomass char gasification rates to be measured at conditions relevant to industrial entrained-flow gasifiers by reacting small particles in entrained-flow at high temperatures and pressures for short times (<0.3 s). Chars of barkless poplar sawdust (PS), switchgrass (SG), and corn stover (CS) were used in the biomass gasification experiments in the HPFFB reactor. Properties of the *raw* biomass fuels were summarized in Table 5.1 and Table 5.2. Although the term *gasification* is sometimes used to describe the pyrolysis of highly volatile biomass, *gasification* of biomass in

[2] The work in this chapter has been published: Lewis, A. D., E. G. Fletcher and T. H. Fletcher, "CO_2 Char Gasification Rates of Sawdust, Switchgrass, and Corn Stover in a Pressurized Entrained-Flow Reactor," *Energy & Fuels*, **28**, 5812-5825 (2014). Parts of this chapter were also included in a technical report (McDermott et al., 2014).

this chapter refers to heterogeneous reaction of the solid residue that results after pyrolysis (i.e., char) with CO_2.

Biomass char particle feeding rates around 0.3 g/hr were used to ensure single-particle behavior and to prevent clogging. The lowest void fraction in the feeding tube was about 0.99899, and in the reactor was 0.99994, corresponding to a spacing between particle centers of at least 12 particle diameters in the reactor (see Appendix D). Sufficient biomass char was fed during a single HPFFB experiment to perform an accurate ash test on the partially gasified collected char (see Section 4.8).

The matrix of biomass gasification experiments in this study is shown in Table 6.1. The experiments were conducted at three gas conditions at total pressures of 10 and 15 atm using peak centerline gas temperatures exceeding 1800 K. These gas temperature measurements as well as any other cited gas temperatures in this chapter have been corrected for radiation losses from a 422 μm-diameter B-type spherical thermocouple bead (see Appendix A). The correction of gas temperature in the near-burner region was approximately 100 K at the utilized HPFFB conditions. Post-flame gas compositions of the three HPFFB conditions are included in Table 6.1; the gasification conditions either contained ~40 or 90 mol% CO_2. The ranges of centerline gas temperatures and bulk CO_2 partial pressures in these experiments were 1266-1891 K and 6.1-13.5 atm, respectively. Complete details of experimental conditions and measured data are summarized in Appendix D.

Particle mass release was measured using Equation (4.6) at a minimum of three residence times per gas condition at typical collection heights of 1, 3, and 5.5 inches above the burner (see Figure 4.2). The first collection height typically near 1” above the burner served as a reference data point, since only the mass released after this first data point was used in the modeling. The

residence time of this first sample location is shown as the 'reference residence time' in Table 6.1. The three gas conditions in this chapter (see Table 6.1) are identified by the maximum centerline gas temperature measured at each condition, the total pressure, and the approximate mole percentage of CO_2 present in the post-flame gases. Details about the calculations for particle residence time were included in Section 4.6.

Table 6.1. Matrix of experiments for biomass CO_2 gasification tests

Total Pressure	Maximum Gas Temperature	Equilibrium CO_2, CO, N_2, H_2O	Reference Residence Time	Biomass Sample	Gasification Residence Times
15 atm	1848 K	89.8, 8.1, 1.2, 0.9 mol%	79 ms	PS	142; 267 ms
			57 ms	SG	139; 262 ms
			56 ms	CS	94; 136; 255 ms
10 atm	1808 K	89.2, 8.4, 1.2, 1.2 mol%	53 ms	PS	127; 239 ms
			51 ms	SG	122; 229 ms
			52 ms	CS	87; 126; 237 ms
15 atm	1891 K	40.8, 11.3, 46.6, 0.7 mol%	68 ms	PS	125; 234 ms
			47 ms	SG	113; 211 ms
			53 ms	CS	89; 128; 240 ms

6.1.1 Char Re-Injection Approach

The HPFFB CO_2 gasification experiments utilized pyrolyzed biomass chars generated at high heating rate as feedstock material. Biomass chars generated during rapid pyrolysis and short residence times have been reported as having high porosity and reactivity (Zanzi et al., 1996). The high volatile yields of biomass solely from pyrolysis (see Sections 2.2 and 5.2.1) required the use of a char re-injection approach to measure accurate mass release values from CO_2 gasification of the biomass chars. Since char gasification focuses on the conversion of the dry and ash-free solid after pyrolysis, this would have left approximately 1, 5, and 7 wt% of the daf starting mass available for conversion for polar sawdust, switchgrass, and corn stover, respectively, had char gasification experiments been conducted following *in-situ* pyrolysis.

The biomass char feedstocks for the HPFFB char gasification experiments were generated at atmospheric pressure and high heating-rate conditions in General Electric's Bench Scale Gasifier (BSG) down-flow drop tube reactor (Maghzi and Rizeq, 2011) (2.25" ID, 10 SLPM) by feeding raw, 150-250 μm biomass particles at a maximum gas temperature near 750 °C using a collection height of 34". The BSG environment in char-generation mode was primarily composed of N_2, but ~2 mol% O_2 was used during biomass char generation experiments to keep tar yields low. The O_2 used in the BSG experiments likely did not contribute to any significant char oxidation since each biomass char lost ~15 wt% daf mass during separate testing at pyrolysis conditions. The fact that the BSG-generated chars were not completely pyrolyzed suggests that the high mass of volatiles moving away from the particles during BSG char-generation experiments likely prevented O_2 from reaching the char surface. The BSG reactor allowed relatively quick production of biomass char due to its ability to feed biomass near 30 g/hr, which is about 45 times higher than the maximum clog-free feed rate of biomass in the HPFFB reactor. To better simulate commercial entrained-flow gasifiers where char gasification typically occurs after *in-situ* pyrolysis, it would have been preferable to have the biomass chars pyrolyzed and later gasified at the same total pressure, but this was not possible in this study due to limitations of both time and reactor configuration.

The method of re-injecting fully pyrolyzed chars to measure char oxidation data has been used previously by others when feeding coal (Hurt et al., 1998; Hecht et al., 2013; Shurtz and Fletcher, 2013) to overcome experimental challenges of measuring accurate mass release for sooty coals. Although the effect of re-injection on biomass char reactivity has not been reported (to the knowledge of the author), Hurt et al. (1998) reported that capture and re-injection of coal

char had little effect on the measured reactivity when feeding Illinois #6 coal through an entrained-flow reactor.

6.1.2 Biomass Char Shape

The BSG-produced poplar sawdust char (see Figure 6.1) was naturally spherical due to the high heating-rate char-generation conditions of the drop-tube reactor. The sawdust char in Figure 6.1 somewhat resembled Group I cenospheric coal char that is classified by large internal voids and thin walls; such coal particles have been reported as being more reactive than coal chars with lower porosity and thicker walls (Wall et al., 2002).

(a) (b)

Figure 6.1. SEM images at two magnifications of BSG-pyrolyzed poplar sawdust char later used in HPFFB CO_2 gasification experiments.

The poplar sawdust char was used directly in subsequent HPFFB gasification experiments without any additional preparation, and 80 wt% of this char was within the 77-139 μm range. It is interesting to note that spherical sawdust char has been observed in other studies after the pyrolysis of different species of wood sawdust at high heating rates (Zhang et al., 2006; Dupont et al., 2008; Lewis, 2011; Lewis and Fletcher, 2013) and has been attributed to melting of the

cell structure and plastic transformations (Cetin et al., 2004; Zhang et al., 2006). In contrast, no major morphological transformations of sawdust particles have been observed during pyrolysis at low heating rates (e.g., at 20 K/s by Cetin et al. (2004)). It appears that spherical sawdust char particles are obtained only after pyrolysis at high heating rates.

Chars generated in the BSG reactor from switchgrass and corn stover were not spherical, so the wheat grinder method (see Section 4.4) was used on these chars to produce near-spherical particles. After grinding these chars using low grinder speeds, these chars were sieved and only the 45-75 μm fraction was used in HPFFB experiments. Use of spherical char particles in char gasification experiments in the HPFFB reactor simplified calculation of residence times, particle temperatures, and gasification rate constants. Feeding only sphere-like char particles at entrained-flow conditions also guaranteed a much tighter distribution of particle residence times from a particular collection height above the burner, thus allowing a more precise time to be used in char gasification modeling.

Figure 6.2 and Figure 6.3 show optical microscope images of BSG-pyrolyzed switchgrass and corn stover chars, respectively, before and after grinding. The images in both figures are shown at the same magnification. The ground and sieved 45-75 μm fractions of switchgrass and corn stover chars are shown in Figure 6.2b and Figure 6.3b, respectively. The small char particles in this study were used to minimize temperature gradients within the particle, and represent a typical particle size used in industrial entrained-flow gasifiers.

The effect of grinding the BSG-pyrolyzed switchgrass char was estimated using particle measurements by ImageJ software (Schneider et al., 2012) from Figure 6.2a and Figure 6.2b (see Appendix D). The mass-mean aspect ratio (ratio of length to width) of particles in Figure 6.2a is 3.9, but was reduced after grinding in Figure 6.2b to 2.3. Grinding the switchgrass char a second

time would likely further decrease the mass-mean aspect ratio of the particles, but was not attempted due to the limited supply of switchgrass char available and concerns about having sufficient sample to complete a full set of char gasification experiments.

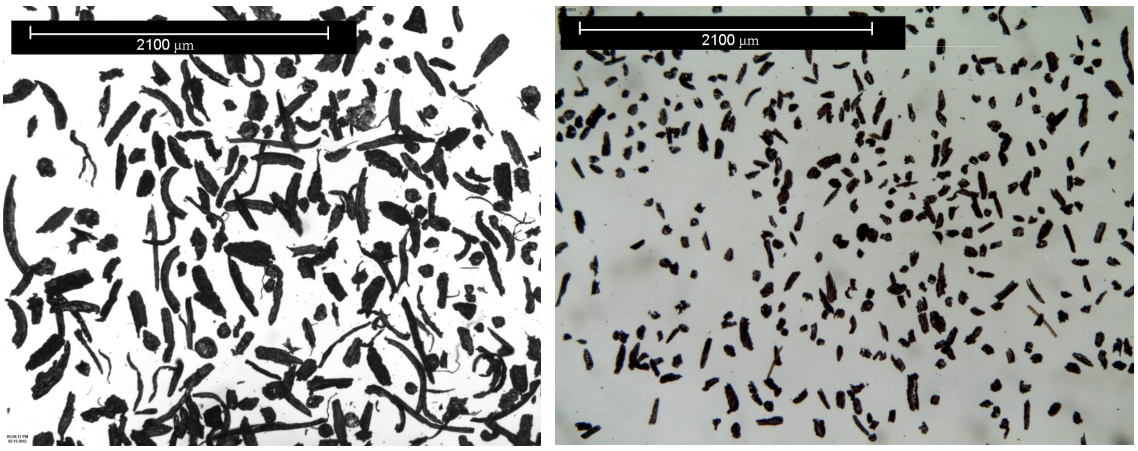

(a) (b)

Figure 6.2. BSG-pyrolyzed switchgrass char (a) before and (b) after grinding using a grinder at 35 volts.

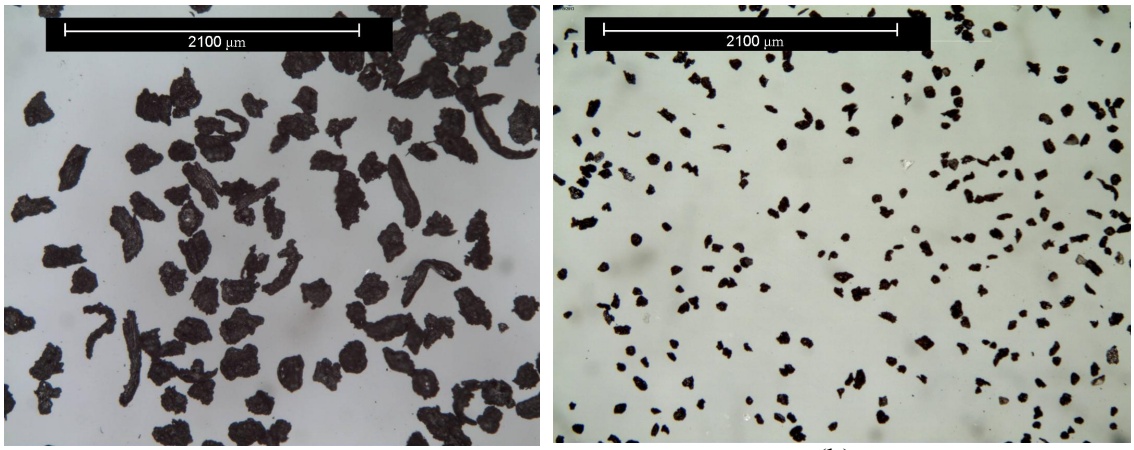

(a) (b)

Figure 6.3. BSG-pyrolyzed corn stover char (a) before and (b) after grinding using a grinder at 25 volts.

The diameters of the BSG-generated biomass chars were measured from optical microscope images of the biomass chars using ImageJ software(Schneider et al., 2012). The 'analyze particles' function of ImageJ was used to find areas of individual particles. Care was

taken not to include any areas from over-lapping particles, since ImageJ would mistakenly count this as one particle. Spherical particle diameters were then back calculated from the measured particle areas. The mass mean (d_m) was calculated from Equation (6.1) where w_i is the mass fraction of particles in a narrow bin size of diameter d_i.

$$d_m = \sum_{i=1}^{n} d_i \cdot w_i \tag{6.1}$$

Figure 6.4 shows the measured particle size distributions of the biomass feedstock chars that acted as feedstock material in HPFFB char gasification experiments. The size distributions in the figure are reported on a mass mean basis from measuring approximately 1200 particles per feedstock. The calculated mass mean diameters for the biomass chars are shown in Table 6.2, along with additional properties of the biomass chars. Three ash tests on the corn stover feedstock char resulted in a relatively large range of values, which explains the ± 8.2 wt% reported for this char in the table. Replicate ash tests on the sawdust and switchgrass chars yielded values within 3% of prior measurements.

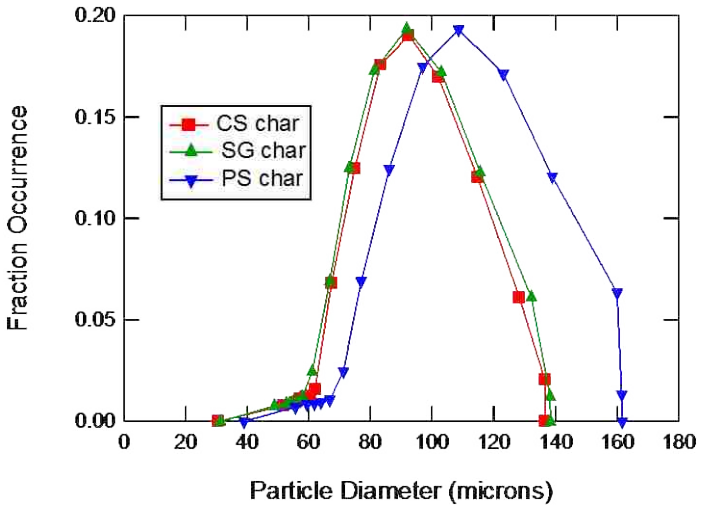

Figure 6.4. Particle size distribution of biomass chars (mass mean basis).

Table 6.2. Properties of biomass chars used in HPFFB char gasification experiments

Feedstock	PS char	SG char	CS char
sieve size (μm)	— [a]	45-75	45-75
mass mean size (μm)	102.7	86.2	87.2
C (wt% daf)	85.00	81.00	82.41
H (wt% daf)	2.43	2.63	2.66
N (wt% daf)	0.43	0.65	1.73
S (wt% daf)	0.07	0.21	0.60
O (wt% daf, by diff.)	12.08	15.50	12.61
ash (wt% dry)	7.01	24.44	65.43 ±8.2[b]
moisture (wt% as rec'd)	4.38	3.49	2.14
apparent density (g/cm^3)	0.283	0.334	0.837
N_2 surface area (m^2/g)	0.64	8.08	3.05
CO_2 surface area (m^2/g)	352	296	143

[a] unsieved, although 80 wt% was within the 77-139 μm range
[b] the ± here represents the difference between the mean value and the maximum or minimum value

6.2 First-Order Char Gasification Model

This section serves as the sole documentation of char gasification modeling in this dissertation. Therefore, this particular section is written in generic terms to include both CO_2 gasification modeling *and* H_2O gasification modeling, even though only CO_2 gasification experiments and modeling were performed for biomass chars (the topic of this chapter).

Numerous char gasification models of differing complexity (Molina and Mondragon, 1998; Liu and Niksa, 2004; Shurtz, 2011; Shurtz and Fletcher, 2013) have been proposed with the common objective of predicting the burnout rate of the char. However, highly complex models often have the drawback of being very computationally expensive, making them sometimes difficult to use in practical applications (Fermoso et al., 2009). Therefore, simpler models are sometimes preferred. The char mass release data from the HPFFB gasification experiments were modeled in this work with a relatively simple first-order global model (Goetz et al., 1982; Sowa, 2009; Lewis, 2011; Lewis et al., 2014b) where the rate (r_p'') is normalized by

particle external surface area. The model is a function of particle temperature, partial pressure of CO_2 or H_2O at the particle surface, external particle surface area, and time:

$$r_p'' = \frac{1}{A_p} \cdot \frac{dm_p}{dt} = -k_{rxn} \cdot P_{reac\tan t,surf} = -\left[A \cdot \exp\left(\frac{-E}{R \cdot T_p} \right) \right] \cdot P_{reac\tan t,surf} \qquad (6.2)$$

where A_p is the external surface area of the spherical particles ($4 \cdot \pi \cdot r^2$), m_p is the particle mass, t is time, k_{rxn} is the gasification rate constant, $P_{reactant,surf}$ is the partial pressure of CO_2 or H_2O at the particle surface, E is activation energy, A is the pre-exponential factor, T_p is the particle temperature, and R is the ideal gas constant. The rate in Equation (6.2) was numerically integrated, and is negative since particle mass is lost during char gasification. The kinetic parameters E and A for the model in Equation (6.2) were determined by minimizing the sum-squared error between measured and predicted particle mass release values from char gasification. Additional details about regressing optimal kinetic parameters for a first-order global gasification model have been documented by Lewis (2011).

Since only the gas temperature (T_{gas}) was measured, T_p was calculated from the transient particle energy balance at each time step:

$$m_p \cdot C_p \cdot \frac{dT_p}{dt} = h_c \cdot A_p \cdot (T_{gas} - T_p) + \varepsilon_p \cdot \sigma \cdot A_p \cdot (T_{surr}{}^4 - T_p{}^4) + \frac{dm_p}{dt} \cdot \Delta H_{rxn} \qquad (6.3)$$

where C_p is the particle heat capacity, h_c is the heat transfer coefficient ($Nu \cdot k_{gas}/d_p$), ε_p is the emissivity of the char particle, σ is the Stefan–Boltzmann constant (5.67×10^{-12} W/cm^2/K), ΔH_{rxn} is the heat of reaction for the CO_2 or H_2O gasification, and T_{surr} is the surroundings temperature of 500 K (see Appendix A). A value of 0.8 (Fletcher, 1989) was used for the emissivity of the char. The left-hand side of Equation (6.3) was set equal to zero with the assumption that the particle temperature is near steady state with its surroundings when using time steps of

approximately 0.15 ms. The first term on the right-hand side of Equation (6.3) represents the convective heat transfer term, which yielded positive values since T_{gas} was always greater than T_p in this gasification study. The second term in Equation (6.3) takes into account radiative heat transfer to the particle, and is negative when $T_p > T_{surr}$. In this study, the final term in Equation (6.3) takes into account particle cooling due to the endothermic H_2O/char or CO_2/char gasification reaction. The dm_p/dt term caused the final term to be negative, and ΔH_{rxn} was positive to account for the endothermic char gasification reaction. The convective heat transfer term was the most dominant of the three terms in the particle energy balance. The relative importance of the radiative heat transfer term compared to the endothermic gasification term in the particle energy balance varied between fuels and reaction conditions in this research. A plot depicting the relevant importance of different terms in the particle energy balance equation for poplar sawdust char is included in Appendix D. Also included in this appendix are the results of a sensitivity analysis where the terms ε_p and T_{surr} were evaluated for their effect on particle temperature.

Although the first-order gasification model in Equation (6.2) only implicitly accounts for any pore diffusion effects in the regressed kinetic parameters, mass transfer through the boundary layer of the particle is explicitly considered at each time step by equating it to the reaction rate:

$$k_{rxn} \cdot P_{reactant,surf} = \nu \cdot h_m \cdot \left(\frac{P_{reactant,\infty}}{R \cdot T_{gas}} - \frac{P_{reactant,surf}}{R \cdot T_p} \right) \tag{6.4}$$

which after algebra results in the following equation for the partial pressure of CO_2 or H_2O at the particle surface:

$$P_{reac\tan t,surf} = \frac{\nu \cdot h_m \cdot P_{reac\tan t,\infty}}{R \cdot T_{gas}\left[k_{rxn} + \frac{\nu \cdot h_m}{R \cdot T_p}\right]} \tag{6.5}$$

where v is the mass of carbon (i.e., char) that react per mole of CO_2 or H_2O reactant, h_m is the mass transfer coefficient ($Sh \cdot D_{AB}/d_p$), and $P_{reactant,\infty}$ is the partial pressure of CO_2 or H_2O in the bulk gas. In the case of CO_2 or H_2O char gasification, v was (12 g C/ (1 mol CO_2 or H_2O)) from the following reactions:

$$C + CO_2 \rightarrow 2\ CO$$
$$C + H_2O \rightarrow CO + H_2$$

Coefficients and correlations from the Gordon-McBride database (McBride et al., 2002) were used to model the heat of reaction, ΔH_{rxn}, for the char/CO_2 or char/H_2O gasification reaction at each particle temperature. The approximate values of ΔH_{rxn} were 13,700 and 11,200 J/gm for the char/CO_2 and char/H_2O gasification reactions, respectively. Char was assumed to have the properties of graphite for the calculations of the heat of reaction, as other researchers have assumed previously (Hurt et al., 1998; Shurtz and Fletcher, 2013). The binary diffusion coefficients (D_{AB}) used to calculate the mass transfer coefficient (h_m) came from published values (Incropera and Dewitt, 2002), those fit to an empirical equation based on Chapman-Enskog kinetic theory (Mitchell, 1980), and those predicted by corresponding-states methods (Bird et al., 2002). The diffusion coefficient was inversely proportional to pressure, directly proportional to temperature raised to a power, and evaluated at the film temperature (average of T_{gas} & T_p). The gas thermal conductivity (k_{gas}) was also evaluated at the film temperature, and estimated using the mole weighted average of individual gas species present in the HPFFB post-flame environments.

6.3 Considerations of Biomass Char Gasification Modeling

The decrease in external surface area with increased char conversion was included in the gasification modeling of sawdust, switchgrass, and corn stover chars. These values came from particle diameter measurements using Image J (Schneider et al., 2012) software of the gasified biomass chars collected from the HPFFB reactor (see Section 6.1.2 & Appendix D).

Similar to the reaction environment in a commercial gasifier, CO and CO_2 both were present in the post-flame region of the HPFFB reactor in the biomass gasification experiments. The amount of CO present in the three gas conditions used in this study was about 10 mol% (see Table 6.1), which is important to at least consider since CO is known to inhibit the CO_2/char gasification reaction (Wall et al., 2002). The Char Conversion Kinetics (CCK) (Shurtz, 2011; Shurtz and Fletcher, 2013) coal model was run for 90 μm Illinois #6 coal char at conditions representative of the 3 conditions used in this study (see Table 6.1) to estimate the effect of the presence of CO on the measured particle mass release in the biomass char gasification HPFFB experiments. The values used to model Illinois #6 coal char by the CCK code were the following: E_7 = 35 kcal/mol, $A_{7,0}$ = $3.943 \cdot 10^8$ s^{-1}, Ψ_0 = 0, and τ/f = 12 (Shurtz and Fletcher, 2013). The CCK model uses a 5-step gasification kinetic mechanism that enables the effect of CO inhibition to be evaluated; the model predicted that the final daf mass release values (char basis) for the coal char were on average 13.6% lower than when the char gasification occurred at conditions free of CO. The CO inhibition effect may have been of similar magnitude in the biomass gasification measurements. However, with the limited data available, the first-order modeling of biomass char gasification performed in this research did not treat the effect of CO inhibition. It is interesting to note that two research groups (Turkdogan and Vinters, 1970; Illerup and Rathmann, 1996) showed that for biomass char the effect of CO inhibition decreases as

temperature increases; the biomass experiments in the current study were conducted at high temperature.

6.4 Mass Release Summary and Representative Temperature Profile

Mass release data were measured for corn stover char at an additional collection height of 2" above the burner after noting that no significant mass release occurred for this biomass between the collection heights of 3 and 5.5 inches. The asymptotic mass release values after the 3" collection height may have been caused by ash inhibition where an inorganic-rich layer creates additional resistance to CO_2 accessing the remaining organic material in the char particle (Hurt et al., 1998). The corn stover char particles collected at the 3" and 5.5" collection heights contained about 90 wt% ash on a dry basis. Other possible explanations for the asymptotic mass release values of corn stover char after the 3" collection height may include thermal annealing and volatilization of catalytically active species. Only the mass release data measured at the collection heights of 1", 2", and 3" were used in the modeling of corn stover char since the model in Equation (6.2) does not consider ash inhibition or other complicating factors.

A summary of the measured biomass char mass release data (on an as-received char basis) from the HPFFB reactor is presented in Table 6.3. Replicate experiments were performed on about one-third of the conditions; the uncertainty in the mass release based on repeated measurements was about ± 3 wt% daf. The data in Table 6.3 were used to fit kinetic coefficients for the gasification model in Equation (6.2), and the results are presented below.

Table 6.3. Summary of mass release data used in gasification modeling on an as-received char basis

Total Pressure	Max Gas Temperature	Equilibrium CO_2	PS Res. Time	PS %MR (daf)	SG Res. Time	SG %MR (daf)	CS Res. Time	CS %MR (daf)
15 atm	1848 K	89.8 mol%	79 ms	45.7	57 ms	44.1	56 ms	40.4
			142 ms	56.4	139 ms	60.8	94 ms	76.8
			267 ms	78.6	262 ms	79.1	136 ms	89.0
10 atm	1808 K	89.2 mol%	53 ms	25.5	51 ms	45.2	52 ms	48.5
			127 ms	42.4	122 ms	51.0	87 ms	71.0
			239 ms	62.4	229 ms	61.9	126 ms	81.5
15 atm	1891 K	40.8 mol%	68 ms	31.0	47 ms	38.0	53 ms	55.5
			125 ms	54.4	113 ms	62.4	89 ms	64.9
			234 ms	67.0	211 ms	79.3	128 ms	81.4

As previously stated, the first collection height typically near 1" above the burner served as a reference data point, and only the mass lost after this first collection height was used in the gasification modeling to prevent uncertainties in the temperature history near the burner from affecting the regressed kinetic parameters in this study. Using the first collection height as a reference for mass loss also prevented any mass released due to incomplete pyrolysis during the BSG-char generation experiments from being falsely attributed to CO_2 gasification of the biomass char in the HPFFB re-injection experiments.

Representative gas and particle temperature profiles are shown in Figure 6.5 for the 45-75 μm switchgrass char at the 15 atm $T_{gas,max}$ = 1891 K HPFFB condition where the post-flame CO_2 concentration was near 40 mol%. Equation (6.3) was used to calculate the particle temperature profile in the figure. Other temperature profiles can be found in Appendix D.

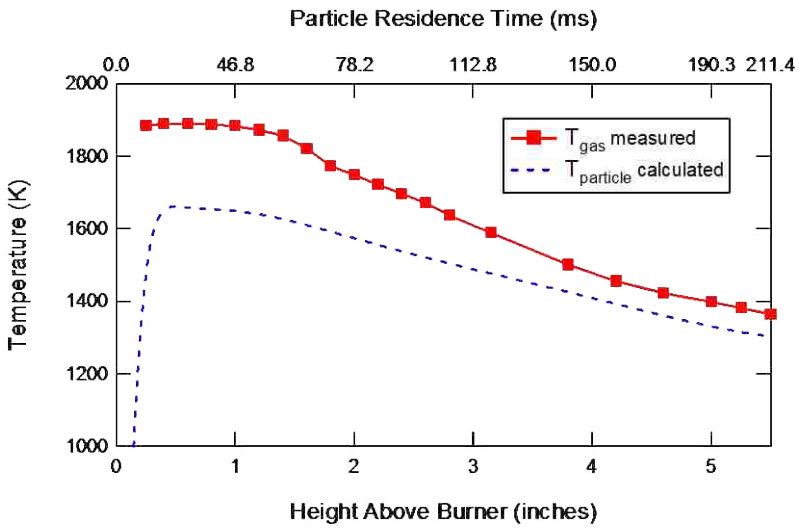

Figure 6.5. Measured centerline gas temperature profile and calculated particle temperature profile at the 15 atm/40 mol% CO_2 HPFFB experimental condition for 45-75 µm near-spherical BSG switchgrass char.

6.5 Biomass Char Gasification Modeling Results

Table 6.4 includes a summary of the optimal biomass kinetic parameters for use in the first-order gasification model in Equation (6.2). The reported kinetic parameters in the table were verified to be independent of time step; changing the time step from ~0.15 ms to ~0.075 ms changed values of the kinetic coefficients by less than 0.25%. Since pyrolysis conditions can affect biomass gasification reactivity (Mermoud et al., 2006), it is important to emphasize that the kinetic parameters in Table 6.4 were for biomass chars of small diameter prepared at high heating rate for short residence times (<3 s) at atmospheric pressure that were then gasified at pressurized conditions of 10 and 15 atm in the HPFFB reactor.

Calculated ranges of T_p and $P_{CO2,surf}$ for the three biomass data sets are included in Table 6.4, as calculated by Equations (6.3) and (6.5), respectively. The ranges of T_p and $P_{CO2,surf}$ for corn stover in the table only include values up to the 3" collection height, since the data at the 5.5" collection height was not included in the modeling, as previously discussed. The +/- values

reported in Table 6.4 for A, T_p, and $P_{CO2,surf}$ for corn stover are included since a relatively large range of ash percentages (i.e., 65.4 ± 8.2 wt%) were measured for this particular biomass feedstock. This uncertainty in ash content affected corn stover char gasification rates, which describe the conversion of the organic material (i.e., dry mass*(1- x_{ash})).

Table 6.4. Summary of first-order kinetic parameters and reaction conditions for CO_2 gasification of biomass chars in the HPFFB reactor

	Poplar Sawdust Char	**Switchgrass Char**	**Corn Stover Char**
A (g/cm^2/s/atm CO_2)	747.92	191.23	622.73 (± 18.2)
E (kJ/mol)	175	175	175
relative error (char basis[c])	5.26%	6.24%	6.01%
pyrolysis conditions	high heating rate at 1 atm	high heating rate at 1 atm	high heating rate at 1 atm
max conversion (daf wt%, char basis[d])	74.8	73.5	87.2
Condition Identifier Total Pressure; $T_{gas,max}$; mol% CO_2	**Poplar Sawdust Char** T_p range $P_{CO2,surf}$ range	**Switchgrass Char** T_p range $P_{CO2,surf}$ range	**Corn Stover Char** T_p range [e] $P_{CO2,surf}$ range [e]
15 atm; 1848 K; ~90% CO_2	1211 – 1441 K 10.2 – 12.8 atm	1227 – 1560 K 10.9 – 13.1 atm	1366 – 1482 K ± 10 9.8 – 12.1 atm ± 0.1
10 atm; 1808 K; ~90% CO_2	1205 – 1493 K 6.6 – 8.5 atm	1219– 1588 K 7.4 – 8.6 atm	1376– 1509 K ± 13 6.7 – 8.1 atm ± 0.1
15 atm; 1891 K ~40% CO_2	1282 – 1534 K 4.3 – 5.7 atm	1303 – 1651 K 4.8 – 5.9 atm	1452 – 1576 K ± 5 4.2 – 5.2 atm ± 0.1

[c] as-received char basis [d] fully pyrolyzed char basis
[e] only includes data measured at collection heights up to 3" above the burner

Several researchers have noted that biomass gasification rates are not constant for the full range of conversions (Espenas, 1993; Illerup and Rathmann, 1996; Marquez-Montesinos et al., 2002; Struis et al., 2002; Ollero et al., 2003; Cetin et al., 2005b; Gomez-Barea et al., 2006; Zhang et al., 2008; Di Blasi, 2009; Yuan et al., 2011). Hence, the kinetic parameters summarized in Table 6.4 gave satisfactory estimates of particle mass release due to CO_2 gasification up to the measured conversions listed in the table. Figure 6.6 illustrates the fit of the first-order model in Equation (6.2) with biomass char gasification mass release data at two conditions, even though

similar plots could be produced for each biomass char and HPFFB gas condition combination (see Table 6.1). Figure 6.6a compares the model fit of measured poplar sawdust char data at the 15 atm ~40 mol% CO_2 HPFFB condition while Figure 6.6b is a similar plot of switchgrass char data at the 15 atm ~90 mol% CO_2 condition. The mass release values measured at the lowest residence times served as initial conditions for the modeling, and the measured mass release values at the two higher particle residence times were used to evaluate predicted gasification rates.

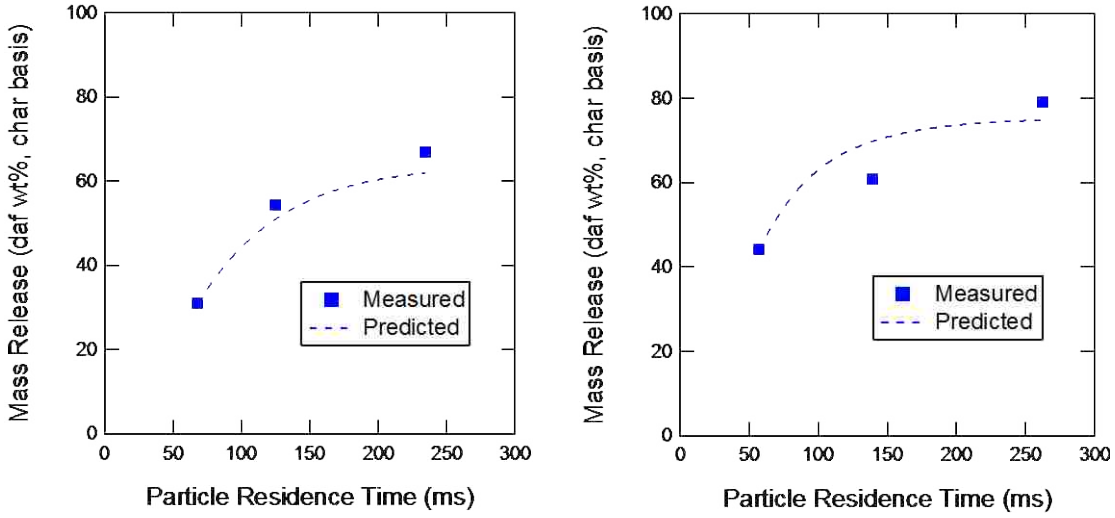

Figure 6.6. Comparison of measured and modeled mass release (as-received char basis) of (a) BSG poplar sawdust char at the 15 atm ~40 mol% CO_2 HPFFB condition and (b) near-spherical BSG switchgrass char at the 15 atm ~90 mol% CO_2 HPFFB condition.

Figure 6.7 includes parity plots for all three biomass data sets, which shows how the predicted first-order gasification rates compared with measured biomass mass release data on a daf char basis. As was the case for Table 6.4, the corn stover data in Figure 6.7c only included values up to the collection height of 3" above the burner. The relative error values reported in Table 6.4 indicate the quality of fit of the model to measured mass release values on a char basis, and were calculated by:

$$\text{Re}\,lative\ Error = \frac{\sqrt{\sum_{i=1}^{n}\left(\frac{X_i^{\,M} - X_i^{\,E}}{X_i^{\,E}}\right)^2}}{n} \times 100 \tag{6.6}$$

where X_i^M and X_i^E are defined as the modeled and experimental particle mass release points, respectively. Maximum relative errors of only 5 to 6% are especially encouraging.

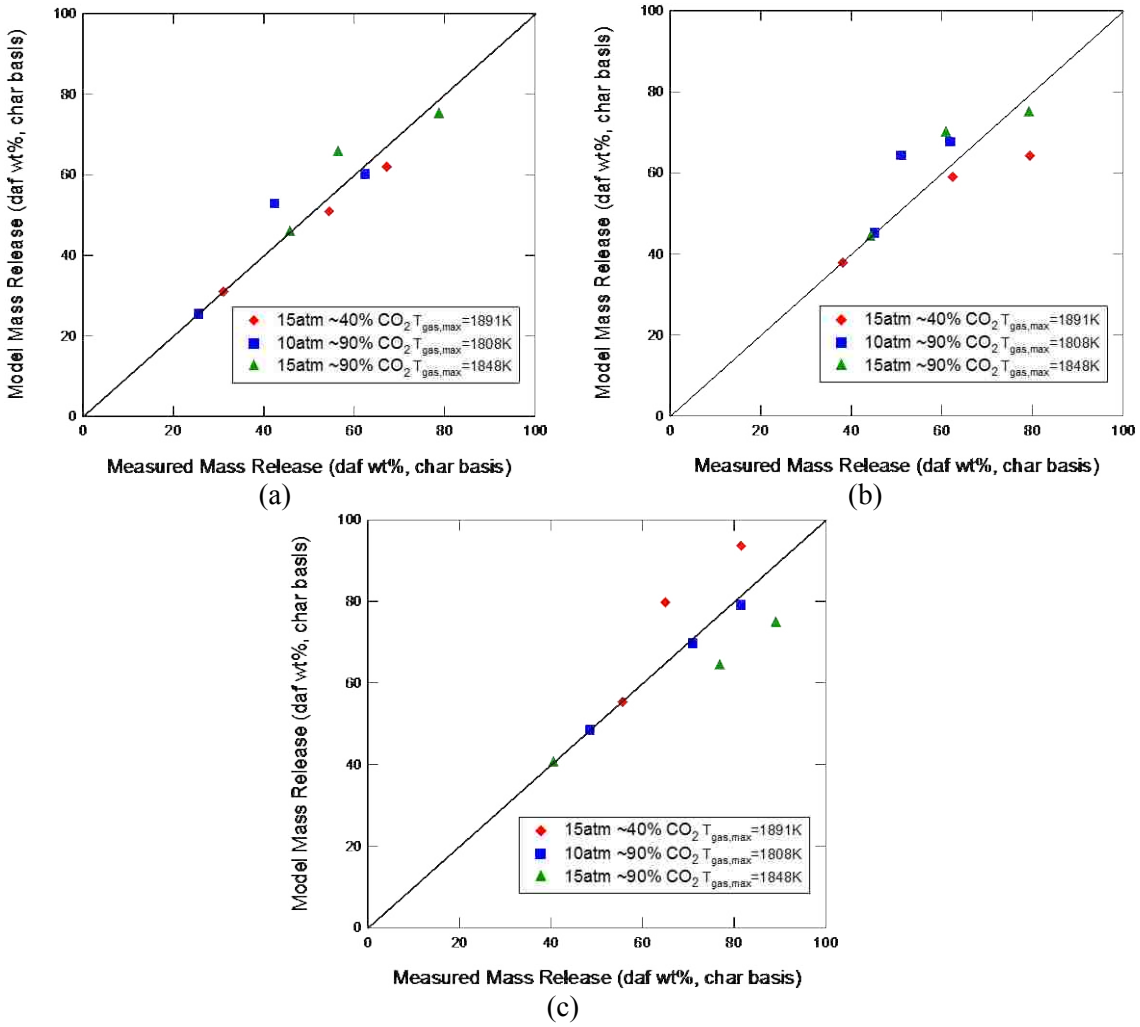

Figure 6.7. Parity plots of HPFFB CO_2 gasification data of (a) poplar sawdust, (b) switchgrass, and (c) corn stover chars with a first-order model on an as-received char basis.

The parameter E was fixed at 175 kJ/mol for all 3 biomass chars since this value provided a good fit of all the biomass data (see Section 6.2). Using the same E value for all the biomass chars made convenient comparisons of gasification rates by simply comparing A values in Table

6.4 of the different biomass chars. For example, the poplar sawdust char/CO_2 gasification rate (r_p'') was about 3.9 (i.e., 748/191) times higher than for switchgrass char. The gasification rate of the sawdust char was only 17 to 24% higher than the corn stover char. The range of values stems back to the uncertainty in the ash fraction (x_{ash}) of the corn stover char feedstock material (see Table 6.2); uncertainty in ash fraction affects daf char gasification rates which describe conversion of the organic fraction (i.e., dry mass*(1- x_{ash})). A visual comparison of the CO_2 gasification rates of the 3 biomass chars is included in Figure 6.8 at a CO_2 partial pressure of 7.4 atm; the range of values shown for corn stover char in the figure are due to ash fraction uncertainty of this feedstock, as just described.

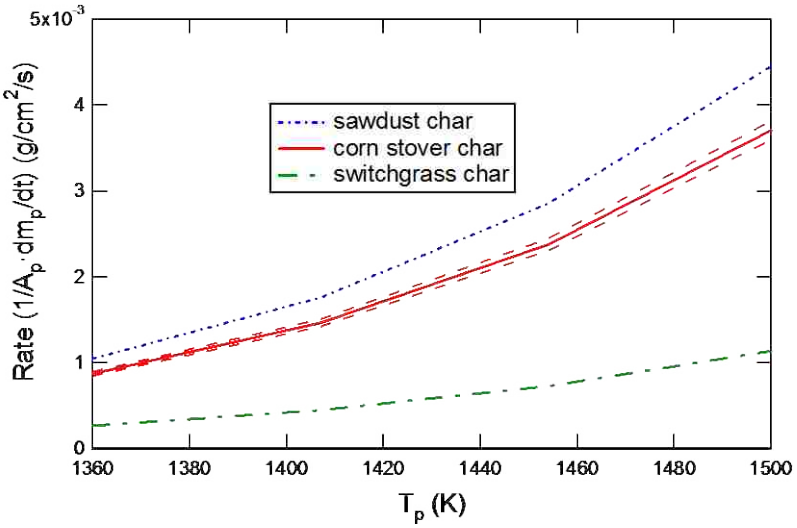

Figure 6.8. Comparison of calculated biomass char/CO_2 gasification rates at $P_{CO2,surf}$ = 7.4 atm using kinetic coefficients in Table 6.4 in Equation (6.2).

It is important when reporting particle rates at high temperature to document the extent that film diffusion of reactant gas through the particle boundary layer affected the measured rates. The maximum rate occurs when the rate is limited entirely by diffusion of reactant gas to the particle surface, which occurs at high temperature when the concentration of reactant gas at the particle surface is approximately zero. The chi factor, χ, (Smith, 1982; Smith et al., 1994)

provides an indication of the effect of film diffusion on heterogeneous rates and was calculated for all the biomass chars at the HPFFB gasification conditions. It is defined as the measured rate divided by the maximum rate under film-diffusion control:

$$\chi = \frac{k_{rxn} \cdot P_{reac\,tant,surf}}{\nu \cdot h_m \cdot \left(C_{reac\,tant,\infty}\right)} = \frac{k_{rxn} \cdot P_{reac\,tant,surf}}{\nu \cdot h_m \cdot \left(\frac{P_{reac\,tant,\infty}}{R \cdot T_{gas}}\right)} \tag{6.7}$$

where $C_{reactant,\infty}$ and $C_{reactant,surf}$ are defined as the concentration of gasification reactant gas in the bulk and at the particle surface, respectively, while all other parameters were defined previously (see Section 6.2). The chi factor ranges from 0 to 1; the surface reaction controls when χ is much less than 1 while film diffusion controls entirely when χ approaches unity. The maximum χ factor in the biomass data sets was 0.17, which indicates that the measured rates did not occur in the Zone III regime (Smoot and Smith, 1985) where film diffusion controls.

The biomass chars in this study were generated at atmospheric pressure in the BSG drop tube reactor, and then gasified at pressurized conditions of 10 and 15 atm in the HPFFB reactor. Hence, the char gasification rates reported in this study may need to be modified slightly to model biomass conversion in an entrained-flow gasifier after *in-situ* pyrolysis, where the high heating-rate biomass char generated at pressurized conditions would be gasified at the same elevated pressure. Insight about this can be drawn from experiments in the literature, which were reviewed in Section 2.2.8.4. Although the three research groups (Illerup and Rathmann, 1996; Cetin et al., 2005b; Okumura et al., 2009) did not reach the same conclusion for the effect of pyrolysis pressure on biomass gasification reactivity, the reported rates in this work would be pertinent to both pressurized staged gasifiers (Mermoud et al., 2006) and char recycling systems

(Matsumoto et al., 2009) which gasify biomass char after atmospheric-pressure pyrolysis in a separate reactor.

6.6 Comparisons with the Literature

Since the maximum residence time available in commercial entrained-flow gasifiers is on the order of seconds, it is known that significant particle conversion due to gasification is achieved in short times at the high temperatures, pressures, and particle heating rates characteristic of such reactors. The current study reports CO_2 gasification of three biomass chars where significant conversions were measured in <270 ms during entrained-flow experiments at high temperatures and CO_2 partial pressures. Matsumoto et al. (2009) also measured significant biomass conversions in short times (<3 s) when gasifying 50-100 μm barkless Japanese cedar char in a drop tube furnace at a total pressure of 4 bar in 50% CO_2 at gas temperatures 900 to 1200 °C.

The current study and the results of Matsumoto et al. (2009) are in contrast to many TGA studies in the literature where appreciable conversion of biomass char by gasification typically required minutes. For example, Gómez-Barea et al. (2006) reported that full conversion of <60 μm wood matter from pressed-oil stone was attained at atmospheric pressure after ~2 minutes at 950 °C in a TGA where the maximum CO_2 partial pressure was 0.5 bar. The data of Yuan et al. (2011) show that 56-180 μm pine sawdust char that had been prepared in a high-frequency furnace reached 50% and 100% conversions in about 2 and 4.5 minutes, respectively, when gasified by pure CO_2 in a TGA at 1000 °C and atmospheric pressure. Mani et al. (2011) reported data where <60 μm wheat straw char that had been pyrolyzed for 45 minutes at 500 °C required about 4.8, 7.8, 12.6, and 44 minutes to reach 50% conversion by pure CO_2 at temperatures of

900, 850, 800, and 750 °C, respectively, in a TGA at atmospheric pressure. The CO_2 gasification TGA data of Cetin et al. (2005b) showed that radiata pine char (120-180 μm) took ~4.5 minutes to reach 73% conversion at 1000 °C and atmospheric pressure. In the same work, Cetin et al. also showed that 120-180 μm radiata pine char generated at 20 bar took about 6 minutes to progress in conversion from 10% to 80% when gasified isothermally in a pressurized TGA at 900 °C using typical sample sizes of 5 g at a total pressure of 20 bar in 50% CO_2. It must be noted that Cetin's 20-bar gasification experiment certainly had mass transfer limitations since a large 5-g bed of low-density biomass char particles was used. Some explanations of the differences in biomass gasification rates measured in the entrained-flow experiments vs TGA experiments include differences in pyrolysis heating rate (Kumar and Gupta, 1994; Zanzi et al., 1996; Chen et al., 1997; Fushimi et al., 2003; Cetin et al., 2005a; Mermoud et al., 2006; Okumura et al., 2009), soaking time (Nandi and Onischak, 1985; Chen et al., 1992; Kumar and Gupta, 1994; Mermoud et al., 2006), CO_2 partial pressure, and the ease at which the reactant gas can access the char particles.

Although the gasification rates of biomass char measured in this research and also by Matsumoto et al. (2009) appear fast compared to many TGA-measured gasification rates, it is interesting that a relatively quick reaction time was predicted for the CO_2 gasification of 75-106 μm pine wood char using a rough calculation that neglected pore diffusion effects. This calculation utilized the TGA-measured rates of Fermoso et al. (2009) at an extrapolated temperature of 1225 °C, where it is predicted that the pine wood char would react to 50% conversion in ~3 s at a total pressure of 10 bar in pure CO_2. This prediction utilized reported (Fermoso et al., 2009) rate constants (E_a =164.4 kJ/mol, k_o =3.14·10^6 min^{-1}, ψ =15.2) in the random pore model. For documentation purposes, the pine char in the study of Fermoso was

generated at atmospheric pressure in a drop tube reactor at 1000 °C using a particle residence time near 7 s.

Although CO_2 gasification rates of biomass char were the focus of this chapter, a short discussion of biomass steam gasification rates relative to CO_2 rates is included here since steam is the other major gasification agent that is generally accepted as more reactive. Rensfelt et al. (1978) reported that steam gasification of wood is about twice as fast as CO_2 gasification after observing that the latter required a higher temperature of 30 degrees to attain the same rate. The data of Ahmed and Gupta (2011) showed that yellow pine woodchip char was 2-3 times more reactive to steam than CO_2 when gasification took place at 900 °C at a total pressure of 2 bars and partial pressures of gasifying agent ranging from 0.6 to 1.5 bars. It was reported by Guizani et al. (2013) that the average gasification reactivity (from 20-90% conversion) of both low and high heating-rate beech wood chars was about twice as high for steam than CO_2 at 900 °C and atmospheric pressure using a partial pressure of reactant gas near 0.2 atm. The gasification rates reported by Matsumoto et al. (2009) for Japanese cedar char indicated that steam gasification rates were only faster than CO_2 gasification rates above a *gas* temperature of 1000 °C in a drop tube furnace operated at 4 bar in the temperature range 900-1200 °C. However, the CO_2 and steam gasification comparisons of Matsumoto et al. would have been more useful had they been reported as a function of *particle* temperature and not *gas* temperature.

6.7 Summary

Gasification rates of near-spherical poplar sawdust, switchgrass, corn stover chars by CO_2 were measured in a pressurized flat-flame burner reactor at conditions relevant to an entrained-flow gasifier. Small char particles (~100 μm) were gasified at total pressures of 10 and

15 atm using peak gas temperatures up to 1891 K at conditions where the bulk phase consisted of ~40 and ~90 mol% CO_2. Mass change due to CO_2 gasification of the char was measured for the 3 biomass feedstocks, and was used to regress optimal kinetic parameters using a global first-order model. The effects of CO inhibition were estimated to be relatively small in these conditions, based on calculations made using the coal CCK model.

A new method was developed to produce near-spherical particles from non-spherical biomass chars, which works well even when only limited quantities of biomass char are available. Poplar sawdust char generated at high heating rates was naturally spherical after passing through a plastic stage during pyrolysis. It appears that spherical sawdust particles are only formed after pyrolysis of small particles at high heating rates.

The corn stover char exhibited possible signs of ash inhibition in the gasification experiments by reaching asymptotic mass release values after ~130 ms when the char was composed of about 90 wt% ash (dry basis). Low χ values indicated that the biomass gasification experiments were far from the film diffusion controlled regime.

Over the range of experimental conditions studied, the char CO_2 gasification rate per external surface area (r_p'') for poplar sawdust char was about 3.9 times faster than for switchgrass char, but only about 20% faster than corn stover char. The entrained flow gasification rates measured in this chapter are much faster than those reported in most TGA studies.

7. CO_2 Gasification of Petroleum Coke

CO_2 gasification rates are reported for two petroleum coke chars generated following *in-situ* pyrolysis in the high-pressure flat-flame burner reactor at elevated pressure (10-15 atm), high temperature ($T_{gas,max}$ > 1800 K), and rapid initial particle heating rate (up to 7.6×10^4 K/s). The morphology of the two petcoke chars was studied using SEM images of the chars. A CO_2 gasification rate comparison between petcoke and coal char at pressurized entrained-flow conditions is also provided.[3]

7.1 Petroleum Coke Samples

Two commercially obtained petroleum coke (see Section 2.1.3), or petcoke, samples were studied in this research. The origin and crude oil feedstock from which the petcoke samples originated are proprietary to the companies that supplied the petcokes. The samples are referred to as 'Petcoke A' and 'Petcoke B' in this work. Petcoke A has been used in previous research (Lewis, 2011). The petcoke samples were ground using an electric grinder (Blendtec Kitchen Mill) and sieved to collect the 45-75 μm size range, which was used in all the experiments. Putting ground petcoke on the sieves tended to clog the sieves with fine particles. To overcome

[3] The work in this chapter has been published: Lewis, A. D., E. G. Fletcher and T. H. Fletcher, "CO_2 Gasification Rates of Petroleum Coke in a Pressurized Flat-Flame Burner Entrained-Flow Reactor," *Energy and Fuels,* **28**, 4447-4457 (2014).

this, a shop vacuum was used to clean the sieves repeatedly during sample preparation. The small particles (45-75 μm) were used in experimentation to ensure a high initial heating rate of the particles, to assume no temperature gradients within the particle for modeling, and to represent the pulverized particle size used in industrial entrained-flow gasifiers.

Figure 7.1 shows SEM images of the sized petcoke samples. Properties of the feedstocks used in this study are included in Table 7.1. Information regarding Illinois #6 coal and its char are included in this table since coal was used in a limited number of experiments reported in this chapter. Recall that details about measurement techniques were included in Section 4.8. The measured values of petcoke properties in Table 7.1 agree well with values in the literature (Kairaitis and Tyler, 1983; Marsh et al., 1985; CONCAWE, 1993; Ellis and Paul, 2000b; Ibrahim, 2005; API, 2007; Malekshahian and Hill, 2011a).

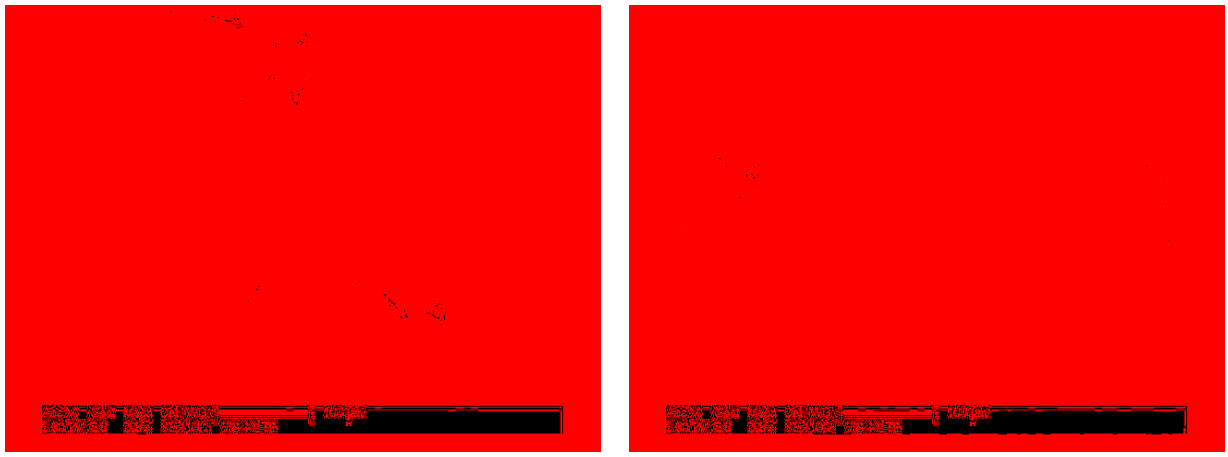

(Petcoke A) (Petcoke B)

Figure 7.1. SEM images of raw petcoke samples collected from the 45-75 micron sieve tray.

Note that the ash composition values in Table 7.1 do not sum to 100, since the elements existed as oxides (i.e., Na_2O, MgO, Al_2O_3, SiO_2, SO_3, K_2O, etc.) after they were collected following an ash test at 750 °C in air. The balance of the ash composition is therefore composed

of elemental oxygen. The parent crude oil from which the petcoke samples originated determined the chemical composition of the ash.

Table 7.1. Properties of petcoke feedstocks

Feedstock	Petcoke A	Petcoke B	ILL #6 coal	ILL #6 char	Composition of Ash[a] (wt%)	Petcoke A	Petcoke B
sieved particle size (μm)	45-75	45-75	45-75	75-106	Na	1.0	3.2
mass mean size (μm)	63.0	57.6	64.3	85.3	Mg	0.1	1.4
C (wt% daf)	87.93	91.09	75.08	—	Al	0.9	6.2
H (wt% daf)	1.82	3.77	5.21	—	Si	3.9	12.3
N (wt% daf)	1.77	1.33	1.34	—	S	0.4	1.1
S (wt% daf)	6.32	2.88	4.35	—	K	0.7	1.4
O (wt% daf, by diff.)	2.16	0.93	14.02	—	Ca	2.2	4.5
volatiles (wt% daf)[b]	8.78	10.52	44.46	—	Ti	0.3	1.0
ash (wt% dry)[b]	0.35	0.30	6.98	13.41	V	37.6	11.2
moisture (wt% as rec'd)[b]	1.29	0.20	3.45	2.4	Fe	9.1	17.5
apparent density (g/cm^3)	1.58	1.21	1.15	0.16	Ni	9.8	7.6
					Cr	1.8	—
N_2 surface area (m^2/g)	7.5	0.3	44.6	189.2	Zn	—	2.2
CO_2 surface area (m^2/g)	187.3	107.4	128.3	342.6	P	—	0.9

[a] prepared at 750 °C. These elements appear as oxides in the ash, but the wt% oxygen is not reported here since the performed analysis reported the non-oxidized metal form. [b] ASTM analysis

7.2 Petcoke Gasification Experiments

The high-pressure flat-flame burner reactor (HPFFB; see Section 4.2) was used to measure mass release caused by CO_2 gasification of the petcoke chars following *in-situ* pyrolysis. The HPFFB reactor allowed petcoke char burnout to be measured at conditions relevant to industrial entrained-flow gasifiers by reacting small particles (45-75 μm) in entrained-flow at high temperatures and pressures for short times (< 0.3 s). Since the petcoke chars in this study were generated and reacted at similar conditions as in commercial entrained-flow gasifiers, the measured rates are especially meaningful. For instance, the petcoke chars for which rates are reported in this study would presumably contain a similar char structure as char generated in industrial entrained-flow gasifiers, thus capturing the effect of representative char structure on the burnout of residual char (Wall et al., 2002).

The matrix of petcoke gasification experiments is shown in Table 7.2. The experiments were conducted at four gas conditions at total pressures of 10 and 15 atm using peak centerline gas temperatures exceeding 1800 K. Gas temperature measurements in this chapter have been corrected for radiation losses from a B-type spherical thermocouple bead (see Appendix A). The correction of gas temperature in the near-burner region was approximately 105 K at the utilized HPFFB conditions. Post-flame gas compositions of the three HPFFB conditions are included in Table 7.2; the gasification conditions either contained ~40 or 90 mol% CO_2. The ranges of centerline gas temperatures and bulk CO_2 partial pressures in these experiments were 1266-1909 K and 4.1-13.5 atm, respectively. Complete details of experimental conditions, and measured data are summarized in Appendix E.

Particle mass release was measured at three residence times per gas condition at typical collection heights of 1, 3, and 5.5 inches above the burner using particle feeding rates around 1 gm/hr. The four gas conditions in this chapter (see Table 7.2) are identified by total pressure, the maximum measured centerline gas temperature, and the mole percentage of CO_2 in the post-flame environment. Petcoke gasification experiments utilized the same HPFFB gas conditions as the biomass gasification experiments (see Table 6.1). However, one additional gas condition (i.e., 10 atm $T_{gas,max}$ = 1909 K ~40 mol% CO_2) was used when feeding petcoke since time permitted these extra experiments to be performed. The first collection height that was near 1" above the burner served as a reference data point, since only the mass release measured after this first collection point was used for gasification modeling. The residence time of this first sample location is included as the 'reference residence time' in Table 7.2. Details about the calculations for particle residence time were included in Section 4.6.

Table 7.2. Matrix of experiments for petcoke CO_2 gasification tests

Total Pressure	Maximum Gas Temperature	Equilibrium CO_2, CO, N_2, H_2O	Pyrolysis / Reference Residence Time	Petcoke Sample	Gasification Residence Times
15 atm	1848 K	89.8, 8.1, 1.2, 0.9 mol%	59 ms	A	142; 265 ms
			60 ms	B	146; 275 ms
10 atm	1808 K	89.2, 8.4, 1.2, 1.2 mol%	73 ms	A	130; 244 ms
			57 ms	B	137; 258 ms
15 atm	1891 K	40.8, 11.3, 46.6, 0.7 mol%	56 ms	A	137; 259 ms
			60 ms	B	124; 231 ms
10 atm	1909 K	40.7, 11.0, 46.8, 0.9 mol%	52 ms	A	125; 232 ms
			57 ms	B	119; 219 ms

7.3 Mass Release of Petcoke

Mass release caused by CO_2 char gasification was measured for Petcokes A and B following *in-situ* pyrolysis in the HPFFB reactor. Measured mass release after the first collection height was attributed solely to CO_2 gasification of the char since pyrolysis was completed by this point. Any mass release from steam gasification was assumed to be negligible due to its low partial pressure (i.e., ~0.12 atm) in the experiments (see Table 7.2). Although it is possible to calculate mass release using ash as a tracer (see Section 4.7), this method was not utilized for petcoke experiments since ash vaporized from Petcoke A when fed through the HPFFB reactor in a previous study (Lewis, 2011). The ash-tracer method of calculating mass release only yields correct values when ash truly acts as a tracer and does not leave the particle.

Mass release values used in the petcoke gasification modeling were calculated from a mass balance. The best possible mass balance was ensured by shutting the reactor down between runs in order to clean out the collection system, and weighing the amount of petcoke fed as well

as the collected char. The use of a short quartz tube immediately around the burner that extended all the way to the collection probe contributed to high collection efficiency (see Figure 4.2). As reported in Section 4.7, the collection efficiency of the HPFFB was measured to be 98.0%.

A summary of the measured petcoke mass release values (on a dry as-received basis) from HPFFB gasification experiments is shown in Table 7.3. A complete summary of measured mass release data of petcoke is included in Appendix E. Each petcoke mass release data point used in modeling was the average mass release from typically 2 to 3 experiments. The average standard deviations in mass release values (as-received basis) at replicate conditions for Petcokes A and B experiments were 3.4 and 3.8 wt% daf, respectively.

Table 7.3. Summary of mass release data used in gasification modeling on a dry as-received basis

Total Pressure	Max Gas Temperature	Equilibrium CO_2	Petcoke A Res. Time	Petcoke A %MR (daf)	Petcoke B Res. Time	Petcoke B %MR (daf)
15 atm	1848 K	89.8 mol%	59 ms	10.7	60 ms	13.2
			142 ms	44.6	146 ms	32.8
			265 ms	59.4	275 ms	47.2
10 atm	1808 K	89.2 mol%	73 ms	22.9	57 ms	15.1
			130 ms	27.7	137 ms	22.3
			244 ms	47.4	258 ms	45.4
15 atm	1891 K	40.8 mol%	56 ms	13.2	60 ms	15.8
			137 ms	25.5	124 ms	27.1
			259 ms	44.3	231 ms	43.1
10 atm	1909 K	40.7 mol%	52 ms	15.3	57 ms	11.1
			125 ms	20.3	119 ms	14.4
			232 ms	29.4	219 ms	30.5

7.4 Pyrolysis Volatile Yields of Petcoke at High Heating Rate

Both Petcokes A and B were fed through the FFB reactor (see Section 4.1) in order to test the effect of particle heating rate on the pyrolysis volatiles yield of petroleum coke at atmospheric pressure. High initial particle heating rate has been shown to increase the volatiles

yield during pyrolysis for other solid fuels such as biomass and some ranks of coal (Jamaluddin et al., 1986; Solomon et al., 1993; Zanzi et al., 1996; Borrego and Alvarez, 2007; Borrego et al., 2009; Tremel et al., 2012; Lewis and Fletcher, 2013).

Both Petcokes A and B were fed through the FFB reactor at different gas conditions where the peak gas temperature ranged from 1320-1929 K using particle residence times in the range 33-102 ms. These experiments served as petcoke pyrolysis experiments at high initial particle heating rate (up to 8.60×10^4 K/s) since no significant mass release due to CO_2 gasification was measured at these conditions where the bulk CO_2 partial pressure was near 0.21 atm. The average volatiles yield from high heating-rate pyrolysis experiments when feeding Petcoke A was 8.86 wt% (daf), while the average mass release of Petcoke B was 10.57 wt% (daf). The results of volatiles yields of Petcokes A and B at both low and high heating-rate conditions are summarized in Table 7.4.

Table 7.4. Summary of mass release from petcoke pyrolysis at low and high heating rates at atmospheric pressure

Sample	ASTM Volatiles wt% (daf)	High Heating Rate Volatiles wt% (daf)
Petcoke A	8.78	8.86
Petcoke B	10.52	10.57

The ASTM volatiles value shown in Table 7.1 serves as a low heating-rate pyrolysis value, whereas the high heating-rate pyrolysis value was taken as the measured mass release during flat-flame burner experiments. There is less than 0.9% difference between the low and high heating-rate pyrolysis mass release values for both petcoke samples. This information is valuable since the char fraction that results from pyrolysis acts as a source of reactants for the thermochemical processes that convert the char, either by combustion or gasification. It is important to note that the comparison in Table 7.4 was for the effect of heating rate on petcoke

volatile yields at atmospheric pressure since increased pressure can result in decreased volatile yields.

Kocaefe et al.(1995) pyrolyzed four kinds of petroleum coke with ASTM volatile yields ranging from 7.2 to 12.0 wt% in a TGA under N_2 at a relatively low heating rate of 2.43 K/s. It was observed that the ASTM volatiles yield was a good approximation of the volatiles that escaped during pyrolysis in the TGA for each of the four varieties of petcoke. From these TGA experiments in the literature as well as the experiments performed at BYU in the FFB reactor, the ASTM volatiles yield of petroleum coke appear to be a good estimate for the volatiles yields during both low and high heating-rate conditions at atmospheric pressure.

7.5 Morphology of Petcoke Char & Tar Formation

Figure 7.2 shows partially gasified Petcoke A char that was collected from the HPFFB reactor and serves as a representative image of other collected samples of Petcoke A char. Recall that SEM images of the raw petcoke samples were included in Figure 7.1. The morphology of Petcoke A char was very similar to that of its parent feedstock material, with the only difference being that the char contains cracks in its surface. Other researchers have also observed cracks and fissures in petcoke char (Zamalloa and Utigard, 1995). Although less than 9 wt% (daf) volatiles were evolved during pyrolysis of Petcoke A, it is thought that the cracks are likely a result of volatiles escaping the particle interior quickly, which is influenced by the high initial particle heating rates characteristic of flat-flame burner reactors. It should be noted that the cracks observed in Petcoke A char were not substantial enough to cause particle fracturing,

which can significantly impact gasification rates. However, the cracks that formed in the petcoke char do create additional surface area that is easily accessible for the reactant gas.

Figure 7.2. SEM image of partially gasified Petcoke A char collected from the HPFFB reactor.

Figure 7.3 shows partially gasified Petcoke B char, which serves as a representative image of other Petcoke B char collected samples. Petcoke B char collected from the HPFFB contained a mixture of two types of particles. Type 1 char particles closely resembled the parent feedstock particles. Type 2 char particles appeared to be highly swollen cenospheres, similar to Group I coal char that is classified by high porosity, thin walls, and large internal voids (Benfell et al., 2000; Wu et al., 2000). Although reactivity differences between Type 1 and Type 2 petcoke particles has not been reported to the knowledge of the authors, Group I coal char was cited as being more reactive than dense Group III coal char (Wall et al., 2002). Figure 7.3b provides some insight on the internal structure of the Type 2 char particles. It appears that the swollen char particles from Petcoke B have thin walls with little to no pore network internally. Note that broken and fragmented char particles from Petcoke B, as seen in Figure 7.3b, were rarely observed in SEM images of the char. Although some cracks were observed in the Type 1 particles of Petcoke B char, the cracks were not nearly as common as was observed in the Petcoke A char particles. It is also noteworthy that other researchers noticed a fraction of

cenospheric petcoke char particles following combustion experiments conducted at high heating rate in a drop tube furnace (Milenkova et al., 2003).

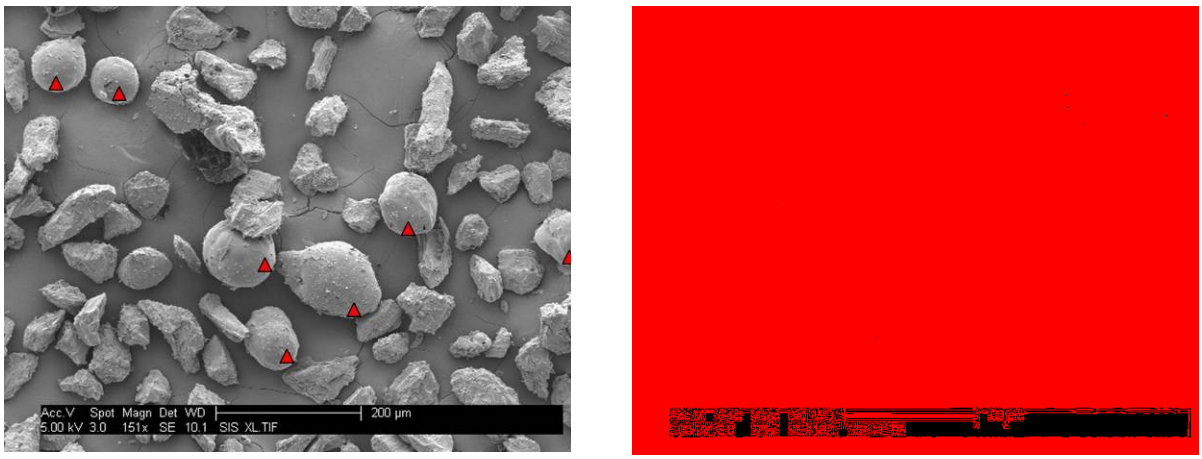

(a) (b)

Figure 7.3. SEM images of partially gasified Petcoke B char collected from the HPFFB reactor. The ▲ symbol identifies Type 2 char particles in figure (a).

The explanation for cenospheric char particles from softening coals is that the metaplast becomes fluid during devolatilization, which results in an entirely new pore structure (Yu et al., 2007). Perhaps this explanation for the differences in coal char morphology can also be applied to Petcoke B. It is interesting to note that although bituminous coals pyrolyzed at high heating rate result in nearly all cenospheric char, the majority of Petcoke B char particles are not cenospheres and did not pass through a plastic stage. Since it is assumed that the differences between the two types of Petcoke B char were caused by transformations during the initial heating of the particle, it would also be assumed that no Type 1 to Type 2 transformation took place during gasification. The different morphologies observed between the chars of Petcokes A and B are possibly attributed to differences in the crude oil feedstock from which the samples originated and perhaps reaction conditions during the coking process, although the exact explanation requires further research.

Although Petcoke B char contained 2 distinct types of particles, Type 1 particles likely comprised most of the sample mass after pyrolysis due to the very low density of cenospheric char particles. For example, cenospheric bituminous coal char particles had apparent densities 2 to 11 times less than their parent coal feedstock (Shurtz, 2011).

Tar was observed on the filters of the HPFFB collection system (see Figure 4.2) when Petcoke B was fed, although essentially no tar was observed when feeding Petcoke A. The tar that resulted from Petcoke B likely originated from the Type 2 char particles. The average tar yield of the experimental runs when feeding Petcoke B in the HPFFB reactor was 1.4 wt%, although tar yields as high as 2.3 wt% were measured. Tar is important to consider because any non-depleted tar yields in industrial processes can cause problems by corroding equipment, causing damage to motors and turbines, lowering catalyst efficiency, and condensing in transfer lines (Vassilatos et al., 1992; Brage et al., 1996; Baumlin et al., 2005).

7.6 Char Gasification Modeling of Petcoke

The same first-order global model described in Section 6.2 was used to model the CO_2 gasification of petcoke char. Decrease in external surface area of Petcoke A with increased conversion was included in the modeling using the following equation that assumes spherical particles:

$$\frac{d_1}{d_0} = \left(\frac{\rho_0}{\rho_1} \cdot \frac{m_1}{m_0} \right)^{\frac{1}{3}} \tag{7.1}$$

where (d_1/d_0) is the diameter ratio of collected char to feedstock material, (ρ_0/ρ_1) is the ratio of apparent densities (see Equation (4.7)) of dried feedstock material to dried collected char, and (m_1/m_0) is the mass ratio of collected char to fed material on a dry basis. Values of ρ_0/ρ_1 in

Equation (7.1) were not affected by choice of ε_b (see Equation (4.7)) with the assumption that feedstock and collected char particles have similar shape. Measurements of Petcoke A used in Equation (7.1) can be found in Appendix E. A constant d_1/d_0 value of 0.9 was used for char gasification modeling of Petcoke B because apparent density measurements (see Section 4.8) of Petcoke B char were not thought to be meaningful due to the mixture of low-density and high-density particles (see Section 7.5).

Representative temperature profiles are shown in Figure 7.4 for Petcoke B fed at the 10 atm $T_{gas,max}$ = 1909 K HPFFB condition with a post-flame CO_2 concentration near 40 mol%. Equation (6.3) was used to calculate the particle temperature profile in the figure. The lowest collection height typically near 1" above the burner served as the initial condition; this collection height was located after the initial rise in particle temperature inside the reactor (see Figure 7.4). Hence, the derived kinetic parameters in this study were not affected by any uncertainties in particle temperature histories between the point of injection and the first collection height.

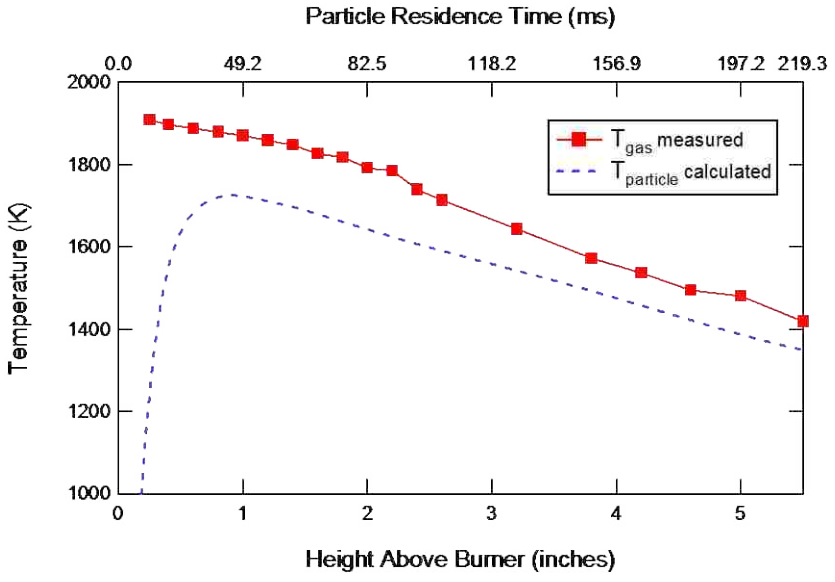

Figure 7.4. Measured centerline gas temperature profile and calculated Petcoke B particle temperature profile at the 10 atm ~40 mol% CO_2 HPFFB condition.

The effect of CO inhibition on measured petcoke mass release values was explored similarly as was done for the biomass chars (see Section 6.3) using the CCK coal model. The CCK model was run for 60 μm Illinois #6 coal char at similar reaction conditions of the petcoke to estimate the effect of CO on the measured particle mass release in the HPFFB petcoke gasification experiments. Estimations from the CCK model revealed that the measured daf mass release values (on a char basis) were on average 16% lower than when the char gasification occurred at conditions free of CO. The CO inhibition effect may have been of similar magnitude in the petcoke gasification measurements. However, with the limited data available, the first-order modeling of petcoke char gasification performed in this research did not treat the effect of CO inhibition.

7.7 Petcoke Gasification Modeling Results

The optimized kinetic parameters regressed from the data sets of Petcoke A and B are summarized in Table 7.5. The relative error (see Equation (6.6)) between measured and modeled particle mass release is listed in the table on the experimental as-received basis and also on a calculated char basis. Since the experimental conditions at which char is generated can affect gasification rates (Mermoud et al., 2006), it is important to note that the reported kinetic parameters in Table 7.5 were for petcoke that was pyrolyzed *in-situ* at high initial particle heating rates and gasified during short reaction times (< 300 ms) at elevated pressure. The maximum initial particle heating rates for Petcokes A and B in the gasification experiments were 6.06×10^4 and 7.55×10^4 K/s, respectively. Calculated ranges of T_p and $P_{CO2,surf}$ for the petcoke data sets are also included in Table 7.5, as calculated by Equations (6.3) and (6.5), respectively.

Table 7.5. Summary of first-order kinetic parameters and reaction conditions for CO_2 gasification of Petcokes A & B in the HPFFB reactor

	Petcoke A	**Petcoke B**
A (g/cm^2/s/atm CO_2)	0.1862	0.0771
E (kJ/mol)	67.5	67.5
relative error (as-received basis)	7.3%	7.2%
relative error (char basis)	17.0%	29.6%
pyrolysis conditions	*in situ* at high heating rate (~5.4·10^4 K/s)	*in situ* at high heating rate (~6.6·10^4 K/s)
max conversion (daf wt%, char basis)	55.5	41.0
Condition Identifier Total Pressure; $T_{gas,max}$; mol% CO_2	**Petcoke A** T_p range $P_{CO2,surf}$ range	**Petcoke B** T_p range $P_{CO2,surf}$ range
15 atm; 1848 K; ~90% CO_2	1174 – 1491 K 9.7 – 12.2 atm	1201 – 1595 K 11.1 – 12.6 atm
10 atm; 1808 K; ~90% CO_2	1184 – 1497 K 7.0 – 8.2 atm	1209– 1630 K 7.6 – 8.5 atm
15 atm; 1891 K ~40% CO_2	1266 – 1636 K 4.5 – 5.5 atm	1293 – 1699 K 5.2 – 5.7 atm
10 atm; 1909 K ~40% CO_2	1322 – 1662 K 3.2 – 3.7 atm	1349 – 1718 K 3.6 – 3.8 atm

The maximum χ factor (see Section 6.5) in the petcoke data sets was only 0.15, which indicates that the measured rates did not occur in the Zone III regime where film diffusion controls.

Figure 7.5 shows an example of the fit of the first-order global model to Petcoke B mass release data collected from the HPFFB reactor at the 15 atm $T_{gas,max}$ = 1848 K condition where the post-flame CO_2 concentration was about 90 mol%. The mass release values measured at the lowest residence time served as the initial condition for the modeling, and the mass release measured at the two higher particle residence times are used to evaluate predicted gasification rates. The parity plots in Figure 7.6 show how the mass release predicted by the first-order gasification model using kinetic parameters in Table 7.5 compared with the measured petcoke mass release data (on a char basis).

When the reactivity data of 2 feedstocks have been fit to the same first-order model and they both have the same E value, convenient rate comparisons can be easily performed by using

ratios of their *A* values. For example, the kinetic parameters in Table 7.5 suggest that Petcoke A is about 2.4 (i.e., 0.1862/0.0771) times more reactive to CO_2 gasification than Petcoke B when the mass release data were fit to the first-order global model in Equation (6.2).

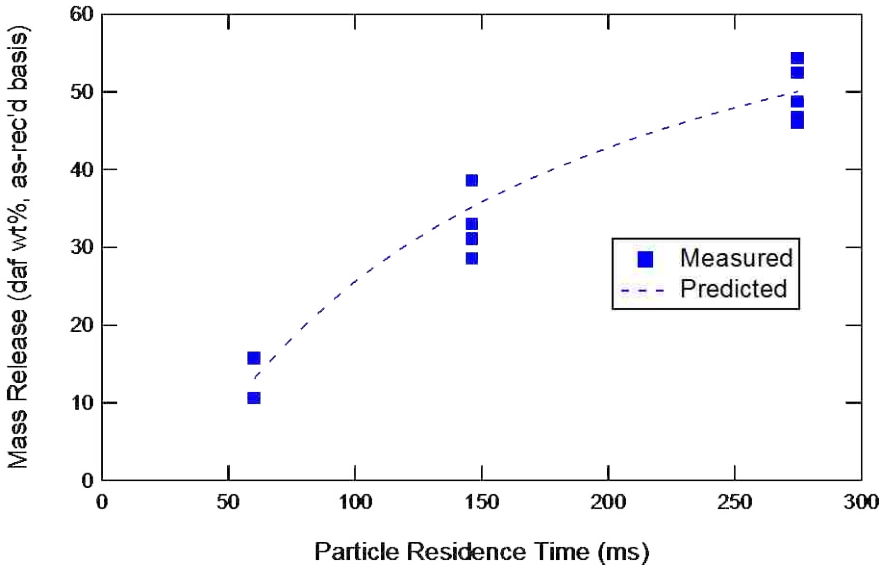

Figure 7.5. Comparison of measured and modeled mass release of Petcoke B at the 15 atm HPFFB condition where $T_{gas,max}$ =1848 K in an environment with ~ 90 mol% CO_2.

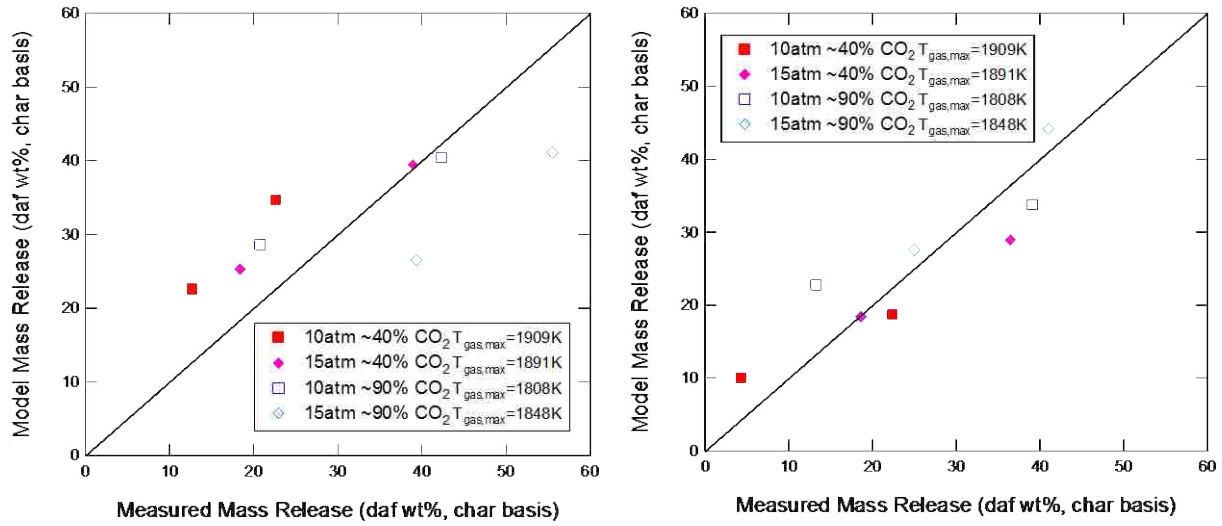

Figure 7.6. Parity plot of HPFFB gasification mass release data (char basis) for (a) Petcoke A and (b) Petcoke B data.

Since gasification rates can be a function of conversion, it is important to note that the reported kinetic parameters in Table 7.5 were for data where Petcokes A and B reached maximum conversions of 55.5 and 41.0 daf wt% on a char basis, respectively. It is unclear from the literature how conversion degree affects CO_2 gasification rates of petcoke. While Gu et al. (2009) measured nearly constant CO_2 gasification rates of petcoke at conversions from about 0.1 to 0.9 at isothermal conditions, Zou et al. (2007) observed a distinct maximum in CO_2 gasification rates near a conversion of 0.3.

The Petcoke A and B char data in this study indicated faster CO_2 gasification rates than a TGA study (Malekshahian and Hill, 2011b) where petcoke char was reacted at similar temperature and CO_2 partial pressure. For example, both Petcoke A and B chars attained conversions of at least 10 wt% (daf char basis) between collection heights of 3 to 5.5 inches above the burner during all 4 of the experimental conditions tested (see Table 7.2). This implies that measurable mass release was observed in this study due to CO_2 gasification of petcoke char in an average time of ~115 ms at average *particle* temperatures between 1238 and 1455 K where average $P_{CO2,surf}$ values were 3.5 to 12.4 atm at total pressures of 10 and 15 atm. However, no measurable mass release occurred in such a short time when petcoke char prepared at atmospheric pressure in N_2 using a heating rate of 20 K/min with a 1-hr hold time at 1248 K and a 2-hr cooling time was gasified in a TGA in undiluted CO_2 at 1248 K at a total pressure of 13.8 atm (Malekshahian and Hill, 2011b). Perhaps this discrepancy can be related to the vastly different pyrolysis conditions of the petcoke chars. However, no significant CO_2 char gasification was measured for either Petcoke A or B at atmospheric pressure in the FFB reactor (see Section 4.1) in a post-flame environment that contained up to 27 mol% CO_2 at conditions where the average *particle* temperatures were between 952 and 1546 K using particle residence

times up to 102 ms, which seems consistent with the low reactivities observed in other studies (Tyler and Smith, 1975; Zamalloa et al., 1995; Zou et al., 2007; Gu et al., 2009; Wu et al., 2009; Malekshahian and Hill, 2011b). Thus the high petcoke reactivities measured in the current study may be limited to petcoke chars generated and gasified at high heating rates and pressures, such as in commercial entrained-flow gasifiers.

While it can be implied that petcoke gasification occurs quickly in commercial entrained-flow gasifiers where the maximum residence time is on the order of seconds, petcoke gasification rates in the current literature (see Section 2.2.10) are on the order of minutes and even hours (at lower temperatures, pressures, and heating rates). In contrast, this study reported CO_2 gasification rates of two petcoke chars where significant conversions were measured in <300 ms when 45-75 μm diameter particles were gasified in entrained flow using total pressures and CO_2 concentrations up to 15 atm and ~90 mol%, respectively.

7.8 Comparison of Petcoke and Coal CO_2 Gasification Rates

Several researchers have reported that the CO_2 gasification reactivity of petcoke is lower than that of coal (Zamalloa et al., 1995; Gu et al., 2009; Wu et al., 2009). However, it is important to note that reactivity comparisons are a function of many variables including coal rank, conditions at which the chars were pyrolyzed, and the reaction condition used to gasify the solid fuels. Since both petcoke and coal are gasified commercially in entrained-flow reactors where the maximum residence time is limited to a few seconds, it would be implied that their reactivities are similar at the high temperature and pressure conditions characteristic of such reactors.

As an aside, it is important in rate comparisons to consider the differences in how rates can be reported. For example, the majority of rates in this study are *dm/dt* normalized by particle external surface area (A_p) while the rates from many TGA studies are reported as $dX/dt = (1/m_{o,daf})\cdot dm/\mathrm{d}t$, where X is conversion, t is time, $m_{o,daf}$ is the starting daf mass of the char sample, and *dm/dt* is the rate of change in particle mass.

Wu et al. (2009) reported gasification conversion times for chars of petcoke and Shenhua coal that had been prepared at a heating rate of 6 K/min with 20-min hold times at 950, 1200 and 1400 °C. When these samples were gasified by CO_2 in a TGA at 950 °C at atmospheric pressure, the petcoke char took 14.9, 4.8, and 1.4 times longer to reach 50% conversion than the coal char when comparing chars pyrolyzed at 950, 1200, and 1400 °C, respectively. Thus, it is seen how pyrolysis conditions (pyrolysis temperature in this case) affected the rate comparisons between petcoke and coal chars. Gu et al. (2009) reported gasification conversion times of both Shenfu coal char that had been pyrolyzed rapidly at 1673 K in a falling reactor and petcoke. The two samples were gasified isothermally by CO_2 at temperatures ranging from 1223 to 1673 K at atmospheric pressure. The reaction times for petcoke to reach 50% conversion were 21.2, 15.6, 7.1, 2.6, 2.3, and 1.9 times longer than the coal char at gasification temperatures of 1223, 1273, 1373, 1473, 1573, and 1673 K, respectively. Thus, it appears that any large discrepancy between petcoke and coal CO_2 gasification rates at low temperature is diminished greatly at higher temperatures. However, the researchers did not analyze the effect of external mass transfer resistance at the high temperatures tested, which makes comparisons difficult.

As part of the current study, CO_2 gasification rates of Illinois #6 coal char and petcoke were compared at the 15 atm condition of the HPFFB reactor in ~ 90 mol% CO_2 where the peak centerline gas temperature was 1848 K (see Table 7.2). Collection heights of 1, 3, and 5.5 inches

were used in the Illinois #6 coal experiments, which corresponded to particle residence times in the range 52 – 247 ms. It would have been ideal to have the coal pyrolyze *in-situ* followed immediately by CO_2 gasification of the char, as was done when feeding the petcoke samples in the HPFFB reactor. However, soot contamination of the coal char obscured the measured extents of gasification, so a char reinjection technique was implemented, similar to the work of others (Hurt et al., 1998; Shurtz and Fletcher, 2013). It has been reported that capture and re-injection of coal char had little effect on the measured reactivity from data taken when feeding Illinois #6 coal through an entrained-flow reactor using a single pass or multiple re-injections (Hurt et al., 1998).

To generate coal char for CO_2 gasification experiments, raw Illinois #6 coal of the size range 45-75 μm was pyrolyzed at 15 atm total pressure in the HPFFB at a peak gas temperature near 1850 K for ~45 ms utilizing a collection height of 0.75" above the burner. A slightly O_2-rich (1.6 mol%) post-flame environment was used in order to oxidize the tar before soot could be formed, which allowed the collection of fully pyrolyzed, soot-free coal char. Both the coal pyrolysis and subsequent CO_2 gasification experiments were conducted at 15 atm total pressure. The Illinois #6 coal char used in subsequent gasification experiments was in the size range 75-106 μm (85.3 μm mass mean) since the particles swelled during pyrolysis and this fraction contained the highest yield of particles. Additional properties of the coal char were included in Table 7.1. Figure 7.7 shows a SEM image of the pyrolyzed Illinios #6 char that acted as the feedstock material during CO_2 char gasification experiments in the HPFFB reactor.

Figure 7.8 summarizes measured mass release values on a daf char basis of Petcoke A, Petcoke B, and Illinois #6 coal char after these feedstocks were fed in the HPFFB at 15 atm $T_{gas,max}$=1848 K condition where the post-flame CO_2 concentration was near 90 mol%.

Figure 7.7. SEM image of 75-106 μm Illinois #6 coal char pyrolyzed at 15 atm in the HPFFB reactor that served as feedstock material for CO_2 gasification experiments.

The measured mass release values for the coal char in Figure 7.8 were the average from 2-3 experiments, and the replicate mass release values were within on average 2.8 wt% of the previously measured value(s). Petcoke mass release values in Figure 7.8 were the average of 2-5 experiments, and the replicate mass release values were within on average 4.3 and 4.8 wt% of the previously measured value(s) for Petcoke A and B, respectively.

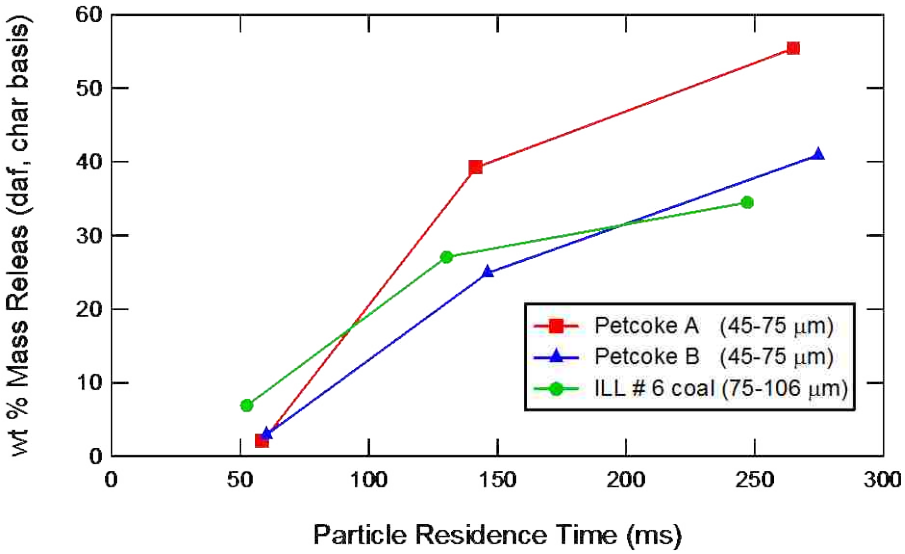

Figure 7.8. Comparison of mass release (char basis) of Petcoke A, Petcoke B, and ILL #6 coal char at 15 atm $T_{gas,max}$=1848 K condition in the HPFFB in ~90 mol% CO_2.

Both petcoke samples gasified to a higher conversion on a char basis when compared to the coal char. However, it is difficult to determine which feedstock had the highest reactivity when compared at the same T_p and $P_{CO2,surf}$ values from simply viewing Figure 7.8 because each feedstock reacted at particle temperature and $P_{CO2,surf}$ histories that were specific to each feedstock.

To equalize the data in Figure 7.8 and make a comparison of char CO_2 gasification rate at the same conditions (T_p and $P_{CO2,surf}$), the optimal kinetic parameters for the first-order model were regressed from the ILL #6 coal data and then compared with the petcoke rates using kinetic parameters in Table 7.5. Regressed values of A and E from the ILL #6 data were 0.6818 g/cm^2/s/atm and 121.3 kJ/mol, respectively. For the reactivity comparison, the first-order rate ($(1/A_p)\ dm/dt$) was converted to dX/dt (or $1/m_{o,daf} \cdot dm/dt$, which is how rates are often compared in other studies) by its multiplication by ($A_p/m_{o,daf}$), where A_p is the external surface area of a particle ($4 \cdot \pi \cdot r^2$), and $m_{o,daf}$ is the constant daf mass of a particle after complete pyrolysis. Values of dX/dt at the same condition ($P_{CO2,surf}$ = 11 atm and T_p = 1500 K) for the 3 feedstocks are summarized in Figure 7.9.

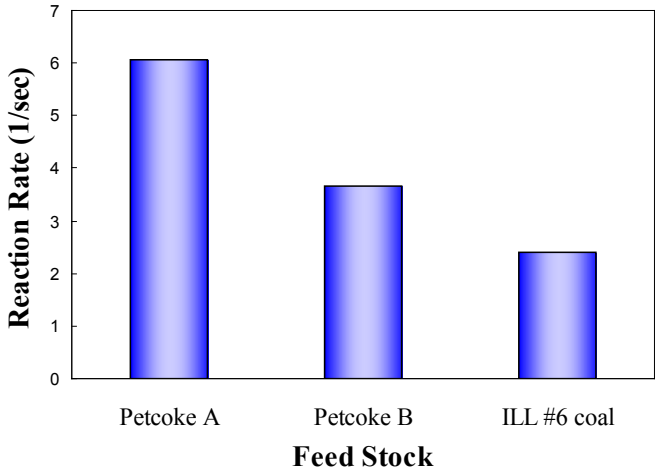

Figure 7.9. Comparison of the CO_2 gasification rates (dX/dt) of Petcoke A, Petcoke B, and ILL #6 coal char at $P_{CO2,surf}$= 11 atm and T_p = 1500 K using kinetic parameters regressed in this study in Equation (6.2).

The CO_2 char gasification reactivities at this condition exhibited the following order: Petcoke A > Petcoke B > Illinois #6 coal. Hence, the reactivity comparison shows that both petcokes had a higher reactivity than the Illinois #6 coal char from entrained-flow experiments conducted at high temperature, pressure, and initial particle heating rates.

The N_2 and CO_2 surface areas of the chars collected from the 15 atm $T_{gas,max}$=1848 K ~90 mol% CO_2 condition (see Figure 7.8) were measured and are summarized in Figure 7.10a and b, respectively. Calculating *dX/dt* as was done for Figure 7.9 using internal surface areas rather than external surface areas yields the same result that both petcoke samples were more reactive than the coal char at the $P_{CO2,surf}$= 11 atm and T_p = 1500 K condition, although using internal surface areas in the calculation causes the rate ratio between petcoke and coal char to increase by factors of about 1.5 and 2 for Petcokes A and B, respectively.

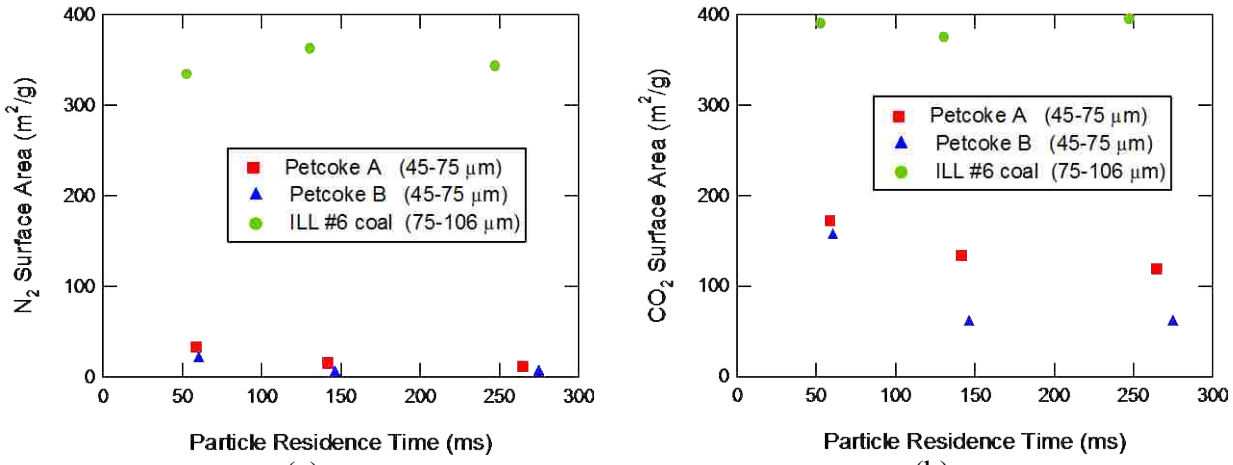

(a) (b)

Figure 7.10. Measured internal surface areas by (a) N_2 and (b) CO_2 of chars used in the petcoke vs ILL #6 coal char comparison and corresponds to data in Figure 7.8.

7.9 Summary

The CO_2 gasification of two petroleum coke samples from industry was studied at conditions of high initial particle heating rate, temperature, and pressure in the HPFFB reactor. The ASTM volatiles values of both Petcokes A and B were good approximations of the pyrolysis mass release at conditions of atmospheric pressure and high particle heating rate, which differs from other solid fuels such as coal and biomass that typically have increased pyrolysis volatile yields at high heating rate. The morphology of Petcokes A and B chars were evaluated using SEM images of partially gasified samples collected from the HPFFB reactor. The structure of Petcoke A had cracks in its surface, but otherwise appeared very similar to that of its raw feedstock. The cracks did not appear to be significant enough to cause particle fracturing, and are believed to be the result of the volatiles during pyrolysis quickly escaping the particle interior at the experimental conditions of high initial particle heating rate. Petcoke B char contained a small fraction of swollen, thin-shelled particles that resembled pyrolyzed bituminous coal chars from high heating rate conditions. These swollen Petcoke B char particles had little to no pore network internally, and likely did not comprise a high mass fraction of the char due to the very low density of cenospheric particles.

The petcoke CO_2 gasification experiments were conducted at total pressures of 10 and 15 atm in the HPFFB reactor at conditions where the bulk phase consisted of ~40 and ~90 mol% CO_2 using peak centerline *gas* temperatures up to 1909 K. Mass release caused by CO_2 char gasification was measured for these two petcoke samples (45-75 μm) following *in-situ* pyrolysis in the HPFFB reactor, and was used to regress optimal kinetic parameters using a global first-order model. Over the range of experimental conditions studied, the char CO_2 gasification rate per external surface area ($1/A_p \cdot dm/dt$) for Petcoke A char was about 2.4 times higher than

Petcoke B char. The CO_2 char gasification conversion rates (*dX/dt*) for both Petcokes A and B were shown to be higher than Illinois #6 coal at conditions in the HPFFB reactor, even though most reactivity comparisons between petcoke and coal at lower temperatures and pressures typically result in coal being more reactive. The reported petcoke char gasification rates in this study are believed to be representative of those from an entrained-flow gasifier since they were measured at similar conditions of elevated temperature and pressure using chars that were pyrolyzed *in-situ* at high heating rates and reacted for short reaction times in entrained flow.

8. Gasification of Coal Char

Steam gasification kinetics of 3 bituminous coal chars (Illinois #6, Utah Skyline, & Pittsburgh #8) were determined from experiments at entrained-flow conditions in the high-pressure flat-flame burner reactor at high temperature ($T_{gas,max}$ up to 1830 K) and elevated pressure (10-15 atm). The steam gasification experiments involved re-injecting fully pyrolyzed coal char in order to overcome experimental challenges of measuring accurate mass release for coals that form soot, especially at elevated pressure. The steam gasification data for the 3 coal chars were fit to a global first-order model. In addition, gasification experiments were conducted for a single coal char (Illinois #6) at conditions where significant char conversion occurred by both H_2O and CO_2.

8.1 Coal Gasification Experiments

The high-pressure flat-flame burner reactor (HPFFB; see Section 4.2) was used to measure steam gasification rates of coal chars at conditions relevant to industrial entrained-flow gasifiers by reacting small particles in entrained-flow at high temperatures and pressures for short times (<0.3 s). The ranges of centerline gas temperature and bulk H_2O partial pressure in these experiments were 1270-1879 K and 0.75-1.16 atm, respectively. It is noteworthy that

Shurtz (2013) measured the CO_2 gasification rates of several coal chars in the HPFFB reactor in a related study.

Chars of 3 bituminous coals (Illinois #6, Utah Skyline, and Pittsburgh #8) were used in the steam gasification experiments in the HPFFB reactor. The abbreviated names of ILL #6, Utah, and Pitt #8 will be used to refer to these coals, respectively. The results of the ultimate and proximate analyses of the 3 raw coals used in this project are shown in Table 8.1.

Table 8.1. Results of the ultimate and proximate analyses of 45-75 μm raw coals

Sample	Apparent Density (g/cm^3)	Moisture (wt%, as rec'd)	Ash (wt%, dry)	Volatiles (wt%, daf [a])	C (wt%, daf)	H (wt%, daf)	N (wt%, daf)	O[b] (wt%, daf)	S (wt%, daf)
ILL #6	1.25	3.45	8.49	43.37	75.09	5.21	1.34	14.02	4.35
Utah	1.25	2.41	7.87	47.06	77.39	5.57	1.57	14.87	0.61
Pitt #8	1.31	1.67	12.41	37.73	80.86	5.39	1.64	10.61	1.49

[a]daf = dry and ash-free basis [b]calculated by difference

8.1.1 Re-Injection Strategy

The HPFFB coal gasification experiments involved re-injecting a sieved fraction of fully pyrolyzed coal char. It would have been ideal to conduct gasification experiments following *in-situ* pyrolysis like occurs in commercial entrained-flow gasifiers, but soot contamination of the char prevented this. A good mass balance for an experimental run (using weights of fed and collected material) is interrupted when a significant amount of soot contaminates the char, since it is experimentally challenging to separate the soot from the char (Shurtz, 2011) and assign accurate mass fractions to each. Soot-laden char also prevents accurate mass release values to be calculated when ash is assumed to act as a tracer (see Equation (4.5)). Hence, the method of re-injecting fully pyrolyzed coal char to measure rates of char conversion was pursued, similarly as was done for biomass char in Chapter 6 (see Section 6.1.1).

The coal chars used in the HPFFB gasification experiments were generated by feeding raw, sized (45-75 μm) coals in the up-flow HPFFB reactor at the same total pressure that the chars would later be re-injected as feedstock material. Experimental optimization studies of char-generation conditions in the HPFFB reactor were performed with the aim of generating nearly soot-free, fully pyrolyzed coal char with minimal char oxidation at total pressures of 10, 12.5, and 15 atm. Different collection heights and post-flame O_2 concentrations were tested. Scanning electron microscope (SEM) images of the chars were also used in the determination of the optimal char-generation conditions of the HPFFB reactor. Figure 8.1a shows coal char collected from a probing char-generation condition that still contained soot. Figure 8.1b shows coal char essentially free of soot at the finalized 12.5 atm char-generation condition of the HPFFB reactor. Note that the SEM images in Figure 8.1 have different magnifications. The finalized HPFFB char-generation conditions had peak gas temperatures near 1850 K using a 0.75" collection height (~40 ms). About 2 mol% O_2 was used in the post-flame environment in order to oxidize the tar before soot could be formed. Details about the char-generation HPFFB conditions at total pressures of 10, 12.5, and 15 atm are located in Appendix F.

(a) (b)

Figure 8.1. SEM images of (a) soot-laden and (b) soot-free coal char.

The coal chars generated in the HPFFB reactor at the 3 total pressures were sieved, and the size fraction of char used during gasification re-injection experiments was determined solely by which size fraction contained the highest yields of particles. The Utah Skyline steam gasification experiments used the 45-75 μm fraction, while both the Illinois #6 and Pittsburgh #8 steam experiments utilized the 75-106 μm fraction. Representative photos of the sieved coal chars that were generated at a total pressure of 15 atm in the HPFFB reactor are shown in Figure 8.2. Additional SEM images of coal chars are included in Appendix F.

(a) ILL #6 15 atm char; 75-106 μm

(b) Utah Skyline 15 atm char; 45-75 μm

(c) Pitt #8 15 atm char; 75-106 μm

Figure 8.2. SEM images of sieved (a) ILL #6, (b) Utah Skyline, and (c) Pitt #8 chars generated at 15 atm that acted as feedstock material for steam gasification HPFFB re-injection experiments at 15 atm.

As an aside, char swelling during high heating-rate pyrolysis (up to 6.7×10^4 K/s) had a greater effect on the Illinois #6 and Pittsburgh #8 coals than the Utah Skyline coal since 45-75 μm raw coal was fed during the generation of all 3 pyrolyzed chars. The chosen size fractions of char (45-75 μm or 75-106 μm) that acted as feedstock material in HPFFB gasification experiments were used to simulate pulverized coal sizes used commercially, but also allowed particle temperature gradients to be ignored in modeling.

8.1.2 Test Matrix and Experimental Details

Two different sets of gas conditions were used in the HPFFB coal gasification experiments. The first set of gas conditions was used to measure particle mass release at total pressures of 10, 12.5, and 15 atm for ILL #6, Utah Skyline, and Pitt #8 coal chars at conditions where the char conversion was primarily due to *steam* gasification. This first set of gas conditions will be referred to as the *steam conditions* in this work. Gasification by CO_2 accounted for some particle mass release when coal char was fed at the first set of gas conditions since it was not possible to have post-flame reaction environments completely absent of CO_2 in the HPFFB reactor. However, the char mass release caused by CO_2 was accounted for in the char gasification modeling. The second set of HPFFB gas conditions was used to study the gasification of a single coal char (ILL #6) at a total pressure of 15 atm using conditions where significant char conversion occurred by both steam *and* CO_2. The second set of gas conditions will be referred to as the *steam/CO_2 conditions* in this work.

The matrix of coal char HPFFB gasification experiments for the first and second set of gas conditions are included in Table 8.2 and Table 8.3, respectively. Also included in the tables are details about the gas conditions including total pressure, maximum measured centerline gas

temperature, and equilibrium composition of the post-flame HPFFB environments as calculated by thermodynamic equilibrium. The gas temperature measurements reported in Table 8.2 and Table 8.3 were corrected for radiation losses from a 422 μm-diameter B-type spherical thermocouple bead (see Appendix A), as were all other gas temperatures reported in this chapter. The correction of gas temperature in the near-burner region was approximately 85 K at the utilized HPFFB conditions. Complete details of experimental conditions and measured coal data are summarized in Appendix F.

Table 8.2. Matrix of experiments for steam gasification tests

Total Pressure	Max Gas Temperature	Equilibrium H_2O, CO_2, CO, N_2	Reference Residence Time	Coal Sample	Gasification Residence Times
10 atm	1814 K	7.5, 14.2, 1.9, 75.7 mol%	42 ms	Utah	107; 183 ms
			45 ms	Pitt #8	116; 199 ms
			45 ms	ILL #6	116; 198 ms
12.5 atm	1782 K	7.7, 14.1, 2.3, 75.1 mol%	47 ms	Utah	118; 202 ms
			52 ms	Pitt #8	135; 232 ms
			52 ms	ILL #6	134; 231 ms
15 atm	1611 K	7.3, 11.4, 2.8, 77.5 mol%	55 ms	Utah	139 ms
			59 ms	Pitt #8	153 ms
			59 ms	ILL #6	153 ms
15 atm	1830 K	8.6, 13.7, 2.5, 74.4 mol%	49 ms	Utah	126; 219 ms
			52 ms	Pitt #8	135; 237 ms
			51 ms	ILL #6	135; 236 ms

Table 8.3. Matrix of experiments for steam/CO_2 gasification tests when feeding 75-106 μm ILL #6 char

Total Pressure	Max Gas Temperature	Equilibrium H_2O, CO_2, CO, N_2	Reference Residence Time	Gasification Residence Times
15 atm	1812 K	7.7, 83.2, 7.9, 1.1	51 ms	130, 222 ms
15 atm	1879 K	7.5, 33.3, 10.5, 47.7	49 ms	130, 224 ms

Particle mass release was typically measured at 3 residence times per gas condition at collection heights of 1, 3, and 5 inches above the burner. The first collection height at 1" above the burner served as a reference data point, since only the particle mass release after this first

data point was used in the modeling. The particle residence time of this first sample location is shown as the 'reference residence time' in Table 8.2 and Table 8.3. The HPFFB gas conditions in this chapter are identified by the total pressure and maximum measured centerline gas temperature. Only 2 residence times were tested at the 15 atm $T_{gas,max}$ = 1611 K condition (see Table 8.2) since water condensation negatively affected particle feeding when collection heights greater than 3" were attempted at this relatively cool condition.

Particle mass release calculated by Equation (4.6) was the primary value used in the gasification modeling of this study, even though ash-tracer mass release values (see Equation (4.5)) were also considered. Ash often was liberated from the bituminous coal chars during experiments, as determined using a mass balance of the ash (see Equation (5.1)). Shurtz (2011) also observed ash liberation from coals fed in the HPFFB reactor at high heating rates, and documented that the mass release values using the ash-tracer method in Equation (4.5) resulted in "very noisy trends." Using Equation (4.6) to calculate particle mass release allowed accurate tracking of the organic mass fraction of the particle even when ash was released to the gas phase during experiments. Sufficient feedstock was fed to the HPFFB reactor at a rate near 0.15 g/hr for an accurate ash test to be performed on the partially gasified collected char after an experiment (see Section 4.8).

The steam concentrations used in this study were limited to less than 9 mol% in the post-flame environment (see Tables Table 8.2 and Table 8.3) due to concerns about damaging the burner head. Supplying extra H_2 to the burner resulted in higher concentrations of steam in the post-flame environment, but also caused the flame to 'sit' closer to the burner surface due to the high flame speed of H_2. Supplying the burner with excessive amounts of H_2 can greatly reduce the life of the burner, thus explaining why only conservative amounts of H_2 were used in this

study. Shurtz (2011) reported that a former HPFFB burner head suffered from high-temperature corrosion after months of using 84 mol% H_2 in the *fuel* stream to the burner. In this project, using H_2 to compose up to 36 mol% of the total fuel stream did not cause any visible damage to the burner head during the 1.5 years that steam gasification experiments were conducted.

Particle residence times for all the experiments were calculated as outlined in Section 4.6. The particle velocity profiles of the 45-75 μm Utah Skyline chars at the HPFFB steam conditions (see Table 8.2) are shown in Figure 8.3. Note that the particle velocities were not constant at the non-isothermal gas conditions of the HPFFB reactor. A complete summary of all the particle velocities is included in Appendix F.

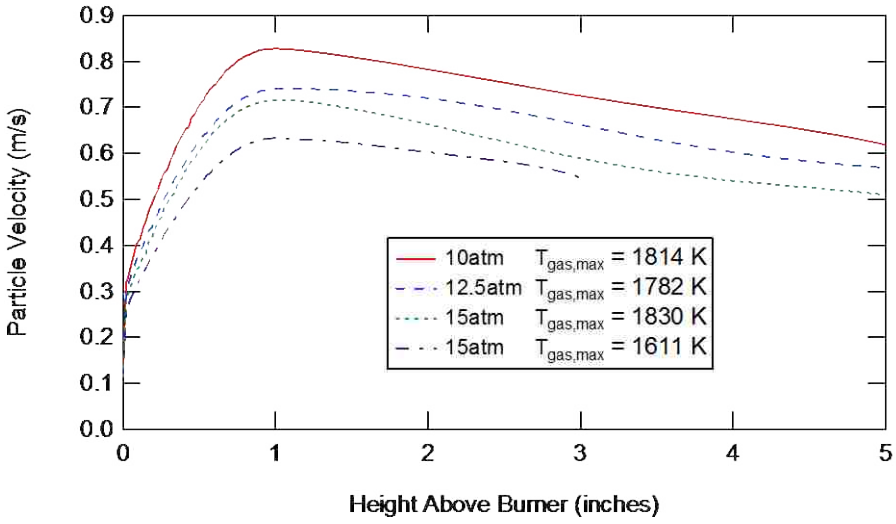

Figure 8.3. Particle velocity profiles of 45-75 μm Utah Skyline chars at steam conditions in the HPFFB reactor.

Table 8.4 provides a summary of the properties of all the coal chars used in the HPFFB gasification experiments. The mass mean diameters (d_m) reported in Table 8.4 were calculated from Equation (6.1) using particle diameter measurements from optical microscope pictures of the chars and ImageJ software (Schneider et al., 2012).

Table 8.4. Properties[c] of coal chars used as feedstock material in HPFFB gasification experiments

Condition at which Char was Feedstock Material	Feedstock	Pyrolysis Pressure (atm)	Ash (wt% dry)	Sieved Size (μm)	Mass Mean (d_m) (μm)	Apparent Density (g/cm^3)
steam[d]	Utah	10	27.8	45-75	61.7	0.242
10 atm; $T_{gas,max}$ = 1814 K	Pitt #8	10	10.6	75-106	85.9	0.161
	ILL #6	10	12.1	75-106	84.5	0.145
steam[d]	Utah	12.5	24.8	45-75	62.7	0.203
12.5 atm; $T_{gas,max}$ = 1782 K	Pitt #8	12.5	9.4	75-106	86.0	0.170
	ILL #6	12.5	15.6	75-106	89.3	0.145
steam[d]	Utah	15	23.6	45-75	68.6	0.186
15 atm; $T_{gas,max}$ = 1611 & 1830 K	Pitt #8	15	10.0	75-106	82.3	0.154
	ILL #6	15	13.9	75-106	78.2	0.144
steam/CO_2[e] 15 atm; $T_{gas,max}$ = 1812 & 1879 K	ILL #6	15	12.9	75-106	86.3	0.144

[c]some surface area data is available in Table F.22, Table F.23, & Table F.24 in Appendix F [d]contains some CO_2; see Table 8.2 [e]see Table 8.3

8.1.3 Centerline Gas Temperature Profiles and Mass Release Summary

The centerline gas temperature profiles were measured at each gas condition (see Table 8.2 and Table 8.3) in the HPFFB reactor as documented in Section 4.5. The measured centerline gas temperature profiles for the 4 steam conditions of the HPFFB reactor (see Table 8.2) are summarized in Figure 8.4. The 10 atm $T_{gas,max}$ = 1850 K temperature profile is also included in Figure 8.4; this additional HPFFB condition essentially did not contain steam and was used to aid in the accounting of char conversion due to CO_2 gasification when coal char was fed at the HPFFB steam conditions (see Table 8.2). The equilibrium post-flame CO_2, H_2O, CO, and N_2 concentrations of this extra condition were 20.8, 0.9, 7.7, and 70.0 mol%, respectively. Other details about this particular HPFFB gas condition can be found in Appendix F.

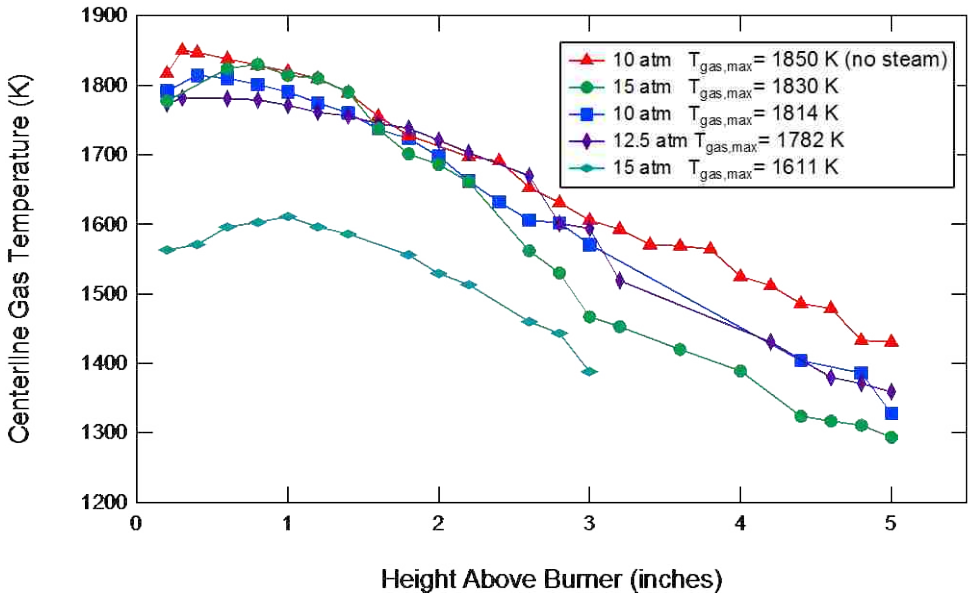

Figure 8.4. Centerline gas temperature profiles of the HPFFB steam conditions corrected for radiation losses from the thermocouple bead.

The temperature profiles corresponding to the second set of HPFFB gas conditions (see Table 8.3) are shown in Figure 8.5. These conditions were used to study the gasification of Illinois #6 coal char at conditions where significant mass release was due to both steam and CO_2 gasification.

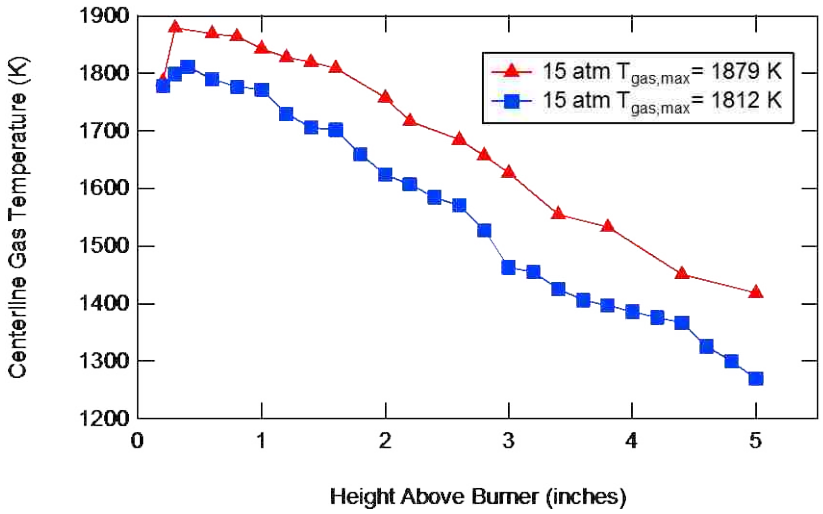

Figure 8.5. Centerline gas temperature profiles of the HPFFB steam/CO_2 conditions corrected for radiation losses from the thermocouple bead.

Replicate HPFFB char gasification experiments were performed at ~30% of the conditions; the repeated mass release measurements were typically within 4 wt% daf of the previously measured values. The data in Table 8.5 and Table 8.6 were used to fit kinetic coefficients to the gasification model. A complete summary of all the measured particle mass release data can be found in Appendix F.

Table 8.5. Summary of averaged mass release measured data at the HPFFB steam conditions

Total Pressure	Max Gas Temperature	Equilibrium H_2O; CO_2	Utah Res. Time	Utah %MR[f] (daf)	Pitt #8 Res. Time	Pitt #8 %MR[f] (daf)	ILL #6 Res. Time	ILL #6 %MR[f] (daf)
10 atm	1814 K	7.5; 14.2 mol%	42 ms	17.7	45 ms	11.6	45 ms	14.0
			107 ms	40.9	116 ms	26.2	116 ms	22.5
			183 ms	46.3	199 ms	40.1	198 ms	24.1
12.5 atm	1782 K	7.7; 14.1 mol%	47 ms	18.9	52 ms	17.1	52 ms	22.6
			118 ms	35.1	135 ms	38.8	134 ms	36.7
			202 ms	72.4	232 ms	60.6	231 ms	41.5
15 atm	1611 K	7.3; 11.4 mol%	55 ms	20.5	59 ms	10.2	59 ms	8.9
			139 ms	26.8	153 ms	18.5	153 ms	27.5
15 atm	1830 K	8.6; 13.7 mol%	49 ms	21.6	52 ms	10.2	51 ms	25.2
			126 ms	49.1	135 ms	44.8	135 ms	57.4
			219 ms	75.9	237 ms	68.7	236 ms	66.3

[f]mass release on a daf char basis

Table 8.6. Summary of averaged mass release measured data at the HPFFB steam/CO_2 conditions

Total Pressure	Max Gas Temperature	Equilibrium H_2O; CO_2	Residence Time	%MR[f] (daf)
15 atm	1812 K	7.7; 83.2 mol%	51 ms	22.3
			130 ms	54.3
			222 ms	68.0
15 atm	1879 K	7.5; 33.3 mol%	49 ms	20.5
			130 ms	64.0
			224 ms	75.5

[f]mass release on a daf char basis

8.2 Coal Char Gasification Modeling

8.2.1 Regressing Kinetic Parameters for Steam Gasification of Coal Char

Kinetic parameters were regressed for the steam gasification of Illinois #6, Utah Skyline, and Pittsburgh #8 coal chars using measured data from the HPFFB reactor at gas conditions (see Table 8.2) where the majority of char conversion was due to steam gasification. The first-order global model described in Section 6.2 was used to model the gasification of coal chars. As described previously, the HPFFB steam conditions contained some CO_2 since it was not possible to have conditions completely free of CO_2 in the post-flame environment of the reactor. Since the global first-order char conversion model is dependent on the partial pressure of a single gasification agent, it was therefore necessary to differentiate the measured particle mass release between that caused by CO_2 gasification and that due to H_2O gasification. To achieve this, particle mass release caused by CO_2 gasification in the HPFFB steam gasification experiments (see Table 8.2) was accounted for using the global first-order model, and the remaining measured particle mass release was attributed to steam gasification. This approach assumed that char gasification rates by CO_2 and H_2O are additive, although there is disagreement in the literature about how to model char gasification in mixed atmospheres of CO_2 and H_2O (Roberts and Harris, 2007; Guizani et al., 2013). The particle mass release due to steam was then used to regress steam gasification kinetic parameters for the first-order model. The decrease in external surface area of the coal chars with increased conversion was included in the modeling using particle diameter predictions from Equation (7.1).

8.2.1.1 Illinois #6 Char

When regressing steam gasification kinetic parameters for ILL #6 char using the measured data from the HPFFB steam conditions, mass release due to CO_2 gasification of ILL #6 coal char was accounted for using published CO_2 gasification rates (Shurtz and Fletcher, 2013). It was convenient since the reported Illinois #6 CO_2 gasification kinetic parameters (i.e., A = 0.8876 g/cm^2/s/atm and E = 121.3 kJ/mol) were for the same first-order model used in this work (see Section 6.2). Illinois #6 coal char (75-106 μm) was also fed in the HPFFB reactor at the 10 atm $T_{gas,max}$ = 1850 K CO_2 condition (see Section 8.1.3) to aid in the accounting of char conversion due to CO_2 gasification. This HPFFB gas condition was specifically chosen since it provided a data point of particle mass release solely due to CO_2 gasification since this condition contained very little steam (0.9 mol%). The 10 atm $T_{gas,max}$ = 1850 K condition also had a similar temperature profile as the steam conditions (see Figure 8.4), yet contained the highest partial pressure of CO_2 (i.e., P_{CO2} = 2.08 atm). Therefore, the measured mass release of coal char at the 10 atm $T_{gas,max}$ = 1850 K condition after ~300 ms provided an upper bound of the particle mass release due to CO_2 gasification in the steam experiments. The mass release data point from the 10 atm $T_{gas,max}$ = 1850 K condition also allowed a quality check of the published CO_2 gasification kinetics (Shurtz and Fletcher, 2013) before these kinetics were used to predict particle mass release due to CO_2 in the steam gasification HPFFB experiments. Since there was only a 2.0 wt% discrepancy (char basis) between the measured and modeled daf mass release at the 10 atm $T_{gas,max}$ = 1850 K condition when feeding ILL #6 coal char, it was concluded that the published ILL #6 CO_2 gasification rates (Shurtz and Fletcher, 2013) provided accurate estimates of the ILL #6 char conversion due to CO_2 at the HPFFB steam conditions (see Table 8.2).

Figure 8.6 shows the prediction of mass release of ILL # 6 char due to CO_2 and H_2O after the first collection height at 1" above the burner at the 15 atm $T_{gas,max}$ = 1830 K HPFFB steam condition. As previously stated, published CO_2 gasification rates (Shurtz and Fletcher, 2013) of ILL #6 coal char were used to account for the char conversion due to CO_2 at this condition. From the figure, it is easily seen that most of the mass release of ILL #6 coal char was due to steam gasification. For example, steam gasification accounted for 83% of the particle mass release at the last collection point at a particle residence time of 236 ms. The 15 atm $T_{gas,max}$ = 1830 K steam condition resulted in the highest char conversion by CO_2 of all 4 steam conditions. Therefore, the particle mass release due to CO_2 in the other 3 steam conditions (see Table 8.2) would be less that that shown in Figure 8.6.

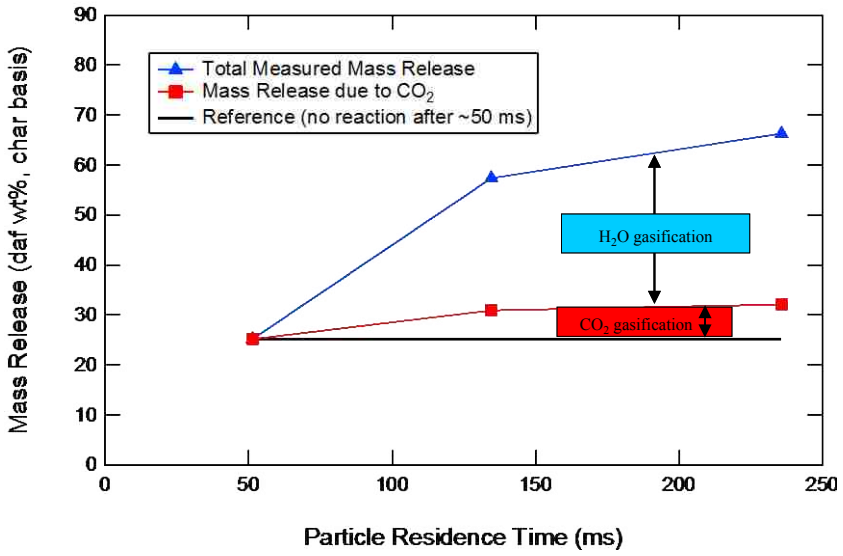

Figure 8.6. Effect of char mass release by H_2O and CO_2 gasification when feeding 15 atm-pyrolyzed 75-106 µm ILL #6 coal char in the HPFFB reactor at the 15 atm $T_{gas,max}$ = 1830 K steam condition.

8.2.1.2 Utah Skyline Char

When regressing steam gasification kinetic parameters for Utah Skyline char using measured HPFFB data, a published empirical correlation (Shurtz and Fletcher, 2013) was evaluated to account for CO_2-induced particle mass release. The published empirical correlation was a function of raw coal composition and predicted the pre-exponential factor, A, at a fixed value of E (123 kJ/mol) for the first-order model described in Section 6.2. The method of using the published empirical correlation to predict the char conversion caused by CO_2 gasification of Utah Skyline char was abandoned when the predicted char mass release on a daf basis was about double that measured (i.e., 58.5% vs 28.6%) when feeding 45-75 μm Utah Skyline char at the 10 atm $T_{gas,max}$ = 1850 K non-steam HPFFB condition using a particle residence time of 285 ms (5.5" collection height).

Instead, CO_2 gasification kinetic constants were regressed for Utah Skyline char using the data collected at the 10 atm $T_{gas,max}$ =1850 K non-steam condition. It would have been ideal to regress CO_2 gasification kinetic parameters of Utah Skyline char with a more complete set of CO_2 gasification data, but this was not possible due to resource constraints of the project. However, it is thought that using the regressed CO_2 gasification kinetic parameters from the limited CO_2 gasification HPFFB data measured in this project yielded more accurate results than if the aforementioned empirical correlation was used.

Setting E = 123 kJ/mol as was done previously for coal chars (Shurtz and Fletcher, 2013), the regressed A parameter was 1.2105 g/cm^2/s/atm for the measured Utah Skyline char CO_2 gasification data at the 10 atm $T_{gas,max}$ =1850 K non-steam condition. As a comparison, A values of 2.679 and 3.006 g/cm^2/s/atm for Utah Skyline char were predicted using the empirical correlations of Shurtz and Fletcher (2013) based on elemental coal composition (C/O daf mass

ratio) and predicted NMR parameters, respectively. The activation energy, E, was ultimately set to 121.3 kJ/mol for gasification of Utah Skyline char in order to make convenient reactivity comparisons with Illinois #6 coal since allowing E to vary for the Utah Skyline data set did not make significant improvements to the model fit. Recall that 121.3 kJ/mol was the published (Shurtz and Fletcher, 2013) first-order model activation energy of ILL #6 char for the CO_2 gasification reaction.

Figure 8.7 shows the prediction of mass release of Utah Skyline char due to CO_2 and H_2O after the first collection height at 1" above the burner at the 15 atm $T_{gas,max}$=1830 K steam HPFFB condition. The regressed parameters (A = 1.0655 g/cm^2/s/atm and E = 121.3 kJ/mol) were used to account for the char conversion due to CO_2 at this condition. From the figure, it is easily seen that most of the mass release of Utah Skyline coal char was due to steam gasification, just as was observed in Figure 8.6 for ILL #6 char. For example, steam gasification accounted for 85% of the char mass release at the last collection point at a particle residence time of 219 ms.

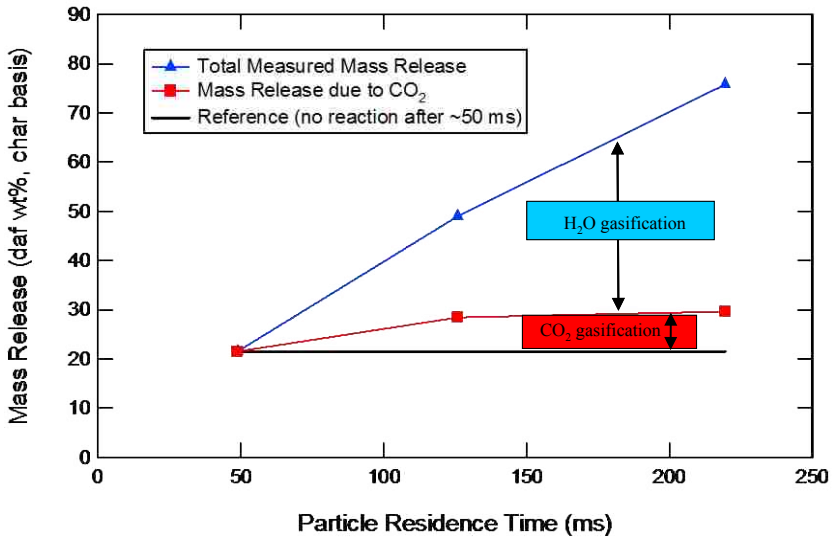

Figure 8.7. Effect of char mass release by H_2O and CO_2 gasification when feeding 15-atm pyrolyzed 45-75 µm Utah Skyline char in the HPFFB reactor at the 15 atm $T_{gas,max}$=1830 K steam condition.

8.2.1.3 Pittsburgh #8 Char

When regressing steam gasification kinetic parameters for Pitt #8 char, mass release due to CO_2 gasification was accounted for in the HPFFB steam gasification experiments using the same aforementioned empirical correlation (Shurtz and Fletcher, 2013) that was a function of the C/O daf mass ratio of the raw coal. The resulting E and A values for the first-order CO_2 gasification model for Pitt #8 char were 123 kJ/mol and 0.7772 g/cm^2/s/atm, respectively. The mass release data collected at ~290 ms (5.5" collection height) when feeding 75-106 μm Pitt #8 10 atm char at the 10 atm $T_{gas,max}$=1850 K non-steam HPFFB condition allowed a quality check of the published empirical correlation for the CO_2 gasification kinetics (Shurtz and Fletcher, 2013) before it was used to predict char conversion by CO_2 in the Pitt #8 HPFFB steam gasification experiments (see Table 8.2). Since there was only a 2.4 wt% discrepancy between the measured and modeled daf mass release at the 10 atm $T_{gas,max}$=1850 K condition when feeding Pitt #8 char, it was concluded that the empirical correlation (Shurtz and Fletcher, 2013) provided a reasonable estimate of the Pitt #8 char conversion due to CO_2 at the HPFFB steam conditions.

Figure 8.8 shows the prediction of mass release of Pitt #8 char due to CO_2 and H_2O after the first collection height at 1" at the 15 atm $T_{gas,max}$=1830 K HPFFB steam condition. As previously stated, char conversion caused by CO_2 gasification was accounted for using predicted kinetic parameters (A = 0.7772 g/cm^2/s/atm and E = 123 kJ/mol) in the first-order model in Section 6.2. From the figure, it is easily observed that the majority of mass release of Pitt #8 coal char was due to steam gasification. For example, steam gasification accounted for 91% of the particle mass release at the last collection point at a particle residence time of 237 ms. The mass release of the Pitt #8 char due to CO_2 gasification in any of the other 3 steam conditions would

be less than that shown in Figure 8.8 since the 15 atm $T_{gas,max}$ =1830 K steam condition resulted in the highest mass release due to CO_2 of all 4 steam conditions.

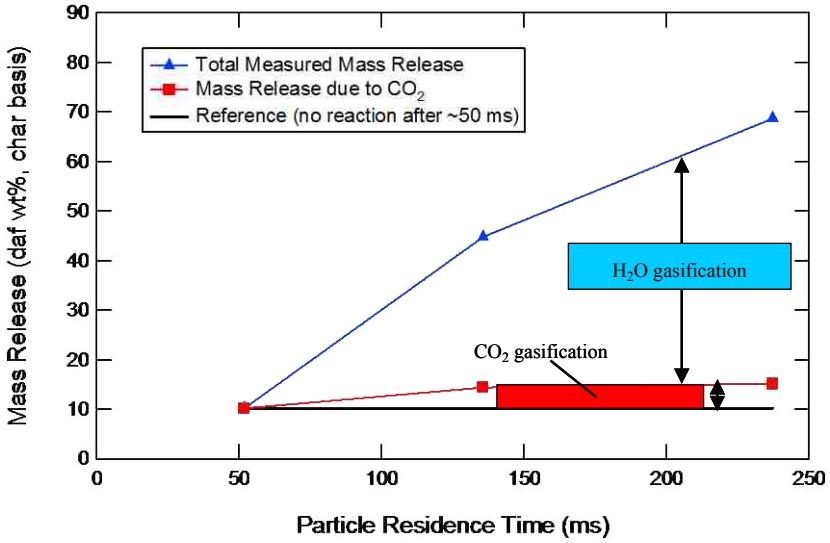

Figure 8.8. Effect of char mass release by H_2O and CO_2 gasification when feeding 15 atm-pyrolyzed 75-106 µm Pitt #8 coal char in the HPFFB reactor at the 15 atm $T_{gas,max}$ = 1830 K steam condition.

8.2.1.4 Coal Char Gasification Modeling Results

In summary, particle mass release caused by CO_2 gasification in the HPFFB steam gasification experiments (see Table 8.2) was accounted for using the global first-order model in Section 6.2 (with CO_2 kinetic parameters from various sources), and the remaining measured particle mass release was attributed to steam gasification. The particle mass release data attributed to steam was then used to regress first-order steam gasification kinetic parameters for each coal char (ILL #6, Utah, Pitt #8) by minimizing the sum squared error between modeled and measured particle mass release data from 4 gas conditions in the HPFFB at typically 3 residence times per gas condition.

The regressed kinetic parameters are summarized in Table 8.7, but should be used with some caution. For example, these values are predicted to yield satisfactory estimates of particle

mass release caused by gasification of coal char for pulverized particle sizes similar to those used in this study (see Table 8.4). However, the first-order global model used in this study assumes no particle temperature gradients, which no longer applies when particle sizes are much beyond about 150-200 μm. The maximum χ factor (see Section 6.5) in the steam gasification data sets was only 0.06, which indicates that the measured rates of char conversion did not occur in the Zone III regime where film diffusion controls.

When the reactivity data of 2 feedstocks have been fit to the same first-order model and they both use the same *E* value, convenient rate comparisons are performed by using ratios of pre-exponential factors. The steam kinetic parameters in Table 8.7 were derived from data where T_p and $P_{H2O,surf}$ values ranged from about 1250-1660 K and 0.65-1.25 atm, respectively. Using data in this table reveals that Utah Skyline char is about 1.5 times (i.e., 7.9418 / 5.3497) more reactive to steam than the ILL #6 char.

Table 8.7. H_2O and CO_2 gasification kinetic parameters for use in the global first-order model

Coal Feedstock	***E*** *(kJ/mol)*	***A*** (H_2O gasification[g]) $\left[\frac{g\ Carbon}{cm^2 \cdot s \cdot atm\ H_2O}\right]$	***A*** (CO_2 gasification) $\left[\frac{g\ Carbon}{cm^2 \cdot s \cdot atm\ CO_2}\right]$
Illinois #6	121.3 (Shurtz and Fletcher, 2013)	5.3497	0.8876 (Shurtz and Fletcher, 2013)
Utah Skyline	121.3	7.9418	1.0655[h]
Pittsburgh #8	123.0	12.5510	0.7772 [i] (Shurtz and Fletcher, 2013)

[g]The steam kinetic parameters were derived from data where T_p and $P_{H2O,surf}$ values ranged from about 1250-1660 K and 0.65-1.25 atm, respectively. [h] This kinetic constant was derived in this project using limited data. [i] This kinetic constant was from a published empirical correlation based on elemental coal composition.

Note in Table 8.7 the slightly higher activation energy for Pitt #8 char that was used to stay consistent with the empirical correlation (Shurtz and Fletcher, 2013) used to model its CO_2 reactivity. However, when modeling the steam gasification data of Pitt #8 char with E = 121.3,

the corresponding *A* value that led to the minimize sum squared error between modeled and measured particle mass release was 10.9746. Using ratios of *A* values, this results that the Pitt #8 char was 2.3 (i.e., 12.5510 / 5.3497) times more reactive to steam than ILL #6 char and 1.6 (i.e., 12.5510 / 7.9418) times more reactive to steam than the Utah Skyline char.

Note also in Table 8.7 that each coal char uses the same *E* value to model both its CO_2 and H_2O gasification rate. This allows rate comparisons of the CO_2 and H_2O gasification reactions of a given coal char using similar ratios of pre-exponential factors. Steam gasification rates of the coal chars were anywhere from 6 (i.e., 5.3497 / 0.8876) to 16 times (i.e., 12.5510 / 0.7772) faster than the corresponding CO_2 gasification rates. These rate comparison values between the steam and CO_2 gasification reactions are similar to those measured in a recent study by Huo et al. (2014) at temperatures of 850 and 900 °C in a TGA reactor. For example, it was reported that the initial rates of steam gasification were about 6-13 and 4-10 times faster than CO_2 gasification of petroleum coke and anthracite coal chars, respectively.

Global kinetic models often provide accurate representations of particle mass release within the range measured in lab experiments. However, large deviations from predicted mass release is known to occur at the latter stages of conversion (Hurt et al., 1998). Hence, the kinetic parameters summarized in Table 8.7 are predicted to yield satisfactory estimates of char mass release due to steam gasification up to the measured conversions of 59, 68, and 64 wt% (daf char basis) for ILL #6, Utah Skyline, and Pitt #8 chars, respectively. Predictions of particle mass release at very high conversions requires accounting for phenomena such as ash inhibition (Hurt et al., 1998).

The parity plots shown in Figure 8.9 show how the measured particle mass release data attributed to steam gasification compared with that predicted by the first-order model using

steam kinetic parameters in Table 8.7. The fits of the first-order model in Figure 8.9 are very encouraging considering the simplicity of the model.

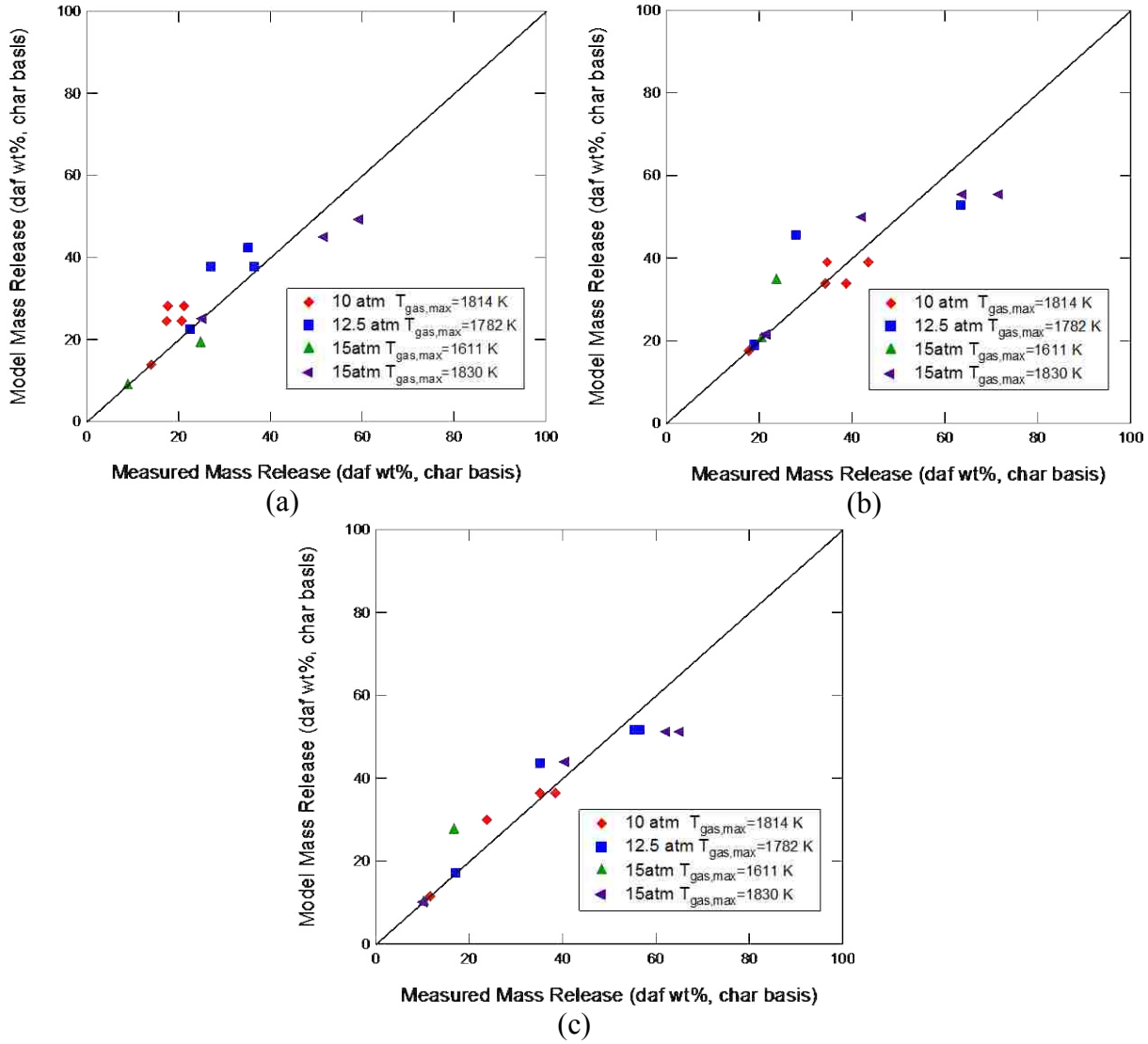

Figure 8.9. Parity plots of HPFFB H_2O gasification data for (a) Illinois #6, (b) Utah Skyline, and (c) Pitt #8 coal chars using particle mass release data attributed to H_2O gasification.

The relative error (see Equation (6.6)) was calculated using experimental steam mass release data from the 4 HPFFB steam conditions and the predictions of the model using kinetic parameters in Table 8.7. The experimental mass release data in this calculation were the values in Table 8.5 with the particle mass release attributed to CO_2 gasification subtracted. The relative

error between the Utah Skyline modeled and measured particle mass release data (daf char basis) was 8.9%. From similar calculations, the ILL #6 and Pitt #8 data had errors of 10.0% and 8.1%, respectively.

8.2.1.5 Comparison to the Literature

The steam gasification rates of the 3 coal chars from the current study (ILL #6, Utah Skyline, & Pitt #8) were compared with published (Shurtz and Fletcher, 2013) CO_2 gasification rates of several different coals in Figure 8.10. Both the steam rates from the current study and the CO_2 rates from the literature were modeled using the same global first-order model described in Section 6.2. The first-order rate constants in Figure 8.10 are each plotted over the particle temperature ranges of the experimental data used to regress the rate parameters. From the figure, it is seen that the steam gasification rates in this study exceeded the CO_2 gasification rates from the literature in every instance. This serves as a quality check of the steam gasification rates in the current work, since the H_2O gasification reaction has been reported in several instances (Walker et al., 1959; Everson et al., 2006; Zhang et al., 2013) as being faster than the CO_2 gasification reaction (although reactivity differences between different coal feedstocks should also be considered). Another quality check of the reported steam gasification rates is made possible since Illinois #6 coal was common to both the current work and the published work (Shurtz and Fletcher, 2013). The ratio of H_2O to CO_2 gasification rates for Illinois #6 coal char is 6, which is on the order of rate ratios reported in the literature for the H_2O and CO_2 gasification reactions (Walker et al., 1959; Moilanen and Muhlen, 1996; Ahmed and Gupta, 2011; Fan et al., 2013; Tremel and Spliethoff, 2013; Zhang et al., 2013; Huo et al., 2014).

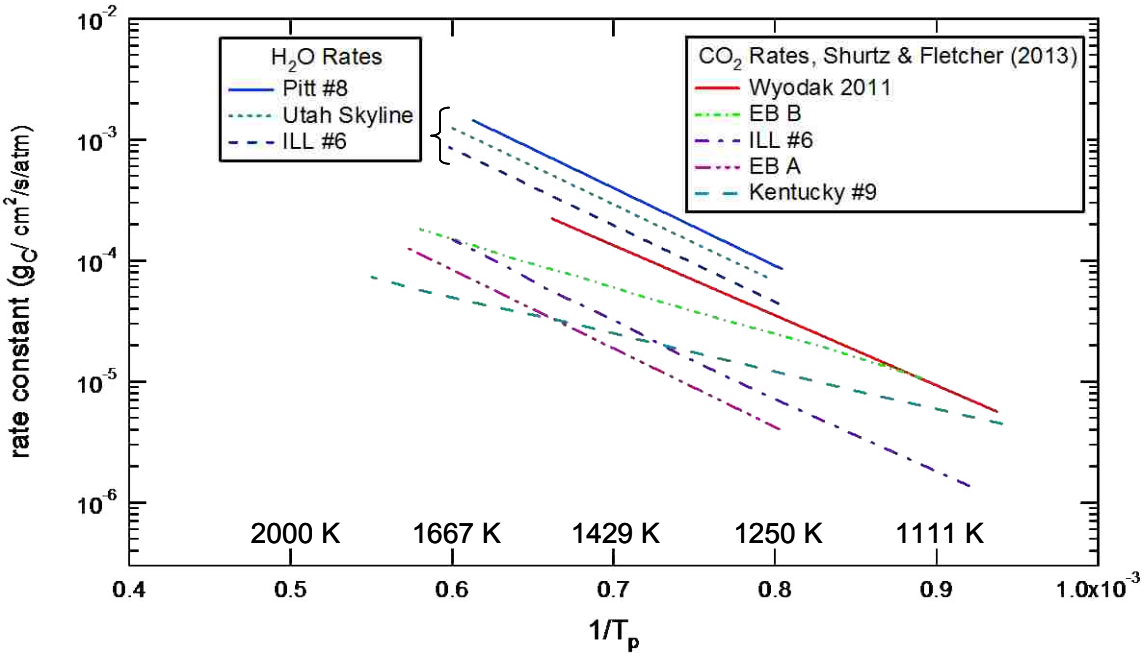

Figure 8.10. Comparison of the steam gasification rate constants of this work with the CO_2 gasification rate constants of Shurtz and Fletcher (2013). The coals EB A and EB B refer to Eastern Bituminous coals A and B, respectively.

8.2.2 Gasification of ILL #6 Coal Char by Both H_2O and CO_2

A single re-injected 75-106 μm coal char (Illinois #6) was gasified at conditions in the HPFFB reactor where significant mass release was due to both steam and CO_2. The re-injected ILL #6 char was generated at 15 atm in the HPFFB reactor (see Section 8.1.1), and the properties of this char feedstock were summarized in Table 8.4. The HPFFB steam/CO_2 conditions (see Table 8.3) contained much higher CO_2 concentrations than the HPFFB steam conditions (see Table 8.2), which allowed CO_2 to account for a much higher fraction of the total particle mass release at the steam/CO_2 conditions. Similar concentrations of H_2O were used in both sets of conditions, since attempting to increase the steam concentration in the HPFFB post-flame environment by supplying the burner with increased H_2 was avoided to prevent damage to the HPFFB burner (see Section 8.1.2). The steam/CO_2 HPFFB experiments utilized 2 gas conditions

(see Table 8.3) at a total pressure of 15 atm, which is the highest operating pressure of the HPFFB reactor. The high pressure was chosen in order to maximize the partial pressures of the two gasification agents, thus guaranteeing the highest extents possible of coal char gasification in the limited particle residence times inside the HPFFB reactor. The composition of the steam/CO_2 post-flame environment was included in Table 8.3, and the measured centerline gas temperature profiles of the 2 steam/CO_2 HPFFB conditions were included in Figure 8.5.

Measured and predicted mass release values of the ILL #6 coal char at the 2 steam/CO_2 conditions of the HPFFB reactor are shown in Figure 8.11. Note that replicates of the measured particle mass release values are shown in the figure.

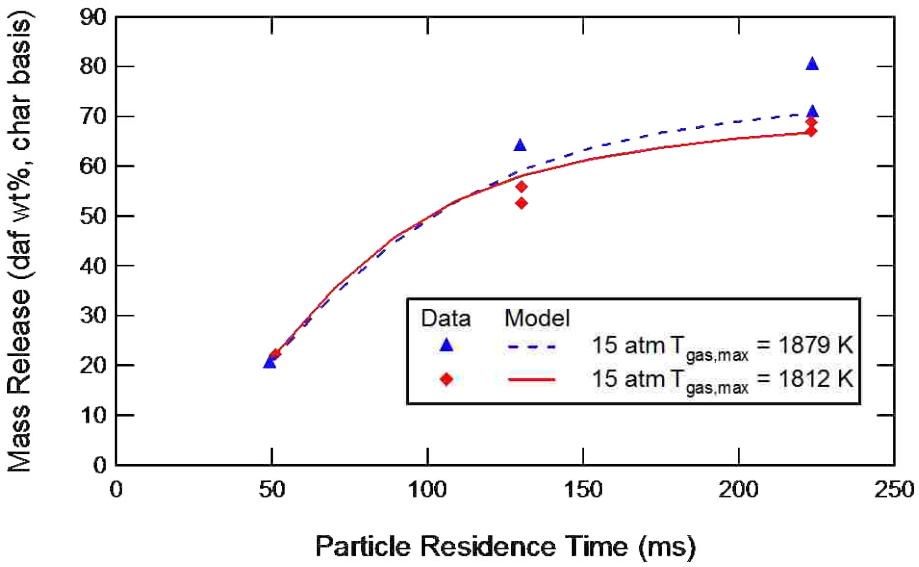

Figure 8.11. Measured and predicted values of daf mass release of 75-106 μm ILL #6 coal char at the steam/CO_2 conditions in the HPFFB reactor at 15 atm.

The predicted mass release curves in Figure 8.11 came from the addition of particle mass release predicted by CO_2 and H_2O gasification using the first-order model with the ILL #6 kinetic parameters in Table 8.7, which included published CO_2 kinetic parameters (Shurtz and Fletcher, 2013) and H_2O kinetic parameters that were regressed in the current study. The prediction of the

particle mass release values agreed well with the measured values at both conditions where the peak gas temperatures were 1812 K and 1879 K.

Although the partial pressure of CO_2 at the 15 atm $T_{gas,max}$ = 1812 K HPFFB condition was 2.5 times higher than at the 15 atm $T_{gas,max}$ = 1879 K condition (see Table 8.3), similar mass release values were measured at both conditions (see Figure 8.11) since rates are exponential with temperature and the 15 atm $T_{gas,max}$ = 1879 K condition was hotter (see Figure 8.5).

Figure 8.12 and Figure 8.13 show the predictions of the global first-order model for the distribution of particle mass release due to H_2O and CO_2 gasification using kinetic parameters in Table 8.7 for the case when 15-atm pyrolyzed 75-106 μm ILL #6 coal char was re-injected at the 15 atm $T_{gas,max}$ = 1812 K and 15 atm $T_{gas,max}$ = 1879 K steam/CO_2 HPFFB conditions, respectively.

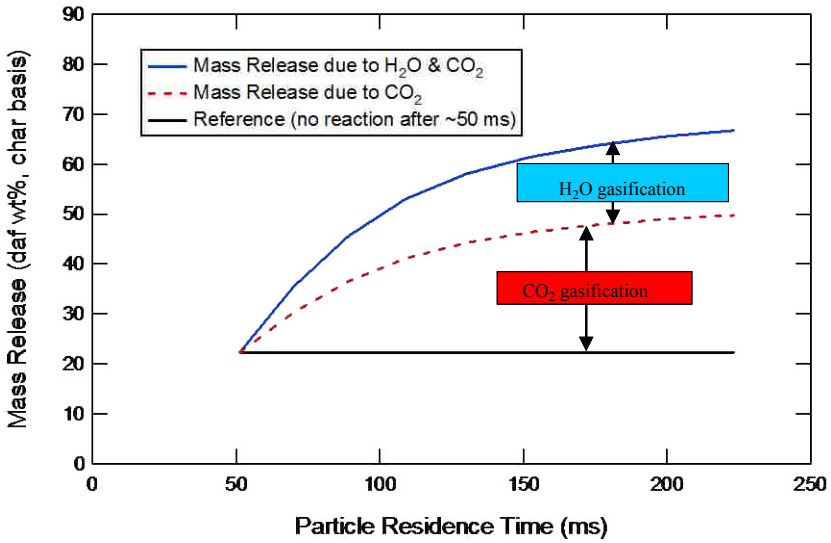

Figure 8.12. First-order model predictions for the distribution of mass release caused by H_2O and CO_2 gasification using kinetic parameters in Table 8.7 for 75-106 μm ILL #6 char reacted at the 15 atm $T_{gas,max}$ = 1812 K steam/CO_2 HPFFB condition.

Although the first-order model predicts similar *total* mass release of ILL #6 coal char at the 2 steam/CO_2 HPFFB conditions, it is predicted that 62% of the total particle mass release is due to CO_2 at the 15 atm $T_{gas,max}$ = 1812 K condition when compared to only 43% at the 15 atm $T_{gas,max}$

= 1879 K condition at particle residence times near 220 ms. The CO_2-induced mass release of ILL #6 char at the 2 steam/CO_2 HPFFB conditions was higher when compared to data summarized in Figure 8.6 partly because P_{CO2} at the 15 atm $T_{gas,max}$ = 1830 K steam condition was 2.4 to 6.1 times lower.

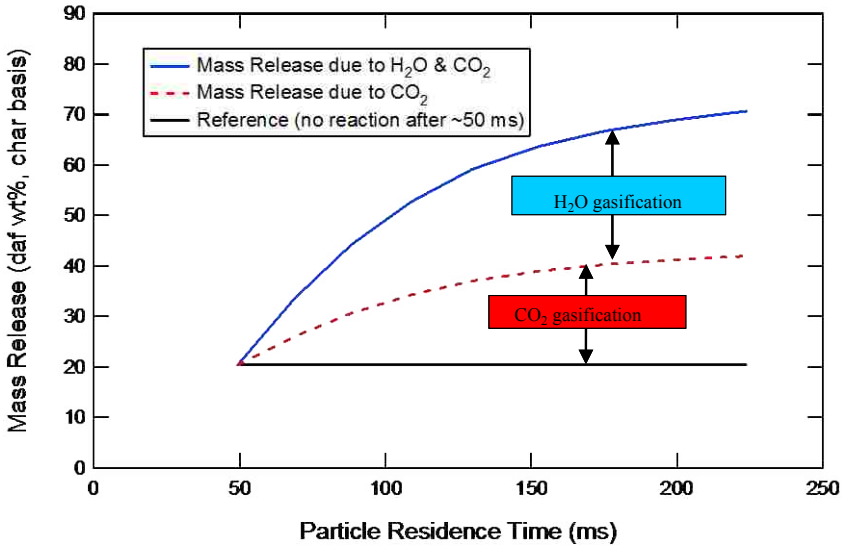

Figure 8.13. First-order model predictions for the distribution of mass release caused by H_2O and CO_2 gasification using kinetic parameters in Table 8.7 for 75-106 μm ILL #6 char reacted at the 15 atm $T_{gas,max}$ = 1879 K steam/CO_2 HPFFB condition.

8.3 Summary

Steam gasification rates of 3 bituminous coal chars (Illinois #6, Utah Skyline, & Pittsburgh #8) were modeled using measured data from the HPFFB reactor at total pressures up to 15 atm and gas temperatures up to 1830 K. The coal chars fed in gasification experiments were generated at conditions of high heating rate at the same total pressure as their respective char gasification experiments. Since the reaction environment in the HPFFB steam gasification experiments contained some CO_2, the CO_2-induced char conversion was taken into account, and the remaining measured particle mass release was attributed to steam gasification. The particle mass release data caused by steam was then used to regress steam gasification kinetic parameters

for a global first-order model. Pitt #8 char was measured to be 2.3 times more reactive to steam than ILL #6 char and 1.6 times more reactive to steam than the Utah Skyline char. Steam gasification rates were measured to be 6 to 16 times faster than CO_2 gasification rates at the conditions studied.

Illinois #6 coal char (75-106 μm) was reacted at conditions at 15 atm in the HPFFB reactor where significant particle mass release occurred by both CO_2 and H_2O. The measured particle mass release data were accurately modeled from the addition of particle mass release predicted by CO_2 and H_2O gasification using the first-order model with the ILL #6 kinetic parameters documented in this chapter.

9. Summary and Conclusions

9.1 Experiments and Modeling of Biomass Pyrolysis

Biomass pyrolysis experiments were performed at atmospheric pressure using conditions of high initial particle heating rate (~7.4×10^4 K/s) in an entrained-flow reactor. A flat-flame burner was used in the reactor to generate well characterized conditions at maximum gas temperatures in the range 1163-1433 K. Pyrolysis yields were measured for 45-75 μm diameter sawdust, switchgrass, corn stover, and straw particles. The high temperatures used in the FFB biomass pyrolysis experiments caused most of the biomass tar to thermally crack into light gas, even at short residence times around 30 ms. Only limited experiments could be performed with corn stover since this feedstock caused serious feeding problems. The measured volatile yields from pyrolysis were 99.3, 94.8, 93.3, and 92.4 wt% daf for poplar sawdust, switchgrass, corn stover, and straw, respectively. Due to the rapid particle heating rates in the entrained-flow reactor, volatile yields of the biomass exceeded the ASTM volatiles value by ~10 wt% daf. A refractory biomass tar yield near 1-2 wt% daf was measured in the reducing environment of the reactor for all 4 biomass feedstocks. On a weight basis, 13-19% of the initial ash content was released to the gas phase during the pyrolysis experiments.

Biomass pyrolysis was modeled using the Chemical Percolation Devolatilization (CPD) model assuming that biomass pyrolysis occurs as a weighted average of its individual

components (cellulose, hemicellulose, and lignin). A kinetic parameter of hemicellulose was modified for use in the CPD model to improve predictions about tar and gas yields from hemicellulose pyrolysis. Kinetic parameters were regressed for a first-order tar-cracking model to describe the rate at which biomass tar thermally cracks into light gas above ~500 °C. The CPD model accurately predicted biomass pyrolysis yields of straw, switchgrass, and 3 species of wood from 3 reactors (flat-flame burner, drop-tube, and TGA).

9.2 Experiments and Modeling of Biomass CO_2 Gasification

Biomass chars of sawdust, switchgrass, and corn stover were generated at high initial particle heating rates (~ 10^4 K/s) in a drop tube reactor at atmospheric pressure using short residence times (<3 s). Near-spherical biomass chars (~100 μm) were then re-injected separately in the high-pressure flat-flame burner (HPFFB) reactor at elevated temperatures ($T_{gas,max}$ > 1800 K) and pressures (10-15 atm) to measure CO_2 gasification rates of the biomass chars at conditions where the bulk phase consisted of ~40 and ~90 mol% CO_2. The optimal kinetic parameters were regressed for each of the chars using a first-order char gasification model.

A new method was developed to produce near-spherical particles from non-spherical biomass chars. This method involved grinding biomass chars with an electric grinder controlled by a variable transformer, and works well even when only limited quantities of biomass char are available. Poplar sawdust char generated at high heating rates was naturally spherical after passing through a plastic stage during pyrolysis. Spherical sawdust char likely only results after pyrolysis of small particles at high heating rates.

Over the range of experimental conditions studied, the char CO_2 gasification rate per external surface area (r_p'') for poplar sawdust char was about 3.9 times faster than for switchgrass

char, but only about 20% faster than corn stover char. Biomass gasification rates measured at entrained-flow conditions appear to be much faster than those reported in most TGA studies.

9.3 Experiments and Modeling of Petroleum Coke CO_2 Gasification

The pyrolysis and CO_2 gasification of 2 industrially obtained petroleum coke samples (referred to as Petcoke A and B) were studied at conditions of high initial particle heating rate and temperature in entrained-flow reactors. The ASTM volatiles value for both Petcokes A and B were good approximations of the pyrolysis mass release at conditions of atmospheric pressure and high particle heating rate, which differs from other solid fuels such as coal and biomass that typically have increased pyrolysis volatile yields at high heating rate. SEM images of the petcoke chars were used to study the morphology of partially gasified samples collected from the HPFFB reactor. The structure of Petcoke A had cracks in its surface, but otherwise appeared very similar to that of its raw feedstock. Petcoke B char contained a small fraction of swollen, thin-shelled particles that resembled pyrolyzed bituminous coal chars from high heating rate conditions.

Petcoke CO_2 char gasification rates were measured following *in-situ* pyrolysis in the HPFFB reactor at total pressures of 10 and 15 atm at conditions where the bulk phase consisted of ~40 and ~90 mol% CO_2 using peak centerline gas temperatures up to 1900 K. Measured data were used to regress optimal kinetic parameters for a first-order model that describes char conversion by CO_2. A reactivity comparison between petcoke and coal was also performed in the HPFFB reactor at 15 atm where the peak centerline gas temperature was 1848 K. The char gasification rates for both petcoke samples were higher than Illinois #6 coal char at $P_{CO2,surf}$ = 11 atm and T_p = 1500 K, even though most reactivity comparisons between petcoke and coal at lower temperatures and pressures typically result in coal being more reactive.

9.4 Experiments and Modeling of Coal Gasification

Steam gasification rates of 3 coal chars (Illinois #6, Utah Skyline, & Pittsburgh #8) were modeled using measured data from the entrained-flow HPFFB reactor at gas temperatures up to 1830 K and total pressures of 10-15 atm. The coal chars fed in gasification experiments were generated at conditions of high heating rate at the same total pressure as their respective char gasification experiments. Since the reaction environment in the HPFFB steam gasification experiments contained some CO_2, the CO_2-induced char conversion was taken into account, and the remaining measured particle mass release was attributed to steam gasification. The particle mass release data caused by steam was then used to regress steam gasification kinetic parameters for a global first-order model. Steam gasification rates were measured to be 6 to 16 times faster than CO_2 gasification rates at the conditions studied. Pittsburgh #8 char was the most reactive to steam, followed by Utah Skyline and Illinois #6 chars.

In addition, Illinois #6 coal char was reacted at high temperature conditions and a pressure of 15 atm in the HPFFB reactor, resulting in significant particle mass release by both CO_2 and H_2O. The measured particle mass release data were accurately modeled by simply adding the first-order CO_2 and H_2O gasification rates obtained in this work for an Illinois #6 coal char.

9.5 How this Research Can Affect Gasifier Design and Operation

The first-order char gasification model and the regressed kinetic parameters in this work (see Section 6.2) allow a prediction of char conversion for pulverized particles in entrained-flow conditions when given 1-D input profiles of residence time, reactant gas concentration, and

temperature. Therefore, the gasification model can find use in CFD codes, by accounting for the exchange of gas species and enthalpy between the char particles and the gas phase (Shurtz and Fletcher, 2013). The insight gained into fuel reactivity will also be of value in the determination of optimal dimensions of future entrained-flow gasifiers, where high char conversions are desired in short residence times, and where any over-design of the gasifier results in hefty capital equipment costs.

The reported char gasification rates in this work can also aid in the optimal operation of commercial entrained-flow gasifiers (Liu et al., 2010b). For example, a sub-stoichiometric amount of oxygen is supplied to a gasifier to react with the fuel since the exothermic combustion reaction provides the heat necessary to drive the endothermic gasification reactions. Although operating the gasifier at an increased O_2/fuel ratio raises the gasifier temperature, a higher concentration of undesired CO_2 and H_2O compose the syngas. Conversely, operating the gasifier at a decreased O_2/fuel ratio results in a higher concentration of desired product gases (i.e., CO & H_2), but the gasifier temperature will decrease which may result in incomplete conversion of the fuel in the limited residence time available in the gasifier. Therefore, char gasification rates provide some insight into the most favorable operating conditions of a gasifier.

9.6 Recommendations for Future Research

It is recommended that the Bio-CPD model be continually improved. Currently, only limited data from the literature was used to determine kinetic parameters of cellulose, hemicellulose, and lignin for the Bio-CPD model. Using a much larger pyrolysis data set from the literature for the main biomass components (cellulose, hemicellulose, & lignin) and

regressing new kinetic parameters for each component may allow even more accurate predictions of biomass pyrolysis yields as a function of time, temperature, pressure, and heating rate.

Biomass pyrolysis yields could be measured at pressurized conditions in the HPFFB reactor to explore the effect of pressure on biomass pyrolysis yields. For these proposed experiments, however, it is suggested that the HPFFB reactor be transformed into a drop-tube reactor. This will enable the measurement of a more meaningful set of pyrolysis data since a Hencken flat-flame burner cannot operate at low enough temperatures to study the extent of pyrolysis. In addition, using the reactor in drop-tube mode in an inert atmosphere for pressurized biomass pyrolysis experiments would prevent mistaking any unintended char gasification for pyrolysis volatile yields, as long as a high enough gas temperature can be achieved in drop tube mode.

The coal char gasification data measured in this work (see Chapter 8) were used to regress kinetic parameters for a first-order model. However, it is recommended that the coal data be fit to a more complex char gasification model, such as the Char Conversion Kinetics (CCK) model developed by Shurtz (2011). Fitting the coal data to the CCK model will likely allow improved predictions of the coal chars at high conversions since the CCK model includes both a thermal deactivation and ash inhibition mechanism.

In this work, the CO_2 char gasification rates of biomass (Chapter 6) and petcoke (Chapter 7) were measured and modeled. However, it is recommended that the H_2O char gasification rates of biomass and petcoke be measured and modeled using the HPFFB reactor. The two fuels could be fed separately at the same HPFFB steam conditions developed in this work for coal (see Table 8.2), or at conditions of higher steam concentrations (see below).

The HPFFB steam concentrations used in this study were limited to less than 9 mol% in the post-flame environment due to concerns about damaging the burner head (see Section 4.2.2). It is recommended that char gasification rates (biomass, coal, & petcoke) be measured in the HPFFB reactor using increased post-flame concentrations of steam. Rather than generating steam by supplying the burner with increased H_2, steam could be generated by pumping liquid water to high pressure using a HPLC pump (since the pressure of the water needs to exceed vessel pressure), vaporizing the water in a furnace, and then heat tracing the lines to the HPFFB burner. The proposed alternative method to generate steam in the HPFFB post-flame environment would be experimentally challenging, but does not have the drawback of causing damage to the burner head when elevated steam concentrations are used in the HPFFB post-flame environment.

Ash was released to the gas phase in the high temperature and heating-rate experiments in this research when feeding separately both biomass and coal chars. It is recommended that the liberated ash elements be identified and quantified. This can be done by performing a mass balance on each element in the ash using ash composition data of the parent feedstock material and also that of collected chars. The ash composition analysis could be performed using the saved ashes from this research, or separate tests could be conducted to collect new samples for analysis.

The morphology of partially gasified petcoke samples from the HPFFB reactor were studied by SEM images in this research (see Section 7.5). The char from the first petcoke sample had small cracks in its surface, while char from the second petcoke sample contained a fraction of swollen, thin-shelled particles. It is recommended to further investigate the morphology of different petcoke char samples collected from conditions of high heating rate to provide understanding about the observed differences in petcoke char morphology. Details about the

utilized coking conditions and the parent crude oil from which the petcoke originated may prove valuable in this investigation.

Reactivity loss in the late stages of coal char conversion has been reported from entrained-flow experiments at high temperature and heating rate (Hurt et al., 1998). However, the author is unaware of any research group that has studied the final stages of *petcoke* conversion in an entrained-flow reactor. It is therefore recommended that the HPFFB reactor be used to study the late stages of petcoke char conversion at gasification conditions. After verifying that re-injection does not affect petcoke gasification rates, a capture and re-injection technique is recommended to reach high char conversions since the available residence time in the HPFFB reactor is limited.

The HPFFB reactor is well suited to study the effect of CO inhibition on the CO_2/char gasification reaction. The reactor could be used to generate chars at meaningful conditions of high pressure, temperature, and initial particle heating rate. The HPFFB reactor could then be transformed into a drop-tube reactor and the generated char could be re-injected at various temperatures, total pressures, and CO:CO_2 ratios.

REFERENCES

Abdullah, H. and H. W. Wu, "Biochar as a Fuel: 1. Properties and Grindability of Biochars Produced from the Pyrolysis of Mallee Wood under Slow-Heating Conditions," *Energy & Fuels,* **23**(8), 4174-4181 (2009).

Ahmed, II and A. K. Gupta, "Kinetics of Woodchips Char Gasification with Steam and Carbon Dioxide," *Applied Energy,* **88**(5), 1613-1619 (2011).

Alen, R., S. Rytkonen and P. McKeough, "Thermogravimetric Behavior of Black Liquors and Their Organic-Constituents," *Journal of Analytical and Applied Pyrolysis,* **31**, 1-13 (1995).

Antal, M. J., "Effects of Reactor Severity on the Gas-Phase Pyrolysis of Celulose-Derived and Kraft Lignin-Derived Volatile Matter," *Industrial & Engineering Chemistry Product Research and Development,* **22**(2), 366-375 (1983).

Antal, M. J. and M. Gronli, "The Art, Science, and Technology of Charcoal Production," *Industrial & Engineering Chemistry Research,* **42**(8), 1619-1640 (2003).

API, "Petroleum Coke Category Analysis and Hazard Characterization," The American Petroleum Institute Petroleum HPV Testing Group (2007).

Bahlawane, N., U. Struckmeier, T. S. Kasper and P. Osswald, "Noncatalytic Thermocouple Coatings Produced with Chemical Vapor Deposition for Flame Temperature Measurements," *Review of Scientific Instruments,* **78**(1) (2007).

Bai, Y. H., Y. L. Wang, S. H. Zhu, L. J. Yan, F. Li and K. C. Xie, "Synergistic Effect between CO_2 and H_2O on Reactivity During Coal Chars Gasification," *Fuel,* **126**, 1-7 (2014).

Barrio, M. and J. E. Hustad, "CO_2 Gasification of Birch Char and the Effect of CO Inhibition on the Calculation of Chemical Kinetics." in *Progress in Thermochemical Biomass Conversion*, (A.V. Bridgwater, ed.), pp. 47-60, Blackwell Science, Oxford (2001).

Batchelder, H. R., R. M. Busche and W. P. Armstrong, "Kinetics of Coal Gasification," *Industrial & Engineering Chemistry* **45**, 1856 (1953).

Baumlin, S., F. Broust, M. Ferrer, N. Meunier, E. Marty and J. Lede, "The Continuous Self Stirred Tank Reactor: Measurement of the Cracking Kinetics of Biomass Pyrolysis Vapours," *Chemical Engineering Science,* **60**(1), 41-55 (2005).

Benfell, K. E., G. S. Liu, D. G. Roberts, D. J. Harris, J. A. Lucas, J. G. Bailey and T. F. Wall, "Modeling Char Combustion: The Influence of Parent Coal Petrography and Pyrolysis Pressure on the Structure and Intrinsic Reactivity of Its Char," *Proceedings of the Combustion Institute,* **28**, 2233-2241 (2000).

Bergman, P. C. A., A. R. Boersma, J. H. A. Kiel, M. J. Prins, K. J. Ptasinski and F. J. J. G. Janssen, "Torrefaction for Entrained-Flow Gasification of Biomass," Petten, The Netherlands, Energy Research Centre of the Netherlands (2005).

Bhat, A., J. V. R. Bheemarasetti and T. R. Rao, "Kinetics of Rice Husk Char Gasification," *Energy Conversion and Management,* **42**(18), 2061-2069 (2001).

Bhatia, S. K. and D. D. Perlmutter, "A Random Pore Model for Fluid-Solid Reactions .1. Isothermal, Kinetic Control," *AIChE Journal,* **26**(3), 379-386 (1980).

Bird, B., W. Stewart and E. Lightfoot, Transport Phenomena, New York, John Wiley & Sons, Inc. (2002).

Borrego, A. G. and D. Alvarez, "Comparison of Chars Obtained under Oxy-Fuel and Conventional Pulverized Coal Combustion Atmospheres," *Energy & Fuels,* **21**(6), 3171-3179 (2007).

Borrego, A. G., L. Garavaglia and W. D. Kalkreuth, "Characteristics of High Heating Rate Biomass Chars Prepared under N_2 and CO_2 Atmospheres," *International Journal of Coal Geology,* **77**(3-4), 409-415 (2009).

Brage, C., Q. H. Yu and K. Sjostrom, "Characteristics of Evolution of Tar from Wood Pyrolysis in a Fixed-Bed Reactor," *Fuel,* **75**(2), 213-219 (1996).

Branca, C. and C. Di Blasi, "Kinetics of the Isothermal Degradation of Wood in the Temperature Range 528-708 K," *Journal of Analytical and Applied Pyrolysis,* **67**(2), 207-219 (2003).

Bridgwater, A. V., "Renewable Fuels and Chemicals by Thermal Processing of Biomass," *Chemical Engineering Journal,* **91**(2-3), 87-102 (2003).

Bridgwater, A. V., "Biomass Fast Pyrolysis," *Thermal Science,* **8**, 21-49 (2004).

Bungay, H. R., Energy, the Biomass Options, New York, John Wiley & Sons (1981).

Cetin, E., B. Moghtaderi, R. Gupta and T. F. Wall, "Influence of Pyrolysis Conditions on the Structure and Gasification Reactivity of Biomass Chars," *Fuel,* **83**(16), 2139-2150 (2004).

Cetin, E., R. Gupta and B. Moghtaderi, "Effect of Pyrolysis Pressure and Heating Rate on Radiata Pine Char Structure and Apparent Gasification Reactivity," *Fuel,* **84**(10), 1328-1334 (2005a).

Cetin, E., B. Moghtaderi, R. Gupta and T. F. Wall, "Biomass Gasification Kinetics: Influences of Pressure and Char Structure," *Combustion Science and Technology,* **177**(4), 765-791 (2005b).

Chen, G. X., K. Sjostrom and E. Bjornbom, "Pyrolysis Gasification of Wood in a Pressurized Fluidized-Bed Reactor," *Industrial & Engineering Chemistry Research,* **31**(12), 2764-2768 (1992).

Chen, G. X., Q. Z. Yu and K. Sjostrom, "Reactivity of Char from Pyrolysis of Birch Wood," *Journal of Analytical and Applied Pyrolysis,* **40-1**, 491-499 (1997).

CONCAWE, "Petroleum Coke," Brussels, Belgium, CONservation of Clean Air and Water in Europe, Product dossier No. 93/105 (1993).

Crawford, R. L., Lignin Biodegradation and Transformation, New York, John Wiley & Sons (1981).

Demirbas, A., "Effect of Initial Moisture Content on the Yields of Oily Products from Pyrolysis of Biomass," *Journal of Analytical and Applied Pyrolysis,* **71**(2), 803-815 (2004).

Di Blasi, C., "Modeling Chemical and Physical Processes of Wood and Biomass Pyrolysis," *Progress in Energy and Combustion Science,* **34**(1), 47-90 (2008).

Di Blasi, C., "Combustion and Gasification Rates of Lignocellulosic Chars," *Progress in Energy and Combustion Science,* **35**(2), 121-140 (2009).

Dupont, C., J. M. Commandre, P. Gauthier, G. Boissonnet, S. Salvador and D. Schweich, "Biomass Pyrolysis Experiments in an Analytical Entrained Flow Reactor between 1073 K and 1273 K," *Fuel,* **87**(7), 1155-1164 (2008).

Ellis, P. J. and C. A. Paul, "Tutorial: Delayed Coking Fundamentals," AIChE Spring National Meeting, Atlanta, GA (2000a).

Ellis, P. J. and C. A. Paul, "Tutorial: Petroleum Coke Calcining and Uses of Calcined Petroleum Coke," AIChE Spring National Meeting, Atlanta, GA (2000b).

Espenas, B. G., "Reactivity of Biomass and Peat Chars Formed and Gasified at Different Conditions." in *Advances in Thermochemical Biomass Conversion,* (A.V. Bridgwater, ed.), pp. 142-159, Blackie Academic and Professional, (1993).

Essenhigh, R. H., "Fundamentals of Coal Combustion." in *Chemistry of Coal Utilization*, 2nd suppl. vol. (M.A. Elliot, ed.), Chapter 19, John Wiley & Sons Inc., New York (1981).

Everson, R. C., H. Neomagus, H. Kasaini and D. Njapha, "Reaction Kinetics of Pulverized Coal-Chars Derived from Inertinite-Rich Coal Discards: Gasification with Carbon Dioxide and Steam," *Fuel,* **85**(7-8), 1076-1082 (2006).

Fagbemi, L., L. Khezami and R. Capart, "Pyrolysis Products from Different Biomasses: Application to the Thermal Cracking of Tar," *Applied Energy,* **69**(4), 293-306 (2001).

Fan, D. M., Z. P. Zhu, Y. J. Na and Q. G. Lu, "Thermogravimetric Analysis of Gasification Reactivity of Coal Chars with Steam and CO_2 at Moderate Temperatures," *Journal of Thermal Analysis and Calorimetry,* **113**(2), 599-607 (2013).

Fermoso, J., C. Stevanov, B. Moghtaderi, B. Arias, C. Pevida, M. G. Plaza, F. Rubiera and J. J. Pis, "High-Pressure Gasification Reactivity of Biomass Chars Produced at Different Temperatures," *Journal of Analytical and Applied Pyrolysis,* **85**(1-2), 287-293 (2009).

Fermoso, J., M. V. Gil, C. Pevida, J. J. Pis and F. Rubiera, "Kinetic Models Comparison for Non-Isothermal Steam Gasification of Coal-Biomass Blend Chars," *Chemical Engineering Journal,* **161**(1-2), 276-284 (2010).

Fermoso, J., M. V. Gil, S. Garcia, C. Pevida, J. J. Pis and F. Rubiera, "Kinetic Parameters and Reactivity for the Steam Gasification of Coal Chars Obtained under Different Pyrolysis Temperatures and Pressures," *Energy & Fuels,* **25**(8), 3574-3580 (2011).

Fisher, P. H., "Personal Communication with Principal Consultant of Pet Coke Consulting LLC located in Greenbrae, CA," A. Lewis (2014).

Fletcher, T. H., "Time-Resolved Temperature Measurements of Individual Coal Particles During Devolatilization," *Combustion Science and Technology,* **63**(1-3), 89-105 (1989).

Fletcher, T. H., A. R. Kerstein, R. J. Pugmire, M. S. Solum and D. M. Grant, "Chemical Percolation Model for Devolatilization. 3. Direct Use of C-13 NMR Data to Predict Effects of Coal Type," *Energy & Fuels,* **6**(4), 414-431 (1992).

Fletcher, T. H., J. L. Ma, J. R. Rigby, A. L. Brown and B. W. Webb, "Soot in Coal Combustion Systems," *Progress in Energy and Combustion Science,* **23**(3), 283-301 (1997).

Fletcher, T. H., H. R. Pond, J. Webster, J. Wooters and L. L. Baxter, "Prediction of Tar and Light Gas During Pyrolysis of Black Liquor and Biomass," *Energy & Fuels,* **26**(6), 3381-3387 (2012).

Franco, C., F. Pinto, I. Gulyurtlu and I. Cabrita, "The Study of Reactions Influencing the Biomass Steam Gasification Process," *Fuel,* **82**(7), 835-842 (2003).

Frandsen, F. J., S. C. van Lith, R. Korbee, P. Yrjas, R. Backman, I. Obernberger, T. Brunner and M. Joller, "Quantification of the Release of Inorganic Elements from Biofuels," *Fuel Processing Technology,* **88**(11-12), 1118-1128 (2007).

Fushimi, C., K. Araki, Y. Yamaguchi and A. Tsutsumi, "Effect of Heating Rate on Steam Gasification of Biomass. 1. Reactivity of Char," *Industrial & Engineering Chemistry Research,* **42**(17), 3922-3928 (2003).

Gale, T. K., C. H. Bartholomew and T. H. Fletcher, "Decreases in the Swelling and Porosity of Bituminous Coals During Devolatilization at High Heating Rates," *Combustion and Flame,* **100**(1-2), 94-100 (1995).

Goetz, G. J., N. Y. Nsakala, R. L. Patel and T. C. Lao, "Combustion and Gasification Kinetics of Chars from Four Commercially Significant Coals of Varying Rank," Second Annual Contractors' Conference on Coal Gasification, Palo Alto, CA (1982).

Gomez-Barea, A., P. Ollero and C. Fernandez-Baco, "Diffusional Effects in CO_2 Gasification Experiments with Single Biomass Char Particles. 1. Experimental Investigation," *Energy & Fuels,* **20**(5), 2202-2210 (2006).

Gray, D., J. G. Cogoli and R. H. Essenhigh, "Problems in Pulverized Coal and Char Combustion," *Advances in Chemistry Series,*(131), 72-91 (1974).

Gu, J., S. Wu, Y. Wu and J. Gao, "CO_2-Gasification Reactivity of Different Carbonaceous Materials at Elevated Temperatures," *Energy Sources Part A-Recovery Utilization and Environmental Effects,* **31**(3), 232-243 (2009).

Guizani, C., F. J. E. Sanz and S. Salvador, "The Gasification Reactivity of High-Heating-Rate Chars in Single and Mixed Atmospheres of H_2O and CO_2," *Fuel,* **108**, 812-823 (2013).

Harris, D. J. and I. W. Smith, "Intrinsic Reactivity of Petroleum Coke and Brown Coal Char to Carbon Dioxide, Steam and Oxygen," Twenty-Third International Symposium on Combustion, The Combustion Institute**:** 1185-1190 (1990).

Hebden, D. and H. J. F. Stroud, "Fundamentals of Coal Combustion." in *Chemistry of Coal Utilization*, 2nd suppl. vol. (M.A. Elliot, ed.), pp.1599-1752, Wiley, New York (1981).

Hecht, E. S., J. S. Lighty and C. R. Shaddix, "Kinetic Rates of Oxidation and Gasification Reactions of Coal Chars Reacting in Oxy-Combustion Environments," 8th U.S. National Combustion Meeting, Park City, UT (2013).

Higman, C. and M. v. d. Burgt, Gasification, London, Elsevier Science (2003).

Hodge, E. M., "The Coal Char-CO_2 Reaction at High Temperature and High Pressure," PhD Dissertation, University of New South Wales (2009).

Howard, J. B., "Fundamentals of Coal Pyrolysis and Hydropyrolysis." in Chemistry of Coal Utilization, 2nd suppl. vol. (M.A. Elliot, ed.), Chapter 12, John Wiley & Sons Inc., New York (1981).

Huang, Z. M., J. S. Zhang, Y. Zhao, H. Zhang, G. X. Yue, T. Suda and M. Narukawa, "Kinetic Studies of Char Gasification by Steam and CO_2 in the Presence of H_2 and CO," *Fuel Processing Technology,* **91**(8), 843-847 (2010).

Huo, W., Z. J. Zhou, F. C. Wang, Y. F. Wang and G. S. Yu, "Experimental Study of Pore Diffusion Effect on Char Gasification with CO_2 and Steam," *Fuel,* **131**, 59-65 (2014).

Hurt, R., J. K. Sun and M. Lunden, "A Kinetic Model of Carbon Burnout in Pulverized Coal Combustion," *Combustion and Flame,* **113**(1-2), 181-197 (1998).

Ibrahim, H. A. H., "The Effect of Thermal Treatment on the True Density of Syrian Green Delayed Petroleum Coke," *Arabian Journal for Science and Engineering,* **30**(2B), 153-161 (2005).

Illerup, J. B. and O. Rathmann, "CO_2 Gasification of Wheat Straw, Barley Straw, Willow and Giganteus," Riso-R-810(EN), Riso National Laboratory, Roskilde, Denmark. (1996).

Incropera, F. P. and D. P. Dewitt, Fundamentals of Heat and Mass Transfer, Chicago, John Wiley & Sons (2002).

Jamaluddin, A. S., J. S. Truelove and T. F. Wall, "Devolatilization of Bituminous Coals at Medium to High Heating Rates," *Combustion and Flame,* **63**(3), 329-337 (1986).

Jarvis, M. W., T. J. Haas, B. S. Donohoe, J. W. Daily, K. R. Gaston, W. J. Frederick and M. R. Nimlos, "Elucidation of Biomass Pyrolysis Products Using a Laminar Entrained Flow Reactor and Char Particle Imaging," *Energy & Fuels,* **25**, 324-336 (2011).

Jenkins, B. M., L. L. Baxter and T. R. Miles, "Combustion Properties of Biomass," *Fuel Processing Technology,* **54**(1-3), 17-46 (1998).

Jimenez, S. and J. Ballester, "Particulate Matter Formation and Emission in the Combustion of Different Pulverized Biomass Fuels," *Combustion Science and Technology,* **178**(4), 655-683 (2006).

Johansen, J. M., J. G. Jakobsen, F. J. Frandsen and P. Glarborg, "Release of K, Cl, and S During Pyrolysis and Combustion of High-Chlorine Biomass," *Energy & Fuels,* **25**(11), 4961-4971 (2011).

Kairaitis, D. A. and R. J. Tyler, "Reactivity of Petroleum Coke to Steam," International Conference on Coal Science, Pittsburgh, Pennsylvania (1983).

Kang, B. S., K. H. Lee, H. J. Park, Y. K. Park and J. S. Kim, "Fast Pyrolysis of Radiata Pine in a Bench Scale Plant with a Fluidized Bed: Influence of a Char Separation System and Reaction Conditions on the Production of Bio-Oil," *Journal of Analytical and Applied Pyrolysis,* **76**(1-2), 32-37 (2006).

Khalil, R., G. Varhegyi, S. Jaschke, M. G. Gronli and J. Hustad, "CO_2 Gasification of Biomass Chars: A Kinetic Study," *Energy & Fuels,* **23**(1), 94-100 (2009).

Klose, W. and M. Wolki, "On the Intrinsic Reaction Rate of Biomass Char Gasification with Carbon Dioxide and Steam," *Fuel,* **84**(7-8), 885-892 (2005).

Kocaefe, D., A. Charette and L. Castonguay, "Green Coke Pyrolysis - Investigation of Simultaneous Changes in Gas and Solid-Phases," *Fuel,* **74**(6), 791-799 (1995).

Koufopanos, C. A., G. Maschio and A. Lucchesi, "Kinetic Modeling of the Pyrolysis of Biomass and Biomass Components," *Canadian Journal of Chemical Engineering,* **67**(1), 75-84 (1989).

Kumar, M. and R. C. Gupta, "Influence of Carbonization Conditions on the Gasification of Acacia and Eucalyptus Wood Chars by Carbon-Dioxide," *Fuel,* **73**(12), 1922-1925 (1994).

Lewis, A. D., "Sawdust Pyrolysis and Petroleum Coke CO_2 Gasification at High Heating Rates," Master's Thesis, Chemical Engineering, Brigham Young University (2011).

Lewis, A. D. and T. H. Fletcher, "Prediction of Sawdust Pyrolysis Yields from a Flat-Flame Burner Using the CPD Model," *Energy & Fuels,* **27**, 942-953 (2013).

Lewis, A. D., E. G. Fletcher and T. H. Fletcher, "CO_2 Gasification Rates of Petroleum Coke in a Pressurized Flat-Flame Burner Entrained-Flow Reactor," *Energy & Fuels*, **28**, 4447-4457 (2014a).

Lewis, A. D., E. G. Fletcher and T. H. Fletcher, "CO_2 Char Gasification Rates of Sawdust, Switchgrass, and Corn Stover in a Pressurized Entrained-Flow Reactor," *Energy & Fuels*, **28**, 5812-5825 (2014b).

Li, F., X. H. Li, R. S. Yao, L. P. Chang and Q. G. Zhang, "A Kinetics Study on the Gasification of Poor Quality Coal," *Energy Sources Part A-Recovery Utilization and Environmental Effects,* **34**(21), 1943-1957 (2012).

Li, S. G., S. P. Xu, S. Q. Liu, C. Yang and Q. H. Lu, "Fast Pyrolysis of Biomass in Free-Fall Reactor for Hydrogen-Rich Gas," *Fuel Processing Technology,* **85**(8-10), 1201-1211 (2004).

Link, S., S. Arvelakis, M. Hupa, P. Yrjas, I. Kulaots and A. Paist, "Reactivity of the Biomass Chars Originating from Reed, Douglas Fir, and Pine," *Energy & Fuels,* **24**, 6533-6539 (2010).

Liu, G. S. and S. Niksa, "Coal Conversion Submodels for Design Applications at Elevated Pressures. Part II. Char Gasification," *Progress in Energy and Combustion Science,* **30**(6), 679-717 (2004).

Liu, H., H. Zhu, M. Kaneko, S. Kato and T. Kojima, "High-Temperature Gasification Reactivity with Steam of Coal Chars Derived under Various Pyrolysis Conditions in a Fluidized Bed," *Energy & Fuels,* **24**, 68-75 (2010a).

Liu, K., Z. Cui and T. H. Fletcher, "Coal Gasification." in *Hydrogen and Syngas Production and Purification Technologies,* (K. Liu, C. Song, and V. Subramani, eds.), pp. 156-218, John Wiley & Sons, New Jersey (2010b).

Lu, H., "Experimental and Modeling Investigations of Biomass Particle Combustion," PhD Dissertation, Brigham Young University (2006).

Ma, J., "Soot Formation During Coal Pyrolysis," PhD Dissertation, Brigham Young University (1996).

Ma, L., "Combustion and Gasification of Chars in Oxygen and Carbon Dioxide at Elevated Pressure," PhD Dissertation, Mechanical Engineering Dept., Stanford University (2006).

Maghzi, S. and G. Rizeq, "Experimental Study of Biomass Pyrolysis in an Entrained Flow Reactor," Western States Section of the Combustion Institute, Riverside, CA (2011).

Malekshahian, M. and J. M. Hill, "Effect of Pyrolysis and CO_2 Gasification Pressure on the Surface Area and Pore Size Distribution of Petroleum Coke," *Energy & Fuels,* **25**(11), 5250-5256 (2011a).

Malekshahian, M. and J. M. Hill, "Kinetic Analysis of CO_2 Gasification of Petroleum Coke at High Pressures," *Energy & Fuels,* **25**(9), 4043-4048 (2011b).

Mani, T., N. Mahinpey and P. Murugan, "Reaction Kinetics and Mass Transfer Studies of Biomass Char Gasification with CO_2," *Chemical Engineering Science,* **66**(1), 36-41 (2011).

Marquez-Montesinos, F., T. Cordero, J. Rodriguez-Mirasol and J. J. Rodriguez, "CO_2 and Steam Gasification of a Grapefruit Skin Char," *Fuel,* **81**(4), 423-429 (2002).

Marsh, H., C. Calvert and J. Bacha, "Structure and Formation of Shot Coke - a Microscopy Study," *Journal of Materials Science,* **20**(1), 289-302 (1985).

Matsumoto, K., K. Takeno, T. Ichinose, T. Ogi and M. Nakanishi, "Gasification Reaction Kinetics on Biomass Char Obtained as a by-Product of Gasification in an Entrained-Flow Gasifier with Steam and Oxygen at 900-1000 Degrees C," *Fuel,* **88**(3), 519-527 (2009).

McBride, B. J., M. Zehe and S. Gordon, "Nasa Glenn Coefficients for Calculating Thermodynamic Properties of Individual Species," NASA TP-2002-215556 (2002).

McDermott, J., X. Bao, D. Bhandari, P. Perez-Diaz, S. Singh, R. Wroczynski, J. Manke, J. Bablin, S. Maghzi, G. Rizeq, L. Baxter, T. Fletcher, A. Lewis, J. Beutler and R. Wu, "Development of Detailed and Simplified Kinetic Models of Biomass Gasification," Final Technical Report, NIFA Award No. 2009-1006-06020 (2014).

Mermoud, F., S. Salvador, L. V. de Steene and F. Golfier, "Influence of the Pyrolysis Heating Rate on the Steam Gasification Rate of Large Wood Char Particles," *Fuel,* **85**(10-11), 1473-1482 (2006).

Milenkova, K. S., A. G. Borrego, D. Alvarez, J. Xiberta and R. Menendez, "Devolatilisation Behaviour of Petroleum Coke under Pulverised Fuel Combustion Conditions," *Fuel,* **82**(15-17), 1883-1891 (2003).

Miller, R. S. and J. Bellan, "A Generalized Biomass Pyrolysis Model Based on Superimposed Cellulose, Hemicellulose and Lignin Kinetics," *Combustion Science and Technology,* **126**(1-6), 97-137 (1997).

Min, F. F., M. X. Zhang, Y. Zhang, Y. Cao and W. P. Pan, "An Experimental Investigation into the Gasification Reactivity and Structure of Agricultural Waste Chars," *Journal of Analytical and Applied Pyrolysis,* **92**(1), 250-257 (2011).

Minchener, A. J., "Coal Gasification for Advanced Power Generation," *Fuel,* **84**(17), 2222-2235 (2005).

Mitchell, R. E., "A Theoretical Model of Chemically Reacting Recirculating Flow," Livermore, CA. Sandia National Laboratory, SAND79-8236 (1980).

Mohan, D., C. U. Pittman and P. H. Steele, "Pyrolysis of Wood/Biomass for Bio-Oil: A Critical Review," *Energy & Fuels,* **20**(3), 848-889 (2006).

Moilanen, A. and H. J. Muhlen, "Characterization of Gasification Reactivity of Peat Char in Pressurized Conditions - Effect of Product Gas Inhibition and Inorganic Material," *Fuel,* **75**(11), 1279-1285 (1996).

Molina, A. and F. Mondragon, "Reactivity of Coal Gasification with Steam and CO_2," *Fuel,* **77**(15), 1831-1839 (1998).

Murthy, B. N., A. N. Sawarkar, N. A. Deshmukh, T. Mathew and J. B. Joshi, "Petroleum Coke Gasification: A Review," *Canadian Journal of Chemical Engineering,* **92**(3), 441-468 (2014).

Nandi, S. P. and M. Onischak, "Gasification of Chars Obtained from Maple and Jack Pine Woods." in *Fundamentals of Thermochemical Biomass Conversion*, (R.P. Overend, A.T. Milne, and K.L. Mudge, eds.), pp. 567-587, Elsevier, New York (1985).

NETL, National Energy Technology Laboratory Gasification Worldwide Database, 2010. http://www.netl.doe.gov/research/coal/energy-systems/gasification/gasification-plant-databases," (accessed Feb. 25, 2014).

Okumura, Y., T. Hanaoka and K. Sakanishi, "Effect of Pyrolysis Conditions on Gasification Reactivity of Woody Biomass-Derived Char," *Proceedings of the Combustion Institute,* **32**, 2013-2020 (2009).

Ollero, P., A. Serrera, R. Arjona and S. Alcantarilla, "The CO_2 Gasification Kinetics of Olive Residue," *Biomass & Bioenergy,* **24**(2), 151-161 (2003).

Orfao, J. J. M., F. J. A. Antunes and J. L. Figueiredo, "Pyrolysis Kinetics of Lignocellulosic Materials - Three Independent Reactions Model," *Fuel,* **78**(3), 349-358 (1999).

Pond, H. R., T. H. Fletcher and L. L. Baxter, "Prediction of Tar and Light Gas During Pyrolysis of Black Liquor and Biomass," 3rd Annual Joint Meeting of the U.S. Sections of the Combustion Institute, Chicago, IL (2003).

Prakash, N. and T. Karunanithi, "Kinetic Modeling in Biomass Pyrolysis - a Review," *Journal of Applied Sciences Research,* **4**(12), 1627-1636 (2008).

Ranzi, E., A. Cuoci, T. Faravelli, A. Frassoldati, G. Migliavacca, S. Pierucci and S. Sommariva, "Chemical Kinetics of Biomass Pyrolysis," *Energy & Fuels,* **22**(6), 4292-4300 (2008).

Rath, J. and G. Staudinger, "Cracking Reactions of Tar from Pyrolysis of Spruce Wood," *Fuel,* **80**(10), 1379-1389 (2001).

Raveendran, K., A. Ganesh and K. C. Khilar, "Pyrolysis Characteristics of Biomass and Biomass Components," *Fuel,* **75**(8), 987-998 (1996).

Ren, L. W., J. L. Yang, F. Gao and J. D. Yan, "Laboratory Study on Gasification Reactivity of Coals and Petcokes in CO_2/Steam at High Temperatures," *Energy & Fuels,* **27**(9), 5054-5068 (2013).

Rensfelt, E., G. Blomkvist and C. Ekstrom, "Energy from Biomass and Wastes," Institute of Gas Technology Symposium, Washington D.C., USA**:** p. 465-94 (1978).

Roberts, D. G. and D. J. Harris, "Char Gasification in Mixtures of CO_2 and H_2O: Competition and Inhibition," *Fuel,* **86**(17-18), 2672-2678 (2007).

Rowell, R. M., The Chemistry of Solid Wood, Washington D.C., American Chemical Society (1984).

Rowley, R. L., W. V. Wilding, J. L. Oscarson, Y. Yang and N. F. Giles, "DIPPR Data Compilation of Pure Chemical Properties, Design Institute for Physical Properties," Provo, Utah, Brigham Young University (2010).

Schneider, C. A., W. S. Rasband and K. W. Eliceiri, "NIH Image to Imagej: 25 Years of Image Analysis," *Nature Methods,* **9**(7), 671-675 (2012).

Scott, D. S. and J. Piskorz, "The Continuous Flash Pyrolysis of Biomass," *Canadian Journal of Chemical Engineering,* **62**(3), 404-412 (1984).

Scott, D. S., J. Piskorz and D. Radlein, "Liquid Products from the Continuous Flash Pyrolysis of Biomass," *Industrial & Engineering Chemistry Process Design and Development,* **24**(3), 581-588 (1985).

Scott, D. S., J. Piskorz, M. A. Bergougnou, R. Graham and R. P. Overend, "The Role of Temperature in the Fast Pyrolysis of Cellulose and Wood," *Industrial & Engineering Chemistry Research,* **27**(1), 8-15 (1988).

Senneca, O., "Kinetics of Pyrolysis, Combustion and Gasification of Three Biomass Fuels," *Fuel Processing Technology,* **88**(1), 87-97 (2007).

Shaddix, C. R., "Correcting Thermocouple Measurements for Radiation Loss: A Critical Review," Proceedings of the 33rd National Heat Transfer Conference, Albuquerque, New Mexico (1999).

Shen, D. K., S. Gu and A. V. Bridgwater, "Study on the Pyrolytic Behaviour of Xylan-Based Hemicellulose Using TG-FTIR and Py-GC-FTIR," *Journal of Analytical and Applied Pyrolysis,* **87**(2), 199-206 (2010).

Shurtz, R., "Effects of Pressure on the Properties of Coal Char under Gasification Conditions at High Initial Heating Rates," PhD Dissertation, Chemical Engineering, Brigham Young University (2011).

Shurtz, R. C., J. W. Hogge, K. C. Fowers, G. S. Sorensen and T. H. Fletcher, "Coal Swelling Model for Pressurized High Particle Heating Rate Pyrolysis Applications," *Energy & Fuels,* **26**(6), 3612-3627 (2012).

Shurtz, R. C. and T. H. Fletcher, "Coal Char-CO_2 Gasification Measurements and Modeling in a Pressurized Flat-Flame Burner," *Energy & Fuels,* **27**(6), 3022-3038 (2013).

Simbeck, D. R., R. L. Dickenson and E. D. Oliver, "Coal Gasification Systems: A Guide to Status, Applications, and Economics," Final Report, Electric Power Research Institute, Palo Alto, CA, Synthetic Fuels Associates, Mountain View, CA, Project 2207, EPRI AP-3109 (1983).

Smith, I. W., "The Combustion Rates of Coal Chars: A Review," Nineteenth Internal Symposium on Combustion, Pittsburgh**:** 1045-1065 (1982).

Smith, K. L., L. D. Smoot, T. H. Fletcher and R. J. Pugmire, The Structure and Reaction Processes of Coal, New York, Plenum Press (1994).

Smoot, L. D. and P. J. Smith, Coal Combustion and Gasification, New York, Plenum Press (1985).

Smoot, L. D., "Coal and Char Combustion." in *Fossil Fuel Combustion*, (W. Bartok and A.F. Sarofim, eds.), pp. 653-768, John Wiley & Sons, New York (1991).

Solomon, P. R., T. H. Fletcher and R. J. Pugmire, "Progress in Coal Pyrolysis," *Fuel,* **72**(5), 587-597 (1993).

Soltes, E. J. and T. J. Elder, "Pyrolysis." in *Organic Chemicals from Biomass*, (I.S. Goldstein, ed.), pp. 63-95, CRC Press, Boca Raton, FL (1981).

Sowa, J. M., "Studies of Coal Nitrogen Release Chemistry for Oxyfuel Combustion and Chemical Additives," M.S. Thesis, Chemical Engineering, Brigham Young University (2009).

Stiles, H. N. and R. Kandiyoti, "Secondary Reactions of Flash Pyrolysis Tars Measured in a Fluidized-Bed Pyrolysis Reactor with Some Novel Design-Features," *Fuel,* **68**(3), 275-282 (1989).

Struis, R., C. von Scala, S. Stucki and R. Prins, "Gasification Reactivity of Charcoal with CO_2. Part I: Conversion and Structural Phenomena," *Chemical Engineering Science,* **57**(17), 3581-3592 (2002).

Tremel, A., T. Haselsteiner, C. Kunze and H. Spliethoff, "Experimental Investigation of High Temperature and High Pressure Coal Gasification," *Applied Energy,* **92**, 279-285 (2012).

Tremel, A. and H. Spliethoff, "Gasification Kinetics During Entrained Flow Gasification - Part II: Intrinsic Char Reaction Rate and Surface Area Development," *Fuel,* **107**, 653-661 (2013).

Trommer, D. and A. Steinfeld, "Kinetic Modeling for the Combined Pyrolysis and Steam Gasification of Petroleum Coke and Experimental Determination of the Rate Constants by Dynamic Thermogravimetry in the 500-1520 K Range," *Energy & Fuels,* **20**(3), 1250-1258 (2006).

Tsai, C. Y. and A. W. Scaroni, "The Structural-Changes of Bituminous Coal Particles During the Initial-Stages of Pulverized-Coal Combustion," *Fuel,* **66**(2), 200-206 (1987).

Turkdogan, E. T. and J. V. Vinters, "Effect of Carbon Monoxide on the Rate of Oxidation of Charcoal, Graphite and Coke in Carbon Dioxide," *Carbon,* **8**, 39-53 (1970).

Tyler, R. J. and I. W. Smith, "Reactivity of Petroleum Coke to Carbon Dioxide between 1030 and 1180 K," *Fuel,* **54**(2), 99-104 (1975).

van Lith, S. C., V. Alonso-Ramirez, P. A. Jensen, F. J. Frandsen and P. Glarborg, "Release to the Gas Phase of Inorganic Elements During Wood Combustion. Part 1: Development and Evaluation of Quantification Methods," *Energy & Fuels,* **20**(3), 964-978 (2006).

van Lith, S. C., P. A. Jensen, F. J. Frandsen and P. Glarborg, "Release to the Gas Phase of Inorganic Elements During Wood Combustion. Part 2: Influence of Fuel Composition," *Energy & Fuels,* **22**(3), 1598-1609 (2008).

Vassilatos, V., G. Taralas, K. Sjostrom and E. Bjornbom, "Catalytic Cracking of Tar in Biomass Pyrolysis-Gas in the Presence of Calcined Dolomite," *Canadian Journal of Chemical Engineering,* **70**(5), 1008-1013 (1992).

Vassilev, S. V., D. Baxter, L. K. Andersen and C. G. Vassileva, "An Overview of the Chemical Composition of Biomass," *Fuel,* **89**(5), 913-933 (2010).

Vassilev, S. V., D. Baxter, L. K. Andersen, C. G. Vassileva and T. J. Morgan, "An Overview of the Organic and Inorganic Phase Composition of Biomass," *Fuel,* **94**(1), 1-33 (2012).

Wagenaar, M., W. Prins and W. P. M. Vanswaaij, "Flash Pyrolysis Kinetics of Pine Wood," *Fuel Processing Technology,* **36**(1-3), 291-298 (1993).

Walker, P. L., F. J. Rusinko and L. G. Austin, "Gas Reactions of Carbon," *Advances in Catalysis,* **11**, 133-221 (1959).

Wall, T. F., G. S. Liu, H. W. Wu, D. G. Roberts, K. E. Benfell, S. Gupta, J. A. Lucas and D. J. Harris, "The Effects of Pressure on Coal Reactions During Pulverised Coal Combustion and Gasification," *Progress in Energy and Combustion Science,* **28**(5), 405-433 (2002).

Ward, S. M. and J. Braslaw, "Experimental Weight-Loss Kinetics of Wood Pyrolysis under Vacuum," *Combustion and Flame,* **61**(3), 261-269 (1985).

White, J. E., W. J. Catallo and B. L. Legendre, "Biomass Pyrolysis Kinetics: A Comparative Critical Review with Relevant Agricultural Residue Case Studies," *Journal of Analytical and Applied Pyrolysis,* **91**(1), 1-33 (2011).

Williams, A., J. M. Jones, L. Ma and M. Pourkashanian, "Pollutants from the Combustion of Solid Biomass Fuels," *Progress in Energy and Combustion Science,* **38**(2), 113-137 (2012).

Williams, T. C. and C. R. Shaddix, "Contamination of Carbon Monoxide with Metal Carbonyls: Implications for Combustion Research," *Combustion Science and Technology,* **179**(6), 1225-1230 (2007).

Wu, H., M. Castro, P. A. Jensen, F. J. Frandsen, P. Glarborg, K. Dam-Johansen, M. Rokke and K. Lundtorp, "Release and Transformation of Inorganic Elements in Combustion of a High-Phosphorus Fuel," *Energy & Fuels,* **25**(7), 2874-2886 (2011).

Wu, H. W., G. Bryant, K. Benfell and T. Wall, "An Experimental Study on the Effect of System Pressure on Char Structure of an Australian Bituminous Coal," *Energy & Fuels,* **14**(2), 282-290 (2000).

Wu, Y. Q., S. Y. Wu, J. Gu and J. S. Gao, "Differences in Physical Properties and CO_2 Gasification Reactivity between Coal Char and Petroleum Coke," *Process Safety and Environmental Protection,* **87**(5), 323-330 (2009).

Wurzenberger, J. C., S. Wallner, H. Raupenstrauch and J. G. Khinast, "Thermal Conversion of Biomass: Comprehensive Reactor and Particle Modeling," *Aiche Journal,* **48**(10), 2398-2411 (2002).

Xu, Q. X., S. S. Pang and T. Levi, "Reaction Kinetics and Producer Gas Compositions of Steam Gasification of Coal and Biomass Blend Chars, Part 1: Experimental Investigation," *Chemical Engineering Science,* **66**(10), 2141-2148 (2011).

Yan, Q. X., J. J. Huang, J. T. Zhao, C. Y. Li, L. S. Xia and Y. T. Fang, "Investigation into the Kinetics of Pressurized Steam Gasification of Chars with Different Coal Ranks," *Journal of Thermal Analysis and Calorimetry,* **116**(1), 519-527 (2014).

Yoon, S. J., Y. C. Choi, S. H. Lee and J. G. Lee, "Thermogravimetric Study of Coal and Petroleum Coke for Co-Gasification," 24(3) (2007).

Yu, J. L., J. A. Lucas and T. F. Wall, "Formation of the Structure of Chars During Devolatilization of Pulverized Coal and Its Thermoproperties: A Review," *Progress in Energy and Combustion Science,* **33**(2), 135-170 (2007).

Yuan, S. A., Z. J. Zhou, J. Li, X. L. Chen and F. C. Wang, "HCN and NH_3 Released from Biomass and Soybean Cake under Rapid Pyrolysis," *Energy & Fuels,* **24**, 6166-6171 (2010).

Yuan, S. A., X. L. Chen, J. Li and F. C. Wang, "CO_2 Gasification Kinetics of Biomass Char Derived from High-Temperature Rapid Pyrolysis," *Energy & Fuels,* **25**(5), 2314-2321 (2011).

Zamalloa, M., D. Ma and T. A. Utigard, "Oxidation Rates of Industrial Cokes with CO_2 and Air," *ISIJ International,* **35**(5), 458-463 (1995).

Zamalloa, M. and T. A. Utigard, "Characterization of Industrial Coke Structures," *ISIJ International,* **35**(5), 449-457 (1995).

Zanzi, R., K. Sjostrom and E. Bjornbom, "Rapid High-Temperature Pyrolysis of Biomass in a Free-Fall Reactor," *Fuel,* **75**(5), 545-550 (1996).

Zeng, D., "Effects of Pressure on Coal Pyrolysis at High Heating Rates and Char Combustion," PhD Dissertation, Brigham Young University (2005).

Zhang, J., H. Toghiani, D. Mohan, C. U. Pittman and R. K. Toghiani, "Product Analysis and Thermodynamic Simulations from the Pyrolysis of Several Biomass Feedstocks," *Energy & Fuels,* **21**(4), 2373-2385 (2007).

Zhang, R., Q. H. Wang, Z. Y. Luo, M. X. Fang and K. F. Cen, "Competition and Inhibition Effects During Coal Char Gasification in the Mixture of H_2O and CO_2," *Energy & Fuels,* **27**(9), 5107-5115 (2013).

Zhang, Y., S. Kajitani, M. Ashizawa and K. Miura, "Peculiarities of Rapid Pyrolysis of Biomass Covering Medium- and High-Temperature Ranges," *Energy & Fuels,* **20**(6), 2705-2712 (2006).

Zhang, Y., M. Ashizawa, S. Kajitani and K. Miura, "Proposal of a Semi-Empirical Kinetic Model to Reconcile with Gasification Reactivity Profiles of Biomass Chars," *Fuel,* **87**(4-5), 475-481 (2008).

Zhang, Z. and T. Wang, "Investigation of Combustion and Thermal-Flow inside a Petroleum Coke Rotary Calcining Kiln with Potential Energy Saving Considerations," *Journal of Thermal Science and Engineering Applications,* **5**, 011008 (2013).

Zou, J. H., Z. J. Zhou, F. C. Wang, W. Zhang, Z. H. Dai, H. F. Liu and Z. H. Yu, "Modeling Reaction Kinetics of Petroleum Coke Gasification with CO_2," *Chemical Engineering and Processing,* **46**(7), 630-636 (2007).

Appendix A. Radiation Correction for Gas Temperature Measurements

The centerline gas temperature profiles of the atmospheric FFB and the HPFFB were measured using a B-type thermocouple with a wire diameter of 0.005". The spherical thermocouple bead sizes were measured using an optical microscope as 555 and 422 μm for the FFB and HPFFB thermocouples, respectively. Calculations were required to solve for the gas temperature since the measured temperatures were actually of the thermocouple bead. It is very important to obtain accurate gas temperature profiles, especially when trying to obtain particle kinetic rate constants. Many important topics about correcting thermocouple measurements for radiation loss are covered in the review article by Shaddix (1999). The gas temperature is solved using an energy balance of the thermocouple bead. The bead is heated by convection and is cooled by radiating heat away to the cooler surroundings. Assuming that the thermocouple bead is at equilibrium, the following energy balance is used:

$$Q_{convection} = Q_{radiation} \tag{A.1}$$

$$h_c \cdot A_{bead} \cdot (T_{gas} - T_{bead}) = A_{bead} \cdot \sigma \cdot \varepsilon \cdot (T_{bead}^{\ 4} - T_{surroundings}^{\ 4}) \tag{A.2}$$

where h_c is the convective heat transfer coefficient, A_{bead} is area of the thermocouple bead (which cancels out), T_{gas} is the gas temperature, T_{bead} is the temperature of the thermocouple bead, $T_{surroundings}$ is the temperature of the surroundings, σ is the Stefan-Boltzmann constant ($5.67 \cdot 10^{-8}$ $W/m^2/K^4$), and ε is the emissivity of the thermocouple bead. Equation (A.2) was used to solve

for the gas temperature in the atmospheric FFB and in the HPFFB. View factors were not used in the HPFFB temperature correction since heaters were not utilized in this study. A constant surroundings temperature ($T_{surroundings}$) of 500 K was used in both the FFB and HPFFB temperature corrections. For the HPFFB reactor, the 500 K estimate of $T_{surroundings}$ was validated by measuring temperatures 506-521 K in the insulation outside of the long quartz tube (see Figure 4.2).

Solving for the gas temperature using Equation (A.2) required iteration because the transport properties (heat capacity, viscosity, & thermal conductivity) of the gases surrounding the thermocouple bead are calculated at the film temperature (average of T_{gas} & T_{bead}), which is not known beforehand. The transport properties of the gases were calculated using DIPPR equations (Rowley et al., 2010) and were determined as the molar average of the four most prevalent post-flame gases of N_2, CO_2, CO, and H_2O as determined from a thermodynamic equilibrium program. The four aforementioned gases comprised at least 98.9 mol% of the post-flame gases. The emissivity (ε) of a B-type thermocouple bead was calculated by the following empirical fit of the emissivity of an S-type thermocouple (Shaddix, 1999; Bahlawane et al., 2007):

$$\varepsilon = -0.1 + 3.24 \cdot 10^{-4} T - 1.25 \cdot 10^{-7} T^2 + 2.18 \cdot 10^{-11} T^3 \qquad \text{(A.3)}$$

where T is the temperature in K. The correlation predicts emissivity values of 0.12 and 0.21 at temperatures of 1000 and 1900 K, respectively.

Determining the values to use in Equation (A.2) is fairly straight forward, except for h which requires numerous calculations and is defined by:

$$h = \frac{Nu \cdot k_{gas}}{D_{bead}} \qquad \text{(A.4)}$$

where D_{bead} is the diameter of the thermocouple bead, k_{gas} is the thermal conductivity of the gases surrounding the bead at the film temperature, and Nu is the Nusselt number. The Nusselt number was calculated using the following falling drop correlation that is applicable to convection past the assumed-spherical thermocouple bead:

$$Nu = 2 + 0.569 \cdot \mathrm{Re}^{1/2} \cdot \mathrm{Pr}^{1/3} \tag{A.5}$$

where Re is the Reynolds number and Pr is the Prandtl number. The Reynolds number is defined as:

$$\mathrm{Re} = \frac{\rho_{gas} \cdot v_{gas} \cdot D_{bead}}{\mu_{gas}} \tag{A.6}$$

where ρ_{gas} is the gas density, v_{gas} is the gas velocity past the thermocouple bead, and μ_{gas} is the gas viscosity at the film temperature. The gas density was calculated as:

$$\rho_{gas} = \frac{P}{R \cdot T_{gas}} \cdot MW_{gas} \tag{A.7}$$

where P is total pressure, R is the ideal gas constant, and MW_{gas} is the molecular weight of the post-combustion gases. The gas velocity (v_{gas}) was taken as the measured particle velocity if this information was available, but was calculated using the following formula in other cases:

$$v_{gas} = \frac{m_{gas}}{Area_{CS} \cdot \rho_{gas}} \tag{A.8}$$

where m_{gas} is the mass flow rate gases to the burner, and $Area_{CS}$ is the cross-sectional area of the flow path (25.81 & 5.31 cm^2 for the FFB and HPFFB facilities, respectively). The measured centerline particle velocity was believed to be a more accurate prediction of the gas velocity than that obtained when using Equation (A.8). Developed flow explains why measured velocities

were always faster than that predicted by Equation (A.8) since velocity along the centerline is faster than the average velocity. The Prandtl number is defined as:

$$\mathrm{Pr} = \frac{C_{pGAS} \cdot \mu_{gas}}{k_{gas}} \tag{A.9}$$

where C_{pGAS} is the gas heat capacity at the film temperature.

Appendix B. Example Particle Mass Release Calculations

This section explains particle mass release in more detail for thermal conversion processes such as pyrolysis, char combustion, or char gasification and provides some sample calculations. The purpose of this section is to help experimental researchers understand how to measure accurate particle mass release in entrained-flow experiments and to correctly assign the mass release to moisture, ash liberation, pyrolysis, or conversion by combustion or gasification. Particle mass release can be reported on a dry basis, and also a dry and ash-free (daf) basis. Reporting particle mass release on a *dry basis* allows the results to not be influenced by initial moisture in the fuel. Reporting particle mass release on a *daf basis* allows comparisons of the organic fraction of the particle during thermal conversion since moisture and ash do not influence the results.

1) **Moisture**: It is important in particle thermal conversion experiments to always measure the moisture content of the feedstock that is being researched. A moisture test is performed by measuring the mass release that occurs when the sample is maintained at 107 °C for an hour or longer; the sample should be allowed to cool for a few minutes after being removed from the hot environment in order to avoid the effect of buoyancy on the mass measurements.

If a raw fuel contains 4 wt% moisture (wet basis), this amount of moisture will leave the fuel during a pyrolysis experiment and this moisture mass loss should *not* be attributed to organic

volatile yields. It is similarly important to measure moisture content if a char re-injection strategy is employed where char is generated in one experiment and then converted in a separate experiment. If there is 3 wt% moisture (wet basis) in the char in an re-injection experiment, then this amount of moisture will leave the char during a char conversion experiment. The moisture mass loss could be mistakenly attributed to char gasification mass loss if one is not careful to attribute mass loss to the correct source.

Example) If 100 g of biomass was fed with 5 wt% moisture (wet basis) in an entrained-flow experiment at high temperature, then 5 g of the measured particle mass loss was due to moisture leaving, and should not be attributed to pyrolysis, char combustion, or char gasification.

2) **Completion of Pyrolysis**: For char re-reinjection experiments (where char that is generated in one experiment is converted in a separate experiment), it is important to quantify the extent that the re-injected char was pyrolyzed. If the temperature or residence time were not sufficiently high in the char-generation experiment, then the char may possibly not be fully pyrolyzed and completion of pyrolysis will account for some of the particle mass release in a char gasification experiment. Falsely high char gasification rates could easily be reported if careful attention is not paid to the appropriate breakdown of the particle mass release between completion of pyrolysis *and* char gasification.

If differences in char mass release after the first collection point are used in the regression of char gasification rate parameters (as was done in this study), then the effect of incomplete pyrolysis likely will not affect the gasification rates since pyrolysis occurs quickly and will likely be completed by the first collection point (assuming the temperature is sufficiently hot). However, if it is desired to accurately report particle mass release values on a char basis from the

char gasification experiment, then one needs to quantify the mass release attributed to incomplete pyrolysis in the char gasification experiment. To quantify the extent of incomplete pyrolysis of the generated char, a separate experiment is required. Re-injecting a fraction of the char at a 'pyrolysis' condition can allow the quantification of the extent of pyrolysis for the char. A 'pyrolysis' condition is defined here as one in which the conditions (i.e., temperature & partial pressure of reactant gas) are not severe enough for measurable char gasification to take place in the allotted residence time of an entrained-flow experiment. The char mass release during such an experiment can be attributed to the completion of pyrolysis, assuming that ash was not liberated during this experiment (and also assuming that mass release due to moisture was correctly accounted for).

Another experiment that could be performed to quantify the extent of incomplete pyrolysis of the char that acts as feedstock in char gasification experiments would be to use a small sample of the char (~ 10 mg) in a TGA experiment at elevated temperature in an inert atmosphere (N_2, Ar, He, etc). The char mass release during the TGA experiment could be attributed to the completion of pyrolysis (assuming that mass release due to moisture was correctly accounted for).

However, a word of caution is given about ash liberation during re-injection experiments. It is possible that a portion of ash will leave the char in an experiment where the extent of pyrolysis is being quantified (as well as in a char gasification experiment). If you do not take the ash release into account, then the mass release due to the completion of pyrolysis may be over-predicted. Ash liberation in a TGA experiment (rather than an entrained-flow experiment) at a lower temperature and lower initial particle heating rate may perhaps be less of a problem. Ash release can be quantified by an ash balance on the ash ($m_1 \cdot x_{1,ash} - m_2 \cdot x_{2,ash} = m_{ash\ liberated}$) where

m_1 and m_2 are the mass of the char used in the experiment (entrained-flow or TGA) and mass of the char after the experiment, respectively. The terms $x_{1,ash}$ and $x_{2,ash}$ are the ash fractions in the respective chars.

Example) 100 g of biomass char was fed that contained 4 wt% moisture in an entrained-flow experiment at a 'pyrolysis' condition in order to determine the mass release due to completion of pyrolysis. 20 g of mass leaves during the experiment, and 4 g (100*0.04) is due to moisture leaving and 16 g (20 - 4) is due to the completion of pyrolysis (assuming no ash liberation). In future char gasification experiments where this same batch of biomass char is fed, it is known that 4 wt% of the initial mass of biomass char will leave as moisture, and 16 wt% of the initial mass of char will leave due to the completion of pyrolysis (assuming no ash liberation). So, if 100 g of biomass char is fed during a char gasification re-injection experiment, and 30 g mass release is measured, then 4 g was due to moisture, 16 g was due to the completion of pyrolysis (assuming no ash liberation), and 10 g (30 – 4 - 16) was due to gasification. That means on a dry char basis that 12.5 wt% [(30 - 4 -16) / (100 - 4 - 16)] of the fully-pyrolyzed mass of char should be attributed to char gasification.

3) **Ash Liberation**: This section has some repetitive material as contained in Section 4.7, but is provided again here to make this section complete. In char re-injection experiments performed in this research for biomass and coal, it was found that a significant amount of ash was liberated from the char. The way to quantify this is to use an ash balance (see section 2) Completion of Pyrolysis which is located above).

Typically, the equation to calculate the mass release on a dry ash-free (daf) basis for pyrolysis, char gasification, or char combustion is Equation (4.4). The numerator in Equation (4.4) is meant to quantify the amount of organic material that was released during the

experiment, but the organic mass release is over-predicted when ash is liberated. A mass balance on the organic fraction of the particle allows the numerator in Equation (4.4) to be changed, and Equation (4.6) results (although this equation assumes an accurate mass balance during the experiment). The numerator in Equation (4.6) now accurately assigns organic mass release of the particle, and is correct even if a large amount of ash is liberated during the char re-injection experiment.

To clarify, the particle mass release due to the completion of pyrolysis requires an additional experiment (either a TGA test, or to feed the char in an entrained-flow experiment at 'pyrolysis' conditions (see above)). However, no extra experiments are necessary to calculate the ash that was released to the gas phase during an experiment. An example problem is shown below where the percentage of ash that liberated in an experiment is calculated.

Example) 100 g of nearly-fully-pyrolyzed char is fed during a re-injection char gasification experiment and 40 g of dry char is collected after the experiment. This means that 60 g (100 – 40) of particle mass release needs to be accounted for.

The feedstock char in the gasification experiment had 4 wt% moisture, and a separate experiment revealed that 16 wt% (dry basis) of the initial dry char mass is released due to the completion of pyrolysis. The ash fraction in the feedstock char was 20 wt% (dry basis). The ash fraction in the partially-gasified char collected after the gasification experiment was 30 wt% (dry basis). The desire is to calculate the percentage of mass release due to char gasification on a dry and ash-free (daf) char basis (i.e. the percentage of the fully-pyrolyzed char that gasified).

Again, we have 60 g (100 - 40) of mass release to account for:

4 g is due to moisture leaving

16 g is due to the completion of pyrolysis

96*0.20 = 19.2 g of ash initially

40*0.30 = 12 g of ash after the run

(19.2 - 12) / 19.2 *100 = 37.5% of the ash was released to the gas phase during this run (assuming an accurate mass balance was obtained)

19.2 - 12 = 7.2 g of mass release is due to ash liberation

This means that 32.8 g of mass release is due to char gasification during this particular run (60 - 4 - 16 – 7.2)

The dry, ash-free (daf) amount of fully-pyrolyzed feedstock char fed (even though partially pyrolyzed char was fed) is 60.8 g or (100 - 4 - 19.2 - 16)

The percentage of mass release due to char gasification on a daf char basis is:

32.8 / 60.8 *100 = 53.95 wt% (daf char basis)

The mass release due to char gasification is the mass that is released beyond moisture loss, the release associated with the completion of pyrolysis, and ash liberation.

Appendix C. Biomass Pyrolysis Data and Additional Information

Table C.1 Gas conditions for FFB biomass pyrolysis experiments

Centerline $T_{gas,max}$[a]	**1163 K**	**1320 K**	**1433 K**	**1751 K**
Gas flow (kg/s)	$4.898 \cdot 10^{-4}$	$5.048 \cdot 10^{-4}$	$5.739 \cdot 10^{-4}$	$8.015 \cdot 10^{-4}$
Φ (Equivalence Ratio)	1.59	1.43	1.29	1.16
Carrier[b] N_2 (SLPM)	0.0367	0.0367	0.0367	0.0367
O_2 (SLPM)	1.49	2.05	2.58	4.47
Oxidizer[c] N_2 (SLPM)	7.75	7.8	12.5	18.5
CO (SLPM)	10.2	9.75	8.85	11.82
H_2 (SLPM)	0.6	0.3	0.45	0.36
Fuel[d] N_2 (SLPM)	5.93	6.5	5.7	6.5
Quench N_2 (SLPM)	60	60	60	60
Equilibrium Post-Flame Gas Compositions				
CO_2 mol%	11.39	16.14	17.56	23.12
H_2O mol%	0.77	0.67	1.21	0.89
CO mol%	30.18	23.84	14.58	8.64
H_2 mol%	1.72	0.56	0.42	0.07
N_2 mol%	55.93	58.80	66.23	67.26

[a]maximum measured radiation-corrected centerline gas temperature [b]N_2 in the feeding tube
[c]N_2 in the oxidizer line [d]N_2 in the fuel line

Table C.2. Radiation-corrected centerline FFB gas temperature profiles

Height Above Burner (inches)	**$T_{gas,max}$ = 1163 K**	**$T_{gas,max}$ = 1320 K**	**$T_{gas,max}$ = 1433 K**	**$T_{gas,max}$ = 1751 K**
0	1003	1163	1314	1552
0.25	1128	1287	1401	1699
0.5	1152	1312	1419	1733
0.75	1160	1318	1429	1749
1	1162	1320	1433	1751
1.5	1163	1316	1430	1745
2	1158	1309	1425	1731
2.5	1152	1300	1418	1716
3	1146	1293	1408	1697
3.5	1140	1283	1400	1677
4	1133	1274	1389	1658
4.5	1123	1264	1376	1638
5	1117	1256	1363	1620
6	1103	1233	1339	1582
7	1087	1213	1311	1543

Sample Input File for CPD Code:

Included below is a sample input file for cellulose that was run using the CPDCP version of the CPD model. The CPDCP version of the code is useful for entrained flow experiments and requires a particle velocity profile and gas temperature profile. The only change that would be made to run this code for hemicellulose or lignin would be to change the structural and kinetic parameters (Lewis and Fletcher, 2013). Other versions of the model are CPD and CPD heat, whose input files are similar enough that they are not included here. This particular sample input file included below would be used to model the sawdust pyrolysis experiments in the FFB reactor at the $T_{gas,max}$ = 1433 K condition.

Input file for cellulose

```
Sawdust_vel_1433.dat        ! Name of Particle Velocity Profile file (included below)
Sawdust_temp_1433.dat       ! Name of Gas Temperature Profile file (included below)
Cell_1433K_1.txt            ! Name of first output file
Cell_1433K_2.txt            ! Name of second output file
Cell_1433K_3.txt            ! Name of third output file

 1.0              TIMAX   !maximum time (seconds)
 300.             TG0
 36.              VG0 !cm/s
 0.653            RHOP !G/CM**3
 0.007            DP !CM
 0.0              swell !(df-d0)/d0
 -106             DELHV !CAL/G (- MEANS ENDOTHERMIC)
 0.024            Omegaw
 0.008            OMEGAA
 0.8              EMIS
 500.             TWALL
 1200             THTR (1700 for high T, 1200 for Low T)
 300.             TTUBE
 1.e-5,5.e-5,10   dt,dtmax,iprint

1.0         !p0     ! structural parameters of cellulose (Lewis and Fletcher, 2013)
0.0         !c0
 3.0         !sig+1
 81          !mw
 22.7        !mdel
 2.0e16      !ab          ! kinetic parameters of cellulose (Lewis and Fletcher, 2013)
```

```
 55400      !eb
 4100       !ebsig
100         !ac=rho
 0.0        !ec
 3.0e15     !ag
 61200       !eg
 8100        !egsig
 3.e15       !Acr (pre-exponential factor for crosslinking rate)
 65000       !Ecr (activation energy for crosslinking rate)

 0       !arad (pre-exponential factor for N attack by free radical)
 0       !erad (activation energy for N attack by free radical, cal.)
 0       !fstable (initial frac. of MW decay with no radical N attack)
 0       !an (high T slow N release pre-exponential factor)
 0       !en (high T slow N release activation energy, calories)
 0       !ensig (deviation bound for distribution of en)

 1.0     !pressure (atm)

.444       %Carbon (DAF)   ! Composition of Cellulose
.062       %H
.00        %N
.494       %O
.00        %S
```

Sawdust_vel_1433.dat file

c 45-75 μm sawdust particle velocities at the $T_{gas,max}$ = 1433 K condition in the FFB reactor
c z(mm) vp (cm/s)

```
0               36.0
0.3115          33.6
0.6334          39.3
0.919           49.0
1.2             51.1
2.4             67.2
3.6             76.8
4.8             82.7
6               88.0
7.2             91.3
8.4             94.9
9.6             97.4
10.8            99.8
12              102.1
25.4            113
38.1            123
```

50.8	122
63.5	130
76.2	132

Sawdust_temp_1433.dat file

c FFB reactor centerline gas temperature profile at the $T_{gas,max}$ = 1433 K pyrolysis condition
c z(mm) Tg (K)

0.00	300
1	1314
6.35	1401
12.70	1419
19.05	1429
25.40	1433
38.10	1430
50.80	1425
63.50	1418
76.20	1408
88.90	1400
101.60	1389
114.30	1376
127.00	1363
139.70	1352
152.40	1339
177.80	1311

Table C.3. Meausured particle velocities (m/s) of 45-75 μm biomass in the FFB reactor

Height Above Burner (inches)	PS[a] $T_{gas,max}$ = 1433 K	PS[a] $T_{gas,max}$ = 1751 K	ST[b] $T_{gas,max}$ = 1433 K	CS[c] $T_{gas,max}$ = 1433 K	SG[d] $T_{gas,max}$ = 1433 K
0.5	1.16 ± [f] 0.06	1.92	-	-	-
1	1.13 ± 0.06	1.92 ± 0.02	1.10 ± 0.03	1.06 ± 0.01	1.10 ± 0.02
1.5	1.23 ± 0.04	2.02 ± 0.08	-	-	-
2	1.22 ± 0.06	2.00 ± 0.06	1.18 ± 0.03	1.13 ± 0.04	1.20 ± 0.02
2.5	1.30 ± 0.04	2.02 ± 0.08			
3	1.32 ± 0.06	2.07 ± 0.04	1.28 ± 0.06	1.28	1.30 ± 0.04
3.5	1.43 ± 0.05	2.13 ± 0.06	-	-	-
4	1.41 ± 0.09	2.22 ± 0.05	-	-	-
4.5	1.44	2.24 ± 0.09	-	-	-
5	1.46	2.30 ± 0.03	-	-	-
Height Above Burner (inches)	PS[a] $T_{gas,max}$ = 1163 K	ST[b] $T_{gas,max}$ = 1163 K	CS[c] $T_{gas,max}$ = 1163 K	SG[d] $T_{gas,max}$ = 1163 K	PS[a] & ST[b] $T_{gas,max}$ = 1320 K
1”	0.84[e]	0.85[e]	0.82[e]	0.85[e]	0.96[e]
2”	0.86[e]	0.91[e]	0.87[e]	0.93[e]	0.99[e]
3”	1.01[e]	0.99[e]	0.99[e]	1.01[e]	-

[a]PS = poplar sawdust [b]ST = straw [c]CS = corn stover [d]SG = switchgrass [e]these are predictions (Lewis, 2011) since the particles were not bright enough to be measured [f]confidence intervals ($T_{stat} \cdot \sigma$ / *sqrt(#points)*) of 95% are shown

Table C.4. Biomass residence times (ms) in FFB reactor at various collection heights

Height Above Burner (inches)	PS[a] $T_{gas,max}$ = 1163 K	PS[a] $T_{gas,max}$ = 1320 K	ST[b] $T_{gas,max}$ = 1163 K	ST[b] $T_{gas,max}$ = 1320 K	CS[c] $T_{gas,max}$ = 1163 K	SG[d] $T_{gas,max}$ = 1163 K
1	34.8	-	33.7	-	-	34.0
2	64.3	58.5	61.5	57.3	-	61.3
3	89.4	-	87.2	-	-	-
4	-	-	112.9	-	-	111.7
5	-	-	-	-	139.6	-
Height Above Burner (inches)	PS[a] $T_{gas,max}$ = 1433 K	PS[a] $T_{gas,max}$ = 1751 K	ST[b] $T_{gas,max}$ = 1433 K	CS[c] $T_{gas,max}$ = 1433 K	SG[d] $T_{gas,max}$ = 1433 K	
1	-	-	-	-	-	
2	49.2	-	48.7	-	49.1	
3	-	-	-	72.6	68.6	
4	-	-	-	-	-	
5	-	-	-	110.3	-	
6	-	76.8	-	128.7	-	
7	-	-	-	147.2	-	
8	156.3	-	-	-	-	

[a]PS = poplar sawdust [b]ST = straw [c]CS = corn stover [d]SG = switchgrass

Table C.5. Biomass (45-75 μm) particle velocity (m/s) profiles at Different conditions in FFB reactor

Height Above Burner (mm)	PS[a] $T_{gas,max}$ = 1163 K	PS[a] $T_{gas,max}$ = 1320 K	PS[a] $T_{gas,max}$ = 1433 K	PS[a] $T_{gas,max}$ = 1751 K	ST[b] $T_{gas,max}$ = 1163 K	ST[b] $T_{gas,max}$ = 1320 K
0	0.075	0.075	0.075	0.075	0.041	0.041
1	0.456	0.488	0.507	0.682	0.518	0.545
3	0.589	0.622	0.718	1.072	0.633	0.678
5	0.669	0.694	0.823	1.303	0.698	0.730
7	0.724	0.741	0.884	1.475	0.744	0.763
9	0.768	0.778	0.929	1.615	0.778	0.792
13	0.819	0.831	0.990	1.821	0.831	0.835
16.5	0.837	0.864	1.027	1.952	0.847	0.864
Height Above Burner (mm)	ST[b] $T_{gas,max}$ = 1433 K	CS[c] $T_{gas,max}$ = 1163 K	CS[c] $T_{gas,max}$ = 1433 K	SG[d] $T_{gas,max}$ = 1163 K	SG[d] $T_{gas,max}$ = 1433 K	
0	0.041	0.098	0.098	0.054	0.054	
1	0.582	0.421	0.444	0.477	0.551	
3	0.807	0.561	0.667	0.621	0.781	
5	0.884	0.640	0.783	0.691	0.859	
7	0.930	0.702	0.853	0.741	0.921	
9	0.963	0.744	0.902	0.776	0.957	
13	1.020	0.802	0.974	0.830	1.019	
16.5	1.057	0.819	1.019	0.846	1.055	

[a]PS = poplar sawdust [b]ST = straw [c]CS = corn stover [d]SG = switchgrass *use measured particle velocities to complete the profiles after 16.5 mm above the burner

Table C.6. Summary of 45-75 μm poplar sawdust pyrolysis data in the FFB reactor

Collection Height Above Burner	Particle Residence Time	wt% Tar (daf)	wt% Char (daf)	wt% Gas (daf) *by difference
$T_{gas,max}$ = 1163 K condition				
1”	35 ms	3.94	2.06	94.00
1”	35 ms	5.49	3.89	90.61
1”	35 ms	5.79	1.37	92.84
1”	35 ms	4.88	2.23	92.88
1”	35 ms	5.45	3.79	90.76
1”	35 ms	7.82	1.59	90.59
1”	35 ms	5.32	1.89	92.79
1”	35 ms	4.59	2.35	93.06
1”	35 ms	4.08	0.84	95.08
1”	35 ms	5.33	1.38	93.29
1”	35 ms	5.30	1.00	93.70
1”	35 ms	4.05	1.36	94.59
1”	35 ms	3.42	1.44	95.14
1”	35 ms	3.35	0.78	95.87
2”	64 ms	1.75	0.67	97.58

Table C.6 continued

Collection Height Above Burner	Particle Residence Time	wt% Tar (daf)	wt% Char (daf)	wt% Gas (daf) *by difference
2”	64 ms	1.92	0.97	97.11
2”	64 ms	1.26	0.42	98.32
2”	64 ms	1.57	0.55	97.88
3”	89 ms	1.00	1.08	97.92
3”	89 ms	1.16	0.68	98.17
3”	89 ms	1.53	0.72	97.76
$T_{gas,max}$ = 1320 K condition				
2”	59 ms	0.45	0.80	98.75
2”	59 ms	0.42	0.54	99.04
$T_{gas,max}$ = 1433 K condition				
2”	49 ms	0.76	0.74	98.49
2”	49 ms	1.66	0.66	97.68
8”	156 ms	1.27	0.60	98.13
$T_{gas,max}$ = 1751 K condition				
6”	77 ms	2.13	0.31	97.56

* ash fractions of the char are not reported for each case because insufficient sawdust was typically fed during a single run for an accurate ash test to be performed on the collected sawdust char.

Table C.7. Summary of 45-75 μm switchgrass pyrolysis data in the FFB reactor

Collection Height Above Burner	Particle Residence Time	wt% Tar (daf)	wt% Char (daf)	wt% Gas (daf) *by diff.	x_{ash} in char (dry basis)	% daf MR[a] by Eqn (4.5)[b]	% daf MR[a] by Eqn (4.6)
$T_{gas,max}$ = 1163 K condition							
1”	34 ms	3.02	9.94	87.03	0.4346	88.33	90.06
1”	34 ms	3.11	8.53	88.36	0.4381	88.50	91.47
1”	34 ms	-[c]	-[c]	-[c]	0.4489	88.99	-[c]
2”	61 ms	1.24	5.60	93.16	0.5726[d]	93.31	94.40
2”	61 ms	1.32	5.31	93.37	0.5726[d]	93.31	94.69
4”	112 ms	1.28	5.36	93.35	0.5874	93.70	94.64
4”	112 ms	1.06	5.43	93.51	0.5999	94.02	94.57
$T_{gas,max}$ = 1433 K condition							
2”	49 ms	1.62	4.56	93.82	0.6150	94.39	95.44
3”	69 ms	-[d]	4.46	-[e]	0.6394	94.94	95.54

[a]mass release [b]assumes ash as a tracer; these values are not trusted as much as the MR values by Eqn (4.6) because a mass balance on the ash revealed that ash was released to the gas phase during the biomass pyrolysis experiments, which would result in falsely low MR values by Eqn (4.5) [c]forgot to weigh feed plunger [d]combined ash test [e]weighed filters incorrectly

Table C.8. Summary of 45-75 μm corn stover pyrolysis data in the FFB reactor

Collection Height Above Burner	Particle Residence Time; % Carrier N_2[a]	wt% Tar (daf)	wt% Char (daf)	wt% Gas (daf) *by diff.	x_{ash} in char (dry basis)	% daf MR[b] by Eqn (4.5)[c]	% daf MR[b] by Eqn (4.6)
$T_{gas,max}$ = 1163 K condition							
5”	140 ms; 70%	1.45	11.19	87.36	0.7034	87.16	88.81
$T_{gas,max}$ = 1433 K condition							
3”	73 ms; 70%	2.01	5.20	92.79	0.7501	89.85	94.80
5”	110 ms; 70%	2.10	6.68	91.22	0.7616	90.47	93.32
6”	129 ms; 65%	2.17	7.08	90.76	0.7974	92.26	92.92
6”	129 ms; 65%	2.39	7.04	90.57	0.7945	92.12	92.96
7”	147 ms; 60%	2.34	6.96	90.70	0.7872	91.77	93.04
7”	147 ms; 60%	2.05	6.77	91.17	0.7871	91.76	93.23
7”	147 ms; 60%	2.00	7.18	90.81	0.7914	91.97	92.82

[a]percentage of max flow of N_2 in feeding tube (max = 0.1 SLPM). These runs contained variable amounts of carrier N_2 since they were somewhat probing experiments to find the least amount of carrier N_2 that could be added for corn stover (CS) to not clog since CS had a tendency to pyrolyze early in the feeding tube and clog [b]mass release [c]assumes ash as a tracer; these values are not trusted as much as the MR values by Eqn (4.6) because a mass balance on the ash revealed that ash was released to the gas phase during the biomass pyrolysis experiments, which would result in falsely low MR values by Eqn (4.5)

Table C.9. Summary of 45-75 μm straw pyrolysis data in the FFB reactor

Collection Height Above Burner	Particle Residence Time	wt% Tar (daf)	wt% Char (daf)	wt% Gas (daf) *by diff.	x_{ash} in char (dry basis)	% daf MR[a] by Eqn (4.5)[b]	% daf MR[a] by Eqn (4.6)
$T_{gas,max}$ = 1163 K condition							
1”	34 ms	2.29	8.74	88.98	0.3117	88.55	91.26
1”	34 ms	2.16	7.69	90.15	0.4310	93.15	92.31
1”	34 ms	2.52	11.94	85.54	0.3100	88.46	88.06
1”	34 ms	2.55	9.84	87.61	0.3085	88.38	90.16
2”	62 ms	1.18	8.65	90.17	0.3562	90.63	91.35
2”	62 ms	0.91	7.34	91.75	0.3526	90.48	92.66
2”	62 ms	1.31	7.21	91.48	0.3433	90.08	92.79
2”	62 ms	0.95	8.20	90.85	0.3661	91.02	91.80
3”	87 ms	0.16	6.88	92.96	0.3568	90.65	93.12
3”	87 ms	1.58	7.85	90.57	0.3708[c]	91.20	92.15
3”	87 ms	0.83	7.98	91.19	0.3708[c]	91.20	92.02
3”	87 ms	1.01	8.78	90.22	0.3708[c]	91.20	91.22
4”	113 ms	0.83	7.77	91.40	0.3472	90.25	92.23
4”	113 ms	1.24	6.91	91.85	0.3576	90.68	93.09
$T_{gas,max}$ = 1320 K condition							
2”	57 ms	1.18	8.84	89.98	0.3116	88.54	91.16
$T_{gas,max}$ = 1433 K condition							
2”	49 ms	1.20	6.02	92.78	0.4074	92.46	93.98
2”	49 ms	1.10	7.03	91.87	0.3582	90.71	92.97

[a]mass release [b]assumes ash as a tracer; these values are not trusted as much as the MR values by Eqn (4.6) because a mass balance on the ash revealed that ash was released to the gas phase during the biomass pyrolysis experiments, which would result in falsely low MR values by Eqn (4.5) [c]combined ash test

Table C.10. Ash liberation data[a] of switchgrass and corn stover from biomass pyrolysis experiments in the FFB reactor

Switchgrass (45-75 µm)				Corn Stover (45-75 µm)			
Collection Height Above Burner	Particle Residence Time	$T_{gas,max}$	% of Ash Liberated (weight basis)	Collection Height Above Burner	Particle Residence Time	$T_{gas,max}$	% of Ash Liberated (weight basis)
1”	34 ms	1163 K	14.8	5”	140 ms	1163 K	12.9
1”	34 ms	1163 K	25.9	6”	129 ms	1433 K	8.6
2”	61 ms	1163 K	16.4	6”	129 ms	1433 K	10.7
2”	61 ms	1163 K	20.7	7”	147 ms	1433 K	15.5
4”	112 ms	1163 K	14.8	7”	147 ms	1433 K	17.8
4”	112 ms	1163 K	9.2	7”	147 ms	1433 K	10.6
2”	49 ms	1433 K	18.8				
3”	69 ms	1433 K	11.8				

[a]this data corresponds to summarized data in Figure 5.7

Table C.11. Ash liberation data of straw from biomass pyrolysis experiments in the FFB reactor

Straw (45-75 µm)			
Collection Height Above Burner	Particle Residence Time	$T_{gas,max}$	% of Ash Liberated (weight basis)
1”	34	1163	23.7
1”	34	1163	15.4
2”	62	1163	7.7
2”	62	1163	22.9
2”	62	1163	27.3
2”	62	1163	8.7
3”	87	1163	26.4
3”	87	1163	10.8
3”	87	1163	9.4
4”	113	1163	20.3
4”	113	1163	25.9
1”	57	1320	22.8
2”	49	1433	20.1
2”	49	1433	24.3

* this data corresponds to summarized data in Figure 5.7

As stated in Chapter 5, there are concerns about the accuracy of gas temperatures and particle residence times reported from biomass pyrolysis data from GE’S bench scale gasifier (BSG) reactor (Maghzi and Rizeq, 2011). For example, particle residence times up to 740 ms were reported in the conference paper. However, particle velocity calculations (Lewis, 2011) suggest that the true particle residence times were approximately 2-4 times longer. In addition, it

is thought that the true gas temperatures were at least 100 °C cooler than those reported in the conference paper (Maghzi and Rizeq, 2011). For example, see the BSG temperature data in Table C.12 below. Since the surroundings temperature (i.e., 2nd column in the table) was hotter than the gas temperature, heat from the reactor wall radiated to the thermocouple bead, making the true gas temperature *cooler* than the raw gas temperature measurements (i.e., 1st column in the table).

Table C.12. BSG reactor temperature measurements

T_{gas}[a]	BSG Wall Temperature[b]	Reported T_{gas}[c]
475 °C	667 °C	590 °C
600 °C	805 °C	700 °C
700 °C	915 °C	800 °C

[a]before temperature correction due to radiation effects (see Appendix A) [b]measured
[c]reported gas temperatures in the conference paper after applying a temperature correction to the raw T_{gas} measurements in the first column

Appendix D. Biomass Char Gasification Data and Additional Information

Void fractions and particle spacing were reported in Chapter 6 for the biomass char gasification experiments. The calculations are presented here:

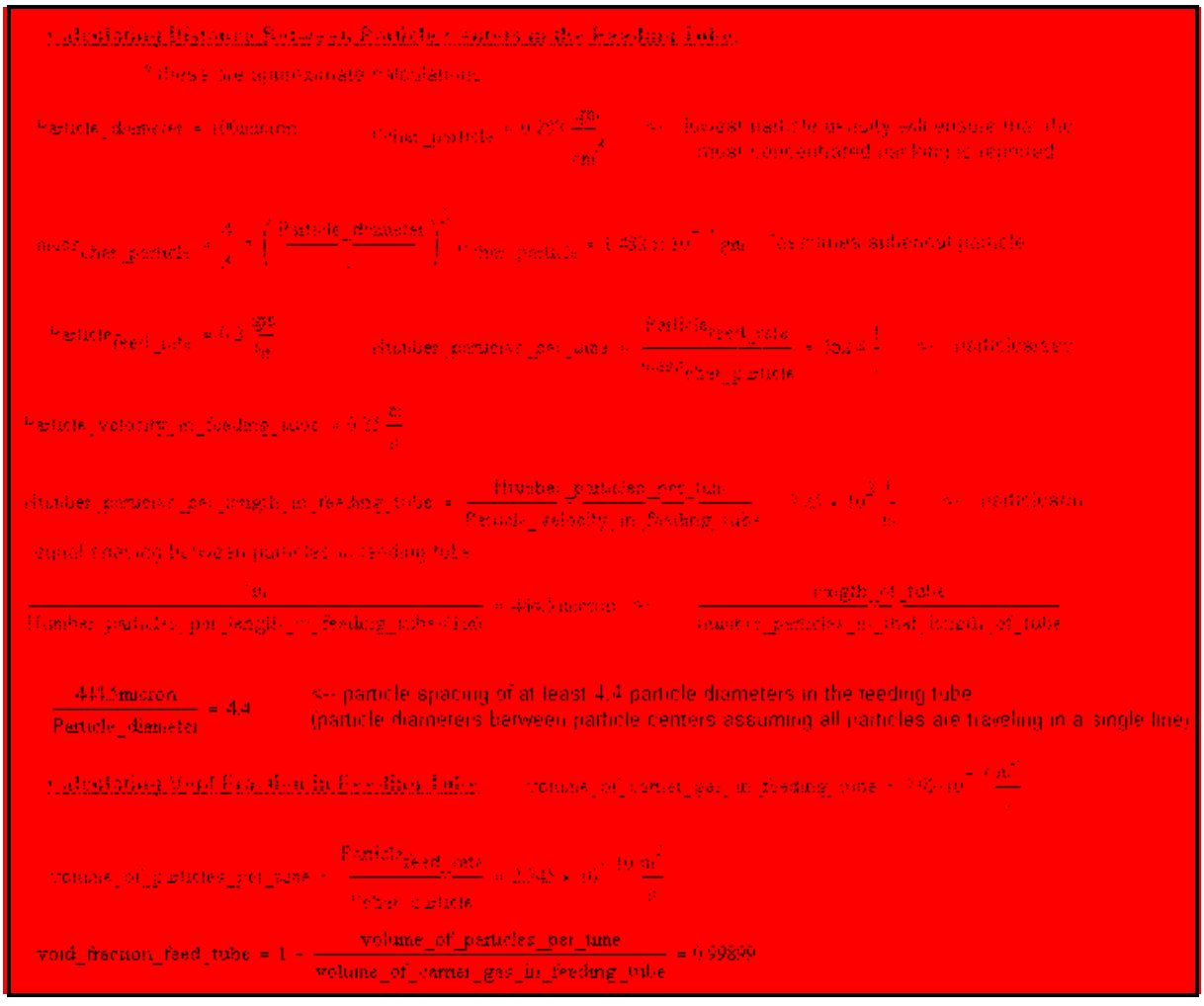

Calculating Distance Between Particle Centers in the Reactor: * these are approximate calculations

* feeding tube diameter in HPFFB reactor: 1.359 mm

* assumes a cylindrical column of gas (3 mm ID) in the reactor (after particles leave the feeding tube) where the particles are contained

Number_particles_per_time = $562.4\,\frac{1}{s}$ <-- solved for above

Particle_velocity_in_reactor := $0.7\,\frac{m}{s}$ <-- measured at 1-inch above burner

$$\text{Number\_particles\_per\_length\_in\_reactor} := \frac{\text{Number\_particles\_per\_time}}{\text{Particle\_velocity\_in\_reactor}} = 803.4\,\frac{1}{m}$$ <--- particles/m

equal spacing between particles in reactor:

$$\frac{1m}{\text{Number\_particles\_per\_length\_in\_reactor}\cdot(1m)} = 1.2\times10^{3}\ \text{micron} \quad \text{<----} \quad \frac{\text{length\_of\_tube}}{\text{number\_particles\_in\_that\_length\_of\_tube}}$$

$\frac{1.2\times10^{3}\ \text{micron}}{\text{Particle\_diameter}} = 12$ <-- particle spacing of at least 12 particle diameters in the reactor (particle diameters between particle centers assuming all particles are traveling in a single line)

Calculating Void Fraction in Reactor:

$$\text{volume\_in\_cylindrical\_column\_of\_gas\_in\_reactor} := \pi\cdot\left(\frac{3mm}{2}\right)^{2}\cdot\text{Particle\_velocity\_in\_reactor} = 4.948\times10^{-6}\,\frac{m^{3}}{s}$$

volume_of_particles_per_time = $2.945\times10^{-10}\,\frac{m^{3}}{s}$ <-- solved for above

$$\text{void\_fraction\_in\_reactor} := 1-\frac{\text{volume\_of\_particles\_per\_time}}{\text{volume\_in\_cylindrical\_column\_of\_gas\_in\_reactor}} = 0.99994$$

Details about the Mass-Mean Aspect Ratio of Switchgrass Particles in Figure 6.2:

The mass-mean aspect ratio of switchgrass char in Figure 6.2a and Figure 6.2b were reported in Chapter 6 to be 3.9 and 2.3, respectively. Length and width measurements of the char particles were obtained by hand measurements using ImageJ software. The mass of each particle was estimated based on the aspect ratio (i.e., length/width). For particles with aspect ratios below 1.5, the particle mass was calculated assuming a sphere where the diameter was the average of length and width measurements. For particles with aspect ratios above 1.5, the particle mass was calculated assuming a cylinder. The mass-mean aspect ratio (AR_m) of particles for each figure was then calculated as:

$$AR_m = \sum_{i=1}^{n} AR_i \cdot w_i \qquad \text{(D. 1)}$$

where AR_i is the aspect ratio of individual particles in the figure and w_i is the weight fraction that each particle represents.

Table D.1. Gas conditions for HPFFB biomass char gasification experiments

Centerline $T_{gas,max}$[a]	**1848 K**	**1808 K**	**1891 K**	**1686 K[b]**	**1734 K[b]**
Total Pressure (atm)	**15**	**10**	**15**	**15**	**15**
Gas flow (kg/s)	$5.476 \cdot 10^{-4}$	$4.075 \cdot 10^{-4}$	$5.366 \cdot 10^{-4}$	$5.434 \cdot 10^{-4}$	$5.481 \cdot 10^{-4}$
Φ (Equivalence Ratio)	1.043	1.045	1.121	1.066	1.137
Carrier[c] N_2 (SLPM)	0.235	0.175	0.235	0.235	0.235
O_2 (SLPM)	2.80	2.09	-	2.41	-
Air (SLPM)	-	-	13.35	-	11.90
CO_2 (SLPM)	11.62	8.64	3.88	11.77	5.22
CO (SLPM)	6.98	5.20	8.02	6.98	8.02
H_2 (SLPM)	0.168	0.168	0.168	0.168	0.168
Quench[d] N_2 (SLPM)	52	40	52	52	52
Equilibrium Post-Flame Gas Compositions					
Ar mol%	-	-	0.55	-	0.48
CO mol%	8.09	8.39	11.31	12.16	13.84
CO_2 mol%	89.79	89.20	40.78	85.73	43.61
H_2 mol%	0.02	0.03	0.04	0.03	0.06
H_2O mol%	0.86	1.16	0.69	0.84	0.67
N_2 mol%	1.24	1.23	46.63	1.23	41.34

[a]maximum radiation-corrected measured centerline gas temperature [b]these conditions were used when feeding poplar sawdust (PS) char. Although the PS data at the 15 atm 1686 K and 15 atm 1734 K conditions are summarized in this appendix, the results were not included in Chapter 6 in order to compare the measured data of all 3 biomass feedstocks on an equal basis (i.e., using data from the same 3 conditions) [c]N_2 in the feeding tube [d]N_2 in the collection probe

Table D.2. Radiation-corrected centerline HPFFB gas temperature profiles

Height[a] (inches) @ 15 atm $T_{gas,max}$ = 1848 K; ~90 mol% CO_2	***T_{gas} (K) @ 15 atm $T_{gas,max}$ = 1848 K; ~90 mol% CO_2***	***Height[a] (inches) @ 10 atm $T_{gas,max}$ = 1808 K; ~90 mol% CO_2***	***T_{gas} (K) @ 10 atm $T_{gas,max}$ = 1808 K; ~90 mol% CO_2***	***Height[a] (inches) @ 15 atm $T_{gas,max}$ = 1891 K; ~40 mol% CO_2***	***T_{gas} (K) @ 15 atm $T_{gas,max}$ = 1891 K; ~40 mol% CO_2***
0.25	1848	0.25	1807	0.25	1885
0.5	1828	0.5	1808	0.4	1891
0.75	1807	0.75	1797	0.6	1890
1	1792	1	1790	0.8	1888
1.25	1748	1.25	1776	1	1884
1.5	1719	1.5	1756	1.2	1873
1.75	1681	1.75	1701	1.4	1857
2	1655	2	1654	1.6	1822
2.5	1566	2.25	1633	1.8	1773
3.4	1424	2.5	1560	2	1749
3.8	1386	2.75	1528	2.2	1722
4.2	1365	3.4	1414	2.4	1697
4.6	1335	3.8	1387	2.6	1672

Table D.2 continued

Height*[a] *(inches) @ 15 atm $T_{gas,max}$ **= 1848 K; ~90 mol% CO_2**	T_{gas} ***(K) @ 15 atm*** $T_{gas,max}$ **= 1848 K; ~90 mol% CO_2**	***Height*[a] *(inches) @ 10 atm*** $T_{gas,max}$ **= 1808 K; ~90 mol% CO_2**	T_{gas} ***(K) @ 10 atm*** $T_{gas,max}$ **= 1808 K; ~90 mol% CO_2**	***Height*[a] *(inches) @ 15 atm*** $T_{gas,max}$ **= 1891 K; ~40 mol% CO_2**	T_{gas} ***(K) @ 15 atm*** $T_{gas,max}$ **= 1891 K; ~40 mol% CO_2**
5	1297	4.2	1361	2.8	1637
5.4	1280	4.6	1324	3.8	1501
5.8	1262	5	1298	4.2	1456
6.2	1231	5.4	1272	4.6	1423
6.6	1205	5.8	1248	5	1399
6.8	1204	6.2	1225	5.4	1371
7	1168	6.6	1181	5.8	1346
		6.8	1167	6.2	1327
		7	1104	6.6	1295
				6.8	1291
				7	1263

[a]height above burner

Table D.3. Radiation-corrected centerline HPFFB gas temperature profiles[a]

Height*[b] *(inches) @ 15 atm $T_{gas,max}$ **= 1686 K; ~90 mol% CO_2**	T_{gas} ***(K) @ 15 atm*** $T_{gas,max}$ **= 1686 K; ~90 mol% CO_2**	***Height*[b] *(inches) @ 15 atm*** $T_{gas,max}$ **= 1734 K; ~40 mol% CO_2**	T_{gas} ***(K) @ 15 atm*** $T_{gas,max}$ **= 1734 K; ~40 mol% CO_2**
0.25	1686	0.25	1731
0.5	1668	0.4	1734
0.75	1651	0.6	1734
1	1636	0.8	1733
1.25	1614	1	1723
1.5	1583	1.2	1709
1.75	1549	1.4	1671
2	1505	1.6	1642
2.25	1467	1.8	1605
2.5	1425	2	1594
3.8	1250	2.2	1574
4.2	1227	2.4	1544
4.6	1205	2.6	1536
5	1194	2.8	1491
5.4	1169	3.4	1421
5.8	1152	3.8	1387
6.2	1138	4.2	1356
6.6	1113	4.6	1334
6.8	1092	5	1306
7	1059	5.4	1279
-	-	5.8	1264

Table D.3 continued

Height*[b] *(inches) @ 15 atm $T_{gas,max}$ **= 1686 K; ~90 mol% CO_2**	***T_{gas} (K) @ 15 atm*** $T_{gas,max}$ **= 1686 K; ~90 mol% CO_2**	***Height*[b] *(inches) @ 15 atm*** $T_{gas,max}$ **= 1734 K; ~40 mol% CO_2**	***T_{gas} (K) @ 15 atm*** $T_{gas,max}$ **= 1734 K; ~40 mol% CO_2**
-	-	6.2	1239
-	-	6.6	1212
-	-	6.8	1194
-	-	7	1183

[a] for poplar sawdust char data (see footnote *b* to Table D.1)
[b]height above burner

Table D.4. Meausured particle velocities (m/s) of biomass char in the HPFFB reactor at 1" above the burner surface

	15 atm $T_{gas,max}$ =1848 K ~90% CO_2	**10 atm $T_{gas,max}$ =1808 K ~90% CO_2**	**15 atm $T_{gas,max}$ =1891 K ~40% CO_2**	**15 atm $T_{gas,max}$ =1686 K ~90% CO_2**	**15 atm $T_{gas,max}$ =1734 K ~40% CO_2**
PS[a] char	0.667 ±[e] 0.018	0.746[d]	0.744 ± 0.018	0.613 ± 0.02	0.641 ± 0.016
CS[b] char	0.700 ± 0.03	0.753 ± 0.015	0.726 ± 0.019	-	-
SG[c] char	0.677 ± 0.03	0.778 ± 0.024	0.828[d]	-	-

[a] poplar sawdust char [b]45-75 μm near-spherical corn stover char [c]45-75 μm near-spherical switchgrass char
[d]this is a prediction [e]confidence intervals ($T_{stat} \cdot \sigma$ / *sqrt(#points)*) of 95% are shown

Table D.5. Biomass char residence times in HPFFB reactor at various collection heights

Height Above Burner (inches)	**PS[a] char 15 atm $T_{gas,max}$ =1848 K ~90% CO_2**	**PS[a] char 10 atm $T_{gas,max}$ =1808 K ~90% CO_2**	**PS[a] char 15 atm $T_{gas,max}$ =1891 K ~40% CO_2**	**PS[a] char 15 atm $T_{gas,max}$ =1686 K ~90% CO_2**	**PS[a] char 15 atm $T_{gas,max}$ =1734 K ~40% CO_2**	
1"	-	52.6 ms	-	-	-	
1.5"	78.9 ms	-	67.8 ms	83.2 ms	76.7 ms	
3"	141.6 ms	126.6 ms	124.6 ms	152.8 ms	142.5 ms	
5.5"	267 ms	239 ms	234.1 ms	290.2 ms	268.1 ms	
7"	350 ms	-	307.1 ms	-	-	
Height Above Burner (inches)	**CS[b] char 15 atm $T_{gas,max}$ =1848 K ~90% CO_2**	**CS[b] char 10 atm $T_{gas,max}$ =1808 K ~90% CO_2**	**CS[b] char 15 atm $T_{gas,max}$ =1891 K ~40% CO_2**	**SG[c] char 15 atm $T_{gas,max}$ =1848 K ~90% CO_2**	**SG[c] char 10 atm $T_{gas,max}$ =1808 K ~90% CO_2**	**SG[c] char 15 atm $T_{gas,max}$ =1891 K ~40% CO_2**
1"	55.9 ms	52.1 ms	52.5 ms	56.7 ms	50.7 ms	46.8 ms
2"	94.1 ms	86.9 ms	88.8 ms	-	-	-
3"	135.9 ms	125.5 ms	128 ms	139 ms	121.6 ms	112.8 ms
5.5"	255.2 ms	236.7 ms	240.3 ms	262.4 ms	229.4 ms	211.4 ms

[a]poplar sawdust char [b]45-75 μm near-sph corn stover char [c]45-75 μm near-sph switchgrass char

Table D.6. Particle velocity (m/s) profiles for poplar sawdust char at different conditions in HPFFB reactor

	PS[a] char	PS[a] char	PS[a] char	PS[a] char	PS[a] char
Height Above Burner	**15 atm $T_{gas,max}$ = 1848 K ~90 mol% CO_2**	**10 atm $T_{gas,max}$ = 1808 K ~90 mol% CO_2**	**15 atm $T_{gas,max}$ = 1891K ~40 mol% CO_2**	**15 atm[b] $T_{gas,max}$ = 1686K ~90 mol% CO_2**	**15 atm[b] $T_{gas,max}$ = 1734K ~40 mol% CO_2**
mm	**V_p (m/s)**	**V_p (m/s)**	**V_p (m/s)**	**V_p (m/s)**	**V_p (m/s)**
0	0.055	0.059	0.055	0.055	0.055
2	0.256	0.274	0.307	0.232	0.275
3	0.289	0.311	0.337	0.273	0.313
6	0.390	0.417	0.436	0.350	0.397
9	0.465	0.516	0.527	0.434	0.466
12	0.540	0.594	0.598	0.493	0.526
15	0.595	0.653	0.656	0.546	0.574
18	0.635	0.705	0.705	0.583	0.612
21	0.659	0.733	0.732	0.604	0.633
24	0.668	0.746	0.744	0.614	0.642
25.4	0.667	0.746	0.744	0.613	0.641
Particle velocities are obtained for distances of x > 25.4 mm above the burner using the equation $v_p = v_p(25.4\text{ mm})*T(x) / T(25.4\text{ mm})$ where T is the centerline gas temperature[c] at height x. T(25.4 mm) values are given below for each of the conditions.					
T(25.4 mm)	1792 K	1790 K	1884 K	1636 K	1723 K

[a]poplar sawdust char [b]see footnote *b* to Table D.1 [c]see Table D.2 and Table D.3 for gas temperature profiles

Table D.7. Particle velocity (m/s) profiles for corn stover and switchgrass chars at different conditions in HPFFB reactor

	CS[a] char	CS[a] char	CS[a] char	SG[b] char	SG[b] char	SG[ab] char
Height Above Burner	**15 atm $T_{gas,max}$ = 1848 K ~90 mol% CO_2**	**10 atm $T_{gas,max}$ = 1808 K ~90 mol% CO_2**	**15 atm $T_{gas,max}$ = 1891K ~40 mol% CO_2**	**15 atm $T_{gas,max}$ = 1848 K ~90 mol% CO_2**	**10 atm $T_{gas,max}$ = 1808 K ~90 mol% CO_2**	**15 atm $T_{gas,max}$ = 1891K ~40 mol% CO_2**
mm	**V_p (m/s)**	**V_p (m/s)**	**V_p (m/s)**	**V_p (m/s)**	**V_p (m/s)**	**V_p (m/s)**
0	0.108	0.117	0.108	0.048	0.052	0.048
2	0.232	0.258	0.272	0.266	0.282	0.314
3	0.270	0.292	0.309	0.298	0.326	0.362
6	0.377	0.404	0.404	0.382	0.437	0.476
9	0.476	0.496	0.499	0.481	0.523	0.580
12	0.554	0.577	0.576	0.546	0.621	0.662
15	0.617	0.658	0.638	0.603	0.682	0.724
18	0.663	0.707	0.685	0.645	0.732	0.784
21	0.691	0.739	0.712	0.668	0.764	0.815
24	0.702	0.753	0.725	0.679	0.778	0.828
25.4	0.701	0.753	0.726	0.678	0.779	0.828
Particle velocities are obtained for distances of x > 25.4 mm above the burner using the equation $v_p = v_p(25.4\text{ mm})*T(x) / T(25.4\text{ mm})$ where T is the centerline gas temperature[c] at height x. T(25.4 mm) values are given below for each of the conditions.						
T(25.4 mm)	1792 K	1790 K	1884 K	1792 K	1790 K	1884 K

[a]45-75 μm near-sph corn stover char [b]45-75 μm near-sph switchgrass char [c]see Table D.2 for gas temp profiles

Table D.8. Particle size distribution[a] for biomass chars

CS[b] char		SG[c] char		PS[d] char	
size range (μm)	Mass Fraction	size range (μm)	Mass Fraction	size range (μm)	Mass Fraction
0 - 30.4	0.0000	0 - 31.2	0.0000	0 - 38.8	0.0000
30.5 - 51.8	0.0079	31.3 - 48.8	0.0076	38.9 - 55.5	0.0071
51.9 - 55.6	0.0092	48.9 - 52.6	0.0087	55.6 - 59.3	0.0086
55.7 - 56.9	0.0109	52.7 - 54.5	0.0093	59.4 - 61.7	0.0087
57 - 59	0.0119	54.6 - 55.9	0.0091	61.8 -63.8	0.0092
59.1 - 60.5	0.0128	56 - 57.7	0.0120	63.9 - 66.7	0.0107
60.6 - 61.9	0.0160	57.8 - 61	0.0244	66.8 - 71.1	0.0246
62 - 67.3	0.0684	61.1 - 66.7	0.0692	71.2 - 76.9	0.0692
67.4 - 74.8	0.1247	66.8 - 73	0.1246	77 - 86	0.1246
74.9 - 83.1	0.1758	73.1 - 81.1	0.1729	86.1 - 96.8	0.1750
83.2 - 92.4	0.1904	81.2 - 91.6	0.1937	96.9 - 108.5	0.1933
92.5 - 101.9	0.1699	91.7 - 102.9	0.1722	108.6 - 123	0.1714
102 - 114.6	0.1204	103 - 115.5	0.1229	123.1 - 138.9	0.1208
114.7 - 128.2	0.0611	115.6 - 132.1	0.0611	139 - 159.9	0.0635
128.3 - 136.5	0.0205	132.2 - 138.2	0.0122	160 - 161.4	0.0133

[a]see Section 6.1.2 [b]45-75 μm near-sph corn stover char [c]45-75 μm near-sph switchgrass char [d]poplar sawdust char

Table D.9. Poplar sawdust char re-injection HPFFB gasification data

Collection Height[a] (inch)	Residence Time (ms)	wt% MR (daf) #1[b]	wt% MR (daf) #2[c]	wt% MR (daf) #3[d]	% of ash liberated[e] (weight basis)	x_{ash} (dry basis)	d/d_o [f]	Apparent Density[g] g/cm^3
15 atm $T_{gas,max}$ = 1848 K ~90 mol% CO_2[l]								
1.5	79	45.72	45.15	36.49	14.54	0.1061	0.81	0.2987
3	142	56.37	63.42[h]	58.75[h]	-5.75	0.1545	0.79	0.2741
5.5	267	80.57[k]	72.69	66.30	42.33	0.1828	0.65[i]	0.2297[i]
5.5	267	76.63[k]	65.67	57.18	45.42	0.1497	0.65[i]	0.2654[i]
10 atm $T_{gas,max}$ = 1808 K ~90 mol% CO_2[l]								
1	53	25.49	33.79[h]	24.77	0.95	0.0911	0.89	0.3051
3	127	42.45	56.14[h]	51.10[h]	-17.70	0.1336	0.86	0.2765
5.5	239	62.43	59.25	52.26	21.30	0.1364	0.79	0.2335
15 atm $T_{gas,max}$ = 1891 K ~40 mol% CO_2[l]								
1.5	68	31.04	36.32[h]	27.26	5.20	0.0939	0.84	0.2951
3	125	54.36	51.06	42.78	20.24	0.1164	0.79	0.2747
5.5	234	67.85	59.58	51.32	33.95	0.1341	0.71	0.2679
5.5	234	66.14	65.24	59.64	16.11	0.1574	0.71	0.2842
15 atm $T_{gas,max}$ = 1686 K[j] ~90 mol% CO_2[l]								
1.5	83	32.28	28.89	17.15	18.26	0.0834	0.85	0.3126
3	153	57.02	48.46	38.51	30.11	0.1092	0.76	0.2907
5.5	290	60.15[k]	47.42	36.02	37.73	0.1054	0.75	0.282
15 atm $T_{gas,max}$ = 1734 K[j] ~40 mol% CO_2[l]								
1.5	77	33.93	34.81	24.79	12.15	0.0911	0.85	0.3111
3	143	42.82	40.96	31.39	16.65	0.0990	0.84	0.2897
3	143	38.91	41.68[h]	33.05	8.75	0.1012	0.84	0.2943
5.5	268	73.62[k]	60.10	49.86	47.39	0.1307	0.80	-
5.5	268	54.66	53.46	45.97	16.08	0.1225	0.80	0.2629

*see footnotes of this table on the next page

Footnotes to **Table D.9:**

[a]above burner [b]wt% mass release (daf, as-received char basis) by Equation (4.6) [c]wt% mass release (daf, as-received char basis) by Equation (4.5) with an assumed 13.5% ash release since 3 re-injection experiments in the FFB reactor at pyrolysis conditions showed that ~13.5% of the ash in the char was released to the gas phase upon re-injection [d]wt% mass release (daf, as-received char basis) by Equation (4.5), but is low if ash leaves the char (see Section 4.7) [e]by Equation (5.1) [f]by Equation (7.1) [g]by Equation (4.7) [h]value is greater than MR #1 so do not use (see Section 4.7) [i]volume of sample used to arrive at this value was on the lower end of where bulk density measurements are accurate (see Section 4.8 and Equation (7.1)) [j]see footnote *b* to Table D.1 [k]note the high ash release of this run which may be explained by collection inefficiencies. Therefore, MR #2 might be more accurate for this run [l]in post-flame environment

Table D.10. Corn stover char[a] re-injection HPFFB gasification data

Collection Height[b] (inch)	Residence Time (ms)	wt% MR (daf) #1[c]	wt% MR (daf) #2[d]	wt% MR (daf) #3[e]	% of ash liberated[f] (weight basis)	x_{ash} (dry basis)	d/d_o [g]	d/d_o [h]	Apparent Density [i] g/cm^3
15 atm $T_{gas,max}$ = 1848 K ~90 mol% CO_2[m]									
1	56	41.07	40.99	32.93	12.13	0.7384	-	0.90 [j]	0.8906 [j]
1	56	39.77	34.18	24.25	20.49	0.7142	0.93	0.95	0.7117
2	94	76.78	75.15	71.49	18.56	0.8691	0.84	0.78 [j]	1.0745 [j]
3	136	89.02	85.61	82.92	35.73	0.9172	0.81	0.64 [j]	1.4816 [j]
5.5	255	89.90	82.34	77.65	54.80	0.8944	0.75	0.57 [j]	1.4699 [j]
10 atm $T_{gas,max}$ = 1808 K ~90 mol% CO_2[m]									
1	52	61.93	65.87[k]	61.76	0.45	0.8319	-	0.85 [j]	1.0504 [j]
1	52	35.06	33.00	23.54	15.08	0.7123	0.91	1	0.6577
2	87	71.00	73.45[k]	70.17	2.80	0.8638	0.79	0.82 [j]	1.1094 [j]
3	126	81.51	81.73[k]	79.27	10.83	0.9013	0.82	0.72 [j]	1.4261 [j]
5.5	237	83.78	78.74	74.77	35.71	0.8824	0.85	0.67 [j]	1.3163 [j]
15 atm $T_{gas,max}$ = 1891 K ~40 mol% CO_2[m]									
1	53	55.53	58.36[k]	53.08	5.22	0.8014	0.99	0.88 [j]	0.9491 [j]
2	89	47.57	49.03[k]	42.30	9.14	0.7664	0.94	0.90 [j]	0.8856 [j]
2	89	80.07	82.20[k]	80.07	0.01	0.9047	-	0.75 [j]	1.4185 [j]
2	89	67.07	74.73[l]	71.69[l]	-16.30[l]	0.8189	-	0.87 [j]	1.0086 [j]
3	128	81.39	81.23	78.64	12.88	0.8986	0.86	0.72 [j]	1.3969 [j]
5.5	240	89.27	85.74	83.04	36.73	0.9178	0.84	0.61 [j]	1.6403 [j]

[a]45-75 μm near-spherical corn stover char [b]above burner [c]wt% mass release (daf, as-received char basis) by Equation (4.6) [d]wt% mass release (daf, as-received char basis) by Equation (4.5) with an assumed 12% ash release [e]wt% mass release (daf, as-received char basis) by Equation (4.5), but is low if ash leaves the char (see Section 4.7) [f]by Equation (5.1) [g]measured using ImageJ software (see Section 6.1.2) [h]by Equation (7.1) [i]by Equation (4.7) [j]this value is most likely not accurate since the volume of sample used for bulk density measurements was below the cutoff at which accurate values are obtained (see Section 4.8 and Equation (7.1)) [k]value is greater than MR #1 so do not use (see Section 4.7) [l]some insulation in the collected char obscured results
[m]in post-flame environment

Table D.11. Switchgrass char[a] re-injection HPFFB gasification data

Collection Height[b] (inch)	Residence Time (ms)	wt% MR (daf) #1[c]	wt% MR (daf) #2[d]	wt% MR (daf) #3[e]	% of ash liberated[f] (weight basis)	x_{ash} (dry basis)	d/d_o [g]	d/d_o [h]	Apparent Density [i] g/cm^3
15 atm $T_{gas,max}$ = 1848 K ~90 mol% CO_2[n]									
1	57	44.12	47.89[j]	40.70	5.76	0.3530	0.96	0.90	0.3012
3	139	60.83	61.60[j]	56.00	11.00	0.4237	0.87	0.81[l]	0.3210[l]
5.5	262	80.66[k]	67.84	58.96	52.88	0.4408	0.92	0.67[m]	0.2945[m]
5.5	262	77.56[k]	68.85	61.99	40.95	0.4598	-	0.70[m]	0.3014[m]
10 atm $T_{gas,max}$ = 1808 K ~90 mol% CO_2[n]									
1	51	46.68	44.40	35.68	17.09	0.3347	-	0.88	0.3017
1	51	43.72	48.70[j]	41.81	3.29	0.3573	0.96	0.88	0.3232
3	122	51.00	51.25[j]	44.02	12.47	0.3662	0.92	0.85	0.3190
5.5	229	61.85	60.48	54.33	16.46	0.4147	0.88	0.81	0.3138
15 atm $T_{gas,max}$ = 1891 K ~40 mol% CO_2[n]									
1	47	60.64[k]	48.76	38.33	36.18	0.3441	-	0.80	0.2959
1	47	37.99	43.42[j]	35.81	3.39	0.3351	0.94	0.89	0.3387
3	113	62.37[k]	56.81	49.24	25.87	0.3892	0.89	0.80	0.2999
5.5	211	80.84[k]	72.05	65.51	44.45	0.4840	0.88	0.70[m]	0.2791[m]
5.5	211	77.71[k]	72.11	66.70	33.06	0.4927	-	0.72[m]	0.2964[m]

[a]45-75 µm near-spherical switchgrass char [b]above burner [c]wt% mass release (daf, as-received char basis) by Equation (4.6) [d]wt% mass release (daf, as-received char basis) by Equation (4.5) with an assumed 13% ash release since a re-injection experiment in the FFB reactor at pyrolysis conditions showed that ~13% of the ash in the char was released to the gas phase upon re-injection [e]wt% mass release (daf, as-received char basis) by Equation (4.5), but is low if ash leaves the char (see Section 4.7) [f]by Equation (5.1) [g]measured using ImageJ software (see Section 6.1.2) [h]by Equation (7.1) [i]by Equation (4.7) [j]value is greater than MR #1 so do not use (see Section 4.7) [k]note the high ash release (6th column) of this run which may be explained by collection inefficiencies. Therefore, MR #2 might be more accurate for this run [l]a coal run was conducted prior to this experiment and it was overlooked to clean the inside of the collection probe so coal char contamination may have affected this measured density [m]volume of sample used to arrive at this value was on the lower end of where bulk density measurements are accurate (see Section 4.8) [n]in post-flame environment

As stated in Section 6.2, the left-hand side of Equation (6.3) was set equal to zero when calculating particle temperatures with the assumption that the particle temperature is near steady state with its surroundings when using time steps of approximately 0.15 ms. The convective heat transfer term was the most dominant of the three terms in the particle energy balance. The relative importance of the radiative heat transfer term compared to the endothermic gasification term in the particle energy balance varied between fuels and reaction conditions in this research. However, Figure D.1 is included to show the fraction of energy that each term (convection, radiation, heat of reaction) represents for poplar char gasifying at the 15 atm $T_{gas,max}$ = 1891 K HPFFB condition as a function of (a) particle temperature and (b) height above the burner. Notice that the convection term in Figure D.1a and b always makes up half of the net energy since the convective heat is always balanced by the cooling terms of radiation and heat of reaction (i.e., endothermic char gasification) since steady state was assumed at each small time step in the calculation of particle temperatures. Notice in Figure D.1a that the heat of reaction term exceeds the radiative term at particle temperatures exceeding ~1400 K in this particular comparison. At higher temperatures, the char gasification reaction occurs more quickly, which increases the relative importance of the heat of reaction term in the overall heat balance. Figure D.1b demonstrates a similar concept; the heat of reaction term exceeds the radiative term in the

near-burner region of the HPFFB reactor, which region is characterized by hotter temperatures (see Figure 6.5 for instance).

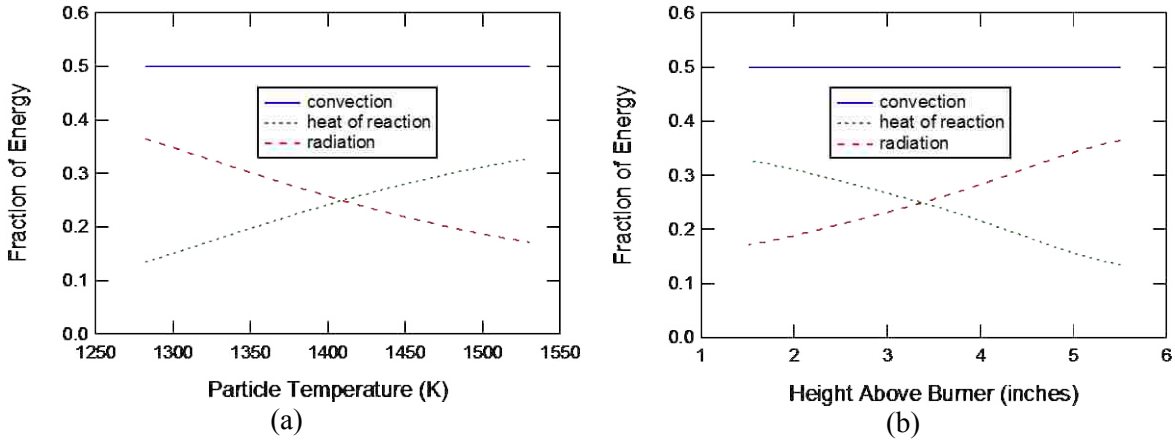

Figure D.1. Fraction of terms in the particle energy balance (see right-hand side of Equation (6.3)) as a function of (a) particle temperature and (b) height above the burner for poplar char gasifying by CO_2 at the 15 atm $T_{gas,max}$ = 1891 K 40 mol% CO_2 HPFFB condition.

Sensitivity Analysis

Values for char emissivity (ε_p) and surroundings temperature (T_{surr}) were evaluated for their effect on the particle temperature as calculated by the particle energy balance in Equation (6.3). In this work, values used for ε_p and T_{surr} were 0.8 and 500 K, respectively. Figure D.2 shows how particle temperature was affected by a range of char emissivity values for sawdust char fed at the HPFFB 10 atm $T_{gas,max}$ = 1808 K condition. The range of emissivity values (0.7-0.9) only affected particle temperature by a maximum difference of 9.6 K. Figure D.3 shows how calculated particle temperature was affected by a range of surroundings temperatures for sawdust char at the same aforementioned HPFFB condition. The true surroundings temperature was certainly between the 300-700 K range, but this range of T_{surr} values only made a maximum difference of 4 K to particle temperatures. Also shown in Figure D.3 is the effect of particle temperature at T_{surr} values of 950 and 1150 K to demonstrate the effect of T_{surr} at higher temperatures. Setting T_{surr} to 950 and 1150 K caused an increase in particle temperature in the ranges of 4-13 and 10-29 K, respectively.

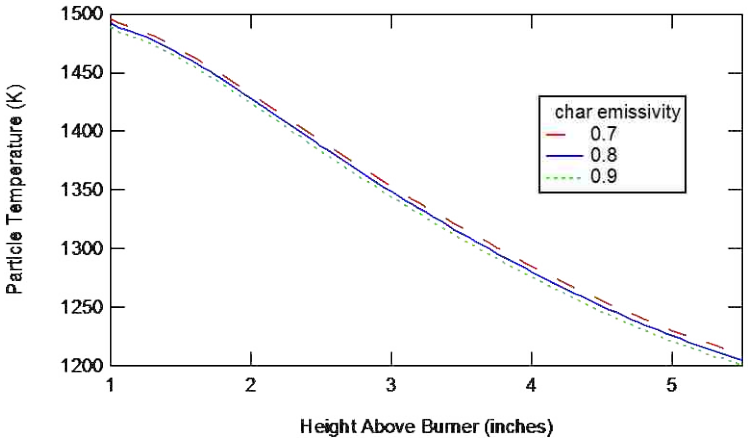

Figure D.2. Effect of char emissivity on particle temperature for poplar sawdust char fed in the HPFFB reactor at the 10 atm $T_{gas,max}$ = 1808 K condition in a post-flame environment consisting of ~90 mol% CO_2.

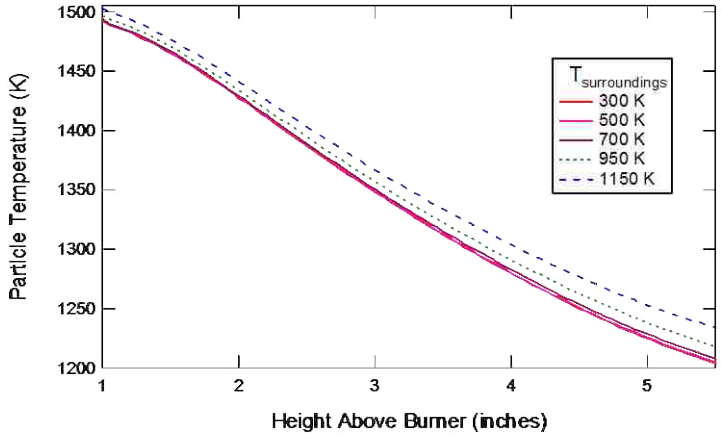

Figure D.3. Effect of surroundings temperature on particle temperature for poplar sawdust char fed in the HPFFB reactor at the 10 atm $T_{gas,max}$ = 1808 K condition in a post-flame environment consisting of ~90 mol% CO_2.

Appendix E. Petcoke Gasification Data and Additional Information

Petroleum coke gasification data were measured using six conditions in the HPFFB reactor (see Table E.1 below). Conditions 1 through 5 in Table E.1 were also used in biomass char gasification experiments. Information regarding the gas conditions and centerline gas temperature profiles will *not* be repeated here for those HPFFB conditions which have been documented elsewhere in this dissertation (see Table D.1, Table D.2, & Table D.3 in Appendix D). However, information regarding condition 6 of Table E.1 will be summarized in this appendix since it has not yet been reported.

Data collected at conditions 4 and 5 in Table E.1 will be summarized in this appendix, although data from these two conditions were not used in the regression of kinetic parameters that were reported in Chapter 7 (see Table 7.5). When the HPFFB reactor was operated using conditions 4 or 5, the outside wall of the reactor was noticeably hotter to the touch than when it was operated with any of the other conditions in Table E.1. This was confusing since conditions 4 and 5 of Table E.1 contained lower gas temperatures. Also, the petcoke particle mass release data measured at conditions 4 or 5 seemed high when compared to the other measured data from the other conditions. Either something was peculiar about HPFFB conditions 4 or 5, or petcoke char gasification sometimes occurs more quickly at less severe reaction conditions (perhaps by affecting evolution of char structure).

Table E.1. HPFFB gas conditions used in petcoke gasification experiments

Condition Number	Centerline $T_{gas,max}$[a]	Total Pressure	Approx. mol% CO_2[b]
1	1848 K	15 atm	90
2	1808 K	10 atm	90
3	1891 K	15 atm	40
4	1686 K	15 atm	90
5	1734 K	15 atm	40
6	1909 K	10 atm	40

[a]maximum radiation-corrected measured centerline gas temperature [b]in post-flame environment

Table E.2. Gas conditions for petcoke experiments

Centerline $T_{gas,max}$[a]	1909 K	1929 K[f]
Reactor	HPFFB	FFB
Total Pressure (atm)	10 atm	~ 1 atm
Gas flow (kg/s)	$5.476 \cdot 10^{-4}$	$7.730 \cdot 10^{-4}$
Φ (Equivalence Ratio)	1.12	1.10
Carrier[b] N_2 (SLPM)	0.18	0.0367
O_2 (SLPM)	-	5.09
Air (SLPM)	10	-
Oxidizer N_2[c] (SLPM)	-	19.16
Fuel N_2[d] (SLPM)	-	3.5
CO_2 (SLPM)	2.91	-
CO (SLPM)	5.90	12
H_2 (SLPM)	0.17	0.32
Quench[e] N_2 (SLPM)	40	60
Equilibrium Post-Flame Gas Compositions		
Ar mol%	0.55	-
CO mol%	10.96	6.74
CO_2 mol%	40.69	27.40
H_2 mol%	0.06	0.04
H_2O mol%	0.93	0.83
N_2 mol%	46.81	64.47

[a]maximum radiation-corrected measured centerline gas temperature
[b]N_2 in the feeding tube [c]N_2 in the oxidizer line [d]N_2 in the fuel line
[e]N_2 in the collection probe [f]this condition was to test petcoke volatile yields at high heating rate

Table E.3. Radiation-corrected centerline gas temperature profiles

Height[a] (inches) @ 10 atm $T_{gas,max}$ = 1909 K; ~40 mol% CO_2[b] (HPFFB reactor)	***T_{gas} (K) @ 10 atm $T_{gas,max}$ = 1909 K; ~40 mol% CO_2[b] (HPFFB reactor)***	***Height[a] (inches) @ 1 atm $T_{gas,max}$ = 1929 K[c] (FFB reactor)***	***T_{gas} (K) @ 1 atm $T_{gas,max}$ = 1929 K[c] (FFB reactor)***
0.25	1909	0.25	1893
0.4	1898	0.5	1918
0.6	1889	0.75	1923
0.8	1880	1	1929
1	1871	1.5	1925
1.2	1859	2	1911
1.4	1848	2.5	1890
1.6	1827	3	1869
1.8	1819	3.5	1846
2	1792	4	1822
2.2	1786	4.5	1796
2.4	1740	5	1770
2.6	1714	6	1721
3.8	1573	7	1673
4.2	1537	8	1620
4.6	1495		
5	1481		
5.4	1427		

Table E.3 continued

Height[a] (inches) @ 10 atm $T_{gas,max}$ = 1909 K; ~40 mol% CO_2[b] (HPFFB reactor)	***T_{gas} (K) @ 10 atm $T_{gas,max}$ = 1909 K; ~40 mol% CO_2[b] (HPFFB reactor)***	***Height[a] (inches) @ 1 atm $T_{gas,max}$ = 1929 K[c] (FFB reactor)***	***T_{gas} (K) @ 1 atm $T_{gas,max}$ = 1929 K[c] (FFB reactor)***
5.8	1394		
6.2	1355		
6.6	1325		
6.8	1293		
7	1263		

[a]above burner [b]in post-flame environment [c]this condition was for testing for petcoke volatile yields at high heating rate

Table E.4. Meausured particle velocities (m/s) of petcoke in the HPFFB reactor at 1" above the burner surface

	15 atm $T_{gas,max}$ = 1848 K ~90 mol% CO_2[b]	**10 atm $T_{gas,max}$ = 1808 K ~90 mol% CO_2[b]**	**15 atm $T_{gas,max}$ = 1891 K ~40 mol% CO_2[b]**	**15 atm $T_{gas,max}$ = 1686 K[a] ~90 mol% CO_2[b]**	**15 atm $T_{gas,max}$ = 1734 K[a] ~40 mol% CO_2[b]**	**10 atm $T_{gas,max}$ = 1909 K ~40 mol% CO_2[b]**
Petcoke A	0.677 ±[c] 0.034	0.739 ± 0.039	0.675 ± 0.029	0.593 ± 0.051	0.653 ± 0.027	0.722 ± 0.025
Petcoke B	0.650 ± 0.019	0.692 ± 0.023	0.760 ± 0.016	0.619 ± 0.029	0.651 ± 0.023	0.768 ± 0.017

[a]see discussion at beginning of Appendix E [b]in post-flame environment [c]confidence intervals ($T_{stat} \cdot \sigma$ / *sqrt(#points)*) of 95% are shown

Table E.5. Petcoke residence times in HPFFB reactor at various collection heights

Height Above Burner (inches)	Petcoke A 15 atm $T_{gas,max}$ = 1848 K ~90 mol% CO_2[a]	Petcoke A 10 atm $T_{gas,max}$ = 1808 K ~90 mol% CO_2[a]	Petcoke A 15 atm $T_{gas,max}$ = 1891 K ~40 mol% CO_2[a]	Petcoke A 15 atm $T_{gas,max}$ = 1686 K[b] ~90 mol% CO_2[a]	Petcoke A 15 atm $T_{gas,max}$ = 1734 K[b] ~40 mol% CO_2[a]	Petcoke A 10 atm $T_{gas,max}$ = 1909 K ~40 mol% CO_2[a]
1"	59 ms	-	56 ms	66 ms	58 ms	52 ms
1.5"[c]	-	73 ms	-	-	-	-
3"	142 ms	130 ms	137 ms	160 ms	143 ms	125 ms
5.5"	265 ms	244 ms	259 ms	302 ms	266 ms	232 ms
Height Above Burner (inches)	**Petcoke B 15 atm $T_{gas,max}$ = 1848 K ~90 mol% CO_2[a]**	**Petcoke B 10 atm $T_{gas,max}$ = 1808 K ~90 mol% CO_2[a]**	**Petcoke B 15 atm $T_{gas,max}$ = 1891 K ~40 mol% CO_2[a]**	**Petcoke B 15 atm $T_{gas,max}$ = 1686 K[b] ~90 mol% CO_2[a]**	**Petcoke B 15 atm $T_{gas,max}$ = 1734 K[b] ~40 mol% CO_2[a]**	**Petcoke B 10 atm $T_{gas,max}$ = 1909 K ~40 mol% CO_2[a]**
1"	60 ms	57 ms	-	64 ms	-	-
1.25"[c]	-	-	60 ms	-	68 ms	57 ms
3"	146 ms	137 ms	124 ms	153 ms	142 ms	119 ms
5.5"	275 ms	258 ms	231 ms	289 ms	266 ms	219 ms

[a]in post-flame environment [b]see discussion at beginning of Appendix E [c]there is no reason why the first collection height was not always 1 inch, even though it does not make a difference with how the data was modeled in this work

Table E.6. Particle velocity (m/s) profiles for Petcoke A at different conditions in the HPFFB reactor

Height Above Burner	15 atm $T_{gas,max}$ = 1848 K ~90 mol% CO_2[a]	10 atm $T_{gas,max}$ = 1808 K ~90 mol% CO_2[a]	15 atm $T_{gas,max}$ = 1891 K ~40 mol% CO_2[a]	15 atm $T_{gas,max}$ = 1686 K[b] ~90 mol% CO_2[a]	15 atm $T_{gas,max}$ = 1734 K[b] ~40 mol% CO_2[a]	10 atm $T_{gas,max}$ = 1909 K ~40 mol% CO_2[a]
mm	**V_p (m/s)**	**V_p (m/s)**	**V_p (m/s)**	**V_p (m/s)**	**V_p (m/s)**	**V_p (m/s)**
0	0.114	0.123	0.114	0.114	0.114	0.123
2	0.212	0.228	0.242	0.199	0.235	0.275
3	0.259	0.271	0.288	0.235	0.276	0.325
6	0.384	0.409	0.400	0.341	0.384	0.448
9	0.497	0.526	0.496	0.432	0.473	0.546
12	0.576	0.613	0.563	0.497	0.543	0.615
15	0.630	0.670	0.616	0.547	0.593	0.671
18	0.661	0.712	0.650	0.578	0.631	0.702
21	0.678	0.734	0.670	0.592	0.649	0.719
24	0.681	0.740	0.676	0.596	0.655	0.724
25.4	0.678	0.739	0.675	0.593	0.653	0.722
Particle velocities are obtained for distances of x > 25.4 mm above the burner using the equation $v_p = v_p(25.4\text{ mm})*T(x) / T(25.4\text{ mm})$ where T is the centerline gas temperature[c] at height x. T(25.4 mm) values are given below for each of the conditions.						
T(25.4 mm)	1792 K	1790 K	1884 K	1636 K	1723 K	1871 K

[a]in post-flame environment [b]see discussion at beginning of Appendix E [c]see Table D.1, Table D.2, & Table E.3 for gas temperature profiles

Table E.7. Particle velocity (m/s) profiles for Petcoke B at different conditions in the HPFFB reactor

Height Above Burner	15 atm $T_{gas,max}$ = 1848 K ~90 mol% CO_2[a]	10 atm $T_{gas,max}$ = 1808 K ~90 mol% CO_2[a]	15 atm $T_{gas,max}$ = 1891 K ~40 mol% CO_2[a]	15 atm $T_{gas,max}$ = 1686 K[b] ~90 mol% CO_2[a]	15 atm $T_{gas,max}$ = 1734 K[b] ~40 mol% CO_2[a]	10 atm $T_{gas,max}$ = 1909 K ~40 mol% CO_2[a]
mm	V_p (m/s)	V_p (m/s)	V_p (m/s)	V_p (m/s)	V_p (m/s)	V_p (m/s)
0	0.080	0.085	0.080	0.080	0.080	0.085
2	0.211	0.230	0.258	0.203	0.242	0.283
3	0.256	0.275	0.311	0.242	0.282	0.338
6	0.379	0.397	0.439	0.353	0.381	0.469
9	0.480	0.498	0.541	0.448	0.473	0.573
12	0.551	0.578	0.630	0.520	0.544	0.654
15	0.605	0.634	0.688	0.570	0.595	0.711
18	0.637	0.668	0.730	0.601	0.627	0.745
21	0.651	0.688	0.752	0.618	0.647	0.764
24	0.653	0.694	0.761	0.622	0.653	0.770
25.4	0.650	0.692	0.760	0.620	0.652	0.768
Particle velocities are obtained for distances of x > 25.4 mm above the burner using the equation $v_p = v_p(25.4\text{ mm})*T(x) / T(25.4\text{ mm})$ where T is the centerline gas temperature[c] at height x. T(25.4 mm) values are given below for each of the conditions.						
T(25.4 mm)	1792 K	1790 K	1884 K	1636 K	1723 K	1871 K

[a]in post-flame environment [b]see discussion at beginning of Appendix E [c]see Table D.1, Table D.2, & Table E.3 for gas temperature profiles

Table E.8. HPFFB gasification data of Petcoke A

Collection Height[a] (inch)	Residence Time (ms)	wt% MR[b] (daf) as-received basis	Apparent Density[c] g/cm^3	d/d_o [d]
15 atm $T_{gas,max}$ =1848 K ~90 mol% CO_2[e]				
1	59	11.44	1.6998[i]	0.94
1	59	10.69	-	-
1	59	9.91	1.6953 [i]	0.94
3	142	34.01	1.7584 [i]	0.84
3	142	47.15	1.9248 [f,i]	0.76 [f]
3	142	44.76	1.7074 [f,i]	0.80 [f]
3	142	52.52	1.6758 [i]	0.77
5.5	265	59.96	1.7497 [i]	0.71
5.5	265	58.79	1.6565 [i]	0.73
10 atm $T_{gas,max}$ =1808 K ~90 mol% CO_2[e]				
1.5	73	24.86	1.6582 [i]	0.89
1.5	73	20.91	-	-
3	130	44.54	1.6266 [i]	0.81
3	130	32.90	1.6696 [i]	0.86
3	130	25.47	1.6829 [i]	0.89
3	130	24.61	1.6614 [i]	0.89
5.5	244	45.20	1.7444 [i]	0.79
5.5	244	47.99	1.7677 [f,i]	0.77 [f]
5.5	244	48.91	1.7781 [f,i]	0.77 [f]

*this table is continued on the next page

Table E.8 continued

Collection Height[a] (inch)	Residence Time (ms)	wt% MR[b] (daf) as-received basis	Apparent Density[c] g/cm^3	d/d_o [d]
15 atm $T_{gas,max}$=1891 K ~40 mol% CO_2[e]				
1	56	13.24	1.7362 [i]	0.92
3	137	17.12	1.7696 [i]	0.90
3	137	34.03	1.6597 [i]	0.86
3	137	20.56	1.7363 [i]	0.90
3	137	21.85	-	-
5.5	259	40.28	1.7612 [i]	0.81
5.5	259	40.64	1.6463 [i]	0.83
5.5	259	49.76	1.6980 [i]	0.78
5.5	259	46.41	1.6973 [i]	0.79
15 atm $T_{gas,max}$=1686 K[g] ~90 mol% CO_2[e]				
1	66	23.55	1.6214 [i]	0.91
1	66	25.18	1.6303 [i]	0.90
1	66	13.48	1.6283 [i]	0.94
3	160	45.57	1.6828 [i]	0.80
3	160	49.46	1.7036 [i]	0.78
3	160	38.32	1.6775 [i]	0.83
5.5	302	50.87	1.7021[h,i]	0.77
5.5	302	46.75	1.7021[h,i]	0.79
15 atm $T_{gas,max}$=1734 K[g] ~40 mol% CO_2[e]				
1	58	19.04	1.6544 [i]	0.92
1	58	10.58	1.7164 [i]	0.94
3	143	26.30	1.6774 [i]	0.89
3	143	35.10	1.7302 [i]	0.84
3	143	30.14	1.7427 [i]	0.86
5.5	266	40.74	1.5316	0.85
5.5	266	41.84	1.6272 [i]	0.83
10 atm $T_{gas,max}$=1909 K ~40 mol% CO_2[e]				
1	52	12.42	1.6121 [i]	0.95
1	52	18.13	1.6647 [i]	0.92
3	125	10.51	1.5746	0.96
3	125	21.58	1.7407 [i]	0.89
3	125	21.36	1.6977 [i]	0.90
3	125	18.05	1.5436	0.94
5.5	232	28.98	1.7444 [i]	0.86
5.5	232	29.88	1.7380 [i]	0.86

[a]above burner [b]particle mass release by Equation (4.4) since insufficient petcoke was fed during a single experiment for an accurate ash test to be performed on the collected char (see Section 4.8); any ash release to the gas phase that may have occurred would not have any appreciable effect on the mass release values due to the low ash content of petcoke [c]by Equation (4.7) [d]by Equation (7.1) [e]in post-flame environment [f]this value is most likely not accurate since the volume of sample used for bulk density measurements was below the cutoff at which accurate values are obtained (see Section 4.8 and Equation (7.1)) [g]see discussion at beginning of Appendix E [h]density measurement was performed by combining 2 char samples together due to the minimal amount of material in either sample [i]petcoke density increases when heated to high temperature (Ellis and Paul, 2000b; Ibrahim, 2005; Zhang and Wang, 2013); compare with the apparent density of raw Petcoke A given in Table 7.1

Table E.9. HPFFB gasification data of Petcoke B

Collection Height[a] (inch)	Residence Time (ms)	wt% MR[b] (daf) as-received basis	x_{ash}[c] (dry basis) in raw feedstock	Apparent Density[d] of raw feedstock (g/cm^3)	Apparent Density[d] of char (g/cm^3)
15 atm $T_{gas,max}$ =1848 K ~90 mol% CO_2[e]					
1	60	10.61	0.00309	1.2033	1.0829[f]
1	60	15.76	0.00309	1.2033	1.0780[f]
3	146	31.13	0.00289	1.2021	0.8874[f]
3	146	38.60	0.00289	1.2021	0.8432[f]
3	146	28.56	0.00309	1.2033	-
3	146	33.07	0.00309	1.2033	1.1143[f]
5.5	275	48.77	0.00248	1.2372	-
5.5	275	46.75	0.00248	1.2372	-
5.5	275	54.31	0.00289	1.2021	0.8646[f]
5.5	275	46.12	0.00309	1.2033	0.9558[f]
5.5	275	39.93	0.00248	1.2372	-
10 atm $T_{gas,max}$ =1808 K ~90 mol% CO_2[e]					
1	57	15.76	0.00309	1.2033	0.9536[f]
1	57	14.45	0.00309	1.2033	0.9530[f]
3	137	22.03	0.00289	1.2021	0.8320[f]
3	137	43.68[g]	0.00309	1.2033	0.9869[f]
3	137	24.58	0.00309	1.2033	1.0063[f]
3	137	20.34	0.00309	1.2033	1.0573[f]
5.5	258	47.70	0.00289	1.2021	0.7927[f]
5.5	258	44.79	0.00289	1.2021	0.7846[f]
5.5	258	42.23	0.00309	1.2033	0.9919[f]
5.5	258	52.08	0.00309	1.2033	0.9750[f]
15 atm $T_{gas,max}$ =1891 K ~40 mol% CO_2[e]					
1.25	60	17.59	0.00309	1.2033	1.0214[f]
1.25	60	13.96	0.00309	1.2033	1.1054[f]
3	124	29.65	0.00289	1.2021	0.8906[f]
3	124	24.63	0.00309	1.2033	1.0165[f]
5.5	231	35.24	0.00289	1.2021	0.8184[f]
5.5	231	53.41	0.00289	1.2021	0.8085[f]
5.5	231	44.24	0.00289	1.2021	0.8348[f]
5.5	231	48.15	0.00623	1.1786	0.8384[f]
5.5	231	41.57	0.00309	1.2033	-
5.5	231	35.84	0.00248	1.2372	0.9493[f]
15 atm $T_{gas,max}$ =1686 K[h] ~90 mol% CO_2[e]					
1	64	13.21	0.00309	1.2033	0.9964[f]
1	64	26.28[g]	0.00309	1.2033	1.0420[f]
3	153	44.98	0.00309	1.2033	1.0673[f]
3	153	44.51	0.00309	1.2033	1.0158[f]
3	153	48.88	0.00248	1.2372	0.9658[f]
5.5	289	52.93	0.00248	1.2372	1.0052[f]
5.5	289	54.53	0.00289	1.2021	0.8778[f]
5.5	289	50.24	0.00289	1.2021	0.9150[f]

*this table is continued on the next page

Table E.9 continued

Collection Height[a] (inch)	Residence Time (ms)	wt% MR[b] (daf) as-received basis	x_{ash}[c] (dry basis) in raw feedstock	Apparent Density[d] of raw feedstock (g/cm^3)	Apparent Density[d] of char (g/cm^3)
15 atm $T_{gas,max}$=1734 K[h] ~40 mol% CO_2[e]					
1.25	68	20.02	0.00309	1.2033	0.9836[f]
3	142	25.19	0.00309	1.2033	1.0235[f]
3	142	29.52	0.00309	1.2033	1.0035[f]
5.5	266	45.23	0.00289	1.2021	0.8048[f]
5.5	266	47.07	0.00289	1.2021	0.8454[f]
10 atm $T_{gas,max}$=1909 K ~40 mol% CO_2[e]					
1.25	57	11.54	0.00309	1.2033	0.9315[f]
1.25	57	10.62	0.00309	1.2033	0.9395[f]
3	119	22.38	0.00309	1.2033	0.9605[f]
3	119	13.73	0.00309	1.2033	0.9172[f]
3	119	10.22	0.00309	1.2033	0.9554[f]
3	119	11.29	0.00309	1.2033	1.0090[f]
5.5	219	39.61	0.00289	1.2021	0.7520[f, i]
5.5	219	36.36	0.00289	1.2021	0.7726[f]
5.5	219	28.60	0.00309	1.2033	0.9362[f]
5.5	219	24.55	0.00309	1.2033	0.9692[f]

[a]above burner [b]particle mass release by Equation (4.4) since insufficient petcoke was fed during a single experiment for an accurate ash test to be performed on the collected char (see Section 4.8); any ash release to the gas phase that may have occurred would not have any appreciable effect on the mass release values due to the low ash content of petcoke [c]fraction of ash in the virgin feedstock of a particular prepared batch; there were a total of 4 ground and sieved (45-75 μm) batches used in this work since insufficient prepared sample was made from a single batch to run all the desired experiments. However, all 4 batches were generated from the same bucket of petcoke sample [d]by Equation (4.7) [e]in post-flame environment [f]this density is not very meaningful due to the mixture of low-density and high-density char particles from Petcoke B (see Section 7.5) [g]not used in the modeling [h]see discussion at beginning of Appendix E [i]this value is most likely not accurate since the volume of sample used for bulk density measurements was below the cutoff at which accurate values are obtained (see Section 4.8)

Chapter 7 contained a comparison of the volatile yields of petroleum coke at low and high heating rates (see Section 7.4). Included below is pertinent data concerning volatile yields of petroleum coke at high heating rates.

Table E.10. Measured particle velocities (m/s) of petcoke in the FFB reactor at atmospheric pressure

Collection Height[a] (inch)	Petcoke A $T_{gas,max}$ [b] = 1751 K[c]	Petcoke A $T_{gas,max}$ [b] = 1929 K[d]	Petcoke B $T_{gas,max}$ [b] = 1433 K[c]
1	2.11 ±[e] 0.15	1.94 ± 0.03	1.13 ± 0.03
1.5	2.04 ± 0.07	-	-
2	-	2.08 ± 0.12	1.22 ± 0.04
3	2.35 ± 0.08	2.18 ± 0.14	1.36 ± 0.04
4	-	2.20 ± 0.09	-
5	-	2.34 ± 0.03	-
6	2.45 ± 0.05	2.41 ± 0.02	-
7	-	2.39 ± 0.11	-
8	2.34	2.52 ± 0.05	-

[a]above burner [b]maximum radiation-corrected measured centerline gas temperature [c]see Table C.1 & Table C.2 [d]see Table E.2 & Table E.3 [e]confidence intervals ($T_{stat} \cdot \sigma$ / *sqrt(#points)*) of 95% are shown

Table E.11. Petcoke Volatile Yields at High Heating-Rate Conditions in FFB Reactor at Atmospheric Pressure

Sample	Residence Time (ms)	$T_{gas,max}$[a] (K)	Collection Height[b] (inch)	wt% MR[c] (daf) as-received basis
Petcoke A	33	1751[e]	2	8.09
Petcoke A	33	1751[e]	2	9.30
Petcoke A	33	1751[e]	2	8.37
Petcoke A	60	1751[e]	4	10.03
Petcoke A	60	1751[e]	4	7.05
Petcoke A	98	1751[e]	8	9.27
Petcoke A	98	1751[e]	8	8.57
Petcoke A	23	1929[f]	1	8.72
Petcoke A	60	1929[f]	4	9.62
Petcoke A	102	1929[f]	8	9.63
Petcoke B	60[d]	1320[e]	2	11.79
Petcoke B	60[d]	1320[e]	2	9.56
Petcoke B	50[d]	1433[e]	2	10.68
Petcoke B	50[d]	1433[e]	2	10.35

[a]maximum radiation-corrected measured centerline gas temperature [b]above burner [c]particle mass release by Equation (4.4) [d]approximate [e]see Table C.1 & Table C.2 [f]see Table E.2 & Table E.3

Chapter 7 contained a comparison of char CO_2 gasification rates between Illinois #6 coal char and two petroleum coke samples (see Section 7.8). Included below is pertinent data concerning this comparison.

Table E.12. HPFFB gas condition[a] used to generate Illinois #6 coal char

Centerline $T_{gas,max}$[b]	1843 K
Total Pressure (atm)	15 atm
Gas flow (kg/s)	$5.009 \cdot 10^{-4}$
Φ (Equivalence Ratio)	0.92
Carrier[c] N_2 (SLPM)	0.215
Air (SLPM)	12.6
Oxidizer N_2[d] (SLPM)	6.2
Fuel N_2[e] (SLPM)	2.5
CO (SLPM)	4.34
H_2 (SLPM)	0.168
Quench[f] N_2 (SLPM)	52
Equilibrium Post-Flame Gas Compositions	
Ar mol%	0.5
O_2 mol%	1.57
CO_2 mol%	18.29
H_2O mol%	0.7
N_2 mol%	78.94

[a]used a collection height of 0.75 inches above the burner (~45 ms)
[b]maximum radiation-corrected measured centerline gas temperature
[c]N_2 in the feeding tube [d]N_2 in the oxidizer line [e]N_2 in the fuel line
[f]N_2 in the collection probe

Table E.13. Radiation-corrected centerline gas temperature profile for Illinois #6 coal char-generation HPFFB condition[a] at 15 atm

Height Above Burner (inches)	***Temperature (K)***
0.3	1843
0.4	1834
0.6	1820
0.8	1801
1	1768
1.2	1729
1.4	1682
1.6	1681
1.8	1635
2	1597
2.2	1558
2.4	1524
2.6	1489
2.8	1418
3	1341

[a]see Table E.12

From the Illinois #6 coal char-generation experiments at the 15 atm $T_{gas,max}$ = 1843 K HPFFB condition, the average collected char yield was 34.0 wt% daf (which assumes no ash release to the gas phase since Equation (4.4) was used for this calculation). The CPD model predicts a fully-pyrolyzed char yield of 42.4 wt% daf for this coal when fed at the HPFFB char-generation condition. However, the discrepancy between these values does not necessarily mean that the entire difference (i.e., 42.4 – 34.0 wt% daf) was due to char combustion in the char-generation experiments. Any ash release to the gas phase that occured in the char-generation experiments would lead to falsely-low calculated values for daf char yield. Unfortunately, an ash test was not performed on the collected coal char prior to sieving so the true daf char yield from the HPFFB char-generation experiments cannot be determined (since some of the size fractions of coal char were discarded after sieving).

Table E.14. Particle velocity (m/s) profile for Illinois #6 coal char (75-106 μm) at the 15 atm $T_{gas,max}$ = 1848 K HPFFB condition in ~90 mol% CO_2[a]

Height Above Burner (mm)	**Particle Velocity (m/s)**
0	0.024
2	0.279
3	0.311
6	0.420
9	0.501
12	0.577
15	0.640
18	0.683
21	0.708
24	0.717
25.4	0.717[b]
Particle velocities are obtained for distances of x > 25.4 mm above the burner using the equation $v_p = v_p(25.4\text{ mm})*T(x) / T(25.4\text{ mm})$ where T is the centerline gas temperature[c] at height x. T(25.4 mm) value is given below.	
T(25.4 mm)	1792 K

[a]in post-flame environment [b]a particle velocity of 0.716 ± 0.018 m/s was measured at 1" above burner [c]see Table D.1 & Table D.2 for gas temperature profile.
*Particle residence times at 1", 3", and 5.5" above the burner were 52, 130, and 247 ms, respectively

The gasification data of the re-injected 75-106 μm Illinois #6 coal char as well as the gasification data following *in-situ* pyrolysis of 45-75 μm Petcoke A and Petcoke B at the 15 atm $T_{gas,max}$ =1848 K ~90 mol% CO_2 HPFFB condition are summarized below for convenience (even though the petcoke data was listed in Table E.8 and Table E.9 above).

Table E.15. HPFFB gasification data of Petcoke A at the 15 atm $T_{gas,max}$ =1848 K ~90 mol% CO_2[a] HPFFB condition

Collection Height[b] (inch)	Residence Time (ms)	wt% MR[c] (daf) as-received basis	wt% MR (daf) char basis	Apparent Density[d] g/cm^3	d/d_o [e]
1	59	11.44	2.91	1.6998[i]	0.94
1	59	10.69	2.10	-	-
1	59	9.91	1.24	1.6953 [i]	0.94
3	142	34.01	27.66	1.7584 [i]	0.84
3	142	47.15	42.07	1.9248 [f,i]	0.76 [f]
3	142	44.76	39.44	1.7074 [f,i]	0.80 [f]
3	142	52.52	47.95	1.6758 [i]	0.77
5.5	265	59.96	56.11	1.7497 [i]	0.71
5.5	265	58.79	54.82	1.6565 [i]	0.73

[a]in post-flame environment [b]above burner [c]particle mass release by Equation (4.4) since insufficient petcoke was fed during a single experiment for an accurate ash test to be performed on the collected char (see Section 4.8); any ash released to the gas phase that may have occurred would not have any appreciable effect on the mass release values due to the low ash content of petcoke [d]by Equation (4.7) [e]by Equation (7.1)

Table E.16. HPFFB gasification data of Petcoke B at the 15 atm $T_{gas,max}$ =1848 K ~90 mol% CO_2[a] HPFFB condition

Collection Height[b] (inch)	Residence Time (ms)	wt% MR[c] (daf) as-received basis	wt% MR (daf) char basis	x_{ash}[d] (dry basis) in raw feedstock	Apparent Density[e] of raw feedstock (g/cm^3)	Apparent Density[e] of char (g/cm^3)
1	60	10.61	0.10	0.00309	1.2033	1.0829[f]
1	60	15.76	5.85	0.00309	1.2033	1.0780[f]
3	146	31.13	23.03	0.00289	1.2021	0.8874[f]
3	146	38.60	31.38	0.00289	1.2021	0.8432[f]
3	146	28.56	20.16	0.00309	1.2033	-
3	146	33.07	25.20	0.00309	1.2033	1.1143[f]
5.5	275	48.77	42.75	0.00248	1.2372	-
5.5	275	46.75	40.49	0.00248	1.2372	-
5.5	275	54.31	48.93	0.00289	1.2021	0.8646[f]
5.5	275	46.12	39.79	0.00309	1.2033	0.9558[f]
5.5	275	39.93	32.87	0.00248	1.2372	-

[a]in post-flame environment [b]above burner [c]particle mass release by Equation (4.4) since insufficient petcoke was fed during a single experiment for an accurate ash test to be performed on the collected char (see Section 4.8); any ash released to the gas phase that may have occurred would not have any appreciable effect on the mass release values due to the low ash content of petcoke [d]fraction of ash in the virgin feedstock of a particular prepared batch; there were a total of 4 ground and sieved (45-75 μm) batches used in this work since insufficient prepared sample was made from a single batch to run all the desired experiments. However, all 4 batches were generated from the same bucket of petcoke sample [e]by Equation (4.7) [f]this density is not very meaningful due to the mixture of low-density and high-density char particles from Petcoke B (see Section 7.5)

Table E.17. HPFFB gasification data of 75-106 μm Illinois #6 coal char at the 15 atm $T_{gas,max}$=1848 K ~90 mol% CO_2[a] HPFFB condition

Collection Height[b] (inch)	Residence Time (ms)	wt% MR (daf) as-received char basis[c]	wt% MR (daf) char basis[d]	x_{ash} (dry basis)	% of ash liberated[e] (weight basis)	Apparent Density[f] g/cm^3	d/d_o [g]
1	52	20.51	10.79	0.1692	-4.53	0.1595	0.940
1	52	13.62	3.06	0.1436	6.47	0.1648	0.946
3	130	34.65	26.67	0.1747	10.71	-	-
3	130	35.50	27.62	0.1962	-1.64	0.1594	0.887
5.5	247	41.62	34.48	0.1718	21.82	0.1664	0.837
5.5	247	40.58	33.31	0.1905	9.70	0.1567	0.866
5.5	247	42.82	35.83	0.1797	19.13	0.1526	0.858

[a]in post-flame environment [b]above burner [c]particle mass release when feeding the prepared char in re-injection gasification HPFFB experiments (see next footnote *d*) [d]when the prepared 75-106 μm coal char was fed in the FFB reactor at a pyrolysis condition ($T_{gas,max}$ = 1320 K condition (see Table C.1 & Table C.2) using a 2-inch collection height and ~60 ms), the char experienced a daf mass release of 10.89%. This mass release was likely either caused by incomplete pyrolysis of the char, or partial combustion of the char as it passed through the flame front (since the char would have little to no volatile matter to keep any O_2 away from the char surface). Certain biomass chars have been fed at the $T_{gas,max}$ = 1320 K FFB condition & they did not lose any significant mass, so perhaps the 10.89% daf mass release of the coal char at the $T_{gas,max}$ = 1320 K FFB condition was not caused by char combustion as it passed through the flame front. The mass release values reported in the 4th column on a char basis assume that the char was not fully pyrolyzed and were used in Figure 7.8. However, the results in Figure 7.9 are not affected by the unknown cause of the 10.89% daf mass release since only the particle mass release after the first collection point (i.e., 1 inch) was used in the char gasification modeling [e]by Equation (5.1) [f]by Equation (4.7) [g]by Equation (7.1)

Table E.18. Surface area data[a] of chars collected at the 15 atm $T_{gas,max}$=1848 K ~90 mol% CO_2[b] HPFFB condition

Collection Height[c] (inch)	Petcoke A Residence Time (ms)	Petcoke A N_2 SA[d] (m^2/g)	Petcoke B Residence Time (ms)	Petcoke B N_2 SA[d] (m^2/g)	Illinois #6 Residence Time (ms)	Illinois #6 N_2 SA[d] (m^2/g)
1	59	33.7	60	20.7	52	336
3	142	15.7	146	5.46	130	364
5.5	265	11.7	275	6.35	247	344
Collection Height[c] (inch)	**Petcoke A Residence Time (ms)**	**Petcoke A CO_2 SA[d] (m^2/g)**	**Petcoke B Residence Time (ms)**	**Petcoke B CO_2 SA[d] (m^2/g)**	**Illinois #6 Residence Time (ms)**	**Illinois #6 CO_2 SA[d] (m^2/g)**
1	59	172	60	156	52	392
3	142	134	146	60.4	130	376
5.5	265	119	275	61.0	247	397

[a]corresponds to Figure 7.10 [b]in post-flame environment [c]above burner [d]surface area

The collection efficiency of the HPFFB reactor was reported as 98.0%. This result came from 5 tests when feeding Petcoke A at a HPFFB gas condition where the CO_2 partial pressure and temperature were not sufficiently high to gasify the petcoke char in the allotted residence time. Information about the utilized HPFFB gas condition and mass release data are reported below.

Table E.19. Gas condition used forHPFFB Collection Efficiency Tests

Centerline $T_{gas,max}$[a]	1804 K
Total Pressure (atm)	5 atm
Gas flow (kg/s)	$2.232 \cdot 10^{-4}$
Φ (Equivalence Ratio)	1.17
Carrier[b] N_2 (SLPM)	0.075
Air (SLPM)	5.45
Oxidizer N_2[c] (SLPM)	3.08
CO (SLPM)	3.0
H_2 (SLPM)	0.17
Quench[d] N_2 (SLPM)	25
Equilibrium Post-Flame Gas Compositions	
CO_2 mol%	20.0
H_2O mol%	1.5
CO mol%	8.2
H_2 mol%	0.1
N_2 mol%	70.2

[a]maximum radiation-corrected measured centerline gas temperature [b]N_2 in the feeding tube [c]N_2 in the oxidizer line [d]N_2 in the collection probe

Table E.20. HPFFB collection efficiency data when feeding Petcoke A at the 5 atm $T_{gas,max}$ = 1804 K gas condition

Collection Height[a] (inch)	**Residence Time (ms)**	**Collection Efficiency**
3	161	98.3
5.5	310	98.5
5.5	310	99.2
9.5	626	82.6[b]
9.5	626	97.6
9.5	626	96.7

[a]above burner [b]this point was not included due to the very high collection efficiencies measured at 9.5" on the 2 following runs. If this point is considered, the collection efficiency would be lowered to 95.5%

Appendix F. Coal Gasification Data and Additional Information

Table F.1. HPFFB gas conditions[a] used to generate coal chars

Centerline $T_{gas,max}$[b]	1856 K	1850 K	1843 K
Total Pressure	10 atm	12.5 atm	15 atm
Gas flow (kg/s)	$3.908 \cdot 10^{-4}$	$4.459 \cdot 10^{-4}$	$5.009 \cdot 10^{-4}$
Φ (Equivalence Ratio)	0.86	0.89	0.92
Carrier[c] N_2 (SLPM)	0.15	0.185	0.215
Air (SLPM)	10.5	11.55	12.6
Oxidizer N_2[d] (SLPM)	4.86	5.53	6.2
Fuel N_2[e] (SLPM)	1.5	2	2.5
CO (SLPM)	3.14	3.74	4.34
H_2 (SLPM)	0.168	0.168	0.168
Quench[f] N_2 (SLPM)	40	46	52
Equilibrium Post-Flame Gas Compositions			
Ar mol%	0.5	0.5	0.5
O_2 mol%	2.88	2.15	1.57
CO_2 mol%	16.86	17.66	18.29
H_2O mol%	0.9	0.79	0.7
N_2 mol%	78.84	78.90	78.94

[a]used a collection height of 0.75 inches above the burner (38 to 44 ms) [b]maximum radiation-corrected measured centerline gas temperature [c]N_2 in the feeding tube [d]N_2 in the oxidizer line [e]N_2 in the fuel line [f]N_2 in the collection probe

Table F.2. Radiation-corrected centerline gas temperature profiles for coal char-generation HPFFB conditions[a]

Height Above Burner (inches)	***T_{gas} (K) @ 10 atm $T_{gas,max}$ =* 1856 K**	***T_{gas} (K) @ 12.5 atm $T_{gas,max}$ =* 1850 K**	***T_{gas} (K) @ 15 atm $T_{gas,max}$ =* 1843 K**
0.3	1856	1850	1843
0.4	1844	1833	1834
0.6	1815	1809	1820
0.8	1790	1788	1801
1	1770	1733	1768
1.2	1743	1720	1729
1.4	1722	1719	1682
1.6	1695	1693	1681
1.8	1641	1640	1635
2	1624	1607	1597

Table F.2 continued

Height Above Burner (inches)	T_{gas} *(K) @ 10 atm* $T_{gas,max}$ = **1856 K**	T_{gas} *(K) @ 12.5 atm* $T_{gas,max}$ = **1850 K**	T_{gas} *(K) @ 15 atm* $T_{gas,max}$ = **1843 K**
2.2	-	1519	1558
2.4	-	1500	1524
2.6	-	1452	1489
2.8	-	1427	1418
3	-	1358	1341

[a]see Table F.1 (a 0.75" collection height was used; 38-44 ms)

(a) (b)

Figure F.1. Illinois #6 coal char (75-106 μm) generated at 15 atm in the HPFFB reactor shown at higher magnification than shown in Figure 8.2a.

(a) (b)

Figure F.2. Utah Skyline coal char (45-75 μm) generated at 15 atm in the HPFFB reactor shown at higher magnification than shown in Figure 8.2b.

(a) (b)

Figure F.3. Pittsburgh #8 coal char (75-106 μm) generated at 15 atm in the HPFFB reactor shown at higher magnification than shown in Figure 8.2c.

Table F.3. Gas conditions for coal steam HPFFB experiments[a]

Centerline $T_{gas,max}$[b]	1814 K	1782 K	1611 K	1830 K	1850 K[f]
Total Pressure	10 atm	12.5 atm	15 atm	15 atm	10 atm
Gas flow (kg/s)	$3.496 \cdot 10^{-4}$	$4.039 \cdot 10^{-4}$	$4.737 \cdot 10^{-4}$	$4.683 \cdot 10^{-4}$	$3.660 \cdot 10^{-4}$
Φ (Equivalence Ratio)	1.06	1.07	1.10	1.07	1.16
Carrier[c] N_2 (SLPM)	0.15	0.185	0.215	0.215	0.15
Air (SLPM)	9.0	10.5	10.75	12.5	8.9
Oxidizer N_2[d] (SLPM)	6.0	6.75	10	7.5	5.0
CO (SLPM)	2.8	3.3	3.4	3.8	4.9
H_2 (SLPM)	1.341	1.613	1.886	2.095	0.17
Quench[e] N_2 (SLPM)	40	46	52	52	40
Equilibrium Post-Flame Gas Compositions					
Ar mol%	0.48	0.49	0.42	0.50	0.48
CO mol%	1.89	2.26	2.75	2.45	7.72
CO_2 mol%	14.21	14.13	11.43	13.74	20.78
H_2 mol%	0.24	0.29	0.51	0.35	0.08
H_2O mol%	7.47	7.71	7.35	8.56	0.91
N_2 mol%	75.71	75.11	77.54	74.39	70.03

[a]corresponds to Table 8.2 [b]maximum radiation-corrected measured centerline gas temperature [c]N_2 in the feeding tube [d]N_2 in the oxidizer line [e]N_2 in the collection probe [f]non-steam condition used to quantify particle mass release due to CO_2 in the coal steam HPFFB experiments (see Section 8.1.3)

Table F.4. Gas conditions for coal steam/CO_2 HPFFB experiments[a]

Centerline $T_{gas,max}$[b]	1879 K	1812 K
Total Pressure	15 atm	15 atm
Gas flow (kg/s)	$5.807 \cdot 10^{-4}$	$5.433 \cdot 10^{-4}$
Φ (Equivalence Ratio)	1.13	1.04
Carrier[c] N_2 (SLPM)	0.215	0.215
Air (SLPM)	15.75	-
O_2 (SLPM)	-	2.98
CO_2 (SLPM)	4.10	11.92
CO (SLPM)	7.4	6.0
H_2 (SLPM)	2.095	1.55
Quench[d] N_2 (SLPM)	52	52
Equilibrium Post-Flame Gas Compositions		
Ar mol%	0.56	0
CO mol%	10.51	7.88
CO_2 mol%	33.29	83.15
H_2 mol%	0.52	0.17
H_2O mol%	7.45	7.70
N_2 mol%	47.66	1.09

[a]corresponds to Table 8.3 [b]maximum radiation-corrected measured centerline gas temperature [c]N_2 in the feeding tube [d]N_2 in the collection probe

Table F.5. Radiation-corrected centerline gas temperature profiles of coal steam HPFFB conditions[a]

Height[b] (inch)	**10 atm steam condition $T_{gas,max}$ = 1814 K**	**12.5 atm steam condition $T_{gas,max}$ = 1782 K**	**15 atm steam condition $T_{gas,max}$ = 1611 K**	**15 atm steam condition $T_{gas,max}$ = 1830 K**
0.2	1792	1773	1563	1777
0.3	-	1782	-	-
0.4	1814	-	1571	-
0.6	1810	1781	1596	1824
0.8	1801	1779	1603	1830
1	1790	1771	1611	1814
1.2	1775	1761	1596	1810
1.4	1760	1756	1586	1790
1.6	1737	1745	-	1737
1.8	1723	1738	1556	1701
2	1698	1721	1529	1686
2.2	1662	1703	1513	1661
2.4	1632	-	-	-
2.6	1606	1670	1460	1562
2.8	1602	1601	1443	1530
3	1571	1594	1388	1467
3.2	-	1519	-	1453
4	-	-	-	1389
4.2	-	1431	-	-
4.4	1404	-	-	1324
4.6		1380	-	1317
4.8	1386	1371	-	1311
5.0	1328	1359	-	1294

[a]see Figure 8.4 and Table F.3 [b]above burner

Table F.6. Radiation-corrected centerline gas temperature profile of the 10 atm $T_{gas,max}$ = 1850 K HPFFB condition[a]

Height[b] (inch)	T_{gas} (K)
0.2	1817
0.3	1850
0.4	1847
0.6	1838
0.8	1829
1	1820
1.2	1810
1.4	1789
1.6	1755
1.8	1728
2.2	1697
2.4	1691
2.6	1653
2.8	1631
3	1606
3.2	1593
3.4	1571
3.6	1569
3.8	1564
4	1525
4.2	1512
4.4	1486
4.6	1479
4.8	1433
5	1431
5.2	1415
5.4	1377
5.6	1344
5.8	1313
6	1312

[a]non-steam condition used to quantify particle mass release due to CO_2 in the coal steam HPFFB experiments (see Section 8.1.3 & Table F.3) [b]above burner

Table F.7. Radiation-corrected centerline gas temperature profiles of coal steam/CO_2 HPFFB conditions[a]

Height Above Burner (inch)	15 atm steam/CO_2 condition $T_{gas,max}$ = 1879 K	Height Above Burner (inch)	15 atm steam/CO_2 condition $T_{gas,max}$ = 1812 K
0.2	1786	0.2	1778
0.3	1879	0.3	1799
0.6	1869	0.4	1812
0.8	1864	0.6	1790
1	1843	0.8	1777
1.2	1828	1	1772
1.4	1820	1.2	1730
1.6	1809	1.4	1706
2	1758	1.6	1702
2.2	1717	1.8	1660
2.6	1685	2	1624
2.8	1657	2.2	1607
3	1627	2.4	1585
3.4	1555	2.6	1570
3.8	1533	2.8	1528
4.4	1451	3	1463
5	1419	3.2	1455
		3.4	1426
		3.6	1406
		3.8	1397
		4	1386
		4.2	1376
		4.4	1367
		4.6	1326
		4.8	1300
		5	1270

[a]see Figure 8.5 & Table F.4

Table F.8. Measured particle velocities of coal chars at HPFFB steam conditions[a] in the HPFFB reactor at 1 inch above the burner surface

	ILL # 6 char (75-106 µm)	**Utah Skyline char (45-75 µm)**	**Pitt # 8 char (75-106 µm)**
Condition	**v_p (m/s)**	**v_p (m/s)**	**v_p (m/s)**
10 atm $T_{gas,max}$ = 1814 K	0.758 ± 0.033	0.828 ± 0.018	0.755[b]
12.5 atm $T_{gas,max}$ = 1782 K	0.641 ± 0.037	0.741 ± 0.019	0.639[b]
15 atm $T_{gas,max}$ = 1611 K	0.572 ± 0.031	0.634[b]	0.569[b]
15 atm $T_{gas,max}$ = 1830 K	0.663 ± 0.033	0.716 ± 0.041	0.660[b]

[a]see Table F.3 & Table F.5 [b]estimated

Table F.9. Measured coal and coal char particle velocities in HPFFB reactor

Steam/CO_2 Conditions[a]		
75-106 µm ILL #6 15 atm[c] char @ 15 atm $T_{gas,max}$ = 1879 K condition	1 inch[b]	0.665 ± 0.019 m/s
75-106 µm ILL #6 15 atm[c] char @ 15 atm $T_{gas,max}$ = 1812 K condition	1 inch[b]	0.704 ± 0.021 m/s
Coal Char Generation Conditions[e]		
45-75 µm raw coal @ 10 atm $T_{gas,max}$ = 1856 K	1 inch[b]	0.841[d] m/s
45-75 µm raw coal @ 12.5 atm $T_{gas,max}$ = 1850 K	1 inch[b]	0.749[d] m/s
45-75 µm raw coal @ 15 atm $T_{gas,max}$ = 1843 K	1 inch[b]	0.713[d] m/s
10 atm $T_{gas,max}$ = 1850 K ~20% CO_2[f]		
45-75 µm Utah Skyline 10 atm[c] char	0.77 inch[b]	0.567[d] m/s
75-106 µm ILL #6 10 atm[c] char	0.77 inch[b]	0.565[d] m/s
75-106 µm Pitt #8 10 atm[c] char	0.77 inch[b]	0.563[d] m/s

[a]see Table F.4 & Table F.7 [b]height at which particle velocity was measured or predicted [c]the fed char was generated at this pressure (see Table F.1 & Table F.2) [d]estimated particle velocity [e]see Table F.1 & Table F.2 [f]non-steam condition used to quantify particle mass release due to CO_2 in the coal steam HPFFB experiments (see Section 8.1.3, Table F.3, & Table F.6)

Table F.10. Coal char residence times in HPFFB reactor at various collection heights and conditions

10 atm $T_{gas,max}$ = 1814 K steam condition[a]			
Height Above Burner (inch)	*10 atm Utah Skyline char*[d] *45-75 μm*	*10 atm ILL #6 char*[d] *75-106 μm*	*10 atm Pitt #8 char*[d] *75-106 μm*
1 inch	42.0 ms	44.8 ms	45.1 ms
3 inch	107.2 ms	115.9 ms	116.4 ms
5 inch	182.7 ms	198.2 ms	199.3 ms
12.5 atm $T_{gas,max}$ = 1782 K steam condition[a]			
Height Above Burner (inch)	*12.5 atm Utah Skyline char*[d] *45-75 μm*	*12.5 atm ILL #6 char*[d] *75-106 μm*	*12.5 atm Pitt #8 char*[d] *75-106 μm*
1 inch	46.6 ms	51.6 ms	51.9 ms
3 inch	117.8 ms	134.1 ms	134.7 ms
5 inch	201.7 ms	231.0 ms	231.7 ms
15 atm $T_{gas,max}$ = 1611 K steam condition[a]			
Height Above Burner (inch)	*15 atm Utah Skyline char*[d] *45-75 μm*	*15 atm ILL #6 char*[d] *75-106 μm*	*15 atm Pitt #8 char*[d] *75-106 μm*
1 inch	54.6 ms	58.7 ms	59.0 ms
3 inch	139.3 ms	152.5 ms	153.3 ms
15 atm $T_{gas,max}$ = 1830 K steam condition[a]			
Height Above Burner (inch)	*15 atm Utah Skyline char*[d] *45-75 μm*	*15 atm ILL #6 char*[d] *75-106 μm*	*15 atm Pitt #8 char*[d] *75-106 μm*
1 inch	48.7 ms	51.4 ms	51.6 ms
3 inch	125.8 ms	134.6 ms	135.4 ms
5 inch	219.4 ms	235.7 ms	237.1 ms
15 atm $T_{gas,max}$ = 1879 K steam/CO_2 condition[b]			
Height Above Burner (inch)	*15 atm ILL #6 char*[d] *75-106 μm*		
1 inch	49.2 ms		
3 inch	129.6 ms		
5 inch	223.5 ms		
15 atm $T_{gas,max}$ = 1812 K steam/CO_2 condition[b]			
Height Above Burner (inch)	*15 atm ILL #6 char*[d] *75-106 μm*		
1 inch	51.1 ms		
3 inch	129.5 ms		
5 inch	222.2 ms		
10 atm $T_{gas,max}$ = 1850 K condition[c]			
Height Above Burner (inch)	*10 atm Utah Skyline char*[d] *45-75 μm*	*10 atm ILL #6 char*[d] *75-106 μm*	*10 atm Pitt #8 char*[d] *75-106 μm*
5.5 inch	285.0 ms	286.0 ms	286.9 ms

[a] see Table F.3 & Table F.5 [b]see Table F.4 & Table F.7 [c]non-steam condition used to quantify particle mass release due to CO_2 in the coal steam HPFFB experiments (see Section 8.1.3, Table F.3, & Table F.6) [d]see Table 8.4

Table F.11. Particle velocity (m/s) profiles for coal chars at different conditions in the HPFFB reactor

Height Above Burner	10 atm $T_{gas,max}$ = 1814 K steam condition[a]	10 atm $T_{gas,max}$ = 1814 K steam condition[a]	10 atm $T_{gas,max}$ = 1814 K steam condition[a]	12.5 atm $T_{gas,max}$ = 1782 K steam condition[a]	12.5 atm $T_{gas,max}$ = 1782 K steam condition[a]	12.5 atm $T_{gas,max}$ = 1782 K steam condition[a]
	Utah 10 atm char[b] 45-75 μm	*ILL #6 10atm char[b] 75-106 μm*	*Pitt #8 10atm char[b] 75-106 μm*	*Utah 12.5atm char[b] 45-75 μm*	*ILL #6 12.5atm char[b] 75-106 μm*	*Pitt #8 12.5atm char[b] 75-106 μm*
mm	**V_p (m/s)**	**V_p (m/s)**	**V_p (m/s)**	**V_p (m/s)**	**V_p (m/s)**	**V_p (m/s)**
0	0.022	0.023	0.026	0.019	0.024	0.027
2	0.392	0.381	0.378	0.354	0.343	0.343
3	0.429	0.406	0.408	0.392	0.366	0.366
6	0.530	0.501	0.490	0.472	0.438	0.428
9	0.617	0.576	0.572	0.551	0.491	0.494
12	0.684	0.639	0.635	0.616	0.542	0.542
15	0.747	0.689	0.685	0.662	0.581	0.577
18	0.789	0.723	0.722	0.702	0.610	0.608
21	0.816	0.749	0.744	0.727	0.631	0.628
24	0.828	0.758	0.755	0.739	0.640	0.638
25.4	0.828	0.758	0.755	0.741	0.641	0.639
Particle velocities are obtained for distances of x > 25.4 mm above the burner using the equation $v_p = v_p(25.4\text{ mm})*T(\text{x}) / T(25.4\text{ mm})$ where T is the centerline gas temperature[c] at height x. T(25.4 mm) values are given below for each of the conditions.						
T(25.4 mm)	1790 K	1790 K	1790 K	1771 K	1771 K	1771 K

[a]see Table F.3 [b]see Table 8.4 for char properties [c]see Table F.5 for gas temperature profile

Table F.12. Particle velocity (m/s) profiles for coal chars at different conditions in the HPFFB reactor

Height Above Burner	15 atm $T_{gas,max}$ = 1611 K steam condition[a]	15 atm $T_{gas,max}$ = 1611 K steam condition[a]	15 atm $T_{gas,max}$ = 1611 K steam condition[a]	15 atm $T_{gas,max}$ = 1830 K steam condition[a]	15 atm $T_{gas,max}$ = 1830 K steam condition[a]	15 atm $T_{gas,max}$ = 1830 K steam condition[a]
	Utah 15atm char[b] 45-75 μm	*ILL #6 15atm char[b] 75-106 μm*	*Pitt #8 15atm char[b] 75-106 μm*	*Utah 15atm char[b] 45-75 μm*	*ILL #6 15atm char[b] 75-106 μm*	*Pitt #8 15atm char[b] 75-106 μm*
mm	**V_p (m/s)**	**V_p (m/s)**	**V_p (m/s)**	**V_p (m/s)**	**V_p (m/s)**	**V_p (m/s)**
0	0.019	0.019	0.022	0.019	0.019	0.022
2	0.305	0.293	0.294	0.337	0.330	0.328
3	0.333	0.320	0.318	0.369	0.357	0.355
6	0.404	0.379	0.377	0.449	0.429	0.426
9	0.467	0.432	0.429	0.533	0.502	0.499
12	0.519	0.477	0.473	0.588	0.551	0.548
15	0.566	0.513	0.512	0.645	0.601	0.598
18	0.598	0.543	0.540	0.679	0.630	0.627

*this table is continued on the next page

Table F.12 continued

Height Above Burner	15 atm $T_{gas,max}$ = 1611 K steam condition[a]	15 atm $T_{gas,max}$ = 1611 K steam condition[a]	15 atm $T_{gas,max}$ = 1611 K steam condition[a]	15 atm $T_{gas,max}$ = 1830 K steam condition[a]	15 atm $T_{gas,max}$ = 1830 K steam condition[a]	15 atm $T_{gas,max}$ = 1830 K steam condition[a]
	Utah 15atm char[b] 45-75 μm	*ILL #6 15atm char[b] 75-106 μm*	*Pitt #8 15atm char[b] 75-106 μm*	*Utah 15atm char[b] 45-75 μm*	*ILL #6 15atm char[b] 75-106 μm*	*Pitt #8 15atm char[b] 75-106 μm*
21	0.621	0.561	0.558	0.706	0.654	0.651
24	0.633	0.571	0.568	0.716	0.663	0.660
25.4	0.634	0.572	0.569	0.716	0.663	0.660
Particle velocities are obtained for distances of x > 25.4 mm above the burner using the equation $v_p = v_p(25.4\text{ mm})*T(x) / T(25.4\text{ mm})$ where T is the centerline gas temperature[c] at height x. T(25.4 mm) values are given below for each of the conditions.						
T(25.4 mm)	1611 K	1611 K	1611 K	1814 K	1814 K	1814 K

[a]see Table F.3 [b]see Table 8.4 for char properties [c]see Table F.5 for gas temperature profile

Table F.13. Particle velocity (m/s) profiles for coal chars at different conditions in the HPFFB reactor

Height Above Burner	10 atm $T_{gas,max}$ = 1850 K condition[a]	10 atm $T_{gas,max}$ = 1850 K condition[a]	10 atm $T_{gas,max}$ = 1850 K condition[a]	15 atm $T_{gas,max}$ = 1812 K steam/CO_2 condition[b]	15 atm $T_{gas,max}$ = 1879 K steam/CO_2 condition[b]
	Utah 10atm char[c] 45-75 μm	*ILL #6 10atm char[c] 75-106 μm*	*Pitt #8 10atm char[c] 75-106 μm*	*ILL #6 15atm char[c] 75-106 μm*	*ILL #6 15atm char[c] 75-106 μm*
mm	**V_p (m/s)**	**V_p (m/s)**	**V_p (m/s)**	**V_p (m/s)**	**V_p (m/s)**
0	0.022	0.023	0.026	0.022	0.022
2	0.358	0.357	0.354	0.304	0.354
3	0.382	0.381	0.387	0.338	0.388
6	0.449	0.447	0.443	0.436	0.459
9	0.494	0.493	0.488	0.518	0.521
12	0.532	0.530	0.523	0.583	0.569
15	0.554	0.553	0.551	0.637	0.613
18	0.566	0.564	0.562	0.673	0.642
19.5	0.567	0.565	0.563	0.688	0.652
21	-	-	-	0.697	0.659
24	-	-	-	0.705	0.666
25.4	-	-	-	0.704	0.665
Particle velocities are obtained for distances greater than the last given value by scaling by temperature using the equation $v_p = v_p(\textit{last measured value})*T(x) / T(\textit{last measured value})$ where T is the centerline gas temperature[d] at height x. T(*last measured value*) is given below for each of the conditions.					
T(*last measured value*)	1820 K	1820 K	1820 K	1772 K	1843 K

[a]see Table F.3 [b]see Table F.4 [c]see Table 8.4 for char properties [d]see Table F.6 & Table F.7 for gas temperature profiles

Table F.14. Illinois #6 (75-106 μm) coal char gasification data at HPFFB steam conditions[a]

Collection Height[b] (inch)	Residence Time (ms)	wt% MR (daf) #1[c]	wt% MR (daf) #2[d]	% of ash liberated[e] (weight basis)	x_{ash} in feedstock char (dry basis)	x_{ash} in collected char (dry basis)	Apparent Density[f] g/cm^3	d/d_o [g]
10 atm $T_{gas,max}$ = 1814 K steam condition[n]								
2; FFB[h]	*~60*	*14.49*	*13.25*	*1.44*	*0.1218*	*0.1379*	-	-
2; FFB[h]	*~60*	*19.50*	*10.03*	*10.52*	*0.1196[m]*	*0.1312*	-	-
1	45	16.15	11.89	4.83	0.1218	0.1360	-	-
3	116	26.04	22.30	4.82	0.1218	0.1515	-	-
3	116	20.89	24.99[k]	-5.48	0.1196[m]	0.1534	0.1419	0.94
5	198	22.15	22.35	-0.26	0.1218	0.1516	-	-
5	198	26.61	25.14	1.96	0.1196[m]	0.1536	-	-
10 atm $T_{gas,max}$ = 1850 K non-steam condition[j n]								
2; FFB[h]	*~60*	*14.49*	*13.25*	*1.44*	*0.1218*	*0.1379*	-	-
2; FFB[h]	*~60*	*19.50*	*10.03*	*10.52*	*0.1196[m]*	*0.1312*	-	-
6	317	18.97[o]	13.70	6.11	0.1218	0.1385	-	-
5	256	23.53	22.67	1.12	0.1196[m]	0.1494	0.1514	0.91
5	256	29.92	23.08	8.89	0.1196[m]	0.1501	0.1532	0.88
12.5 atm $T_{gas,max}$ = 1782 K steam condition[n]								
2; FFB[h i]	*~60*	*16.79 [i]*	*-2.34 [i]*	*18.69 [i]*	*0.2248 [i]*	*0.2208 [i]*	-	-
1	52	22.61	23.89[k]	-1.68	0.1564	0.1959	0.1666	0.89
3	134	57.88	32.07	38.00	0.1564	0.2144	0.1736	0.72
3	134	41.41	18.55[l]	28.06	0.1564	0.1854	0.1392	0.86
5	231	41.49	6.53[l]	37.40	0.1564	0.1655	0.1685	0.80
15 atm $T_{gas,max}$ = 1611 K steam condition[n]								
2; FFB[h]	*~60*	*6.06*	*-32.59*	*29.15*	*0.1389*	*0.1085*	-	-
2; FFB[h]	*~60*	*10.93*	*-15.69*	*23.01*	*0.1389*	*0.1224*	-	-
1	59	9.29	-5.73[l]	14.21	0.1389	0.1324	-	-
3	153	27.50	1.92[l]	26.08	0.1389	0.1413	-	-
15 atm $T_{gas,max}$ = 1830 K steam condition[n]								
2; FFB[h]	*~60*	*6.06*	*-32.59*	*29.15*	*0.1389*	*0.1085*	-	-
2; FFB[h]	*~60*	*10.93*	*-15.69*	*23.01*	*0.1389*	*0.1224*	-	-
1	51	25.18	13.70[l]	13.31	0.1389	0.1575	-	-
3	135	57.40	28.53[l]	40.40	0.1389	0.1842	-	-
5	236	66.29	48.00[l]	35.17	0.1389	0.2368	-	-

[a]see Table 8.2 & Table F.3 [b]above burner [c]wt% particle mass release (daf, char basis) by Equation (4.6) [d]wt% mass release (daf, char basis) by Equation (4.5), but is low if ash leaves the char (see Section 4.7) [e]by Equation (5.1) [f]by Equation (4.7) [g]by Equation (7.1) [h]chars were fed in the FFB reactor at atmospheric pressure at the $T_{gas,max}$ = 1320 K pyrolysis condition (see Table C.1 & Table C.2) to gain insight about ash release upon re-injection and volatile content of the chars [i]the 45-75 μm fraction was fed in the FFB reactor instead of the 75-106 μm fraction due to insufficient quanities of the latter feedstock; see footnote *h* [j]non-steam condition used to quantify particle mass release due to CO_2 in the coal steam HPFFB experiments (see Section 8.1.3) [k]MR #2 exceeded MR #1 so this value was not used in the modeling (see Section 4.7) [l]these values were not used in the modeling since ash liberation likely caused these values to be low (see Section 4.7; also see footnote *h* & the % of ash that was liberated in the *FFB* experiments in the 5th column) [m]the 1st batch of 75-106 μm ILL #6 char that was generated at 10 atm in the HPFFB was depleted so a 2nd batch was generated to run replicate experiments [n]see Table 8.4 for the properties of the coal chars used at these conditions; the char generation pressure and the subsequent gasification pressure were the same (i.e., a char generated at 10 atm in the HPFFB reactor only acted as feedstock material for HPFFB gasification experiments at 10 atm) [o]this value was not used in the modeling since the mass balance of this run was slightly disturbed

Table F.15. Illinois #6 (75-106 μm) coal char gasification data at HPFFB steam/CO_2 conditions[a]

Collection Height[b] (inch)	Residence Time (ms)	wt% MR (daf) #1[c]	wt% MR (daf) #2[d]	% of ash liberated[e] (weight basis)	x_{ash} in feedstock char (dry basis)	x_{ash} in collected char (dry basis)	Apparent Density[f] g/cm^3	d/d_o [g]
15 atm $T_{gas,max}$ = 1812 K steam/CO_2 condition[i]								
2; FFB[h]	*~60*	*11.47*	*6.89*	*4.92*	*0.1285*	*0.1367*	*0.1403*	*0.97*
1	51	22.9	21.83	1.32	0.1285	0.1587	0.1284	0.96
3	130	59.1	52.84	13.37	0.1285	0.2382	0.1119	0.84
3	130	55.4	49.87	11.07	0.1285	0.2273	0.1217	0.84
5	224	75.6[j]	67.33[j]	25.35	0.1285	0.3109	0.1082	0.74
5	224	81.9[k]	65.43[k]	47.53	0.1285	0.2990	0.1006	0.69
15 atm $T_{gas,max}$ = 1879 K steam/CO_2 condition[i]								
2; FFB[h]	*~60*	*11.47*	*6.89*	*4.92*	*0.1285*	*0.1367*	*0.1403*	*0.97*
1	49	21.95	18.99	3.66	0.1285	0.1540	0.1333	0.95
3	130	63.96	65.08[l]	-3.21	0.1285	0.2969	0.1123	0.83
5	224	81.41	79.27	10.32	0.1285	0.4156	0.1155	0.70
5	224	70.72	73.37[l]	-9.95	0.1285	0.3564	0.1190	0.78

[a]see Table 8.3 & Table F.4 [b]above burner [c]wt% particle mass release (daf, char basis) by Equation (4.6) [d]wt% mass release (daf, char basis) by Equation (4.5), but is low if ash leaves the char (see Section 4.7) although wt% MR values by ash-tracer were thought to yield accurate values in these experiments [e]by Equation (5.1) [f]by Equation (4.7) [g]by Equation (7.1) [h]chars were fed in the FFB reactor at atmospheric pressure at the $T_{gas,max}$ = 1320 K pyrolysis condition (see Table C.1 & Table C.2) to gain insight about ash release upon re-injection and volatile content of the chars [i]see Table 8.4 for the properties of the coal char used at these conditions; the char generation pressure and the subsequent gasification pressure were the same (i.e., the char was generated at 15 atm in the HPFFB reactor since the subsequent HPFFB char gasification experiments were conducted at 15 atm) [j]wt% MR value used in the modeling was obtained by weighting MR #1 by 20% and MR #2 by 80% since the relatively high ash liberation values (see 5th column) likely indicate inefficiencies of the collection system rather than ash being released to the gas phase [k]wt% MR value used in the modeling was obtained by weighting MR #1 by 10% and MR #2 by 90% since the relatively high ash liberation values (see 5th column) likely indicate collection inefficienies of the collection probe rather than ash being released to the gas phase [l]MR #2 exceeded MR #1 so this value was not used in the modeling (see Section 4.7)

Table F.16. Utah Skyline (45-75 μm) coal char gasification data at HPFFB steam conditions[a]

Collection Height[b] (inch)	Residence Time (ms)	wt% MR (daf) #1[c]	wt% MR (daf) #2[d]	% of ash liberated[e] (weight basis)	x_{ash} in feedstock char (dry basis)	x_{ash} in collected char (dry basis)	Apparent Density[f] g/cm^3	d/d_o [g]
10 atm $T_{gas,max}$ = 1814 K steam condition [p]								
2; FFB[h]	*~60*	*16.77*	*-24.36*	*33.07*	*0.2780*	*0.2364*	-	-
2; FFB[h i]	*~60*	*13.29* [i]	*5.87* [i]	*7.88* [i]	*0.2362* [i]	*0.2473* [i]	*0.2649* [i]	*0.85* [i]
1	42	17.66	-6.74[m]	22.86	0.2780	0.2650	0.2635	0.91
3	107	43.13	18.73[m]	30.02	0.2780	0.3214	0.2373	0.85
3	107	38.63	3.49[m]	36.41	0.2780	0.2851	0.2130	0.89
5	183	49.28	20.46[m]	36.23	0.2780	0.3261	0.2284	0.83
5	183	41.91[o]	38.88[o]	4.95	0.2362[o]	0.3360	0.2595	0.78
10 atm $T_{gas,max}$ = 1850 K non-steam condition [p q]								
2; FFB[h]	*~60*	*16.77*	*-24.36*	*33.07*	*0.2780*	*0.2364*	-	-
2; FFB[h i]	*~60*	*13.29* [i]	*5.87* [i]	*7.88* [i]	*0.2362* [i]	*0.2473* [i]	*0.2649* [i]	*0.85* [i]
5[k]	256	54.17[k]	-36.23[k]	66.36[k]	0.2780	0.2203[k]	0.2108[k]	0.79[k]
5.5	285	29.72	10.02[m]	21.89	0.2780	0.2996	0.2656	0.87
5.5	285	26.87 [o]	22.26[m o]	5.93	0.2362 [o]	0.2846	0.2375	0.85
5.5	285	29.12 [o]	-0.99[m o]	29.81	0.2362 [o]	0.2344	0.2251	0.84
12.5 atm $T_{gas,max}$ = 1782 K steam condition [p]								
2; FFB[h]	*~60*	*17.01*	*21.79*	*-6.11*	*0.2484*	*0.2970*	*0.2792*	*0.86*
2; FFB[h j]	*~60*	*14.72* [j]	*-11.54* [j]	*23.54* [j]	*0.1335* [j]	*0.1213* [j]	-	-
1	47	18.94	-14.91[m]	29.46	0.2484	0.2234	0.2187	0.90
3	118	35.15	5.26[m]	31.54	0.2484	0.2586	0.2124	0.86
5	202	72.42	61.09[m]	29.12	0.2484	0.4593	0.2526	0.68
5[l]	202	61.95[l n]	23.34[l n]	50.36[l n]	0.2484	0.3013[l n]	0.2351[l]	0.71[l]
15 atm $T_{gas,max}$ = 1611 K steam condition [p]								
2; FFB[h]	*~60*	*13.29*	*5.87*	*7.88*	*0.2362*	*0.2473*	*0.2649*	*0.85*
1	55	19.87	21.17	-1.65	0.2362	0.2818	0.2597	0.85
3	139	26.82	-29.33[m]	43.42	0.2362	0.1930	0.2056	0.86
15 atm $T_{gas,max}$ = 1830 K steam condition [p]								
2; FFB[h]	*~60*	*13.29*	*5.87*	*7.88*	*0.2362*	*0.2473*	*0.2649*	*0.85*
1	49	21.59	13.42[m]	9.44	0.2362	0.2632	0.2528	0.84
3	126	49.10	17.40[m]	38.38	0.2362	0.2724	0.1889	0.81
5	219	84.01	75.42	34.95	0.2362	0.5572	0.2311	0.61
5	219	71.98	1.63[m]	71.52	0.2362	0.2392	0.2087	0.63

[a]see Table 8.2 & Table F.3 [b]above burner [c]wt% particle mass release (daf, char basis) by Equation (4.6) [d]wt% mass release (daf, char basis) by Equation (4.5), but is low if ash leaves the char (see Section 4.7) [e]by Equation (5.1) [f]by Equation (4.7) [g]by Equation (7.1) [h]chars were fed in the FFB reactor at atmospheric pressure at the $T_{gas,max}$ = 1320 K pyrolysis condition (see Table C.1 & Table C.2) to gain insight about ash release upon re-injection and volatile content of the chars [i]the FFB data when feeding 15 atm Utah Skyline char (45-75 μm) is shown here since 15 atm char was used as feedstock material at 10 atm HPFFB conditions to obtain replicate data after the 10 atm Utah Skyline char (45-75 μm) was depleted [j]fed 12.5 atm Utah Skyline char (75-106 μm) at the FFB condition after the 12.5 atm (45-75 μm) feedstock Utah Skyline char was depleted to get additional data about ash release and volatile content of the 12.5 atm Utah Skyline chars [k]data from this experiment was not included in the modeling since MR #1 appears high when compared with the replicate data at this condition; the high ash release (5th column) of this run likely indicate inefficiencies of the collection system rather than ash being released to the gas phase [l]some ash spilled after an ash test on the char collected from this condition, but it is at least known that MR #1 from this experiment is greater than 61.95 wt% daf [m]these values were not used in the modeling since ash liberation likely caused these values to be low (see Section 4.7) [n]these values are not accurate; see footnote *l* [o]15 atm char was fed at 10 atm HPFFB conditions to obtain replicate data after the 10 atm Utah Skyline char (45-75 μm) was depleted [p]see Table 8.4 for additional properties of the coal chars used at these conditions [q]non-steam condition used to quantify particle mass release due to CO_2 in the coal steam HPFFB experiments (see Section 8.1.3)

Table F.17. Pittsburgh #8 (75-106 μm) coal char gasification data at HPFFB steam conditions[a]

Collection Height[b] (inch)	Residence Time (ms)	wt% MR (daf) #1[c]	wt% MR (daf) #2[d]	% of ash liberated[e] (weight basis)	x_{ash} in feedstock char (dry basis)	x_{ash} in collected char (dry basis)	Apparent Density[f] g/cm^3	d/d_o [g]
10 atm $T_{gas,max}$ = 1814 K steam condition [r]								
2; FFB[h]	*~60*	*15.27[m]*	*-12.48*	*24.67*	*0.1055*	*0.0949*	*0.1638*	*0.94*
1	45	8.26[n]	15.46[l]	-8.52	0.1055	0.1224	0.1833	0.94
3	116	17.88[o]	22.10[l]	-5.42	0.1055	0.1314	0.1668	0.93
3	116	15.80[o]	-11.49[l]	24.47	0.1055	0.0956	0.1635	0.94
3	116	26.21	-41.47[l]	47.84	0.1055	0.0769	0.1464	0.92
5	199	38.37	39.00	-1.04	0.1055	0.1620	0.1475	0.90
5	199	41.74	3.48[l]	39.64	0.1055	0.1088	0.1355	0.89
10 atm $T_{gas,max}$ = 1850 K non-steam condition [r s]								
2; FFB[h]	*~60*	*15.27*	*-12.48*	*24.67*	*0.1055*	*0.0949*	*0.1638*	*0.94*
2; FFB[h i]	*~60*	*12.41[i]*	*13.76[i]*	*-1.56[i]*	*0.1002[i]*	*0.1143[i]*	-	-
5.5	287	10.25	21.13[l]	-13.79	0.1055	0.1300	0.1728	0.95
5.5	287	12.57	8.79[l]	4.15	0.1055	0.1145	0.1727	0.94
5.5	287	20.61[j o]	-1.13[j l]	21.50	0.1002[j]	0.0991	0.1707	0.91
5.5	287	11.44[j]	-22.15[j l]	27.50	0.1002[j]	0.0835	0.1626	0.95
12.5 atm $T_{gas,max}$ = 1782 K steam condition [r]								
2; FFB[h]	*~60*	*21.64[p]*	*19.44*	*2.72[p]*	*0.0936*	*0.1136*	*0.1665*	*0.94*
2; FFB[h]	*~60*	*17.14*	*-23.46*	*32.88*	*0.0936*	*0.0772*	-	-
1	52	7.46[q]	20.34[l]	-16.16	0.0936	0.1147	0.1720	0.98
3	135	38.81	20.78[l]	22.76	0.0936	0.1153	0.1430	0.91
5	232	61.24	23.86[l]	49.10	0.0936	0.1194	0.1227	0.82
5	232	60.02	25.96[l]	45.99	0.0936	0.1224	0.1278	0.82
15 atm $T_{gas,max}$ = 1611 K steam condition [r]								
2; FFB[h]	*~60*	*12.41*	*13.76*	*-1.56*	*0.1002*	*0.1143*	-	-
1	59	8.00	-6.81[l]	13.86	0.1002	0.0944	0.1665	0.95
3	153	18.53	3.86[l]	15.25	0.1002	0.1038	0.1746	0.90
15 atm $T_{gas,max}$ = 1830 K steam condition [r]								
2; FFB[h]	*~60*	*12.41*	*13.76*	*-1.56*	*0.1002*	*0.1143*	-	-
1	52	10.22	2.39[l]	8.02	0.1002	0.1024	0.1687	0.94
3	135	44.81	23.61[l]	27.76	0.1002	0.1272	0.1452	0.85
5	237	67.21	54.04[l]	28.64	0.1002	0.1950	0.1362[k]	0.75[k]
5	237	70.17	57.59[l]	29.66	0.1002	0.2079	0.1169[k]	0.76[k]

[a]see Table 8.2 & Table F.3 [b]above burner [c]wt% particle mass release (daf, char basis) by Equation (4.6) [d]wt% mass release (daf, char basis) by Equation (4.5), but is low if ash leaves the char (see Section 4.7) [e]by Equation (5.1) [f]by Equation (4.7) [g]by Equation (7.1) [h]chars were fed in the FFB reactor at atmospheric pressure at the $T_{gas,max}$ = 1320 K pyrolysis condition (see Table C.1 & Table C.2) to gain insight about ash release upon re-injection and volatile content of the chars [i]the FFB data when feeding 15 atm Pitt #8 char (75-106 μm) is shown here since 15 atm char was used as feedstock material at 10 atm HPFFB conditions to obtain replicate data after the 10 atm Pitt #8 char (75-106 μm) was depleted [j]15 atm (75-106 μm) Pitt #8 char was fed at 10 atm HPFFB conditions to obtain replicate data after the 10 atm Pitt #8 char (75-106 μm) was depleted [k]scale was being jittery during 'tap density' test so these values may be incorrect [l]these values were not used in the modeling since ash liberation likely caused these values to be low (see Section 4.7) [m]there was some residual material in the feeder after this run so this value would be less than 15.27 wt% [n]the moisture content of this collected char had to be estimated, so this value could be higher if the moisture content was under-estimated; a MR value of 11.59% daf was used in the modeling for this collection height [o]this data was not included in the modeling [p]the mass balance of this experiment could be a little off [q]was not used in the modeling; the MR value used in the modeling for this collection height was taken as 17.14% daf [r]see Table 8.4 for additional properties of the coal chars used at these conditions [s]non-steam condition used to quantify particle mass release due to CO_2 in the coal steam HPFFB experiments (see Section 8.1.3)

Table F.18. Illinois #6 (75-106 μm) coal char mass release summary at HPFFB steam conditions[a]

Collection Height[b] (inch)	Residence Time (ms)	Average Measured wt% MR[c] (daf)	Predicted wt% MR[c] (daf) by CO_2	Predicted wt% MR[c] (daf) by H_2O
10 atm $T_{gas,max}$ = 1814 K steam condition[d]				
1	45	14.02	14.02	14.02
3	116	22.53	17.53	19.02
5	198	24.06	18.72	19.36
12.5 atm $T_{gas,max}$ = 1782 K steam condition[d]				
1	52	22.61	22.61	22.61
3	134	36.74	27.54	31.81
5	231	41.49	28.97	35.12
15 atm $T_{gas,max}$ = 1611 K steam condition[d]				
1	59	8.89	8.89	8.89
3	153	27.50	11.65	24.74
15 atm $T_{gas,max}$ = 1830 K steam condition[d]				
1	51	25.18	25.18	25.18
3	135	57.40	30.89	51.69
5	236	66.29	32.06	59.41

[a]see Table 8.2 & Table F.3 [b]above burner [c]particle mass release on a daf char basis [d]see Table 8.4 for additional properties of the coal chars used at these conditions

Table F.19. Utah Skyline (45-75μm) coal char mass release summary at HPFFB steam conditions[a]

Collection Height[b] (inch)	Residence Time (ms)	Average Measured wt% MR[c] (daf)	Predicted wt% MR[c] (daf) by CO_2	Predicted wt% MR[c] (daf) by H_2O
10 atm $T_{gas,max}$ = 1814 K steam condition[d]				
1	42	17.66	17.66	17.66
3	107	40.88	22.11	36.43
5	183	46.32	23.47	40.51
12.5 atm $T_{gas,max}$ = 1782 K steam condition[d]				
1	47	18.94	18.94	18.94
3	118	35.15	26.09	28.00
5	202	72.42	27.93	63.43
15 atm $T_{gas,max}$ = 1611 K steam condition[d]				
1	55	20.52	20.52	20.52
3	139	26.82	23.69	23.65
15 atm $T_{gas,max}$ = 1830 K steam condition[d]				
1	49	21.59	21.59	21.59
3	126	49.10	28.49	42.20
5	219	75.85	29.71	67.73

[a]see Table 8.2 & Table F.3 [b]above burner [c]particle mass release on a daf char basis [d]see Table 8.4 for additional properties of the coal chars used at these conditions

Table F.20. Pittsburgh #8 (75-106 μm) coal char mass release summary at HPFFB steam conditions[a]

Collection Height[b] (inch)	Residence Time (ms)	Average Measured wt% MR[c] (daf)	Predicted wt% MR[c] (daf) by CO_2	Predicted wt% MR[c] (daf) by H_2O
10 atm $T_{gas,max}$ = 1814 K steam condition[d]				
1	45	11.59	11.59	11.59
3	116	26.21	14.11	23.69
5	199	40.05	14.92	36.72
12.5 atm $T_{gas,max}$ = 1782 K steam condition[d]				
1	52	17.14	17.14	17.14
3	135	38.81	20.77	35.18
5	232	60.63	21.76	56.01
15 atm $T_{gas,max}$ = 1611 K steam condition[d]				
1	59	10.22	10.22	10.22
3	153	18.53	12.10	16.64
15 atm $T_{gas,max}$ = 1830 K steam condition[d]				
1	52	10.22	10.22	10.22
3	135	44.81	14.43	40.60
5	237	68.69	15.20	63.71

[a]see Table 8.2 & Table F.3 [b]above burner [c]particle mass release on a daf char basis [d]see Table 8.4 for additional properties of the coal chars used at these conditions

Table F.21. Illinois #6 (75-106 μm) coal char mass release summary at HPFFB steam/CO_2 conditions[a]

Collection Height[b] (inch)	Residence Time (ms)	Average Measured wt% MR[c] (daf)	Total Predicted wt% MR[c] (daf)	Predicted wt% MR[c] (daf) by CO_2	Predicted wt% MR[c] (daf) by H_2O
15 atm $T_{gas,max}$ = 1812 K steam/CO_2 condition[d]					
1	51	22.35	22.35	22.35	22.35
3	130	54.32	58.15	44.34	36.15
5	222	67.12	66.80	49.80	39.35
15 atm $T_{gas,max}$ = 1879 K steam/CO_2 condition[d]					
1	49	20.47	20.47	20.47	20.47
3	130	48.56	59.22	37.10	42.58
5	224	75.53	70.72	42.02	49.17

[a]see Table 8.3 & Table F.4 [b]above burner [c]particle mass release on a daf char basis [d]see Table 8.4 for the properties of the coal char used at these conditions

The coal char gasification experiments utilized the 45-75 μm sieved fractions of Utah Skyline char, and the 75-106 μm sieved fractions of Illinois #6 and Pittsburgh #8 chars. Only the 45-75 μm Utah Skyline chars were measured for its CO_2 and N_2 surface area. It was overlooked (excluding the ILL #6 10 atm 75-106 μm sample) to measure the surface area of the 75-106 μm fractions of the Illinois #6 and Pittsburgh #8 chars before these chars were depleted. However, CO_2 and N_2 surface areas were measured for the other sieved fractions of these 2 coals that were not used in char gasification experiments in order to provide some insight.

N_2 surface areas were calculated using the Brunauer-Emmett-Teller (BET) equation. Carbon dioxide adsorption was performed at 298 K (using an ice water bath), and provides insight regarding the micropores of the particle. CO_2 surface areas below were calculated using density functional theory (DFT), and represent the total area in the pores $\geq \sim 4.8$ angstroms.

Table F.22. Surface area of Illinois #6 coal chars[a]

Pyrolysis Pressure[b] (atm)	Sieved Fraction	wt% ash (dry)	Apparent Density[c] (g/cm^3)	CO_2 SA[d] (m^2/g)	N_2 SA[d] (m^2/g)
10	45-75 μm	18.4	0.193	286	133
12.5	45-75 μm	21.2	0.222	280	113
15	45-75 μm	27.1	0.322	215	92.2
10[e]	**75-106 μm**	**12.1[e]**	**0.145[e]**	**326[e]**	**98.6[e]**
12.5	**75-106 μm**	**15.6**	**0.145**	**-**	**-**
15	**75-106 μm**	**13.9**	**0.144**	**-**	**-**
15[f]	**75-106 μm**	**12.9[f]**	**0.144[f]**	**-**	**-**
10	106-150 μm	13.7	0.121	362	214
12.5	106-150 μm	13.0	0.122	360	226
15	106-150 μm	12.5	0.128	332	212

[a]bold values in the table show the chars that were fed during char gasification HPFFB experiments [b]total pressure that the char was generated at in the HPFFB reactor (see Table F.1 & Table F.2) [c]by Equation (4.7) [d]surface area [e]one of two batches of char generated (see Table F.14, foonote *m*) [f]char fed at the steam/CO_2 conditions (see Table 8.3, Table F.4, & Table F.15)

Table F.23. Surface area of Utah Skyline coal chars[a]

Pyrolysis Pressure[b] (atm)	Sieved Fraction	wt% ash (dry)	Apparent Density[c] (g/cm^3)	CO_2 SA[d] (m^2/g)	N_2 SA[d] (m^2/g)
10	**45-75 μm**	**27.8**	**0.242**	**275**	**89.3**
12.5	**45-75 μm**	**24.8**	**0.203**	**264**	**90.1**
15	**45-75 μm**	**23.6**	**0.186**	**257**	**105**
10	75-106 μm	11.9	0.172	334	155
12.5	75-106 μm	17.4	0.195	312	142
15	75-106 μm	6.1	0.140	319	180
10	106-150 μm	19.0	0.178	318	170
12.5	106-150 μm	18.5	0.175	318	192
15	106-150 μm	19.1	0.190	309	198

[a]bold values in the table show the chars that were fed during char gasification HPFFB experiments [b]total pressure that the char was generated at in the HPFFB reactor (see Table F.1 & Table F.2) [c]by Equation (4.7) [d]surface area

Table F.24. Surface area of Pittsburgh #8 coal chars[a]

Pyrolysis Pressure[b] (atm)	Sieved Fraction	wt% ash (dry)	Apparent Density[c] (g/cm^3)	CO_2 SA[d] (m^2/g)	N_2 SA[d] (m^2/g)
10	45-75 μm	55.2	0.470	191	76.2
12.5	45-75 μm	50.2	0.443	137	52.2
15	45-75 μm	48.3	0.412	158	49.0
10	**75-106 μm**	**10.6**	**0.161**	**-**	**-**
12.5	**75-106 μm**	**9.4**	**0.170**	**-**	**-**
15	**75-106 μm**	**10.0**	**0.154**	**-**	**-**
10	106-150 μm	7.7	0.118	354	174
12.5	106-150 μm	9.0	0.120	266	112
15	106-150 μm	8.4	0.127	303	144
10	> 150 μm	15.4	-	-	-
12.5	> 150 μm	14.7	-	-	-
15	> 150 μm	10.4	-	-	-

[a]bold values in the table show the chars that were fed during char gasification HPFFB experiments [b]total pressure that the char was generated at in the HPFFB reactor (see Table F.1 & Table F.2) [c]by Equation (4.7) [d]surface area

Appendix G. HPFFB Reactor Additional Information

Included in this appendix are instructions on how to start-up and shut down the HPFFB reactor. Also included below are instructions on how to shut down the HPFFB reactor in emergency situations. Lastly, this appendix contains schematics of the controllers, plumbing, and layout of gas tanks for the HPFFB reactor.

HPFFB Start-Up: Also consult the dissertation appendix of Randy Shurtz (2011).

1) Make sure everything has been cleaned and is ready for an experiment by doing the following:
   - blow out collection system with compressed air
   - use wire to poke out feed line
   - blow compressed air through the oxidizer line of the burner after removing the quick-release fitting. After blowing compressed air, replace the fitting to its initial position.
   - blow compressed air through the feed line for ~20 seconds from feeder side (no feed plunger should be in place yet)
   - wipe off o-rings that reside in the filters flanges of the collection system
   - weigh and load new filters
   - wipe off o-rings on top and bottom caps of the vessel (since dirty o-rings can cause pressure leaks)
   - center the short quartz tube (see Figure 4.2) with your fingers through the bottom hole in the bottom vessel cap. Then insert the burner into the vessel using the crank system until the etched double line (located ~3.25" below the top of the burner) on the burner is lined up with the entrance into the vessel. Verify that the burner entered the small quartz tube by using a measuring tape through the top hole in the vessel cap. Measure the distance from the top cap to the top of the small quartz tube. It is possible that the burner did not enter the quartz tube, and instead raised the quartz tube (see Figure G.1 below). You want the small quartz tube to be resting on the bottom cap of the vessel, not on the burner. If the burner pushed the quartz tube up, it will be smashed later on when you lower the collection probe.

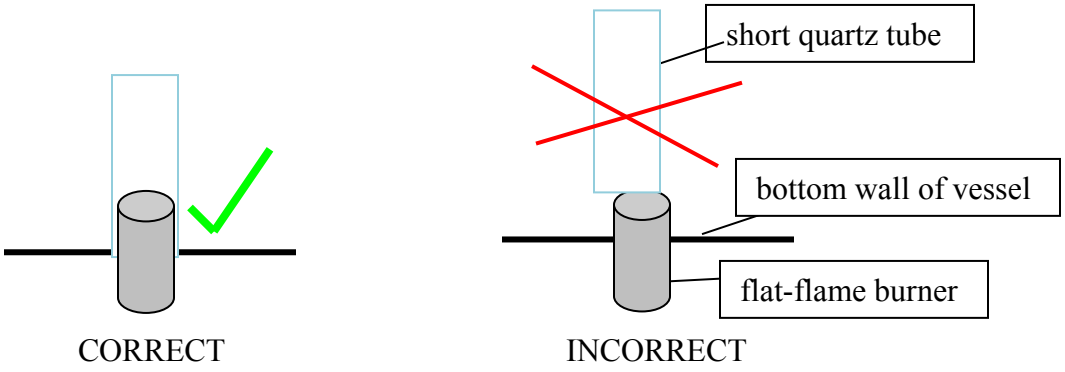

Figure G.1. Positioning of HPFFB burner into small quartz tube.

- weigh the feedstock material on a tared weigh paper before you load it into the feed plunger (see Figure 4.5)
- Make sure there is new parafilm around ferrules on the feed plunger. Parafilm on the ferrules helps prevent gas leaks.
- weigh the loaded plunger (with a cork inserted into the end of the feed plunger to prevent feedstock from falling out).

- check for continuity in glow plug with multimeter by unplugging the cord from the variac and testing for continuity across the electrical prongs. If no continuity, take off top cap of vessel and replace the glow plug.
- attach char trap to collection system
- make sure burner and collection probe are inserted into the vessel
- power on small CO personal monitor and put it near the reactor
- verify the correct gas cylinders are hooked up and that unused gas lines have closed valves on the gas rack

2) Make sure valves on collection system are appropriately open or closed (Filters 2 & 3 should normally be open while Filter 1 is normally closed)
   - secure in place the wheel of the crank burner system using a zip tie
3) Close manual vent valve, Filter #2 valve, and Filter #3 valve on board (in preparation for a pressure test)
4) Turn on cooling water (which supplies water to the probe, bottom cap brass insert, and filter flanges).
5) Conduct pressure test by doing the following:
   - turn on both power strips to the right of the mass flow controller boxes
   - The point of a pressure test is to verify the reactor has no leaks before CO is introduced to the vessel. The pressure tests involves using N_2 to pressurize the reactor to about 10-15 psi above the pressure you will be operating and applying a soapy water solution to fittings and leak-prone areas (feeder, top and bottom cap, filter flanges, char trap, etc.). Bubbles indicate a leak. A second way to tell that a leak exists is if vessel pressure drops while outlet streams to the vessel are closed and also while there is not any gas flowing to the vessel.

- make sure all flows are set to zero on the mass flow controllers and also that the manual quench N_2 and secondary N_2 valves (which delivers N_2 near the bottom of the vessel cap) are closed
  - set carrier N_2 (channel L2, i.e. Left mass flow controller box, channel 2) to ~ 90% on mass flow controller box
  - pressurize vessel with quench N_2 (channel TL5 which indicates Top Left box, channel 5) at a flow that displays 0.8 to 1.0 on the mass flow meter display (which equates to 40-50 SLPM)
- if reactor doesn't pressurize or pressurizes slowly, turn off quench N_2 flow rate and find out why.
  - Stop pressurizing vessel with quench N_2 and snoop (i.e. apply soapy water solution & see if bubbles appear which indicates a leak) the reactor at increments of ~70 psi in pressure. It is safer to find the leak at a lower pressure, which is why the pressure test is conducted in increments.
    - i.e., stop & snoop at 70 psi, 135 psi, 225 psi for a 15 atm run
    - i.e., stop & snoop at 70 psi, 135 psi , and 185 psi for a 12.5 atm run
    - i.e., stop & snoop at 70 psi and 150 psi for a 10 atm run

  Places to snoop: everywhere that has been opened since the last pressure test
  - feed plunger connections
  - feed line where it enters burner
  - filter flanges
  - char trap
  - top cap where probe enters vessel
  - any new plumbing that has been performed
  - around the top or bottom caps of the vessel if these have been opened

6) Blow off feed plunger and char trap with compressed air to remove residual soapy water solution after a pressure test is complete.
7) Decrease vessel pressure to 5 atm (~60 psi on the digital box) for ignition
   - snoop the filter valves on the board after they are partially open. If they leak, repair them since you do not want CO-rich gas leaking into the room during an experiment.
8) Start flowing quench N_2 (channel TL5) at a value of 0.5 on mass flow meter display (which equates to 25 SLPM)
9) Dial in the ignition settings and double-check them, but start with H_2 (channel R3) at 0%.
   - wait until step 13 to turn H_2 on (since ignition is all about proper amount of H_2 and introducing it too soon can delay ignition time)

Ignition Settings

In the recent past, the HPFFB reactor has been used with 3 different gas tank setups (see Figure G.2 to Figure G.6 towards the end of Appendix G), which allow the post-flame environment to consist of approximately 20, 40, and 90 mol% CO_2. Each gas setup requires a different set of ignition settings, which are listed below.

Ex) L2 means Left mass flow controller box, channel 2. R4 means Right box, channel 4.

Tank Setup 1 (~20% CO_2 run) uses air & N_2 in the oxidizer line. For ignition at 5 atm, use:

	Quench N_2	Carrier N_2	N_2	Air	CO	H_2 *don't add yet
Mass Flow Controller Channel	TL5	L2	L3	L1	R4	R3
Mas Flow Controller Setpoint	0.5	90%	5%	14.2%	22.8%	5.5%
Actual Flow (SLPM)	25	0.45	0.5	7.1	4.56	0.23

Tank Setup 2 (~40% CO_2 run) uses air & CO_2 in the oxidizer line. For ignition at 5 atm, use:

	Quench N_2	Carrier N_2	CO_2	Air	CO	H_2 *don't add yet
Mass Flow Controller Channel	TL5	L2	L3	L1	R4	R3
Mas Flow Controller Setpoint	0.5	90%	0%	13.6%	19.5%	5.5%
Actual Flow (SLPM)	25	0.45	0	6.8	3.9	0.23

Tank Setup 3 (~90% CO_2 run) uses CO_2 & O_2 in the oxidizer line. For ignition at 5 atm, use:

	Quench N_2	Carrier N_2	O_2	CO_2	CO	H_2 *don't add yet
Mass Flow Controller Channel	TL5	L2	L3	L1	R4	R3
Mas Flow Controller Setpoint	0.5	90%	16.8%	11.4%	22.8%	5.5%
Actual Flow (SLPM)	25	0.45	1.67	4.25	4.56	0.23

---

10) Open all other tanks except fuel tanks (any of these possible combinations: air & N_2 for ~20% CO_2 conditions, air & CO_2 for ~40% CO_2 conditions, CO_2 & O_2 for ~90% CO_2 conditions).
11) Once vessel pressure is near 5 atm, turn on the glow plug using the variac (turn off light in room for better glow plug visibility through the top port of the vessel). Set the variac voltage to ~2% of 120 volts to power the glow plug. The glow plug should glow orange.
12) Turn on ventilation fan for safety during ignition. Also turn on small fan in corner of room.
13) Open H_2 and CO tanks.

- Verify vessel pressure is still at 5 atm for ignition before you flip the CO/N_2 valve (above CO gas cabinet) which introduces CO to the vessel. Before this point, N_2 is flowing through the CO plumbing to the burner.
- Dial in mass flow controller H_2 setting (see 'Ignition Settings' above) 10-20 seconds after the CO/N_2 valve is flipped and CO has started flowing to the burner.

Ignition is all about the right amount of H_2.

- Too much H_2 makes the flame drop very quickly, but will not light the burner.
- Insufficient H_2 will cause the flame to hang out in the top of the vessel, but never drop (if you are using a B-type thermocouple wire as the glow plug, but not if you use 22 gauge nichrome 60 wire as the glow plug) (see Section 4.2.1).

If a flame is hanging out in the top of the vessel but does not drop, turn off fuels on the mass flow controllers (H_2 and CO) [i.e., channels R3 & R4], turn off glow plug, and wait for the flame to extinguish.

Wait ~2 minutes, turn on glow plug, and then dial the ignition H_2 setting and then slowly dial the CO to its setting slowly (over ~1 min).

If flame drops super fast but does not ignite the burner, then this means that there is too much H_2. Turn off fuels (H_2 and CO) on the mass flow controllers, wait ~5 minutes, and then dial in the H_2 and CO settings and try again.

- Be patient. Typical ignition time can range from 5 to 20 minutes.

---

14) After the burner is lit, dial in stable settings appropriate for the 5-atm vessel pressure.
15) Turn on cooling or secondary N_2 to bottom cap (channel TL1) near 15 (on mass flow meter display)

- open up manual Filter 2 or 3 valves enough on the board so that this additional flow will not pressurize the vessel (if the pressure regulator is not functioning). Having the cooling N_2 on while you lower the probe helps prevent thermal shock to the big quartz tube. If the big quartz tube breaks from thermal shock, a new one costs about $50 and it will requires about 2-3 hours to take off the bottom cap to replace it).

16) Turn on the light in the room.
17) Snoop the top cap where probe enters the vessel.
18) Lower the collection probe slowly to the desired height (so the probe sits about 1/8" above the small quartz tube (see Figure 4.2). Make sure chain is attached to the collection probe crank wheel so that there is no risk of the collection probe moving or shooting out during a pressurized run).
19) Turn off cooling or secondary N_2 to bottom cap (channel TL1) since thermal shock is no longer a concern since the water-cooled collection probe is in place.
20) Raise/lower burner to desired height using the burner crank system. *With the burner inserted into the vessel where the etched double line on the burner (located ~3.25" below the top of the burner) is flush with the visible entrance into the bottom brass insert of the vessel, the burner has 1" movement up or down to change residence times of a run. Secure the bottom crank wheel using zip ties after you are done adjusting it.
21) Double check all gas flow rates on the mass flow controllers.
22) Pressurize from 5 atm to the experimental operating pressure. As the vessel is pressurizing, slowly increase the gas settings to the burner.
23) Stabilize pressure by adjusting Filters 2 and 3 on the board (if the pressure regulator is not working, although the pressure regulator will keep the pressure at its setpoint if it is functioning

properly). The flow through Filter 2 should be greater than the flow through Filter 3 for the collection system to operate as designed.
24) Turn off ventilation fan (unless you desire its use during the run).
25) Check to make sure the burner is at correct height (since pressure can push it out slightly from where you set it in Step 20). Adjust if necessary and secure the crank wheel of the burner system using a zip tie.
26) Check which gas cylinder pressures are low to know which tanks you will closely track during the experiment. The lab has the necessary plumbing to switch tanks mid-run for most of the gases.
27) Put a piece of masking tape on the stepper motor screw (to track its movement and to be detect if it stops moving unexpectedly during the run).
28) Plug in the vibrator(s) (i.e., off-centered cpu fans) on the feed line
29) Attach and turn on the pneumatic vibrator on the feed plunger while watching the particle bed with a flashlight.
- take care to ensure that particles do not drop off the feed plunger yet

30) Keep carrier N_2 (channel L2) at ~90% until you start feeding.
- use stepper motor to start particles feeding
- If feeding is going well, drop carrier N_2 to the actual flow rate

31) Set a timer when the particles begin to feed to calculate the particle feed rate later
32) The reactor is now operating at steady state.
- adjust vessel pressure by opening/closing valves for Filters 1 & 2 on the board (if pressure regulator is not working, although the pressure regulator will keep the pressure at its setpoint if it is functioning properly).
- tap the feed line gently with a combination wrench where the feedl line enters the bottom of the burner to ensure good feeding. Verify that the compression fitting stays tight while you are providing vibration.
- keep an eye on tank pressures (change them at ~500 psi).
- make sure feeding tower does not lean. If it does, stop the run. The tower will not lean if there is good alignment between the plunger & the stepper motor screw.
- make sure stepper motor screw is progressing forward
- pressurized feeder vessel indicates a clogged feed line. If the feed line is clogged, shut down the reactor, clean it out, and repeat the run.

HPFFB Shut-Down: Also consult the dissertation appendix of Randy Shurtz (2011).

1) Turn off pneumatic vibrator on feed plunger.
2) Let all the particles in the feed line continue to feed until no more particles pass through the reactor.
3) Turn off CPU vibrators on feed line.
4) Record the time that the particles were feeding in the lab book to calculate a particle feed rate.
5) Close the valves on top of the CO and H_2 tanks.

Dial your oxygen source to 0% on the mass flow controller to extinguish the flame.
- If you're at 20% or 40% CO_2 gas conditions, turn off air (channel L1)
- If you're at 90% CO_2 gas conditions, turn off oxygen (channel L3)

6) When the flame goes out, relieve pressure in the vessel by:

- opening the manual vent and the valves for Filters 2 and 3 (all are located on the board).

7) When vessel pressure is < 10 psi, flip the N_2/CO valve above the CO cabinet to let N_2 purge the CO line.
8) Turn up the mass flow controller on the CO line (channel R4) to about 60%.
   - N_2 is now flowing through the CO line
9) Turn off quench N_2 (channel TL5) since it does not purge the vessel.
10) Turn on the secondary or cooling N_2 that enters through the bottom cap (channel TL1) above 20 (on the display) to purge the vessel.
11) Raise the probe until it's ~10 inches above the burner so there is more room between burner and collection probe. ***Caution***: do not raise the probe out of the pressurized vessel!
12) Set a timer since it takes about 13 minutes for the vessel to purge (for CO concentrations to drop to zero inside the vessel).
13) Turn off all other gas tanks besides the N_2 tanks.
14) If you are using fuel N_2 (channel TL4) for coal pyrolysis, dial the set point to 0%.
15) Dial your oxygen source to about 20% on the mass flow controller to drain that line.
   - If you're at 20% or 40% CO_2 gas conditions, this is air (channel L1)
   -If you're at 90% CO2 gas conditions, this is oxygen (channel L3)
16) When your oxygen source has depleted, turn up H_2 to about 25% on the mass flow controller to drain that line.
   (We do not want H_2 and an oxidizer gas flowing at the same time since a combustible mixture of gases will be present in the vessel.)
17) After 13 minutes or purging, turn off the N_2 tanks.
18) When the N_2 tanks have drained and vessel pressure is at 1 atm, dial remaining channels on the mass flow controllers to 0%.
19) Make sure the needle valves are completely closed for quench N_2 (flow rate displayed on channel TL5) and secondary or cooling N_2 (displayed on channel TL1).
20) Turn off power to mass flow controllers.
21) Turn on ventilation fan.
22) Put the personal CO monitor on the top of the vessel and raise the probe out of the vessel to make sure the CO levels are safe. If there is still residual CO, then re-insert the collection probe into the vessel, purge longer with N_2, and repeat this step.

- Weigh char in char trap.
- Weigh plunger
- Weigh material in plunger
- Weigh filters
- Blow through collection system with the char trap on to try to collect additional char stuck in the collection system for a better mass balance. This is done by the following: while both Filter 2 and 3 flanges are undone, place your hand over the bottom of the collection probe while blowing compressed air through Filter 3 while Filter 2 valve is closed (with char trap secured to catch any char that may still be present in the collection system). Then blow compressed air through Filter 2 while Filter 3 valve is closed, with your hand still over the bottom of the collection probe.

Shut Down of HPFFB Reactor in Emergency Scenarios

1) Gas Leak in Room

- Turn on ventilation fan.
- Open up exhaust valves (#2 and #3) and manual valve on board
- Turn off mass flow controller switch and leave the room until CO levels drop.

2) Power Outage

The danger is venting the CO-rich pressurized vessel safely.

- If the vented fuel cabinets have lost power, follow 'Path A Instructions."
- If the vented fuel cabinets have power, follow 'Path B Instructions."

Path A Instructions:

- Put the metal covers over the outside ports so that CO will not enter the room in later steps.
- Turn off ventilation fan switch (if it was on when the power went out).
- Attach CO-monitor to your person.
- Turn off power to the mass flow controllers.
- Turn the valve near the table that will re-direct the exhaust gases out the window.
- Open up exhaust valves (#2 and #3) and manual valve on board slowly until vessel is vented.
- Close gas tanks.

Path B Instructions:

- Attach CO-monitor to your person
- Turn off power to the mass flow controllers.
- Open up exhaust valves (#2 and #3) and manual valve on board slowly until vessel is vented.
- Close gas tanks.

3) Fire Alarm

- Close fuel tanks (CO & H_2).
- Flip the CO/N_2 valve above the CO ventilated cabinet to allow N_2 to flow.
- Open up exhaust valves (#2 and #3) and manual valve on board to de-pressurize.
- Close all other tanks besides N_2 if there is time.

The following HPFFB plumbing diagrams are helpful in determining which gas tanks are used for a particular set of HPFFB conditions. Mitch Withers is acknowledged for creating the following diagrams. The dissertation appendix of Randy Shurtz (2011) has other helpful diagrams and documentation concerning the HPFFB reactor.

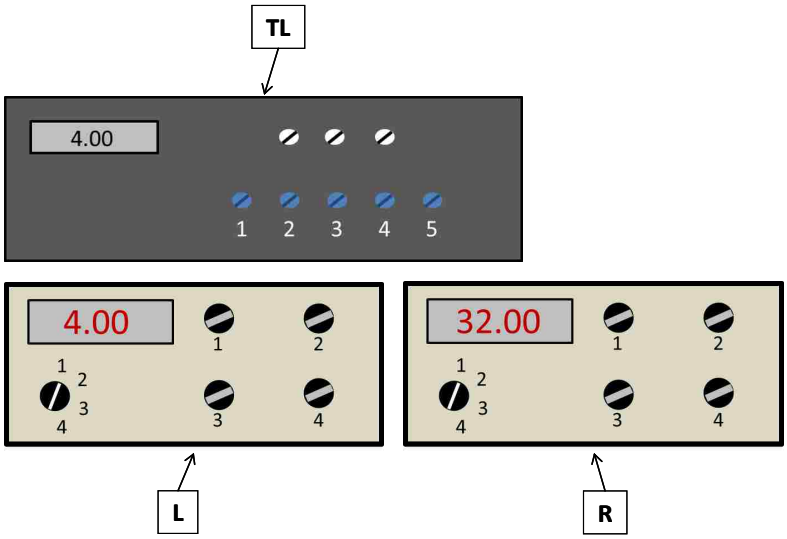

Figure G.2. HPFFB controller setup used to control mass flow controllers and display readouts from mass flow meters. TL = Top Left box; L = Left box; R = Right box

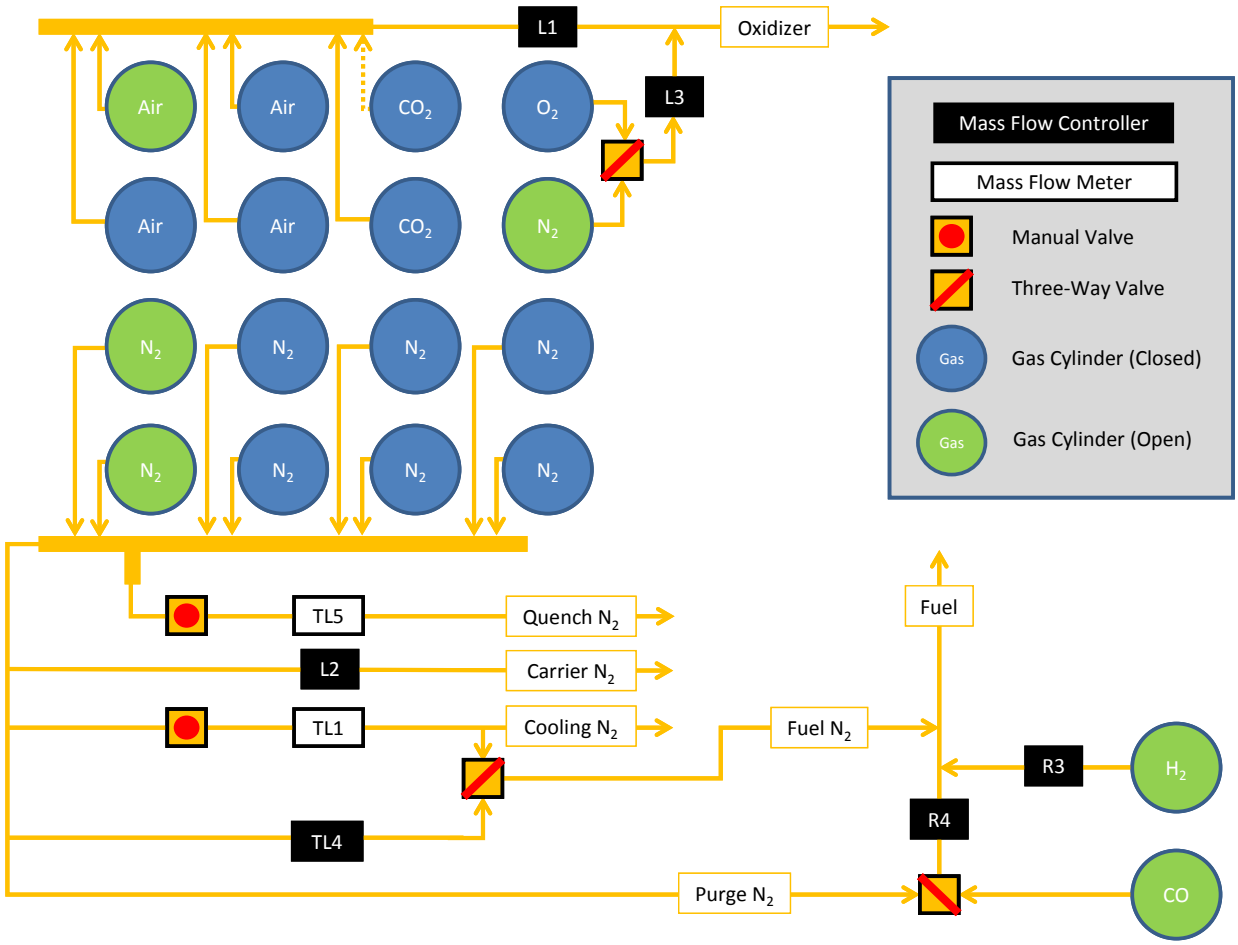

Figure G.3. HPFFB gas supply system to the HPFFB reactor.

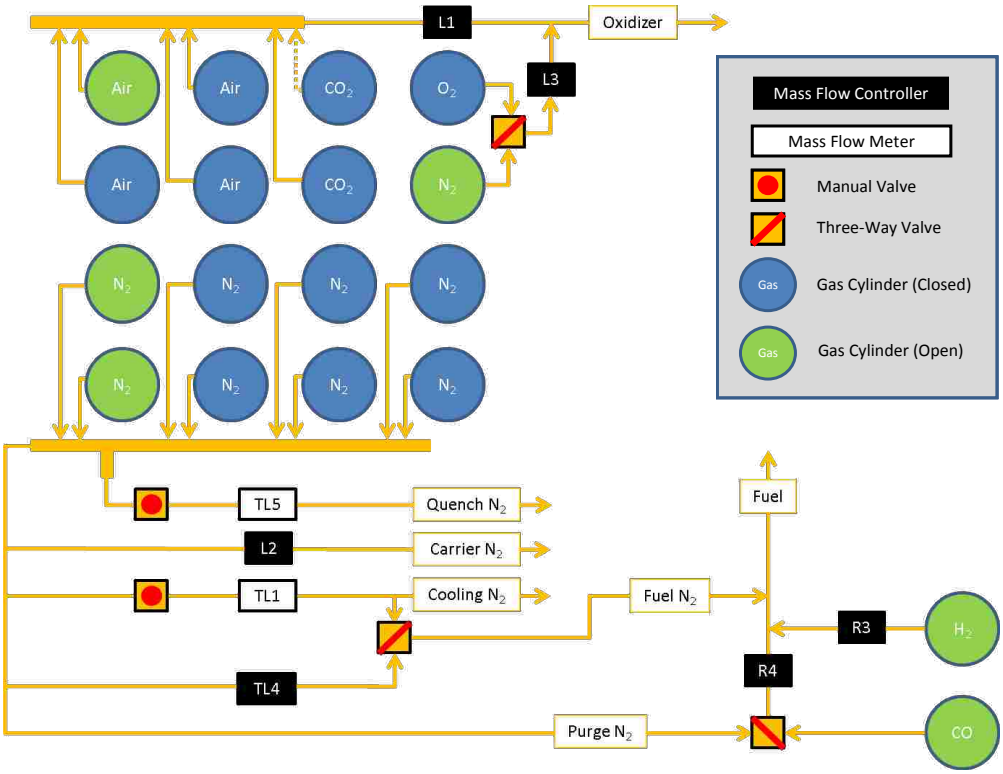

Figure G.4. HPFFB gas setup at conditions where the post-flame environment consists of approximately 20 mol% CO_2.

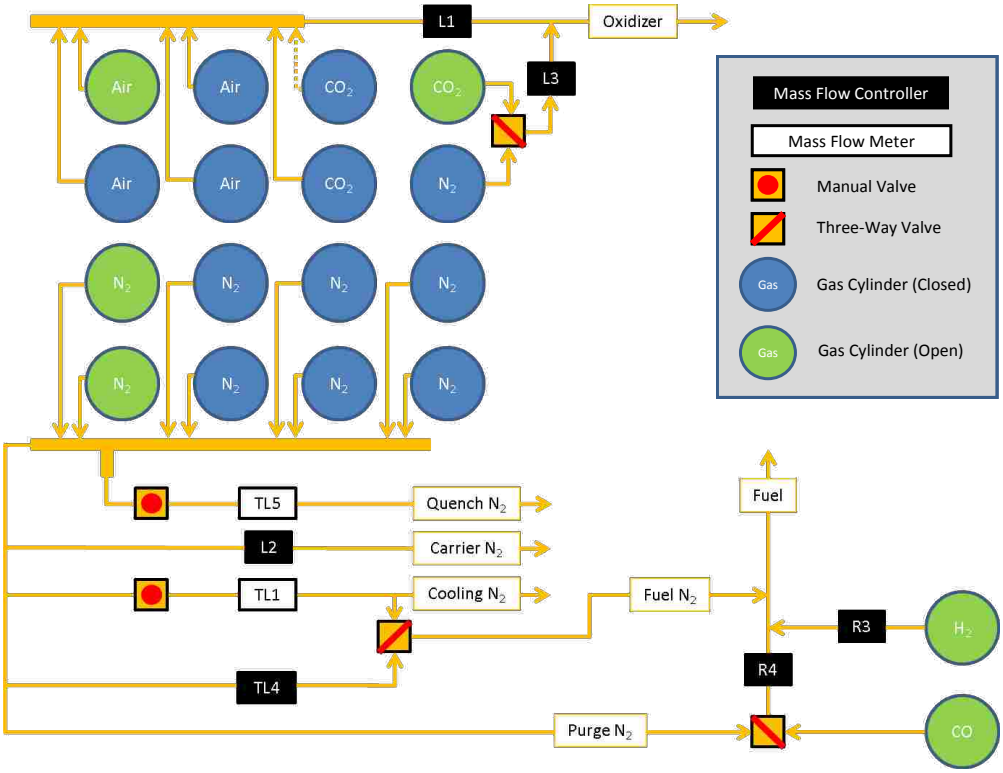

Figure G.5. HPFFB gas setup at conditions where the post-flame environment consists of approximately 40 mol% CO_2.

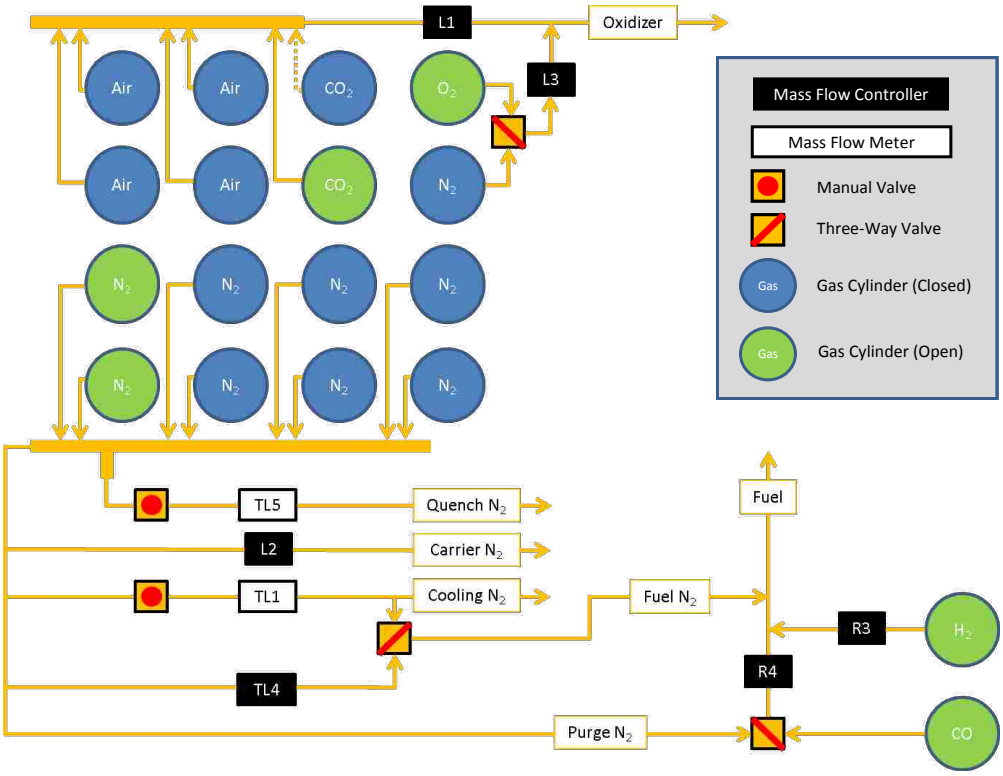

Figure G.6. HPFFB gas setup at conditions where the post-flame environment consists of approximately 90 mol% CO_2.